

***INVESTIGATIONS OF VARIABILITY IN
SPACE WEATHER CONDITIONS: USING
ADVANCED WAVELET ANALYSIS
TECHNIQUES***

Thesis Submitted for the degree

of

Doctor of Philosophy

in

Physics

May - 2017

by

Satish Kumar Kasde

Supervisor

Prof. A.K. Gwal (Retd.)

Former Professor & Head

Department of Physics

Barkatullah University, Bhopal-462026

***Space Science Laboratory, Department of Physics
Barkatullah University Bhopal - 462026, India***

CERTIFICATE

This is to certify that the thesis entitled "**Investigations of Variability in Space Weather Conditions: Using Advanced Wavelet Analysis Techniques**" is a faithful record of research work carried out by **Mr. Satish Kumar Kasde** under my guidance and supervision for the degree of Doctor of Philosophy in Physics at Department of Physics, Barkatullah University, Bhopal, India. The candidate has put in an attendance of more than 200 days with me.

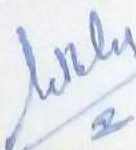
To the best of my knowledge and belief the thesis:

- embodies the work of the candidate himself;
- has duly been completed;
- fulfils the requirements of the ordinance relating to the Ph.D. degree of the University; and
- is upto the standard both in respect of contents and language for being referred to the examiner.



(Prof. A.K. Gwal)
Supervisor

Forwarded by


26/5/17

(Dr. Sadhna Singh)
Head, Department of Physics
Barkatullah University, Bhopal

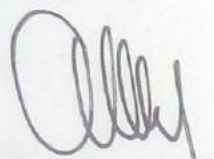
DECLARATION

I do hereby declare that the thesis entitled "**Investigations of Variability in Space Weather Conditions: using Advanced Wavelet Analysis Techniques**" is my own work conducted under the supervision of **Prof. A. K. Gwal (Retd.)** at the Department of Physics, Barkatullah University, Bhopal, India, approved by Research Degree Committee. I have put in more than 200 days of attendance with the supervisor at the center.

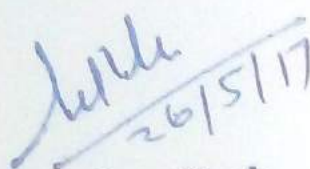
I further declare that to the best of my knowledge the thesis does not contain any part of any work which has been submitted for the award of any degree either in this University or in any other University/Deemed University, without proper citation.



(Satish Kumar Kasde)
Candidate



Prof. A. K. Gwal
(Supervisor)


26/5/17

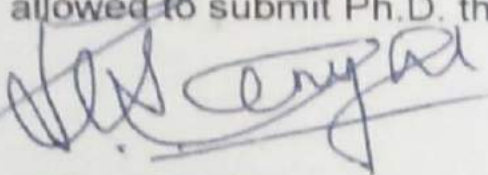
Dr. Sadhna Singh
Head

Department of Physics,
Barkatullah University, Bhopal, (M.P.)

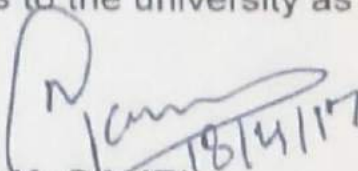
**BARKATULLAH UNIVERSITY, BHOPAL
DEPARTMENT OF PHYSICS**

Pre-Ph.D. Presentation

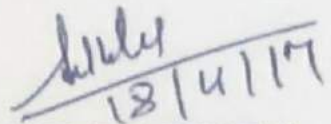
As per the approval of the Hon'ble Vice-Chancellor, Barkatullah University, Bhopal a pre-Ph.D. (Physics) of Mr. Satish Kumar Kasde has been conducted on 18.4.2017 at 12.00 Noon in the committee room of Department of Physics, Barkatullah University, Bhopal. The faculty members, research scholars and students were present in the presentation. Mr. Satish Kumar Kasde gave satisfactory presentation about the research work carried out by him and answered the questions properly. The committee recommends that he may be allowed to submit Ph.D. thesis to the university as per the UGC regulations 2009.



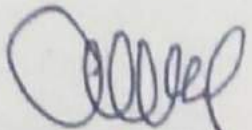
(S.P.SANYAL)
Chairman BoS


18/4/17

(N.K. GAUR)
HoD, Electronics
Dr. N.K. GAUR
Head, Electronics Department
Barkatullah University
BHOPAL-462026


18/4/17

(SADHNA SINGH)
Head, Physics Department
Barkatullah University
BHOPAL- 462026



(A.K. GWAL)
Supervisor

18.4.17



BARKATULLAH VISHWAVIDYALAYA, BHOPAL

(FORMERLY BHOPAL UNIVERSITY, BHOPAL)

CERTIFICATE

No : 1895 / 114

Bhopal Date 01/08/2014

This is to Certify that

Shri SATISH KUMAR KASDE

S/o, W/o, D/o SHRI BAJUSINGH KASDE

Has Appeared in Ph.D. Course Work Examination in the Subject
PHYSICS

Under the Faculty of
SCIENCE

with Enrollment No D-38171

Roll No 29114

Month & Year AUG 2014

and he / she has Qualified the Ph.D. Course Work Examination as per University Rules. He / She Fulfills the eligibility criteria according to University Grant Commission (Minimum standard for award of Ph.D. Degree) Regulation 2009.

Deputy Registrar (Academics)
Barkatullah Vishwavidyalaya, Bhopal (M.P.)
DY Reg. (Academic)

Preface

“Space weather” means changes in the near Earth space environment. It is caused by varying conditions within the Sun’s atmosphere. The Sun emits a continuous stream of highly energetic particles and radiation of varying intensity. The surface of the Sun covers the large scale strong magnetic field as the Sunspots. After the discovery of telescope around 1610, the systematic observation of sunspots started. It was found that the number of sunspots on the surface of the Sun varies cyclically with time, going through repeated descending and ascending phase of a cycle. This cyclic variation of the sunspot number has the average period of about 11 years and is known as the solar cycle or the sunspot cycle or the solar activity cycle. Sunspots are the main sources of several events like the solar flares, eruptions, and coronal mass ejections. These events have serious and sometimes hazardous effects on space weather as well as satellites, air traffic on polar routes and modern-day technologies (telecommunication and electric power grids at high latitudes).

We may also mention that the sunspot cycle has an important effect on the space environment and the Earth climate system. In the pre-industrial era the Sun was the main driver for the earth’s global temperature. Therefore, understanding the solar cycle is not only important to the solar and the stellar physics communities, but also to the space weather and the Earth climate communities. Solar activities are related with the magnetic fields of Sun. The strength of magnetic field at a typical point on the solar surface is a few gauss. However, it can be much higher in sunspots. Sometimes the value of magnetic field was so strong due to which Solar flares occur. Solar flares cause geomagnetic storms, which affect the earth in numerous significant ways. The origin of the Solar wind is complex and the region of Solar wind acceleration has not been probed properly. Several publications discuss the variation in Solar

wind parameters which have durations of hours and boundary widths of tens of minutes. These variations in the Solar wind parameter can also lead to better understanding of the nature and properties of the Solar wind plasma, the stability (or lack thereof) of these structures and the character of plasma instabilities.

The present thesis entitled ***“Investigations of variability in Space Weather conditions: Using Advanced Wavelet Analysis Techniques”*** notify the research work done by me during my Ph.D. work. The thesis reports variability in space weather activity parameter using advanced non-linear techniques.

The **First Chapter** entitled ***“Evaluation of Solar Activities by Advanced Computational Techniques”*** described the Sun and its variable parameters as well as used advanced computational techniques. The Sun is the ancestry of space weather and dynamical star. Solar dynamic and phenomena related to it, is a key part of understanding “Space Weather” conditions. During Solar flares and coronal mass ejection (CMEs) particles travel outwards in the form of Solar wind, which is associated with magnetic field of Sun. The electromagnetic radiation takes about 8 minutes to move from Sun to Earth; on the other hand the charged particles takes few hours to several days as move from Sun to Earth. The radiation and particles interact with the Earth's (geo) magnetic field and outer atmosphere in complex ways, causing concentrations of energetic particles to collect and electric currents to flow in regions of the outer atmosphere (magnetosphere and ionosphere).

The **Chapter Two** named ***“Analysis of Sunspot Time Series during the Ascending Phase of Solar Cycle 24 using the Wavelet Transform”*** revealed that sunspots are widely used to measure the rotational rate of solar surface. We are interested in the analysis of the temporal evaluation of the short-term period present in sunspot time series (i.e. sunspot number and area) during the ascending phase of Solar Cycle 24. For the better understanding of variation in solar activity originated at different layers of the solar atmosphere with respect

to Solar cycles, we study the phase relation between sunspot numbers and sunspot areas using cross correlation analysis techniques based on extended wavelet based approaches such as continuous wavelet transform (CWT), cross - wavelet transform (XWT) and wavelet coherence (WTC). In this study we found the short-term periodicity “27 days-rotational rate of Sun” for current solar cycle 24 (January 2008-May 2013), which suggested that the Solar Cycle 24 has minimum solar activity. We have also investigated the correlation between both parameters and identify the unusual conditions in space weather.

In **Third Chapter** entitled “***Analysis of Short Term Periodic variation in Solar and Terrestrial Parameters***” we analyze the solar wind plasma parameters such as interplanetary magnetic field, solar wind plasma temperature, density, speed and geomagnetic indices Dst, Kp and AE in the time range of ascending phase of the current solar cycle 24. We have chosen the time period from January 2008 to December 2014. This study shows the periodic variations of Solar wind plasma parameters and corresponding change in geomagnetic indices. We conclude that solar rotational periodicity of 27 days was the most prominent period than short range periodicities *i.e.* 2, 9 and 14 days. It suggests that solar wind parameters are highly active at the equatorial location. Thus we conclude that wavelet transform is more suitable for short-term periodic analysis.

In **Chapter Four** named “***Phase Relationship between Sunspot Numbers and F10.7 cm Solar Radio-Flux using Cross-Recurrence Plots and Wavelet -Transform Techniques***” deals with the investigations of phase relation between daily and monthly counts of sunspots and solar radio-flux at 10.7 cm during complete Solar Cycle 23 and the ascending phase of current Cycle 24. The nonlinear approaches such as cross-recurrence plots and advanced wavelet techniques are used to study the asynchronous behaviors of sunspot numbers with F10.7 cm solar radio flux. The results are in agreement with the past findings that solar activity maxima occur at least twice during a cycle: first, near the end of the increasing activity phase and then in the early

beginning years of the declining phase. We also found that the odd and even numbered Solar Cycles 23 and 24 are essentially not in phase and have a phase difference of two months. The sunspot number and solar radio-flux are in phase at the significant period of 27 days, which corresponds to one solar rotation, during the maximum phase of the cycles.

The **Chapter Five** entitled ***“Multifractal Analysis of Sunspot Number time Series during Solar Cycles 20-23 and Ascending Phase of Solar Cycle 24 ”*** deals with the Multifractal analysis of complex dynamical fluctuations in sunspot number data including Solar Cycles 20-23 and ascending phase of current Solar Cycle 24. To reveal the multifractal characteristic of monthly sunspot number are analyzed by singularity spectrum and multi resolution wavelet analysis technique. The result shows that singularities spectrum of sunspot data was well Gaussian in shape, which suggested the multifractal characteristic of data. Thus it was conclude that multifractal character provides a local and adaptive description of the cyclic components of sunspot number time series. The multifractality in sunspot number generates turbulence with the typical characteristics of the anomalous process governing the magnetosphere and interior of Sun.

The **Chapter Six** ***“Multifractal Detrended Fluctuation Analysis (MF-DFA) of Solar Wind Plasma Parameters during Solar Cycle 23”*** quantifies the multifractality in solar wind parameters precisely. Solar wind (SW) plasma parameters are continuously measured by many satellites based techniques. The data used for this study are the daily counts of Solar wind plasma parameters as temperature, density and speed from January 1996 to December 2006 (*i.e.* nearly the time span of Solar Cycle 23). The data were analyzed using the multifractal detrended fluctuation analysis technique in order to characterize the intrinsic scaling property of Solar wind plasma parameters. The Multifractal Detrended Fluctuation Analysis (MFDFA) method allows a reliable multifractal characterization of multifractal non-stationary time series of Solar wind plasma

parameters. One reason to employ the DFA method is to avoid spurious detection of correlations that are artifacts of non - stationarities in the time series.

In this thesis we analyze the periodicities and multifractal properties of various solar activity and solar wind parameters. The rotational periodicity of the sun is expected to provide useful information about solar interior dynamics and mechanism of generation of the solar magnetic field and its emergence on the solar surfaces. We found that wavelet power spectrum and global wavelet spectrum methods are very useful to identify the short term periodicities of interplanetary magnetic field, solar wind plasma parameter and terrestrial geomagnetic indices. The cross wavelet transform shows the strong phase interaction at the maximum phase of cycles and has the periodicity of 27 days associated with the average solar rotation period for active regions. Multifractal spectra provide information where singularities occur in data. Our findings suggested that multifractal analysis techniques are more efficient to capture the inherent richness of time series properties of solar wind plasma parameters. This research work surely gives some innovative idea to early researchers to investigate some new phenomena related to solar activity and solar wind parameters.

(S. K. Kasde)

Contents

<i>Preface</i>	(i)
<i>Contents</i>	(vi)
<i>Acknowledgement</i>	(x)

Chapter-1

Evaluation of Solar Activities by Advanced Computational Techniques

1.1	<i>Introduction: Space Weather</i>	1
1.2	<i>The Sun as a Star</i>	2
	1.2.1 <i>The Stellar Equations of Structure</i>	4
1.3	<i>Structure of the Sun</i>	6
	1.3.1 <i>The Core</i>	7
	1.3.2 <i>The Radiation Zone</i>	8
	1.3.3 <i>The Convection Zone</i>	9
	1.3.4 <i>Atmospheric Layers of Sun</i>	10
	1.3.4.1 <i>The Visible Surface (The Photosphere)</i>	10
	1.3.4.2 <i>The Chromosphere (The red Layer)</i>	11
	1.3.4.3 <i>The Corona (The Sun's Corona)</i>	11
	1.3.4.4 <i>Solar Flares</i>	13
	1.3.4.5 <i>Prominences</i>	14
	1.3.4.6 <i>Coronal Mass Ejections (CMEs)</i>	15
1.4	<i>The Solar Cycle</i>	17
1.5	<i>Variation of Solar Rotation with Latitudes</i>	19
1.6	<i>Solar activity and its parameters</i>	20
	1.6.1 <i>Sunspot Regions</i>	20
	1.6.2 <i>Solar Radio Flux (F10.7 cm)</i>	23
	1.6.3 <i>Solar Wind Plasma</i>	23
	1.6.4 <i>Interplanetary Magnetic Field (IMF)</i>	25
	1.6.5 <i>Geomagnetic Storms</i>	25
1.7	<i>Space Plasma and Magnetohydrodynamics (MHD)</i>	27
	1.7.1 <i>The Solar wind as a Fluid</i>	27
	1.7.2 <i>The Frozen-in Flux Theorem</i>	28
	1.7.3 <i>Magneto-hydro-dynamic (MHD) waves</i>	31
	1.7.4 <i>Magnetic Reconnection</i>	31
1.8	<i>Solar wind - Magnetosphere Coupling</i>	32
1.9	<i>Methods of Analysis</i>	35
	1.9.1 <i>Wavelet Transform</i>	35
	1.9.1.1 <i>Discrete Wavelet Transform (DWT)</i>	36
	1.9.1.2 <i>Continuous Wavelet Transform (CWT)</i>	36

1.9.1.3	Cross Wavelet Transform (XWT)	36
1.9.1.4	Wavelet Coherence Transform (WTC).....	37
1.9.2	Cross Recurrence Plots (CRPs)	37
1.9.3	Multifractal.....	37
1.10	Review of Work Done.....	38
1.11	Future Scope of Work.....	41
1.12	Research Publications.....	42

Chapter-2

Analysis of Sunspot Time Series during the ascending Phase of Solar Cycle 24 using the Wavelet Transform

2.1	Introduction.....	44
2.2	Data Source.....	47
2.3	The Wavelet Techniques (WT)	47
2.3.1	Continuous Wavelet Transform Analysis (CWT).....	47
2.3.2	Wavelet Coherence Analysis (WTC).....	48
2.3.3	Cross Wavelet Transform Analysis (XWT).....	49
2.4	Results and Discussion.....	49
2.5	Conclusions.....	53

Chapter-3

Analysis of Short term Periodic variation in Solar and Terrestrial parameters

3.1	Introduction.....	55
3.2	Prominent Periodicities.....	56
3.2.1	13.5 Day period.....	56
3.2.2	27 Day Period.....	57
3.2.3	154 Day Period.....	57
3.2.4	11 Year Sunspot Cycle.....	58
3.2.5	22 Year magnetic cycle.....	58
3.3	Method: Wavelet Transform.....	58
3.4	Data Set.....	59
3.5	Results	60
3.5.1	IMF B _x Component.....	60
3.5.2	IMF B _y Component.....	61
3.5.3	IMF B _z Component.....	62
3.5.4	Solar Wind Temperature.....	63
3.5.5	Solar Wind Plasma density.....	64
3.5.6	Solar wind Plasma speed.....	65
3.5.7	Geomagnetic Dst index.....	66
3.5.8	Geomagnetic activity index Ap.....	67

3.5.9	Geomagnetic activity index AE.....	68
3.6	Conclusions.....	69

Chapter-4

Phase relationship between Sunspot number and F10.7 cm Solar radio Flux using Wavelet transform Technique

4.1	Introduction.....	72
4.2	Data Set.....	74
4.3	Analysis With Various Techniques	75
4.3.1	Mutual Information and Embedding Dimension.....	75
4.3.2	Cross Recurrence Plots (CRPs)	75
4.3.3	Advanced Wavelet Techniques.....	76
4.4	Results and Discussion.....	76
4.5	Conclusions.....	85

Chapter-5

Multifractal Analysis of Sunspot Number time Series during Solar Cycles 20-23 and Ascending Phase of Solar cycle 24

5.1	Introduction.....	88
5.2	Data set.....	89
5.3	Theoretical Background	90
5.3.1	Time series decomposition via the Discrete Wavelet Transform (DWT)	90
5.3.2	Wavelet Based Multifractal Formalism	90
5.3.3	Partition Function.....	91
5.4	Analysis	92
5.4.1	Wavelet Analysis of Sunspot Numbers.....	92
5.4.2	Multifractal Analysis of Sunspot Numbers.....	99
5.5	Conclusions.....	108

Chapter-6

Multifractal Detrended Fluctuation Analysis (MF-DFA) of Solar Wind Parameters during Solar Cycle 23

6.1	Introduction.....	110
6.2	Data Source.....	113
6.3	Multifractal Detrended Fluctuation Analysis (MF-DFA)	113
6.4	Results and Discussion.....	117
6.5	Conclusions.....	120

Bibliography..... 123
Reprints

Acknowledgments

It is a great pleasure to convey hearty gratitude to my supervisor Prof. A.K. Gwal, for his constant help, encouragement and precious guidance. He has been a constant source of inspiration for me. Despite my shortcomings and slow progress in research, he has been very cooperative and helpful to me. His encyclopedic knowledge of Physics and Astrophysics, and the intuitive and clever ways of solving difficult problems amaze me. Due to his encouragement and support to participate in conferences and workshop, I have been able to interact and work with many good scientists on various problems during my research. His patience and support helped me to overcome the many critical situations and finish this thesis. Heartfelt thanks also go to Mrs. Pramila Gwal for her affection, sympathy and love showed on me. I deeply acknowledge for her splendid, marvelous and cheerful nature.

I am delighted to express my obligation and heartfelt regards to Dr. Sadhna Singh, Head, Department of Physics, Barkatullah University, Bhopal for her continuous encouragement, appreciation and insistence which helped me to complete this thesis well in time. I take this opportunity to express my obligation and heartfelt regards to Prof. S.P. Sanyal, Dr. N.K. Gaur, Dr. Vilas Shelke and Dr. M.C. Shah for their support, motivation and cheering me all along the tenure of research.

I am very grateful to Dr. D.K. Sondhiya for his extraordinary help with the programming in MATLAB to get the right values for the analysis and discussions on the science of both Solar Physics and Ionospheric theory. His constant help, encouragement, suggestion and discussion made me to complete the thesis in short time. By collaborating with him I have identified various research problems in solar physics and find the solutions for that. It is a privilege to thank Mrs. Vandna Sondhiya for her nice, helpful and encouraging nature.

I am delighted to express my obligation and heartfelt regards to each and every individual of the Department of Physics and Barkatullah University, Bhopal for all the support I have received from them and for making it a wonderful experience of my life.

I also like to thank Dr. G. Panda, Dr. S. Raghuwanshi, Dr. J. Pataiya, Dr. C.B. Makode, M. Raghuwanshi, Rahul Shrivastava, Vinod Ranaut, D.R.Upwar, S. Ghaneker, Manoj, Krishna and Ritesh for their special support. Various people have helped through different capacity to make this research as present. I owe my gratitude to all those people who have made this thesis possible and because of whom; my research experience has been one I will cherish forever.

My sincere appreciation goes to University Grants Commission (UGC), New Delhi by awarding me the Rajiv Gandhi National Fellowship (RGNF), without this financial support, it would have been really hard to complete this thesis.

I acknowledge NASA Solar Science, National Geophysical Data Center (NGDC), World Data Center (WDC) Kyoto, NOAA, NASA and satellite mission teams especially ACE, SOHO and GOES for providing access to various data sets on which studies contained in the thesis is based. This work contained in the thesis would have been impossible without the availability of these data sets. For the computations made in this work, we acknowledge the use of the *Matlab* software package (<http://www.mathworks.com>), *Matlab's Wavelet Toolbox* and the free software programs: *Wavelab* (Stanford University – <http://wwwstat.stanford.edu/~wavelab>), *Fraclab*, *A Fractal Analysis Software* (INRIA-<http://fractales.inria.fr/>) and other *Matlab* routines (<http://paos.colorado.edu/research/wavelets/>).

I appreciate the supports of every staff member (both the academic and non-academic) of the Department of Physics and Electronics, Barkatullah University, Bhopal.

I would like to convey my heartfelt thanks to my loving parents, (late) grandfather, and sister for constant encouragement and support and immense helpfulness when it was utmost required throughout the course.

Finally, I acknowledge each and every individual who have directly or indirectly helped me in this work, whether mentioned or remained unmentioned, for making it a unique and memorable experience of my life.

(S. K. Kasde)

Evaluation of Solar Activities by Advanced Computational Techniques

1.1 Introduction: Space weather

Space weather refers to the interaction of solar particles and magnetic fields with the magnetosphere of Earth. During Solar flares and coronal mass ejection (CMEs) particles travel outwards in the form of Solar wind, which is associated with magnetic field of Sun. The electromagnetic radiation takes about 8 minutes to move from Sun to Earth; on the other hand the charged particles takes few hours to several days as move from Sun to Earth. The radiation and particles interact with the Earth's (geo) magnetic field and outer atmosphere in complex ways, causing change in concentrations of energetic particles and electric currents to flow in regions of the outer atmosphere (magnetosphere and ionosphere).

Figure 1.1 illustrated that Space weather not only affects the functioning of technical systems in space and on Earth, but may also endanger human life and health (Hill et al., 2000; Carlowicz and Lopez, 2002). It also affect electronic system (Love et al., 2000; Dorman, 2005), immediate and long term hazards to astronauts and aircraft crews (Garret and Hoffman, 2000; Jokiaho, 2004; Defise et al., 2005), changes in electronic charging of satellites (Lai, 1996, 1999; Baker, 2000), interruptions in telecommunications and navigational systems (Boteler et al., 1998; Kikuchi, 2003), power transmission failures (Kappenman, 1999; Pirjola, 1998; Daglis et al., 2004) and disruption to rail traffic signals (Label and Barth, 2000; Pirjola, 2003). Space weather is thus a lot more than the impressive auroras at high latitudes, with which are familiar and risk hazards due to space weather exotic phenomena pose serious threat

motivating rapid search for accurate analyzing, modeling and prediction methods (Turner, 2000; Bothmer, 2004).



Courtesy: http://www.nasa.gov/mission_pages/sunearth/science/Solar-rotation.html

Figure - 1.1: Interaction of the space weather with Earth's atmosphere

1.2 The Sun as a Star

The sun is one of the billions of stars that make up our galaxy. Its continuation is the consequence of the disintegration of interstellar gas clouds and dust which primarily reached in equilibrium state between the inward gravitation force and outward pressure forces, which include successive energy release from nuclear fusion. The total mass of sun is 4.6×10^9 kg, of which 73.46% hydrogen, 24.85% helium, and small traces of large elements such as oxygen, iron, magnesium and silicon.

In the standard stellar model of sun, it was assume that the interior of sun is in hydrostatic equilibrium state. In this state force of gravity compresses material radially inward, resulting in an opposing force due to the resulting gradient in gas pressure,

$$\frac{dP}{dr} = \frac{-GM_r \rho}{r^2} \quad \dots \dots \dots (1.1)$$

Where,

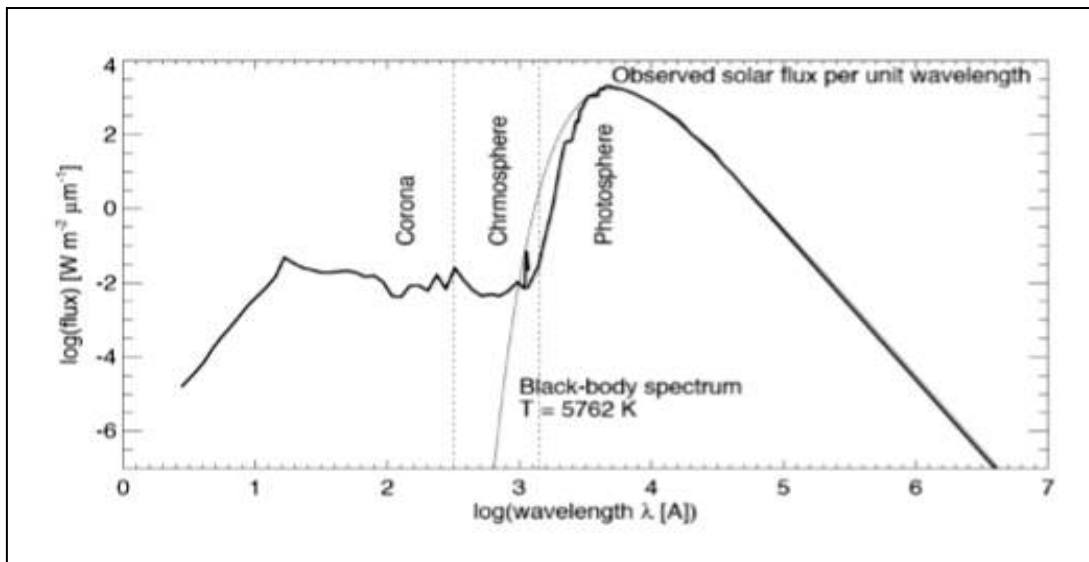
M_r = The mass contained within a given radius

G = Gravitational constant

P = Pressure

ρ = Density

It was assumed that from the center to the solar surface pressure, density and temperature (T) decrease monotonically with radius. The gas pressure is helped by radiation originating from fusion in the core, contributing to internal heating as well as a radiative pressure force and due to the fact local thermodynamic equilibrium (LTE) is reached, implying that stellar material is thermalised and both the material and radiation field are in equilibrium. In this state the materials are assumed to be radiated as black-body. But the sun is not a perfect blackbody, as shown in Figure 1.2 by the comparison between theory and data. In figure thick line shows the observed solar spectrum with emission and absorption lines at short and long wavelengths, respectively and 5762 K black body spectrum is indicated by the thin line.



Courtesy: Aschwanden, 2005

Figure - 1.2 Comparison between theoretical and observed solar flux over wavelength

In black body spectrum, the peak in emission wavelength, λ_m is inversely related to temperature as,

$$\lambda_m T = 0.290[\text{cmK}], \quad \dots \dots \dots (1.2)$$

Here λ_m is given in cm. This is known as Wien's displacement law. It was found that the peaks of solar emission were found in green region of visible spectrum corresponding to temperature of 5770 K at $\lambda_m = 5030 \text{ \AA}$. But the average of whole visible spectrum appears to white.

The total energy emitted by any star is determined by integrating all equation of black body leads the Stephan-Boltzmann law, which is given as

$$J_{bb} = \sigma_{sb} T^4 \quad \dots \dots \dots (1.3)$$

Equation (1.3) gives the power radiated through a surface element of a black body. Here, $\sigma_{sb} = 5.67 \times 10^{-8} \text{ Js}^{-1} \text{ m}^{-2} \text{ K}^{-4}$, known as Stephan-Boltzmann constant. Integration of J_{bb} over a spherical surface yielding a monochromatic luminosity (given in equation 1.4), which is independent of wavelength λ .

$$L_{bb} = 4\pi R_{\odot}^2 \sigma_{sb} T^4 \text{ ergs}^{-1} \quad \dots \dots \dots (1.4)$$

Where R_{\odot} = the solar radius.

1.2.1 The Stellar Equations of Structure

The stellar equations of structure describe the stellar energy released in fusion from the core and transport all over the interior. The following equations form a closed system, known as the stellar equation of structure:

- Equation of State:

$$P = \frac{\rho k_{\beta} T}{\mu m_H} \quad \dots \dots \dots (1.5)$$

- Mass Continuity:

$$\frac{dM_r}{dr} = 4\pi r^2 \rho \quad \dots \dots \dots (1.6)$$

- Energy Source

$$\frac{dL_r}{dr} = 4\pi r^2 \rho \epsilon \quad \dots \dots \dots (1.7)$$

- Radiative Transport:

$$\frac{dT}{dr} = -\frac{3}{4a_r c} \frac{k_{\rho}}{T^3} \frac{L_r}{4\pi r^2} \quad \dots \dots \dots (1.8)$$

- Convective Transport:

$$\frac{dT}{dr} = - \left(1 - \frac{1}{\gamma}\right) \frac{\mu m_H}{k_B} \frac{GM_r}{r^2} \dots \dots \dots (1.9)$$

Where

μ = The mean molecular weight,

m_H = The mass of hydrogen,

M_r = The integrated mass from the centre to a given radius,

ϵ = The total energy emitted by nuclear reactions and gravitational heating (contraction) or cooling (expansion) per gram per second,

a_r = The radiation constant ($a_r = 4\sigma_{SB}/c$),

κ = The mean opacity (averaged over wavelength),

L_r = The integrated luminosity to a given radius,

γ = The ratio of specific heat a constant pressure (CP) to that at constant volume (CV).

By using numerical methods equation 1.5 to 1.9 provide first-order prediction of the temperature, pressure, and density profiles within the solar interior. Figure 1.3 shows a highly detailed numerical solution of that equations proposed by Bahcall & Pinsonneault (Bahcall & Pinsonneault, 2004).

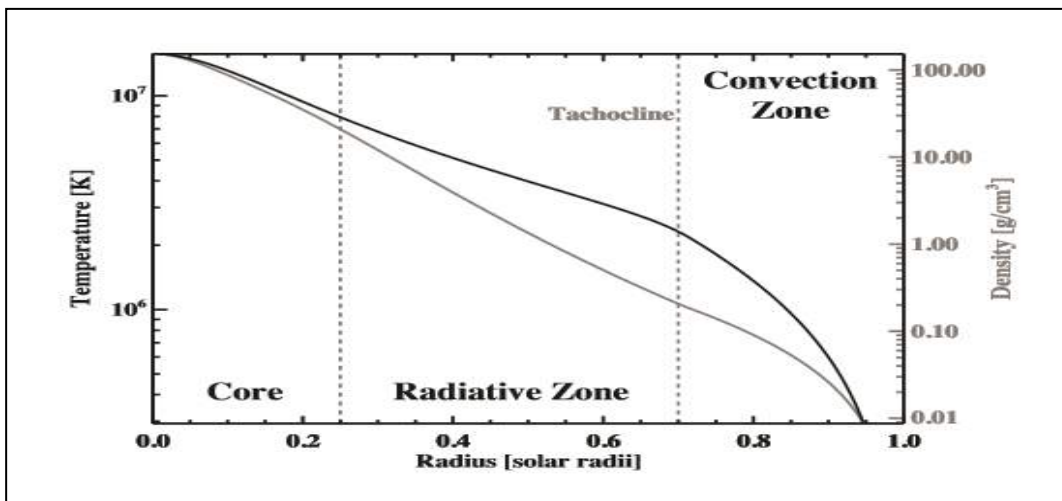


Figure - 1.3: The BP2004 numerical model (Bahcall & Pinsonneault, 2004) of the solar interior.

Stars undergoing fusion in their cores are governed by a mass-luminosity scaling law. The Sun falls on this stellar “main-sequence” (as shown in Figure 1.4) while undergoing fusion, which lasts for the order of 10¹⁰ years.

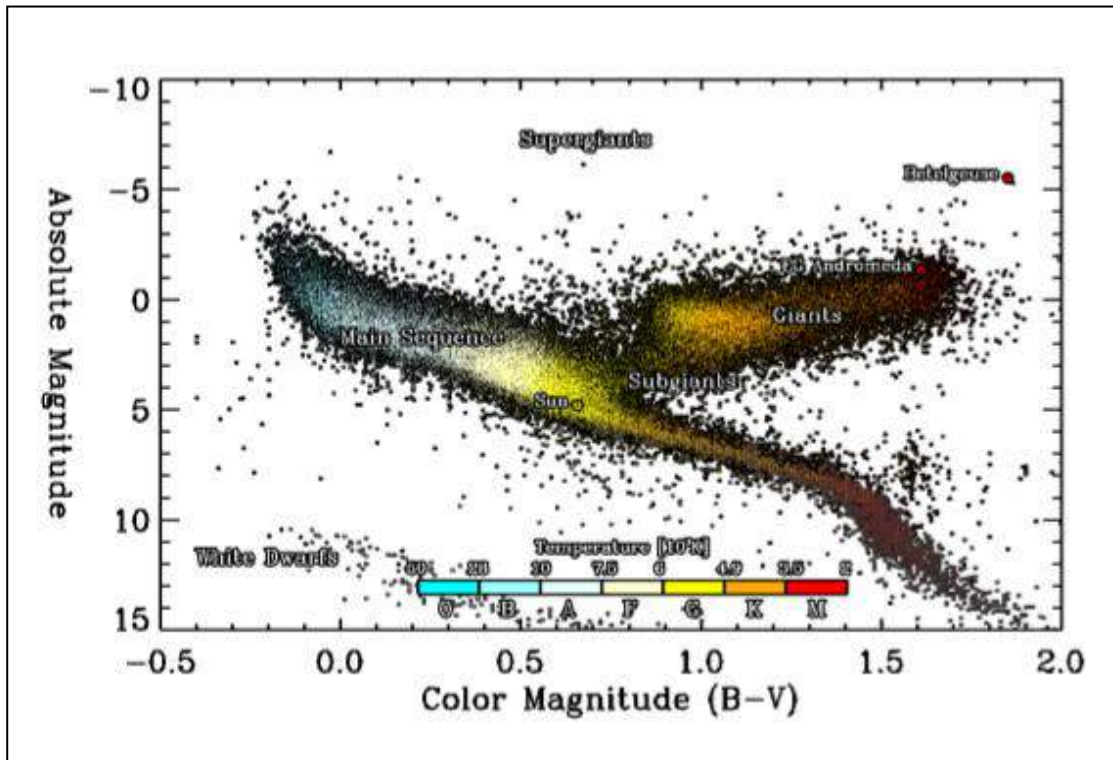


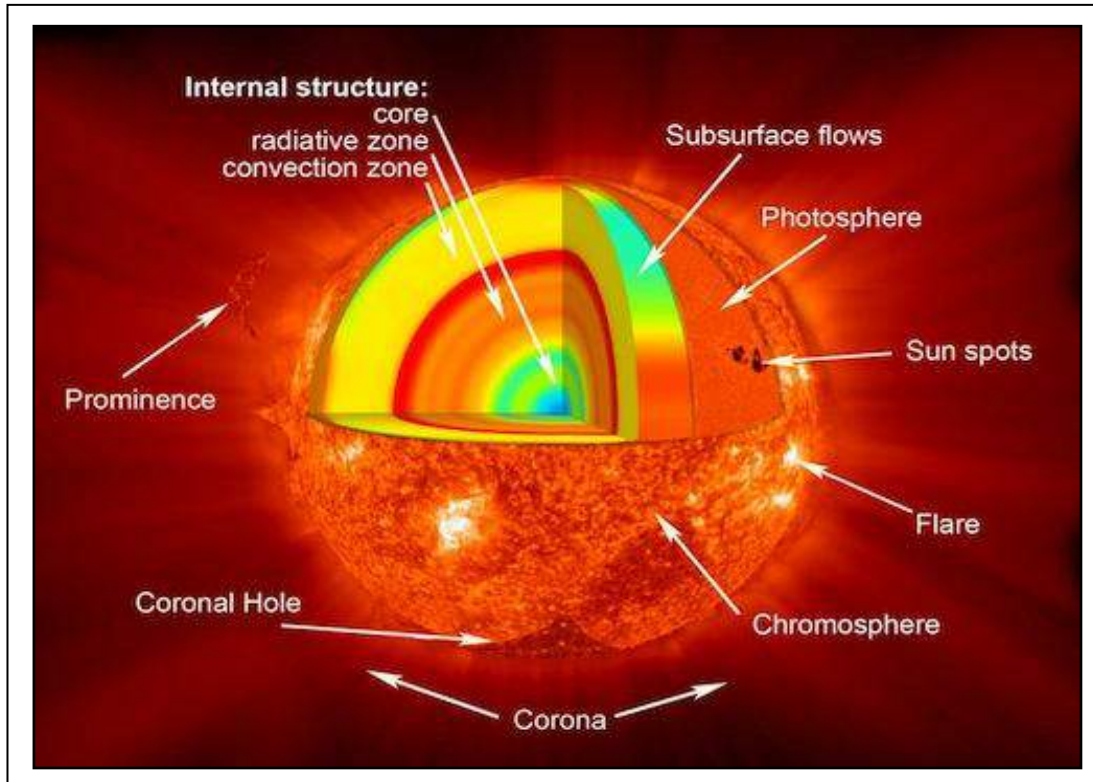
Figure - 1.4: A Hertzsprung-Russell color-magnitude diagram. The color bar indicates the spectral class and temperature range. The HIPPARCOS (black dots) and “Gliese 1991” (dark gray dots) catalogues have been used, excluding binary systems. The main stars studied in the Astrophysics Research Group at Trinity College Dublin are highlighted.

Stars in non-fusion phases of evolution fall to the upper-right (red giants) and lower-left (white-dwarfs) of the main sequence. Stars on the main sequence can be classified by their spectra, which are related to their surface temperatures. The Sun is a G2 (yellowish) star. Stars may vary in their subsurface layers depending on mass and their stage of evolution.

1.3 Structure of the Sun

The standard model of the Sun is shown in Figure 1.5. The Sun has a dense core, where temperatures reach about $13MK$. The temperature and density are sufficient to support nuclear fusion. The core is surrounded by a dense radioactive zone. It is so dense that the individual photons created in the core take about 10^6 years to reach the surface. Surrounding the radiation zone there is the convective zone, where energy is transported by large scale convective cells driven by the temperature difference between the inner and outer layers of the Sun. The surface of the Sun is known as the photosphere and is the boundary between the solar interior and atmosphere. The Solar

atmosphere consists of the chromospheres, transition zone and corona. The brief description of Sun and its various parts are described in next sub-sections.



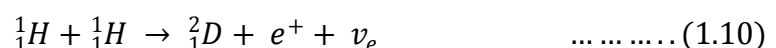
Courtesy: http://www.nasa.gov/mission_pages/sunearth/science/Solar-rotation.html

Figure - 1.5: The standard model of the Sun

1.3.1 The Core

The Sun's core is the central region with a temperature of ~15MK and the density is about 150 g/cm³ (about 10 times the density of gold or lead). Both the temperature and the density decrease as one moves outward from the centre of the Sun. At this extremely high temperature and pressure nuclear reactions consume hydrogen to form helium. Burning of hydrogen in the core creates helium, which may diffuse outwards and form a shell as fusion continues. At this stage a chain of particle interactions start that begins with hydrogen nuclei and ends with helium nuclei, known as proton-proton (PP) chain. This is summarized as follow,

- Two hydrogen nuclei (H) fuse to form a deuterium (D) nucleus, a positron (e^+), and an electron neutrino (ν_e);



- The positron immediately annihilates with a nearby electron, producing two gamma rays (γ);



- The deuterium fuses with another hydrogen nucleus resulting in a helium(He) isotope with one neutron and another gamma ray is released;



- Finally, two helium isotopes fuse, resulting in a helium nucleus with two neutrons and two protons. This process is represented by the following equations,



In the process about 25 MeV energy is generated. In the Sun, step I generates about 85% of the total energy, step II about 15%, with step III only contributing about 0.02%. The neutrinos generated by this process predominantly leave the core unhindered. Neutrinos pass right through the overlying layers of the Sun and can be detected on Earth, using large and complex detectors.

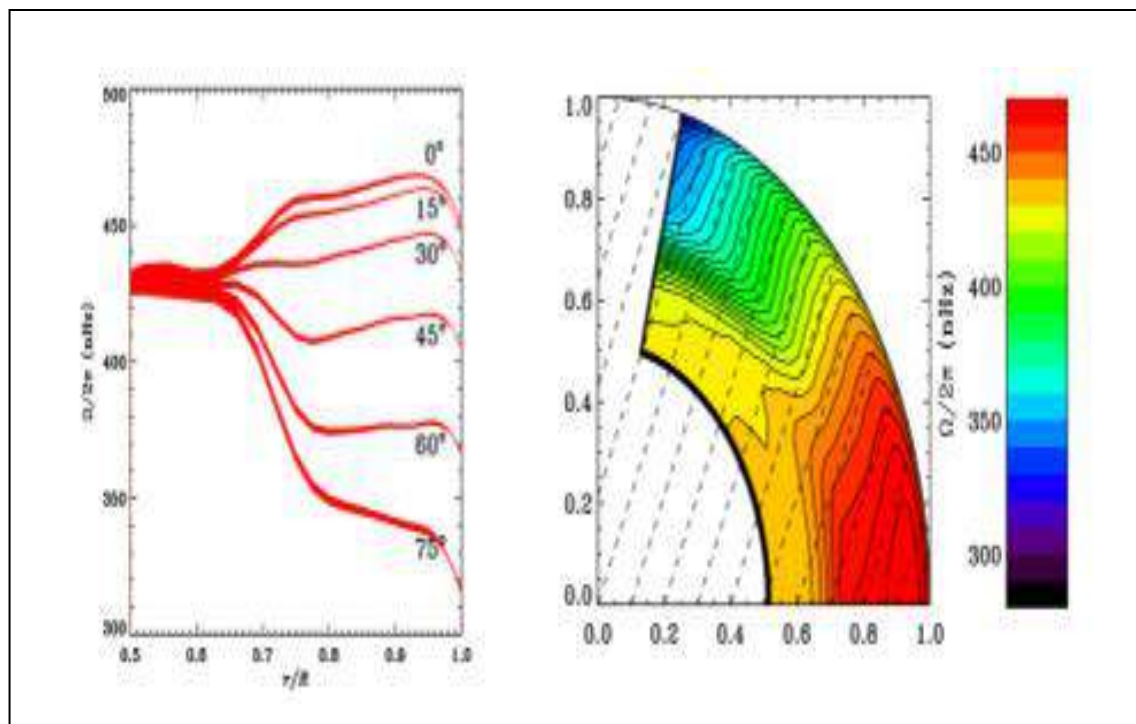
1.3.2 The Radiation Zone

In this region the energy is transported from the super hot interior to the colder outer layers by photons. Technically, this also includes the core. It extends from 0.25 to 0.75 R_{\odot} , (*i.e.* solar radii) with a temperature range of 10 MK – 5 MK. Due to the high densities in the core and radiation zone the gamma rays produced due to p-p chain constantly scatter when they meet with free electrons, protons and atomic nuclei. The scattering takes place, when an electron is completely free (Thompson), loosely bound with the photon wavelength being much smaller than the atom (Compton) or with the wavelength being much larger than the atom (Rayleigh). When a bound electron absorbs a photon bound-bound scattering takes place, in this process a electron transitioning to a less bound state, and are responsible for the spectral absorption lines in stellar spectra. In bound-free absorption energy of the absorbed photon is large enough to free the electron and also for ionizing the atom. During the free-free absorption process an unbound electron near an

ion absorbs a photon as a result the kinetic energy of the electron increases. For the solar interior, free-free and bound-free absorption dominates. Kramers' states that when absorption cross-section for a given amount of material known as opacity, is dominated by bound-free and free-free absorption, $\kappa \propto \rho T^{-7/2}$. Thus κ is indicative of the amount of absorption and increases rapidly with decreasing temperature, reducing the rate of radiative transport and further steepening the temperature gradient.

1.3.3 The Convection Zone

The visible surface of the Sun, extending down about 200000 km, is known the convection zone. In this region, the largest part of the energy is transported to the surface in convection cells, where hotter plasma rises, cools and sinks again. The size of convection cells is strongly depends on the depth owing to strong ranging pressure scale height.



Courtesy: Global Oscillation Network Group (GONG: Harvey et al., 1996).

Figure - 1.6: The internal differential rotation of the Sun as obtained from helioseismology. The bottom of the convection zone lies at $r=0.713 R_\odot$

The region below the convection zone known as radioactive zone moving with constant speed. On the other hand overlying convection zone has latitudinally depends on rotation and leads to a region of strong velocity gradients (shear) at the bottom of the convection zone, which is known as the tachocline (Spiegel and Weiss, 1980). A similar, but thinner region exists close to the surface, which is the Near Surface Shear Layer (NSSL), (see e.g. Thompson et al., 1996; Schou et al., 1998). The overall rotation is clearly not a profile of cylindrical rotation, but the contours of constant rotation are parallel to the rotation axis. In the Sun the contours are spoke-like, i.e. they are pointing radially outward. Proper motion of Sunspot indicates a meridional circulation in the solar convection zone; first found by Tuominen (1941). The direction of this flow is poleward near the surface and equator ward inside the convection zone. The various dynamics process and the structure of the convection zone is vital field of research, because the turbulent motions and differential rotation are able to generate a large-scale magnetic field. That there is a mechanism of creating a magnetic field, called solar dynamo is not disputed either.

1.3.4 Atmospheric Layers of Sun

The energy of the Sun comes from its inner part (i.e. core) to the outer layers of its atmosphere. As we have discussed in the previous section through radiation zone to convection zone large amount of energy transported from the Sun's core. The short description of Sun's atmosphere and various phenomena related to it is given in following sub-sections.

1.3.4.1 The Visible Surface (The Photosphere)

The visible surface of the Sun is known as the photosphere (photo from the Greek for "light"), where optical depth τ for 500 nm light is unity, which is often denoted as τ_{500} and can be thought of as a surface of last scattering for solar optical photon. Its temperature at the bottom is around 6500 K, while at the top that is about 500 km above the "temperature minimum" is 4400 K. In this layer bubbles of hotter material well up from within the sun, divide the surface of the photosphere into bright granules that expand and fade in several minutes. Sometimes huge bundles of magnetic field break through the photosphere

disturbing this boiling layer with a set of conditions known collectively as solar activity and create cool and dark regions known as sunspots. The detail discussion and 11 year cycle variation of sunspot is given in section 1.4.

1.3.4.2 The Chromosphere (The Red Layer)

The region just above the photosphere is called the chromospheres. It is about 1500 *km* thick and characterized by a temperature higher than that of the photosphere (about 10000 K compared to the 5800 K temperature of the photosphere). The density of the plasma (the amount of light emitted) drops rapidly with height in the chromospheres. The chromospheres can be very dynamic with hot jets of gas (spicules) extending high above the surface. These can extend thousands of kilometers above the Solar surface at velocities of about 20 to 100 $km\ s^{-1}$. The chromospheric temperature is inversely proportional to density, so it increases rapidly with height. Spicules and Solar prominences tend to be found at the edges of these cells. Filaments observed above the limb of the Sun, called prominences, are often characterized by their loop-like appearance.

1.3.4.3 The Corona (The Sun's Crown)

The outer atmosphere of the Sun, which is visible during the Solar eclipse are called Solar corona. The corona (Latin for crown) expands out into space supersonically. The Solar gas that escapes into interplanetary space is called the Solar wind. The corona is not spherically symmetric or equally bright in all directions. The visible photosphere is a million times brighter than the corona, and therefore the corona can only be seen when photographic plate is blocked. It is customary to subdivide the Solar corona into three zones, which all vary their size during the Solar cycle: (a) active regions, (b) quiet Sun regions, and (c) coronal holes.

(i) Active Regions

Active regions are located in areas of strong magnetic field concentrations, visible as sunspot groups in optical wavelengths or magnetograms. Because of this bipolar nature active regions are mainly made

up of closed magnetic field lines. Due to the permanent magnetic activity in terms of magnetic flux emergence, flux cancellation, magnetic reconfigurations, and magnetic reconnection processes, a number of dynamic processes such as plasma heating, flares, and coronal mass ejections occur in active regions. The heliographic position of active regions is typically confined within latitudes of $\pm 40^\circ$ from the Solar equator. Active regions, also known as sunspots, appear within $\pm 40^\circ$ of the Solar equator and can grow to cover 1% of the Solar disk (Zirin, 1988). The dark interior of a sunspot is known as the umbra and the lighter area surrounding this is known as the penumbra. The penumbra consists of finer filaments which point radially away from the umbra in simple sunspots.

(ii) Quiet Sun

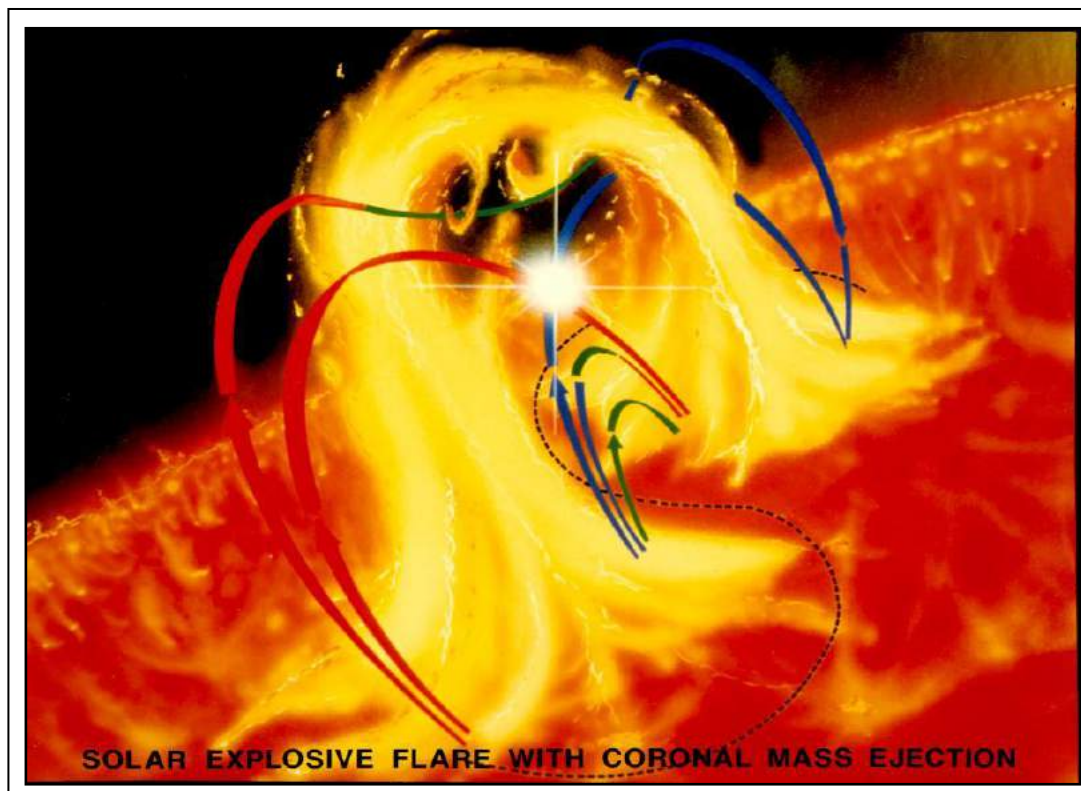
The remaining areas outside of active regions were dubbed quiet Sun regions. Many dynamic processes have been discovered all over the solar surface, so that the term quiet Sun is considered as a misnomer, as justified in relative terms. Dynamic processes in the quiet Sun range from small-scale phenomena such as network heating events, nano-flares, explosive events, bright points, and soft X-ray jets, to large-scale structures, such as Trans-equatorial loops or coronal arches. The distinction between active regions and quiet Sun regions becomes more and more blurred because most of the large-scale structures that overarch quiet Sun regions are rooted in active regions.

(iii) Coronal Holes

The northern and southern polar zones of the solar globe have generally been found to be darker than the equatorial zones during solar eclipses. Max Waldmeier thus coined those zones as “Koronale Löcher” (in German *i.e.* coronal holes). These zones are dominated by open magnetic field lines that act as efficient conduits for flushing heated plasma from the corona into the Solar wind, if there are any chromospheric up flows at their foot points. Due to transport mechanism, coronal holes are empty of plasma most of the time, and thus appear much darker than the quiet Sun, where heated plasma up flowing from the chromosphere remains trapped until it cools down and precipitates back to the chromosphere. Like our Earth atmosphere displays a large variety

of cloud shapes, from bulky stratocumulus to fine-structured cirrus clouds, the solar corona exhibits an equally rich menagerie of loop morphologies, which can reveal important clues about the underlying magnetic reconnection and reconfiguration processes. Pointed and cusp-shaped structures may pinpoint coronal null points of X-type magnetic reconnection points, while circular geometries may indicate relaxed, near-dipolar magnetic field geometries.

1.3.4.4 Solar Flares



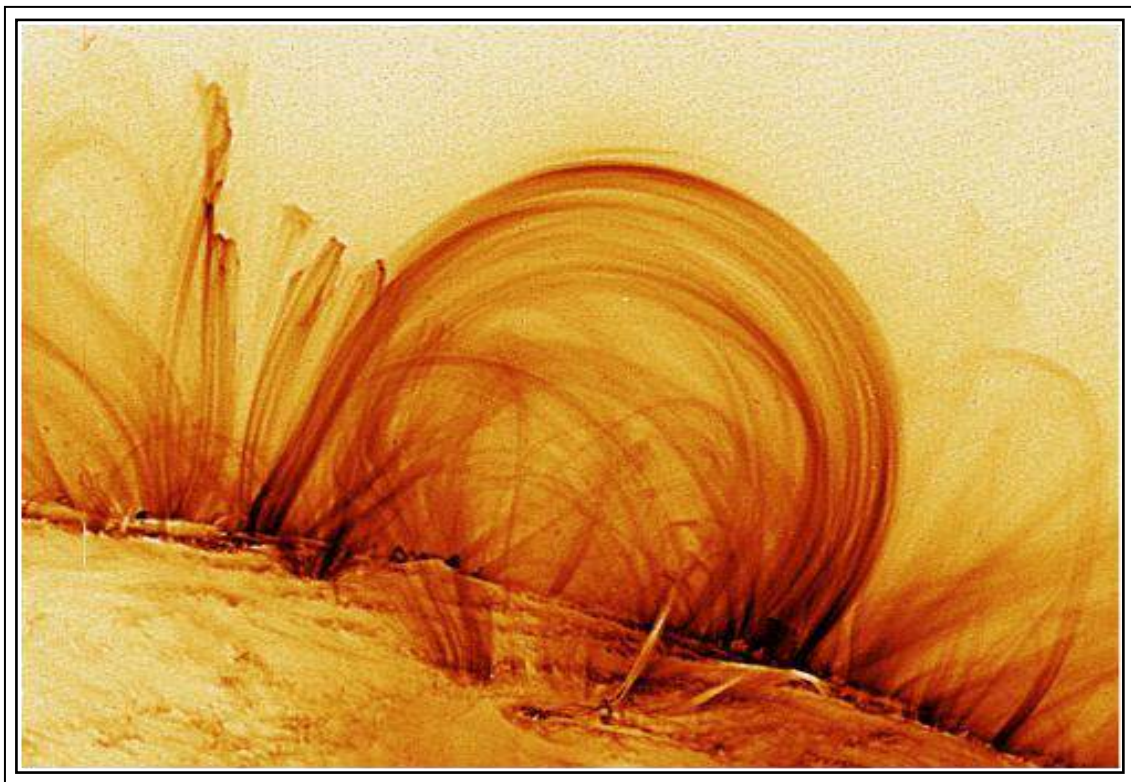
Courtesy: http://www.nasa.gov/mission_pages/sunearth/science/Solar-rotation.html

Figure - 1.7: Solar explosive flare with coronal mass ejection

Solar flares are sudden brightening in the solar atmosphere above sunspot groups (active regions). Richard Carrington was the first observed the first Solar flares in 1859. Solar flares are powered by the sudden release of magnetic energy stored in the corona. It states that the energy is enlightened in the corona, and bigger the flares, the deeper layer is affected by it. According to the energy Solar flares can be classified as A, B, C, M and X, according to the peak flux (W/m^2) of 100 to 800 picometer X – rays near Earth, measured by the GOES spacecraft. Because of the plasma heating, charged particles (electrons,

protons and heavier ions) accelerate by the Solar flares near the speed of light. They create electromagnetic radiation across the electromagnetic spectrum at all wavelengths from radio wave to the gamma rays of shortest wavelength. Our local space weather strongly influence by the Solar flares and associated coronal mass ejections (CMEs) depicted in Figure 1.7. Radars and other devices operating at decimetric wavelengths may disturb their orientation. Solar flares turn out in Solar wind (highly energetic particles) that can induce hazards radiation to Earth's magnetosphere, spacecrafts and astronauts.

1.3.4.5 Prominences

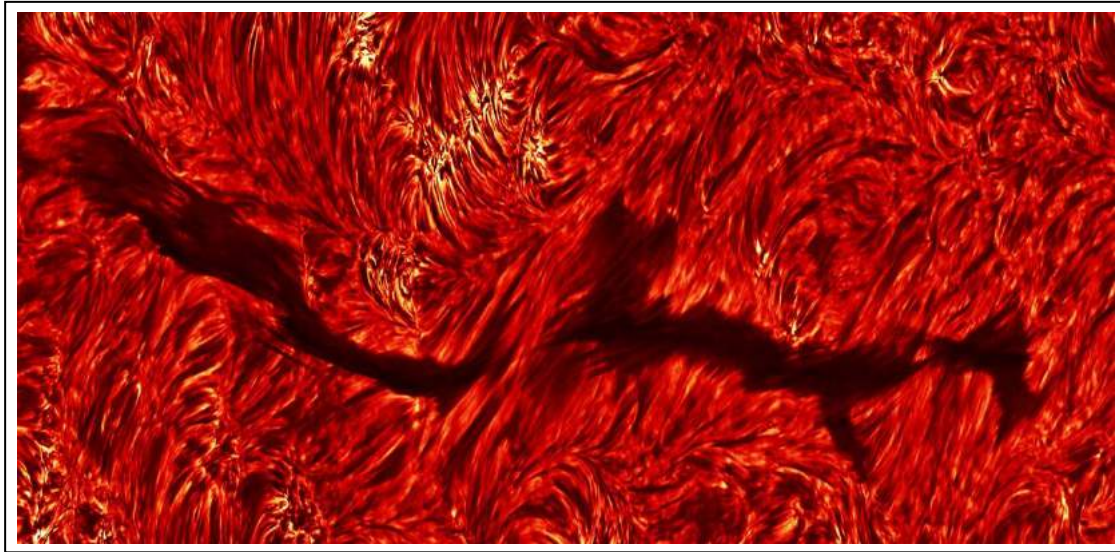


Courtesy: http://www.nasa.gov/mission_pages/sunearth/science/Solar-rotation.html

Figure - 1.8: Prominences are one of the largest “entity” magnetic features of the Sun

The prominences shown in Figure 1.8 are one of the largest “entity” magnetic features on the Sun. Prominences are normally found during the total Solar eclipses and described to it as “burning holes” or “red flames” (Vassenius, 1733), however before the 19th century some observations were done. In 1870s Angelo Secchi was the first distinguished the prominences between quiescent

and eruptive prominences depicted in Figure 1.9 (Galsgaard and Lomgbottom, 1999).



Courtesy: Dutch open Telescope (DOT), www.staff.science.uu.nl

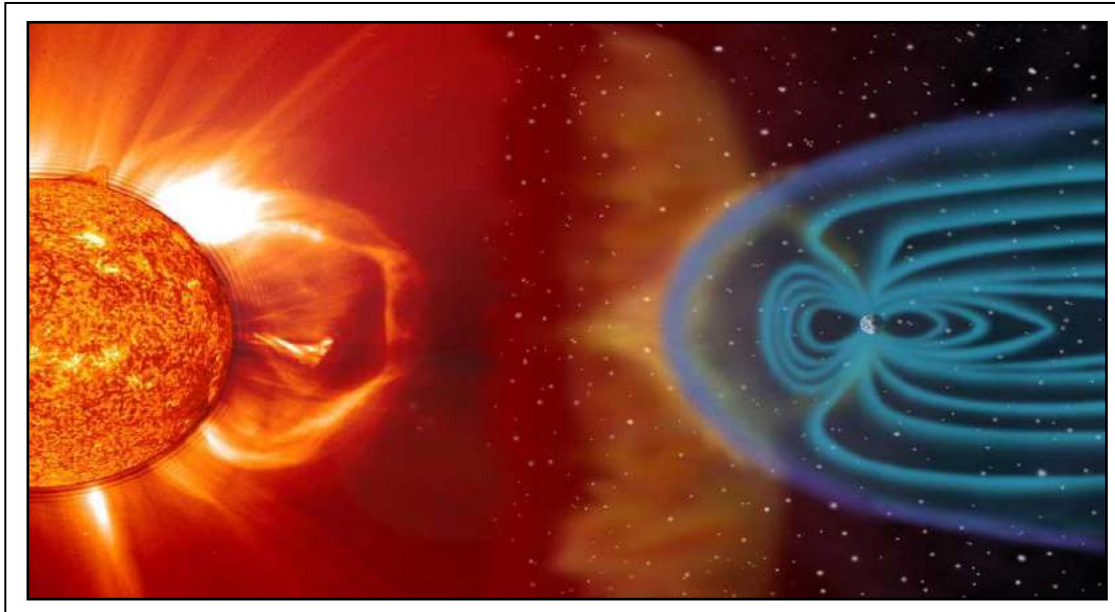
Figure – 1.9: Sun showing quiescent prominence (Filament) The full length of filament taken in Halpha on October 6, 2004.

Quiescent prominences are one of the largest magnetic features of the sun. They form on the time scales of a day and typically remains “unchanged for up to a month and often end their existence through an eruption of Coronal Mass Ejections (CMEs). Prominences are located in the solar corona and consist of plasma that has parameters comparable to that of the chromosphere. Quiescent prominences have a length of 60 to 600 Mm , with a width of 5 to 15 Mm , its temperature varies from 4300 to 5500 K . It has average electron density of 10^{10} to 10^{11} cm^{-3} , and pressure of 0.1 to 1 dyn/cm^2 with magnetic field strength of 4 to 20 G (Bommier et al. 1994; Leroy et al. 1983, Athay et al. 1983). There internal motion have a speed below 10 km/s .

1.3.4.6 Coronal Mass Ejections (CMEs)

The Sun erupt large amount of mass and magnetic field which is known as coronal mass ejections (CME). R. Tousey was the first who detected the Coronal mass ejections (CME) on December 14, 1971 using the 7th Orbiting Solar Observatory (OSO-7). Presently, Large Angle and Spectrometric Coronagraph Experiment (LASCO) instrument on board of SOHO is monitoring the CMEs continuously from 1995. Based on SOHO/LASCO measurments an

average speed of Coronal Mass Ejections range from 20kms^{-1} to $27,000\text{kms}^{-1}$. The effects of CMEs found indirectly at Earth for many thousands of years, due to it on the Earth's magnetosphere an aurora occur. Figure 1.10 shows the interaction of CME with the magnetosphere of Earth.



Courtesy: http://www.nasa.gov/mission_pages/sunearth/science/Solar-rotation.html

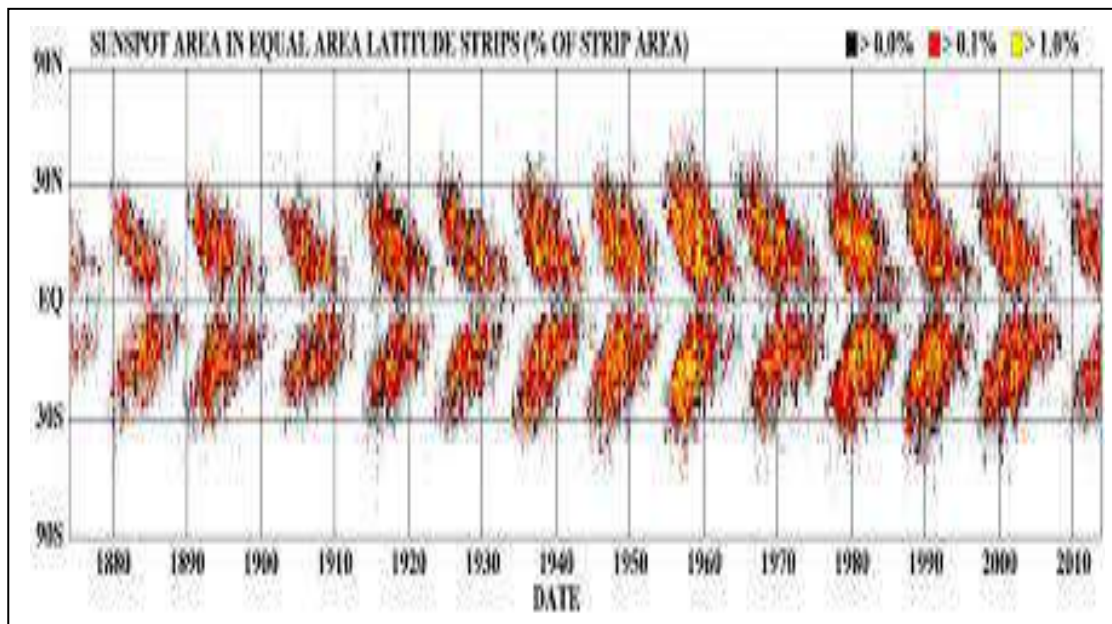
Figure - 1.10: Interaction of Coronal Mass Ejection towards the Earth's atmosphere.

When the ejecta come towards the Earth as an Interplanetary Coronal Mass Ejections (ICME), it disrupt the Earth's magnetosphere it compressed it on the dayside and extend the nightside tail. It creates trillions of watts of power which is directed back towards the Earth's upper atmosphere. This process can cause particularly strong aurora also known as the Aurora Borealis (Northern Hemisphere), and Aurora Australis (Southern Hemisphere). CME dealings with Solar flares, can disrupt radio transmissions, cause blackouts, damage to satellites and electrical transmission lines. The morphology of CMEs consists of a three part structure: a bright leading edge, dark cavity and a bright core or kernel (Illing and Hundhausen 1986, Plunkett et al. 2000). CMEs originate from active regions, having closed magnetic field lines. When amount of magnetic field is sufficient to allow the restraint of the plasma. The frequency of ejections depends on the phase of the Solar cycle: from about one every other day near Solar minimum to 5-6 per day near Solar maximum.

These values are also lower limits of frequency because CMEs propagating away from the Earth (“backside CMEs”) usually not detected by coronagraphs.

1.4 The Solar Cycle

Schwabe suggested that the sunspots appear in quasi-periodic patterns of about 11 years Solar cycle (Schwabe, 1844).

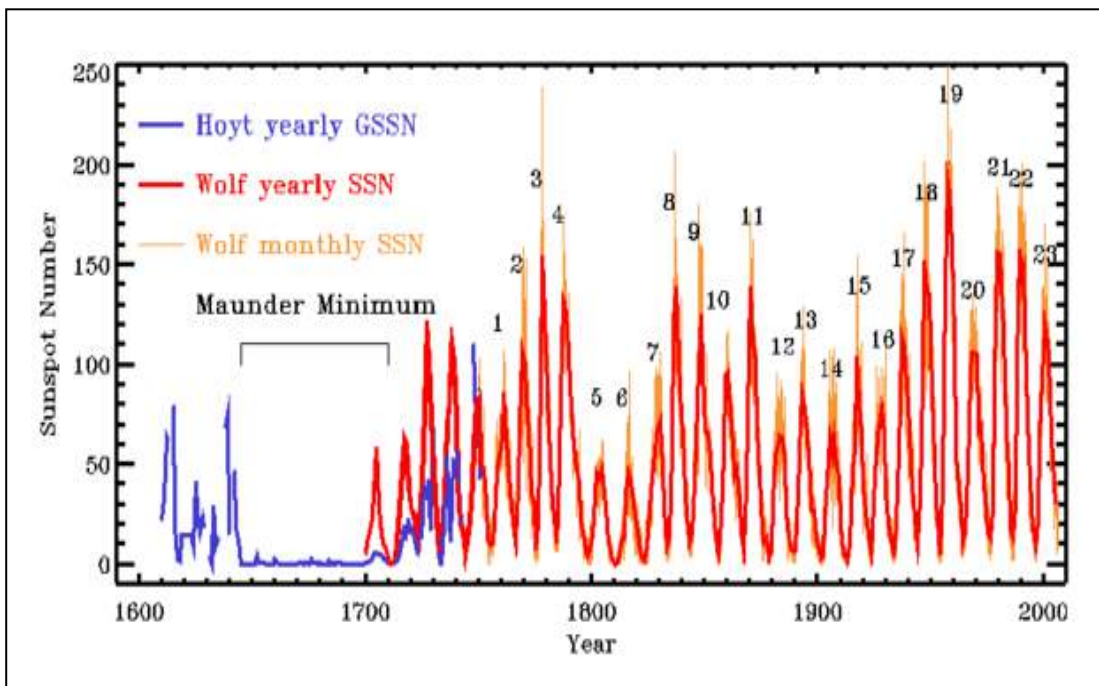


Courtesy: NASA Marshall Space Flight Center

Figure – 1.11: The sunspot butterfly diagram.

The sunspots life time is relatively short from a days to weeks and start to appear at mid-latitudes (about 30-40⁰) on both hemispheres while the time spends mostly new sunspots appear closer and closer to the equator and given use to famous butterfly diagram shown in Figure 1.11. The cyclic pattern of Solar activity from 1749-2000 was illustrated in Figure 1.12. It is divided in the period of Dalton minimum, End of Little Ice Age and Modern Warm Period that is current Solar cycle 24. The number of sunspots on the Sun waxes and wanes over an 11-year called the **Solar Cycle**. Since sunspots are associated with solar activity (i.e., flares and other rapid releases of energy that can heat localized regions of the atmosphere of the Sun to many millions of degrees Kelvin), the Solar cycle also describes the level of activity and variability of the Sun. The sunspots typically have lifetime of 1 to 100 days but the total number

of sunspots changes with this quasi-regular 11-year cycle. The sunspots are regions of intense magnetic fields and the variation in their number indicates that the variation Sun's magnetic field. During Solar minimum the Sun's field is relatively simple and well ordered and resembles a dipole magnetic field, with the magnetic field coming out of one hemisphere and going in the other. Over the next five to six years, as the Sun approaches Solar maximum, the nice dipole configuration slowly disappears and the Sun becomes magnetically disorganized and highly structured.



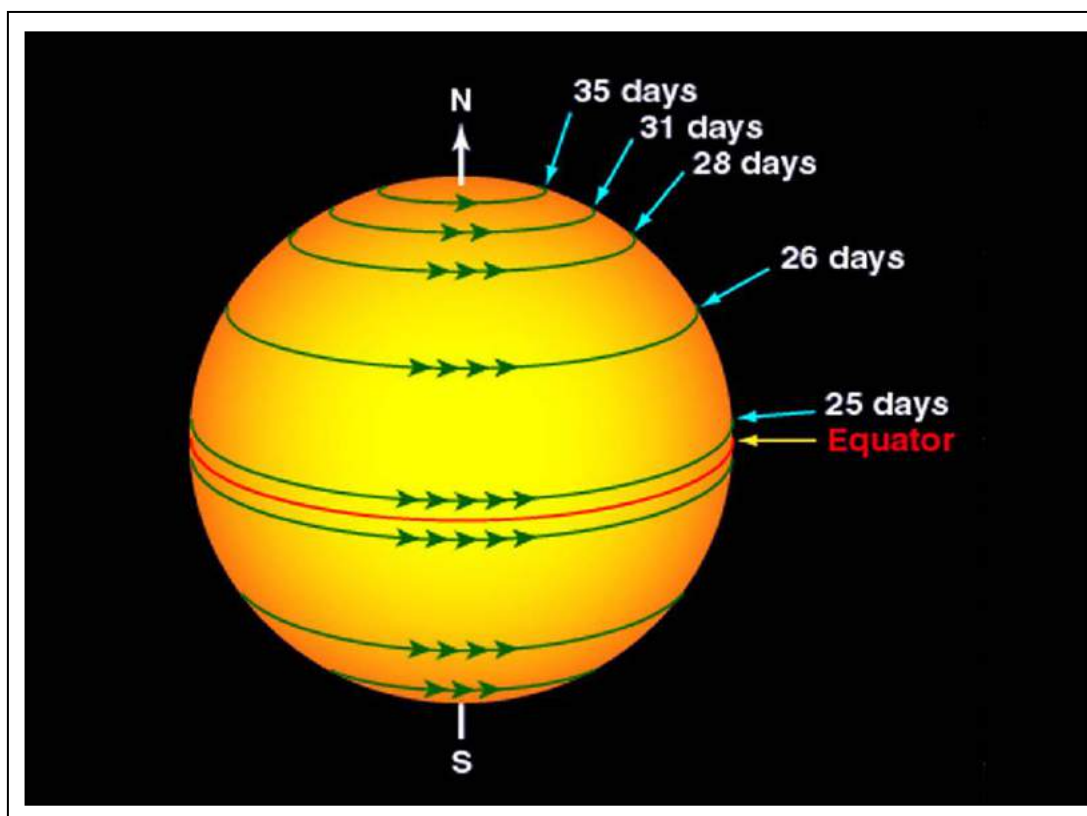
Courtesy: http://www.nasa.gov/mission_pages/sunearth/science/Solar-rotation.html

Figure - 1.12: The Long term Sunspot number variations form 1600 to 2000

Solar maximum, over the next five to six years the magnetic field again becomes more organized and more dipolar. In this transition the tilt of the weak dipole field can be very large with respect to the spin axis of the Sun, but as solar minimum approaches, the dipole axis orientation becomes more and more aligned with the spin axis. When the dipole field is reformed, it has the opposite polarity to the previous one. This change in polarity is what defines the 22-year magnetic cycle of the Sun, sometimes called the double Solar cycle or the Hale cycle.

The polarity of sunspot pairs also follows this cycle. For the first 11 years of the magnetic cycle, the leading spots of a particular hemisphere always have the same polarity, which is opposite to the polarity of the leading spot in the other hemisphere. The sunspot polarities then reverse for the next 11 years. Since the amount of solar activity follows this sunspot or Solar cycle, one would expect that the number of Solar disturbances that impact Earth would also follow this cycle.

1.5 Variation of Solar Rotation with Latitudes



Courtesy: http://www.nasa.gov/mission_pages/sunearth/science/Solar-rotation.html

Figure - 1.13: Rotational rate of the Sun at different latitudes

The Solar rotation was discovered instantly after the invention of telescope in about 1610. Carrington established the physically unique way to define the longitude on the differentially rotating surface of Sun. Therefore, Carrington proposed a notation and divided time into intervals of 27.27 days. First rotation was defined on November 9, 1853. Carrington rotations are related to the motion of the Earth around the Sun (i.e. the “same place” at the Solar equator is toward the Earth after one Carrington rotation). The Sun is not

a solid object, but it is a ball of gas and plasma consequently, it does not rotate at the same rate as the other solid like Earth shown in Figure 1.13. The regions near the equator of Sun rotate with the period of 25 days. The rotation rate of Sun decreases with increasing latitude, therefore the rate of rotation is slowest near the poles. At its poles the Sun rotates with the period of 36 days. The interior of the Sun does not spin the same way as does its surface. The boundary between the inner parts of the Sun that spin together as a whole and the outer parts that spin at different rates is called the "tachocline".

The behavior of the Sun's magnetic field is strongly influenced by the combination of convective currents and differential rotation of the outer layers, convective current bring the charged plasma from deep within the Sun to the surface of Sun. Differential rotation is apparently the main driver of the 11-year sunspot cycle and the associated 22 - year Solar cycle. The notion of differential rotation and convective motion drive these cycles was first put forth in 1961 by the American astronomer Horace Babcock, and is now known as the Babcock Model.

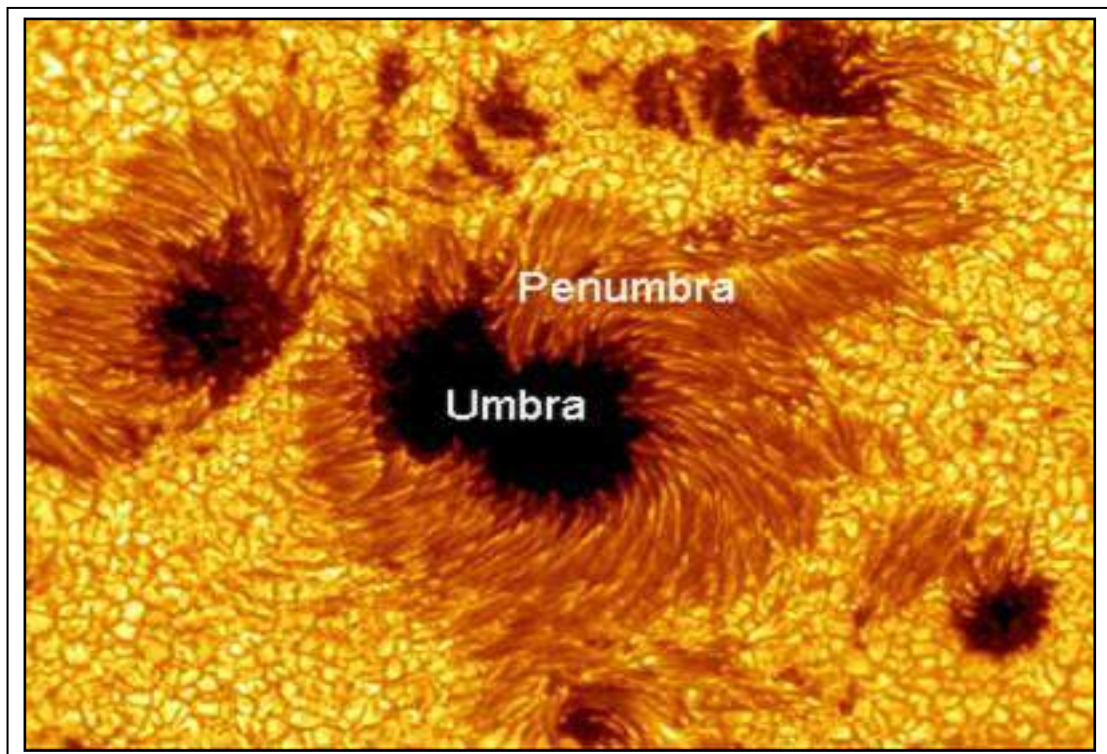
1.6 Solar activity and its parameters

1.6.1 Sunspot Regions

Hale in 1908 was the first who found that the magnetic field of the Sun is very complicated both in space and time. On the surface of Sun spots are darker because they have lower temperature than their surroundings (Kirchhoff's emission law). Sunspots are regions of decreased brightness in the photosphere, or surface layer of Sun, associated with strong magnetic fields. They are thought to be manifestations of an interior magnetic dynamo and are associated with activity in the atmosphere such as flaring and coronal mass ejections. Sunspot corresponds to an intense magnetic flux tube emerging from the convection zone of photosphere. Parker in 1955 explained the magnetic field of sunspot emerging from one spot and return to another because the sunspots usually appear in larger groups or in pairs. The sunspots and the magnetic field are closely related to each other. The strong magnetic field of the sunspots is due to the low temperature and the total pressure as well as

magnetic energy density ought to be in balance. The maximum diameter of biggest sunspot have about 20 000 km. The center of the spot is called **umbra** (its temperature is about 4100 deg K and magnetic field about 0.3 T) and surrounding the spot there may be **penumbra** it consists of dark and bright filaments as shown in Figure 1.14.

Sunspot numbers are used to estimate the Sun's contribution to climate change (Lean and Rind, 2008) and to the modulation of galactic cosmic rays and the radioisotopes they produce in Earth's atmosphere (Usoskin, 2013). About 2,800 years ago, Chinese astronomers made the first recorded observation of sunspots (Clark and Stephenson, 1978).



Courtesy: http://www.nasa.gov/mission_pages/sunearth/science/Solar-rotation.html

Figure - 1.14: Image of a sunspot and Solar granulation obtained from Hinode spacecraft.

The first regular daily (when weather permitted) observations of sunspots began in 1749 at the Zurich Observatory in Switzerland. Using data from Zurich, Samuel Heinrich Schwabe (1789–1875) recognized the occurrence of 11-year Solar cycle in about 1844. He discovered the 11-year sunspot cycle. Swiss astronomer Johann Rudolf Wolf later characterized the 11-year period for

the Solar cycle and developed a formula for quantifying sunspot activity, the Wolf number, which is still in use today (Hathaway, 2010) the cycle is not exactly 11 years but has varied from 9 to 14 years. In mid-nineteenth century, it had been clearly demonstrated that sunspots exist on the Sun and they have an 11-year cycle during which their number waxes and wanes.

The relative sunspot numbers R is a measure of solar activity on the entire disk of the Sun. The relevance of the relative sunspot numbers lies particularly in longest time series of solar activity indices available. Thus, relative sunspot numbers provide the foundation of a continuous data set for research on the solar cycle and its long-term variations. Analytically relative sunspot number R is defined as

$$R = K (10g + f) \quad \dots \dots \dots (1.14)$$

Where, g is the number of observed sunspot groups, f the number of spots and K is an observatory related correction factor.

The Wolf number was introduced in 1848 by Rudolph Wolf, who was the first to compile daily Sunspot Numbers. The concept of correction factor K is introduced by Wolf's successors in 1882 at the Zurich Observatory to convert the actual daily measurements to the scale originated by Wolf (Waldmeier 1961). This compilation of the so-called Zurich relative sunspot numbers is one of the most commonly used databases of Solar activity (Hoyt and Schatten 1998a, b). Beginning with 1981, the Zurich relative sunspot program was replaced by the Sunspot Index Data Center (SIDC) in Brussels, which is the World Data Center for Sunspot Indices (Rishbeth 1991; Ruttenberg and Rishbeth 1994). In principle, sunspot areas are a more direct physical parameter, being closely related to the magnetic field. However, the reliable measurement of sunspot areas is not an easy task, and the results derived by different techniques and different observatories may differ by an order of magnitude (Pettauer and Brandt, 1997). This poses in particular problems for mid- and long-term investigations of solar activity. Sunspot areas are thought to be more physical measures of solar activity. Sunspot areas were given in units of millionths of a solar hemisphere (μHem).

1.6.2 Solar radio flux (F10.7 cm)

The 10.7 cm Solar Radio Flux is the disc-integrated emission from the Sun at the radio wavelength of 10.7 cm (2800 MHz) (see Tapping and Charrois, 1994). Measurements of this flux have been taken daily by the Canadian Solar Radio Monitoring Programme since 1946. Several measurements are taken each day and care is taken to avoid reporting values influenced by flaring activity. Observations were made in the Ottawa area from 1946 to 1990. In 1990, a new flux monitor was installed at Penticton, British Columbia and run in parallel with the Ottawa monitor for six months before moving the Ottawa monitor itself to Penticton as a back-up. The F10.7 Solar radio flux, proposed by Covington from 1947 (Tapping et al., 2003) has become a standard measure of solar activity. It represents the microwave flux density at 10.7 cm wavelength, which corresponds to the electron Larmor frequency for $|B| = 103$ G. Shortly after its introduction, routine observations in Japan began at a set of four fixed frequencies (1.0, 2.0, 3.75, and 9.4 GHz), straddling the F10.7 frequency (2.8 GHz) and encompassing the gyroresonance signature in the Solar microwave spectrum. Tanaka et al. (1973) used these and other data to establish a uniform absolute photometric standard for the microwave range.

Since 1947, the measurements of F10.7 emission from the whole Solar disc at 2800 MHz (10.7cm wavelength) have been made by the National Research Council of Canada (NRCC). Until May 31, 1991 the observations were made at the Algonquin Radio Observatory, near Ottawa. Over 1990-1991 the Solar radio flux F10.7 is measured at the Dominion Radio Astrophysical observatory in Penticton, British Columbia by the Solar Radio Monitoring Programme and available online at <http://www.ngdc.noaa.gov/stp/space-weather/>.

1.6.3 Solar Wind Plasma

The Sun's gives off enormous gravity continuously evaporating into interplanetary space: the Solar Wind. As highly magnetized plasma it dominates a huge volume around the Sun which is called the heliosphere. The existence of the Solar wind was theoretically modeled by E Parker in 1958 and

experimentally verified in 1962. It has been observed throughout wide parts of the heliosphere, as close as 0.29 AU and as far as 70 AU from the Sun, mainly in the ecliptic plane, but also both solar poles. The Solar wind as we see it from the Earth's orbit is characterized by an enormous variability in all its basic properties. The Solar wind proves one key link between the solar atmosphere and the Earth. The Solar wind varies in density, velocity, temperature and magnetic field properties with the Solar cycle, heliographic latitude, heliocentric distance and rotational period. It also varies in response to shocks, waves, and turbulences that perturb the interplanetary flow.

The Solar wind mainly consists of two components: slow Solar wind (speed ~ 400 km/s), which originates from areas of closed magnetic fields on the Sun, and fast Solar wind (speed $\sim 600 - 800$ km/s), which originates from areas of open magnetic fields on the Sun, co-called coronal holes. Predominant location of coronal holes varies with the Solar cycle: during Solar minimum, coronal holes (of opposite polarity) are concentrated at the poles, whereas during the Solar maximum, numerous coronal holes appear at low latitudes, near the Solar equator. Characteristics of different Solar wind types at solar activity minimum are:

- The fast Solar wind emerges from magnetically open coronal holes which are representative of the inactive Sun (*i.e.* the quite Sun). Consistently the 'quite' type Solar wind is found in high-speed streams. Although the major coronal holes usually cover the polar caps at latitudes beyond $40^{\circ} - 60^{\circ}$, the Solar wind emerging there over-expands significantly and fills up all heliosphere except for the 40° wide streamer belts close to the heliomagnetic equator.
- The slow Solar wind of the minimum type originates from above the more active regions on the Sun. It is constrained to the warped streamer belt and comprises the large-scale heliospheric current sheet. The low helium content in this type of Solar wind indicates a larger release height.

- Plasma clouds released in huge eruptions at the Sun can often be discerned by the unusually high helium percentages (~30%) and other signatures.

1.6.4 Interplanetary Magnetic Field (IMF)

The IMF is a vector quantity with three directional components (*i.e.* B_x , B_y and B_z) are oriented parallel to the ecliptic and B_z is perpendicular to the ecliptic. It is created by waves or other disturbances of the Solar wind. When the IMF and geomagnetic field lines are oriented anti parallel to each other, they can reconnect, resulting in the transfer of energy, mass and momentum from the Solar wind to the magnetosphere. The strongest coupling with the most dramatic magnetospheric effects occurs when the B_z component is oriented southward. The IMF is a part of Sun's magnetic field that is carried into interplanetary space by the Solar wind, because its field lines are frozen-in to the Solar wind's plasma. Due to Sun's rotation solar wind travels outwards in a spiral pattern (Parker Spirals). The IMF field is a weak field varying in strength near the Earth from 1 to 37 nT with an average value of $\sim 5 nT$.

1.6.5 Geomagnetic Storms

Storms and sub storms are major constituents of geomagnetic activity and play a crucial role in efforts to define space weather (Kamide *et al.*, 1998a; Freeman, 2001; Angelopoulos, 2008). Intense geomagnetic storms occurring at extreme solar events can affect modern life by disturbing technological systems (Baker, 2000; Daglis *et al.*, 2001). The strength of geomagnetic storms is mainly reflected by the Dst index (<http://swdcwww.kugi.kyoto-u.ac.jp/>). The internal mechanism of geomagnetic fluctuations accompanying the development of geomagnetic storms and substorms is a complex nonlinear system. Some previous works have demonstrated the statistical self-affinity properties observed in the geomagnetic times series (Chang, 1999; Sitnov *et al.*, 2001; Uritsky *et al.*, 2001, Kovacs *et al.*, 2001; Lui, 2002; Wanliss, 2005a; Balasis *et al.*, 2006; Wanliss and Dobias, 2007). It has been found that variations of external geomagnetic field exhibit a power law spectrum with a spectral exponent varying over different lengths of time. This behaviour

indicates that the external geomagnetic field is a multiscale process (Uritsky *et al.*, 2001; Balasis *et al.*, 2006). Considering current efforts in understanding the magnetic geo-environment and improving space weather forecasting, it is evident that the use of classical methods, such as the Fourier Transform for analysing the magnetic signal, or the geomagnetic index Dst, cannot yield any information on the temporal evolution of geomagnetic storm activity (Balasis *et al.*, 2006).

Geomagnetic storms are large disturbances in the geo-magnetosphere often persisting for several days or more. It occurs when interplanetary magnetic field turns southward remains so for a prolonged period of time (Russel *et al.*, 1974; Rostoker and Falthammar, 1967; Tsurutani *et al.*, 1992). Reconnection between the southward directed (relative to the ecliptic plane) component of the Solar wind carried magnetic field (B), B_z and the northward directed geomagnetic field can occur at the dayside magnetopause, resulting in the transfer of significant amounts of energy from the Solar wind into the Earth's magnetosphere. During a typical storm, an enhanced ring current is created and the auroral electro jets in both hemispheres move dramatically equator ward. This is evidenced by a decrease in the geomagnetic field at near-equatorial magnetic stations and a large decrease in the Dst index that is currently compiled from the records from four selected stations (Sugiura, 1991).

During geomagnetic storms, the magnetic field measured at the Earth's surface is perturbed by strong electric currents flowing within both the magnetosphere and ionosphere. The aurora brightens and extends to low magnetic latitudes and intense fluxes energetic charge particles are generated within the magnetosphere. The variation of earth's magnetic field is usually expressed through magnetograms of declination (D), vertical intensity (Z) and horizontal intensity (H). The disturbance storm time index (Dst) has been introduced by the Sugiura (1964).

A geomagnetic storm occurs if the following criteria are satisfied: (1) a significant disturbance occurs which means that the minimum Dst is less than -30 nT ; (2) a disturbance has obvious onset, main and recovery phase. The

isolated geomagnetic storms have important research values in all geomagnetic storms. The criterion using Dst_{min} given by Loewe has been adopted (Loewe and Pross, 1997), as listed in Table 1.1.

Table - 1.1: Classification of geomagnetic storm intensity

Storm class	Weak	Moderate	Strong	Severe	Great
<i>Dst_{min} range/nT</i>	-50~-30	-100~-50	-200~-100	-350~-200	≤-350

1.7 Space Plasmas and Magnetohydrodynamics (MHD)

In MHD, the space plasmas are considered as electrically conducting fluid. It has successfully been applied to the contemporary field of heliosphere space plasma research to evaluate the “macroscopic picture of various phenomena related with solar plasma by the use of conductivity fluid equation and numerical modeling and simulation. Short description of basic concept relevant to this work is given in next sub-sections.

1.7.1 The Solar Wind as a Fluid

In a first order of approximation solar wind plasma is to be considered as fully ionized plasma consisting of half protons and half electrons. Within the plasma charged particles are shield form one other according to length scale. In the presence of other ions within the plasma potential around the particle is mathematically given as

$$\phi_v = \frac{qe^{\frac{-r}{\lambda_D}}}{4\pi r} \dots \dots \dots (1.15)$$

Where q is the charge on the test particles and λ_D is the Debye length given by

$$\lambda_D = \sqrt{\frac{k_B T}{N_e q^2}} \dots \dots \dots (1.16)$$

If the value of $\frac{-r}{\lambda_D}$ is large the potential is small and test particles does not affect the surrounding ions. For solar wind the value of λ_D is approximately 10 meters in length at 1 AU. For effective shielding, the total number of particle within the Debye sphere must be very large. The total number of particles N_D , must be analytically given by

$$N_D = \frac{4}{3} \pi N_e \lambda_D^3 \dots \dots \dots (1.17)$$

Within the solar wind value of N_D approximately equal to 10^{10} . Hence the solar wind can be considered as ideal plasma and it possible to describe it using the ideal gas law. Due to overlapping of Debye sphere of many particles, the plasma exhibits fluid behaviour and can be modelled using magnetohydro dynamics (MHD) (de Pater and Lissauer, 2001) and the solar wind can be considered collisionless.

1.7.2 The Frozen-in Flux Theorem

It states that the magnetic field within the moving plasma like space plasma will move with the velocity of plasma. Even when the surface moves with the plasma, the flux remains the same. This is equivalent to saying that the flux is frozen within the plasma or that the field lines move with the plasma. This theorem is proven in most plasma physics textbooks. We will follow closely the concise but clear discussion given by Schmidt (1979). Now we first consider the induction equation displayed below

$$\frac{\delta \vec{B}}{\delta t} = \nabla \times (\vec{v} \times \vec{B}) + \frac{\nabla^2 \vec{B}}{\mu_0 \sigma} \dots \dots \dots (1.18)$$

Here μ_0 is the permeability of free space and σ is the plasma conductivity. The first term in the right side of the equation (1.18) shows the convective term and the second term shows the diffusive term. The ratio of these term are taken as magnetic Reynolds number R_m , and given as

$$R_m \approx \mu_0 \sigma v_c L_c \dots \dots \dots (1.19)$$

Where v_c and L_c are characteristics speed and scale length respectively.

If $R_m \gg 1$, the convection term dominates and the plasma is said to be in its convective limit. With this limit the induction equation (1.18) as be rewritten as

$$\frac{\delta \vec{B}}{\delta t} = \nabla \times (\vec{v} \times \vec{B}) \dots \dots \dots (1.20)$$

The differential form of Faradays law for electric field vector \vec{E} is given as

$$\frac{\delta \vec{B}}{\delta t} = -\nabla \times \vec{E} \dots \dots \dots (1.21)$$

Now under the convective limit, we are able to write the electric field vector \vec{E} as

$$\vec{E} = -v \times \vec{B} \dots \dots \dots (1.22)$$

And vector \vec{v} as

$$\vec{v} = \frac{\vec{E} \times \vec{B}}{B^2} \dots \dots \dots (1.23)$$

To derive an frozen-in flux theorem, let us consider a surface in space as shown in Figure 1.15 which is threaded by a magnetic flux, F , in a plasma of $R_m \gg 1$ (i.e. for the solar wind).

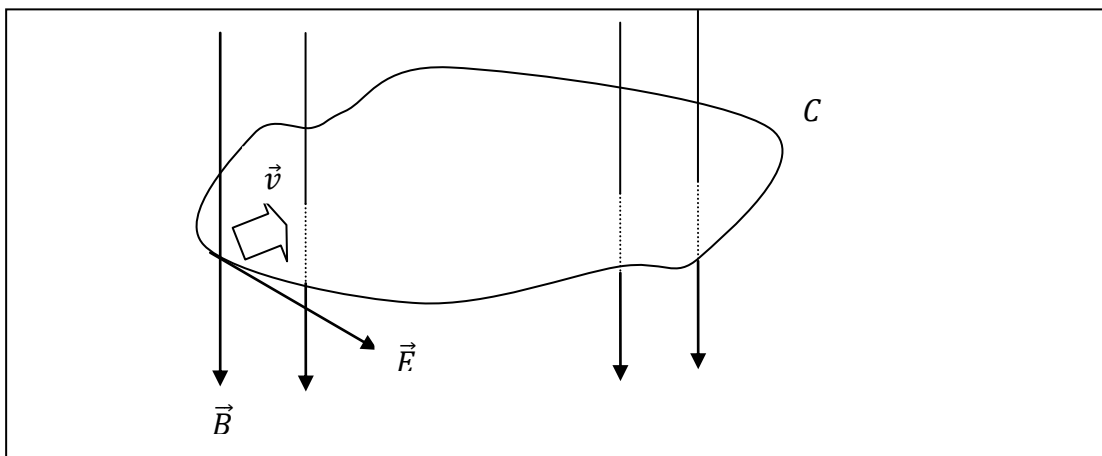


Figure - 1.15: Surface C in space threaded by a magnetic field \vec{B} and perpendicular electric field \vec{E}

Now we start with the integral form of Faradays law

$$\frac{\delta F}{\delta t} = - \oint_c \vec{E} \cdot d\vec{l} = \oint_c [\vec{V} \times \vec{B}] \cdot d\vec{l} \quad \dots \dots \dots (1.24)$$

Now, consider a small segment of length dl of the surface in Cartesian coordinate, where x is aligned with the surface, y is towards the center of the surface and z is normal to the plane of the surface, as depicted in Figure 1.16.

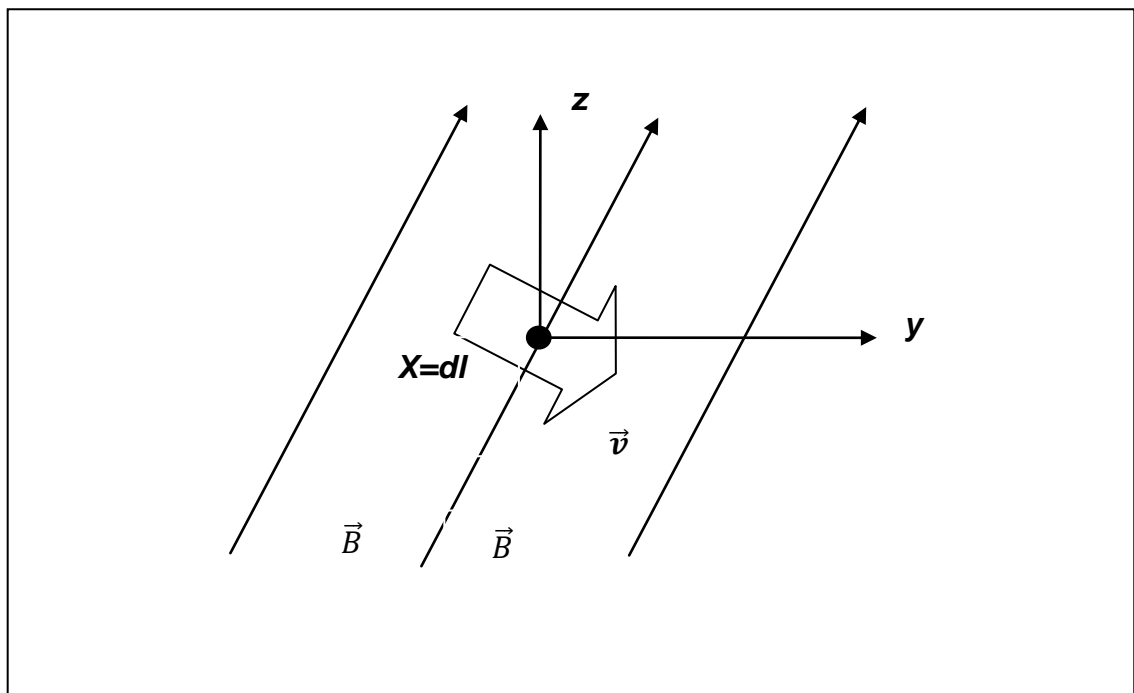


Figure - 1.16: Diagram of a segment of surface, C

If the magnetic field moves with the velocity \vec{v} , then the rate of magnetic flux transfer across the length dl is given by the equation

$$\frac{dF}{dt} = vBdl = [\vec{v} \times \vec{B}] \cdot d\vec{l} \quad \dots \dots \dots (1.25)$$

Now taking the integration across whole surface equation (1.25) can be rewritten as

$$\frac{dF}{dt} = - \oint_c \frac{dF}{dt} = \oint_c [\vec{v} \times \vec{B}] \cdot d\vec{l} \quad \dots \dots \dots (1.26)$$

As the equation (1.24) and (1.26) is in the same form, then the assumption that the magnetic field must move with the plasma velocity must be true for $R_m \gg 1$.

1.7.3 Magneto-hydro-dynamic (MHD) waves

Magnetohydrodynamic waves are found in a wide variety of space plasma. These MHD waves are produced by restoring magnetic and thermal forces in the solar wind. Alfvén waves are transverse waves which produce changes in the local magnetic field perpendicular to the magnetic field lines, but do not compress the solar wind plasma. The detection of MHD waves in space plasma is habitually indirect, by matching the corresponding properties like propagation speed or variation in pressure and also with theoretically deduced properties while the magnetosphere and solar wind offer direct in situ measurements. A difficulty in the detection of MHD waves in space plasmas has been the comprehension that generally such plasmas are strongly inhomogeneous, structured by magnetism, plasma density and temperature variations, or by plasma flows. This strong inhomogeneity brings about complications in the description of magnetohydrodynamic wave phenomena, with magnetic flux tubes and plasma flow tubes being of special interest. In the solar atmosphere, sunspots, solar photospheric magnetic flux tubes, coronal loops and polar plumes are examples of flux tube structure, and oscillatory phenomena have been detected in all of them. Oscillations have also been detected in solar prominences and generated by solar flares.

1.7.4 Magnetic Reconnection

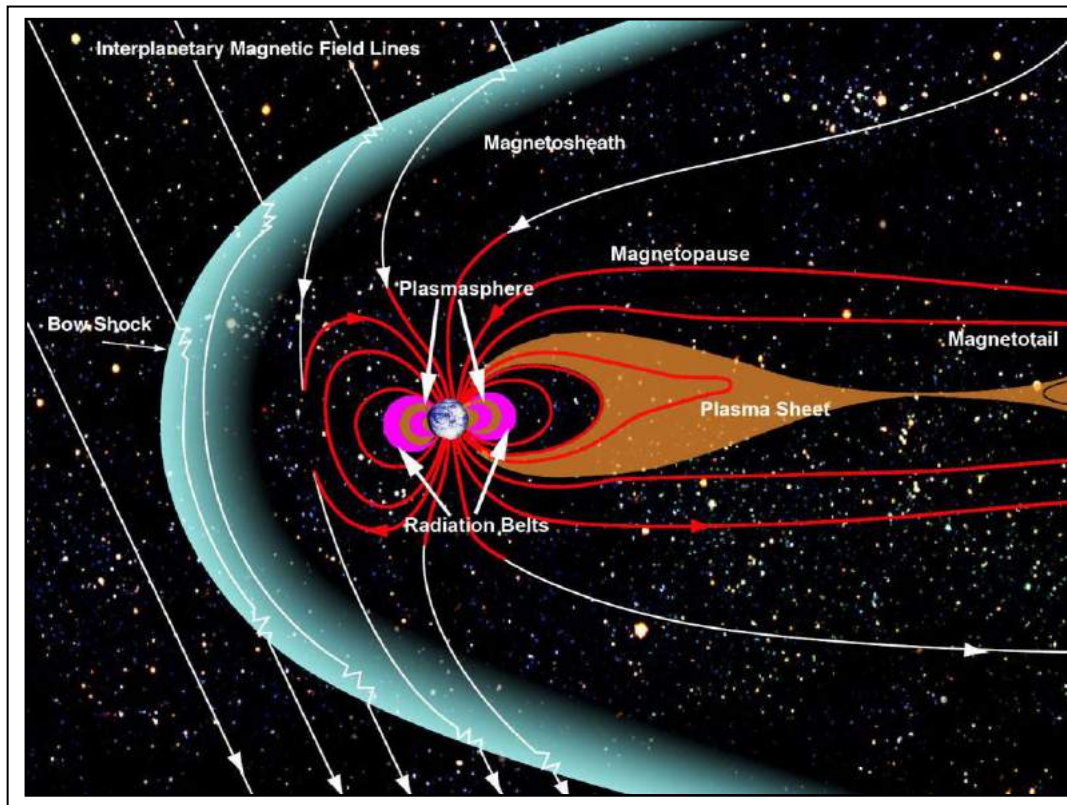
Magnetic reconnection is a fundamental dynamical process that is ubiquitous in astrophysical plasmas. Reconnection is universally established to be a key component in many astrophysical phenomena. Historically, the concepts of reconnection are based on the original two-dimensional (2D), steady-state models which employed a magnetohydrodynamic (MHD) description of the plasma. On typical dynamical time scales adequately hot spatially extended plasma behaves something like as an ideal fluid in the sense that resistive effects are ignorable. As a result, the magnetic field is 'frozen' to the plasma motion and magnetic topology is conserved. This sets strong

limitations on the accessible dynamical states. Large-scale magnetic flux tubes, which are strongly stretched out by the plasma pressure, as for instance observed in planetary magnetospheres or in stellar coronas, would be unable to release large amounts of their energy and return to a correspondingly relaxed state, as long as the plasma is trapped in the flux tubes. Beginning in the late 1950s, several authors, including P A Sweet, E N Parker, H E Petschek and J W Dungey, introduced magnetic reconnection as the central process allowing for efficient magnetic to kinetic energy conversion in solar flares and for interaction between the magnetized interplanetary medium and the magnetosphere of earth.

1.8 Solar Wind-Magnetosphere Coupling

In our solar system many planets have their own magnetic fields, in form of magnetic “bubbles” within the Heliospheric Magnetic Field (HMF) and protect the planetary atmospheres and surfaces from the solar wind and energetic particles. Inside this magnetic bubble the plasma is mostly frozen-in to the magnetic field and because the magnetic pressure dominates, the bubbles are called “magnetospheres”. According to frozen-in theorem it is impossible to enter the solar wind in to the magnetosphere. Due to variation in field inside and outside the magnetosphere there is a sheet between two which is known as “magnetopause”. The width of this sheet is so small which allow the breakdowns in the frozen-in theorem because the field can diffuse through the plasma. Particular, in region where the fields are oppositely directed magnetic reconnection can occur which reconfigures the fields to produce open magnetospheric field lines that thread the magnetopause and connect the magnetospheric field to the interplanetary field. Some solar wind plasma can flow along these field lines into the magnetosphere. The shape of each magnetosphere is not an ideal magnetic dipole but it depends on variation in the solar wind speed and pressure. Generally the shape of magnetospheres is extended tear-drop shapes with a compressed dayside and an extended tail on the nightside. Local enhancements in the solar wind speed and pressure cause the planetary magnetospheres to become increasingly distorted with a more compressed dayside and a more compacted tail (Sibeck et al., 1991). A

schematic of Earth's magnetosphere is given in Figure 1.17 from Pulkkinen (2007), which displays the key regions of the magnetosphere.



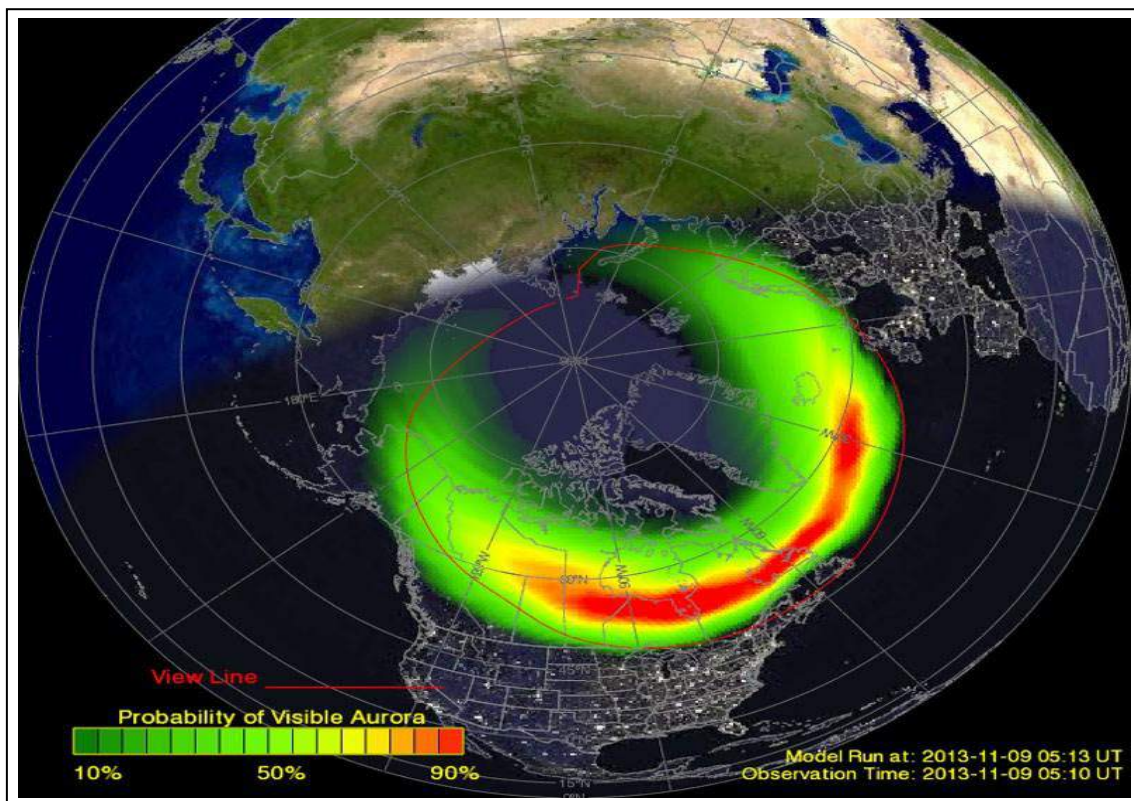
Courtesy: *Space Weather Prediction Center homage*

Figure - 1.17: Model of the magnetosphere.

The component of B_z in the HMF (if HMF is northward directed with respect to the Earth's magnetic dipole) has a great impact on the transport of plasma through the magnetosphere and impacts plasma populations, currents and phenomena such as the aurora borealis at Earth (Milan et al. 2000). On the other hand if B_z is negative (*i.e.* the HMF is southward-directed), then magnetic reconnection can occur at the dayside magnetopause, given that the magnetospheric field here is positive (Tsurutani and Gonzales, 1997). It allows the solar wind plasma to travel along the HMF lines to access magnetospheric field lines by flowing along the open field lines across the magnetopause.

On the dayside, the field aligned inflow and convection join to permit the plasma entering along open field lines to reach right down into the upper atmosphere and can generate a characteristic red aurora there. Due to magnetic reconnection the dayside magnetosphere is wrinkled as field lines are

opened and dragged into tail. These tail comprises field lines which pointing away from the Earth in the southern hemisphere and towards it in the north, between these two field orientation a current sheet must exist which is called “cross-tail current” sheet. In this region open field lines connected with the north and south polar caps of Earth assemble and reconnect to become closed again. The annual average of variable orientation of the IMF gives a constant factor and the mean B_z is proportional to the mean HMF field strength (Lockwood, 2013). The strength of the convection circulation in the magnetosphere and all associated currents in Earth’s ionosphere, depend on the IMF B_z component. Negative B_z and enhanced strength of HMF generate additional open flux in the magnetosphere and expand the polar caps. The reconnection of magnetic field lines generate green and ultraviolet aurora and collapse down towards the Earth. They bring auroral particles down into the Earth’s upper atmosphere and forming a ring around the polar cap called “auroral oval” (see Figure 1.18).



Courtesy: NOAA

Figure – 1.18: A model of the auroral oval as seen from the space over on top of the visible image of earth

The solar wind dynamic pressure compresses the tail field, so the peak moves towards the Earth. So open flux increases in the tail and auroral expands towards the equator. The pole ward edge of the auroral oval is the open-closed field line boundary. However, there is often a dark region between the two where aurora is sub-visual because in response to adding open flux the oval moves further equator-ward than the polar cap boundary. Usually aurora is expanding to fill the dark region between it and becomes more structured and dynamic.

1.9 Methods of Analysis

A great variety of non-linear techniques based on wavelet and cross-recurrence plots (CRPs) have been used in this thesis to analyze various Solar activity index such as sunspot number and area, Solar radio flux (F10.7cm flux), Solar wind plasma parameters and interplanetary magnetic field (IMF) .

1.9.1 Wavelet Transform

Wavelet analysis performs the estimation of the spectral characteristics of a time series as a function of time, revealing how the different periodic components of the time series change over time. It is appropriate to analyze irregular distributed events and time series that contain non-stationary power at many different frequencies. One major advantage of the wavelet transform is the ability to perform natural local analysis of a time series the wavelet stretches into a long function to measure the low frequency movements, and it compresses into a short function to measure the high frequency movements. The discrete wavelet transform (DWT) rely in many works by (Ramsey and Lampart, 1998a and 1998b and Ramsey, 1999 and 2002; Gencay, et al., 2001a; 2005, Connor and Rossiter 2005, Gallegati and Gallegati, 2007).

Several applied fields are making use of wavelets such as astronomy, acoustics, data compression, nuclear engineering, sub-band coding, signal and image processing, neurophysiology, music, magnetic resonance imaging, speech discrimination, optics, fractals, radar, human vision, pure mathematics, and geophysics such as tropical convection, the El Nino-Southern Oscillation,

atmospheric cold fronts, temperature variability, the dispersion of ocean waves, wave growth and breaking, structures in turbulent flows, and stream flow characterization (Farge, 1992; Graps, 1995; Torrence and Compo, 1998).

1.9.1.1 Discrete Wavelet Transform (DWT)

The Discrete Wavelet Transform (DWT) is usually based on the dyadic calculation of position and scale of a signal (Chou, 2007). The DWT is excellent for denoising the signals (Fugal, 2009). The DWT of a vector is the outcome of a linear transformation resulting in a new vector that has equal dimensions to those of the initial vector (Chou, 2011). This transformation is the decomposition process. In this study all the time series (for all the Solar Cycles 20-23 and current Solar Cycle 24) decomposed using the Daubechies and Coifman wavelets. Daubechies wavelet provides compact support (Vonesch et al., 2007), indicating that the wavelets have non-zero basis functions over a finite interval, as well as full scaling and translational orthonormality properties (Popivanov and Miller, 2002; de Artigas et al., 2006). These features are very important for localizing events in the time-dependent signals (Popivanov et al., 2002). DWT decompose the time series into approximation and detail components.

1.9.1.2 Continuous Wavelet Transform (CWT)

The continuous wavelet transform (CWT) maps the original time series, which is a function of just one variable time it transform into a function of two variables time and frequency, providing highly redundant information. The CWT are becoming more widely used by many researchers (Raihan et al., 2005; Jagric et al., 2004; Crowley et al., 2008; Aguiar-Conraria, et al., 2008, Baubeau and Cazelles, 2009; Rua and Nunes, 2009; Rua, 2010 and Aguiar-Conraria and Soares, 2011a and b) provide some examples of useful economic applications of these tools.

1.9.1.3 Cross Wavelet Transform (XWT)

The cross wavelet transform (XWT) is an extension of wavelet transforms to expose their common power and relative phase in time-frequency

space between the two time series (Li et al. 2005). The cross wavelet transform of the two time series X and Y is defined as

$$W^{XY} = W^X W^{Y*}, \quad \dots\dots\dots (1.27)$$

where * denotes complex conjugation, and W^X and W^Y are the continuous wavelet transforms (Grinsted et al. 2004). The complex argument $arg(W^{XY})$ can be interpreted as a local relative phase between X and Y in time-frequency space. Cross-wavelet power reveals areas with high common power.

1.9.1.4 Wavelet Coherence Transform (WTC)

The wavelet coherence (WTC) is an estimator of the confidence level for detection of a time-space region of high common power and consistent phase relationship calculated by the cross wavelet transform between two time series. The measure of wavelet coherence is defined between two continuous wavelet transforms and it may indicate coherence with high confidence level even though the common power is low; it closely resembles a localized correlation coefficient in time – frequency space and varies between 0 and 1.

1.9.2 Cross Recurrence Plots (CRPs)

The CRPs is the extension of recurrence plots able to investigate the time dependent behavior of two processes which are both recorded in a single time series (Zbilut et al., 1998; Marwan and Kurths, 2002; Marwan et al., 2002a). The fundamental approach of this method is to compare the phase space trajectories of two processes in the same phase space. The detail information of this method was given in Chapter- 4.

1.9.3 Multifractal

The process fractal was found by Mandelbrot (1983) to distinguish a rough or fragmented geometric shape that displays a large degree of self similarities within its own fractional dimensions. In recent years, fractal patterns have been extensively studied in diverse fields, ranging from physics to finance. Hurst (Hurst, 1951) introduced the rescaled adjusted range analysis (R&S analysis) for his hydrological study. Peng et al., (1994) overcome this difficulty and proposed the detrended fluctuation analysis (DFA) method in order to

analyses DNA sequence. DFA become a widely used method for the determination of monofractal scaling properties and it can't be applied to describe the multiscale and fractal subsets of the time series. Kantelhardt et al. (Kantelhardt, 2001) advanced the DFA to multifractal detrended fluctuation analysis (MFDFA) for the multifractal characterization of non-stationary time series. The MFDFA applied to various fields of researches including international crude oil markets (Gu, et al., 2010), foreign exchange markets (Norouzzadeh, et al., 2006), stock markets (Yuan, et al., 2009), gold markets (Wang, et al., 2010), and agricultural commodity futures markets (Li, et al., 2011). By researchers generalising DFA and MF-DFA analyses with an emphasis on detrended covariance considered the cross-correlations between two non-stationary time series (Podobnik, et al., 2008; Podobnik, et al., 2009; Zhou, 2008; Li, et al., 2012). For detail discussion of method see the chapter 6.

1.10 Review of Work Done

The Sun is the ultimate source of all space weather on or near the Earth. Space weather process includes variations in interplanetary magnetic field, Coronal Mass Ejections (CMEs) from the Sun and Earth's magnetic field (Tsurutanini et al., 1995; Gapalswamy, 2009). The sunspots and the magnetic field are intimately related to each other. The sunspots are related to the convective motion below the solar surface. The solar wind carries magnetic field from the Sun to the interplanetary space known as the interplanetary magnetic field (IMF). Since the Sun is gaseous body it has differential rotation, meaning the Sun's fastest rotation is at the equator (about 24 - 27 days) and the slowest is at the poles (about 30 - 35 days). Certainly, sunspots and related activities have been analyzed by various methods, including correlation analysis (Temmer et al., 2002; Bogart, 1982), chaos analysis (Veronig et al., 2000; Jevtic et al., 2001) and multifractal analysis (Abramenko, 2005; Movahed et al., 2006; McAteer et al., 2007). Recently, the statistical properties of Sun activity were investigated by chaos theory (Veronig et al., 2000) and multifractal analysis (Abramenko, 2005). The north-south asymmetries and rotational behavior concerning solar activity was investigated by using the wavelet and auto-correlation function (Temmer et al., 2002). In some works determined the

cross-correlation functions between monthly mean sunspot areas and sunspot numbers (Temmer et al., 2002). When temperature, density and magnetic fields are enhanced F10.7 radio flux is used to measure the general solar activity (Bruevich et al., 2012).

The Solar wind plasma parameters are continuously measured by many satellites based techniques. The variations in the solar wind parameters can also lead to better understanding of the nature and properties of the solar wind Plasma, the stability of these structures and the character of plasma instabilities. These variations are generally characterized by multifractality and intermittence phenomena. The multifractal techniques provide an elegant statistical characterization of many complex dynamical variations in Nature and engineering (Gao et al., 2006; 2007). It is conceivable that it may enrich characterization of the sun's magnetic activity and its dynamical modeling (Howe et al., 2000).

There are several mathematical transformations that can be applied to study the astronomical and solar data. Among this Fourier transform is widely used as popular method. Because it has some limitations when higher performance is required, to overcome this limitation Wavelet Transform is applied. However, it has time and frequency localization property decomposing or transforming a one dimensional time series into a diffuse two dimensional time-frequency image, simultaneously. The wavelet analysis always uses a wavelet of the exact shape, only the size scales is up or down with the size of the window. In addition to the amplitude of any periodic signals, it is worth to get information on the phase. The overall works done in this thesis are summarized as following:

- In this thesis, wavelet transform has been applied to analyze the solar wind parameters to characterize the solar wind and the selection of periodic variations that could be the subject of geomagnetic disturbances. Wavelet spectral analysis provides a natural basis to estimate the time - frequency characteristics of the analyzed data. In the wavelet analysis of signals, the time series of solar wind parameters

level variation is mapped into different scales and time instants, using a Morlet wavelet function.

- We have used the wavelet transform techniques such as continuous wavelet transform (CWT), Cross - wavelet transform (XWT) and Wavelet coherence. These techniques were applied on sunspot numbers and area to study the rotational periodicity of Sun. The rotational periodicity of 27 days was found, which corresponds to the Sun's rotation at the equator.
- We performed the Global Wavelet Spectrum (GWS) to study the dominant periods of the solar wind parameters for the current solar cycle 24. These GWS provide an unbiased and consistent estimation of the true power spectrum of the time series, and thus they are a simple and robust way to characterize the time series periodic variations.
- We have shown that phase relationship between F10.7 cm solar radio flux and Sunspot numbers with the associated Coronal index using the non - linear techniques such as XWT, WTC and Cross Recurrence Plots (CRPs). Also calculate the embedding dimension of analyzed data using Cao algorithm (Cao, 1997).
- The sunspots and its cycle remain the best known parameters of solar magnetic activity and thus have been a subject of extensive research. We have studied multifractality of sunspot numbers during the solar cycles 20 - 23 and ascending phase of solar cycle 24. The result of this work provides a general view of the pattern of sunspot number data of different solar cycles along (*i.e.* Studied solar cycles 20 - 24). The Multifractal Detrended Fluctuation Analysis (MF-DFA) method is used to find the multifractal spectrum of solar wind plasma parameters (*i.e.* solar wind plasma speed, density and temperature respectively). It shows less bias and being likely to give a false positive result with respect to the Wavelet transform Modulus Maxima (WTMM). Therefore, MF-DFA is well suited for this work.

1.11 Scope of Future Work

We will continue investigate each of the areas presented in present thesis. Studies presented to have answered one or more questions about variation in Sunspot number and Solar wind plasma during the Solar cycles and Multifractal behavior of Solar wind plasma parameters. Often, more unanswered questions emerge, provoked by the analysis results. In the following sections, the prospects for future work in each area of investigation are described, leading on from the results presented in this thesis.

- The amplitude and spatial configuration of Sun's magnetic field is change with time. Due to formation and decay of strong magnetic fields in the atmosphere of Sun there is a variation in electromagnetic radiation emitted from the Sun, also variation in intensity of plasma flows coming out from the Sun, and the number of sunspots on the surface of Sun. The analysis of variation in number of sunspots on the Sun's surface has a cyclic structure vary in every 11 years. Which affect the environment of Earth in various ways therefore prediction of an extended solar minimum and maximum is extremely important because of the severity of its impact on the near-earth space. Here, we analyze the variation in Sunspot number in various solar cycles using wavelet based techniques. Which provide very reliable information regarding the short term periodicities in Sunspot number and area, also in many Solar wind parameters. Presently, more than half age of 11-years cycle passes, which strongly validate that its solar activity is very weak and it influence the space-weather condition. The continuous long duration and constant low solar activity of present solar cycle during all over the cycle period to till now could provide us a unique opportunity for understanding the solar variation. The availability of solar data from SDO, other various satellites and ground based telescopes around the world will continue to increase in the coming years and advanced methods, such as the ones presented in this thesis, may well become the only way to reliably analyses all of the incoming information and will prove invaluable for the continued understanding of our own Star.

- The most important result achieved in present thesis is the identification of fractal structure and the multifractal properties of solar wind parameters, which is of key significance in studying solar wind turbulence. Hence multifractal analysis of the time series reflects some properties which are not shared by the same analysis on the original time series. There exist three main multifractal spectra, viz. the Hausdroff, large deviation and Legendre spectra. Basically, any of these three spectra provides information as to which singularities occur in the data. This suggests a potentially useful method to explore Solar plasma data. Our Sun is one of such systems, and solar physics can gain much by utilizing these concepts, along with a rich set of developed tools, in further understanding of our closest star seemingly unpredictable behavior.
- Our analysis provides a general view of the pattern of sunspot number of different Solar cycles along with the whole cycles. Balasis *et al.* (2008) found out the emergence of two distinct phases: (i) the phase where the intense magnetic storms cause a higher degree of magnetic field organization, and (ii) the phase which characterizes the normal periods with lower magnetic field coherence. Proper analysis of this feature may help improve the sunspot number prediction.

1.12 Research Publications

- **Kasde, S.K., Sondhiya, D.K., Gwal, A.K.:** Study of Sunspot Time Series Using Wavelet - Based Multifractal Analysis during Solar Cycle 23 and Ascending Phase of Cycle 24, *Physical Science International Journal*, 13 (4), 1 - 12, 2017.
- **Kasde, S.K., Sondhiya, D.K., Gwal, A.K.:** Analysis of Sunspot Time Series During the Ascending Phase of Solar Cycle 24 Using the Wavelet Transform, *American Journal of Modern Physics*, 5, 79-86, 2016.
- **Sondhiya, D.K., Kasde, S.K., Shrivastava, R., Raghuwanshi, M., Gwal, A.K.:** Fine Structure Analysis of Very Low Frequency (VLF) Signal

Transients using Wavelet Transform Modulus Maxima (WTMM) Technique, *International Journal of Pure and Applied Physics*. ISSN 0973-1776, 11 (1), 19 - 27, 2015.

- Sonakia, A., Sondhiya, D.K., **Kasde, S.K.**, Jalori, H., Gwal, A.K.: Detection of Seismo-ionospheric Anomalies using Wavelet based techniques, *IOSR Journal of Applied Physics (IOSR-JAP)*, 6 (3), 74 - 91, 2014.

Analysis of Sunspot Time Series during the Ascending Phase of Solar Cycle 24 using the Wavelet Transform

2.1 Introduction

The important features of the sun's outer regions are the existence of a reasonably strong magnetic field. To the lowest order of approximation, the Sun's magnetic field is dipolar in character and is axis symmetric. All Solar activities are driven by the Sun's magnetic fields. Solar activities are produced due to the emergence of magnetic flux from the photosphere forming active regions which including sunspots. Schwabe (1844) found that 11 year cycle is the most characteristic feature of solar activity. He also described an anomalous variations and fluctuations in the cycle duration as well as in the individual shape and maximum intensity. Hale (1919) discovered that in every 11 years duration the polarity of the Sun's magnetic field reverses. Rotational periodicity is the most noticeable periodicity with the period of 28 days which is associated with rotation of Sun. All quasi-periodic oscillations having periods between the rotational periodicity and 11 year periodicity are usually known as middle-range or intermediate-term periodicities.

The study of all these periodicities except the rotational one is expected to provide useful information about Solar interior dynamics and mechanisms of generation of the Solar magnetic field and its emergence on the Solar surface (Ichimoto et al. 1985; Sturrock and Bai 1992). In addition, all ongoing periodicities can be useful for making predictions of Solar activity (Bai 1992). This feature has been explained for the first time by the dynamo model introduced by Babcock (1961).

Recent helioseismic probing of the Solar interior has shown that the rotation rate of the Sun near the base of its convective zone changes with a period of roughly 1.3 years (Howe et al. 2000). The differential rotation of the Sun is one of the main ingredients of the dynamo located at the base of the convection zone, which generates the magnetic field that is observed at the solar surface. We expect that any fluctuation in the dynamo process will manifest itself most clearly in relatively freshly emerged flux, i.e. in young active regions.

Sunspots, due to their relatively short lifetimes, are good tracers of young active regions. Here we inspect sunspot areas (SSA) and sunspot numbers (SSN) as representatives of the freshly emerged Solar surface magnetic field for a periodicity around 27 days. The long-term evolution of Solar activity has been studied from different perspectives using various short and long-term Solar activity indicators. Mid-term quasi-periodicities in various diagnostics of Solar flare activities and sunspot numbers or areas during few years around the Solar maximum phase have been extensively searched and monitored at many electromagnetic wavelengths (Rieger et al., 1984; Kiplinger et al., 1984; Dennis, 1985; Ichimoto et al., 1985; Delache et al., 1985; Bogart and Bai, 1985; Bai and Sturrock 1987; Oliver et al., 1988; Ribes et al., 1987; Lean and Brueckner, 1989; Ozguc and Atac, 1989; Lean 1990; Carbonell and Ballester, 1990; Dröge et al. 1990; Pap et al. 1990; Kile and Cliver, 1991; Verma et al., 1992; Cane et al., 1998; Ballester et al., 1999; Krivova and Solanki, 2002; Kilic, 2008; Chowdhury et al., 2009b, 2010a). Sunspot activity is usually described by either sunspot numbers (SSN) or sunspot areas (SSA). Both are direct Solar activity indices that are historically most frequently used (Li *et al.*, 2005). The daily SSA is the measure of the area of the Solar surface covered by spots (in the sunspot area unit, namely, parts per million (ppm) of the Solar hemisphere) in a day.

In previous studies basic statistical techniques such as cross-spectral regression analysis visual assessment of plots (Crowley and Berner, 2001; Shaviv and Veizer, 2003; Royer, 2006) were used. Statistical methods and trend analysis are techniques significantly determine the relationships between

two non-stationary time-series. However, the performance of these methods may be compromised if analyzed time - series consists of same wavelength and phase shift. If the phase shift approaches to $\Phi = \pi/2$, both time-series appear to be uncorrelated. Cross-correlation and cross-spectral analysis are able to detect such phase shifts, but only as average values but not represent the condition of non-stationary. This limitation are overcome by using Fourier based techniques. The Fourier transform may generate artifacts when they are applied to analysis the real world process. The use of discrete Fourier transform to normalized time series leads to misleading results (Ballester et al., 2005). Due to the fact, many advanced analysis approaches, such as the cross wavelet transform (XWT), wavelet coherence (WTC) and cross-recurrence plots (CRPs) are widely used to study the non linear behavior of time series (Li, 2008). The wavelet transform decomposes a time series into time-frequency space, thus enabling the determination of the frequency spectrum of the variations as a function of time. It is therefore ideally suited for our purpose.

Cross-wavelet analysis permits detection and extraction of relationships between two non-stationary signals simultaneously in frequency (or scale) and time (or location) (Grinsted et al., 2004). A range of analysis approaches namely continuous wavelet, cross wavelet, and wavelet coherence analysis are employed to study the phase relationship between the smoothed monthly mean sunspot number and F10.7 cm solar radio flux (F10.7) (Zhang Xue et al., 2012). Analysis shows that there is a region of high spectral power construction across the Schwabe cycle belt, where the relative sunspot number and sunspot groups are in phase (Le, 2004). However, analysis of the cross-wavelet transform and wavelet coherence unveils asynchronous behavior featured with phase mixing in the high-frequency components of sunspot activity and Solar F10.7 cm solar radio flux. The comprehensive explanations of wavelet squared coherency and cross-wavelet phase angle using Morlet wavelet based on continuous cross-wavelet transform are given in Torrence and Webster (1999) and Grinsted et al. (2004) and references therein. They use Monte Carlo simulations to provide frequency-specific probability distribution (Global Wavelet Spectrum).

The main concern of this chapter is to apply the advanced wavelet based technique for the detection and quantification of relationship between SSN and SSA time series.

2.2 Data Source

We have used data of daily and total (both the Northern and Southern hemisphere) sunspot numbers (SSN) and sunspot areas (SSA) prior to January 2008 to May 2012. The daily values of sunspot number of the whole Solar disk, northern and southern hemispheres of the Sun are published by the “Solar Influences Data Analysis Centre” which is available online at <http://sidc.oma.be/sunspot-data/>. The sunspot area data were taken from Royal Greenwich Observatory available online at <http://www.Solarscience.msfc.nasa.gov>.

2.3 The Wavelet Techniques (WT)

Wavelet analysis is a tool for analyzing localized variations of power spectra within a time series (Torrence and Compo, 1998; Grinsted et al., 2004). It can be employed to analyze time series that contain non-stationary power at different frequencies. The wavelet technique decomposes a one-dimensional time series into a two-dimensional time-frequency space. Therefore, this method determines not only the periodicities of the dominant modes of variability, but also shows how the modes vary in time. Moreover, the wavelet technique is suitable to detect a signal which is relatively weak and intermittent in nature (Torrence and Compo, 1998; Knaack et al., 2005).

2.3.1 Continuous Wavelet Transform Analysis (CWT)

The continuous wavelet transform of the sunspot data is given by

$$W_{\Psi}(s, t) = \frac{1}{\sqrt{s}} \int_{-\infty}^{\infty} f(t) \Psi^* \left(\frac{t-a}{s} \right) dt \quad \dots \dots (2.1)$$

Where $f(t)$ the time series of the sunspot data is Ψ^* is the complex conjugate of continuous wavelet function Ψ , $s > 0$ the scaling factor controlling the dilation of the mother wavelet and a is the translation parameter

determining the shift of the mother wavelet. The method of wavelet transform can yield periodic information in time and frequency domains simultaneously. For these purposes, we study sunspot data using the Morlet wavelet function,

$$\Psi(t) = \pi^{-\frac{1}{4}} e^{i\omega_0 t} e^{-\frac{t^2}{2}} \quad \dots \dots (2.2)$$

where ω_0 is the dimensionless frequency and η is the dimensionless time. Detailed technical information about the Morlet wavelet is available online at <http://atoc.colorado.edu/research/wavelets/wavelet2.html>.

2.3.2 Wavelet Coherence Analysis (WTC)

The wavelet coherence is closely related with localized correlation coefficient in time- frequency space (Grinsted et al., 2004). It is used to find significant coherence between two time series, even though the common power is low. The WTC between SSN and SSA is defined as

$$R_{ns}^2(s) = \frac{|S(s^{-1}W_{(SSN)(SSA)}^n(s))|^2}{S(s^{-1}|W_{(SSN)}^n(s)|^2) * S(s^{-1}|W_{(SSA)}^n(s)|^2)} \quad \dots \dots (2.3)$$

Where S is smoothing operator, which is defined as

$$S(W) = S_{scale} (S_{time} (W^n(S))) \quad \dots \dots (2.4)$$

Where S_{scale} denotes smoothing along the wavelet scale axis, and S_{time} smoothing along the time axis. For the Morlet wavelet, the smoothing operator is given as (Grinsted et al., 2004)

$$S_{time} (W)|_s = \left(W^n(S) * c_1^{\frac{-t^2}{2s^2}} \right) \Big|_s \quad \dots \dots (2.5)$$

$$S_{scale} (W)|_s = (W^n(S) * c_2 \Pi(0.6s)) \Big|_n \quad \dots \dots (2.6)$$

Where c_1 and c_2 are normalization constants and Π is a rectangle function. The factor 0.6 is a scale decorrelation length determined empirically for the Morlet wavelet (Christopher et al., 1998). The squared wavelet

coherency is a measure of the intensity of the covariance of the two series in time-frequency space (Torrence and Compo, 1998).

2.3.3 Cross Wavelet Transform Analysis (XWT)

The cross wavelet transform (XWT) of SSN and SSA is defined as

$$W^{(SSN)(SSA)} = W^{(SSN)}W^{(SSA)*} \quad \dots \dots \dots (2.7)$$

where * denotes complex conjugation and W^{SSN} and W^{SSA} are the continuous wavelet transforms (Grinsted et al., 2004). The complex argument $arg(W^{(SSN)(SSA)})$ can be interpreted as the local relative phase between SSN and SSA in time frequency space. The cross wavelet transform reveals regions with high common power and further reveals information about the phase relationship. The univariate wavelet power spectrum can be extended to compare SSN and SSA. The wavelet cross spectrum is the expected value of the product of the corresponding SSN and SSA is mathematically given by (Jury et al., 2002)

$$W_{(SSN)(SSA)}(s, t) = W_{SSN}(s, t)W_{SSA}^*(s, t) \quad \dots \dots \dots (2.8)$$

where * denotes the complex conjugate and $W_{SSN}(s, t)$ and $W_{SSA}(s, t)$ are the continuous wavelet transform of SSN and SSA respectively. It not only determines the periodicities of the dominant modes of variability, but also shows how the modes vary in time.

2.4 Results and Discussion

Using the well known wavelet tools, developed by Torrence and Compo (1998), we have analyzed the data from January 2008 - May 2013 on the basis of daily grouped SSN and SSA. Figure 2.1 displayed the variations in SSN and SSA. It was noticed that SSN and SSA Solar indices never peak at the same time, and the SSN peaks appear earlier than the SSA. However, the SSA and SSN develop with the same magnetic field variations on the photosphere of the Sun and the magnetic field strength increases according to the ascending epochs. An understanding of complexity in the periodicities of SSA and SSN

may provide insight into the complex dynamics of the solar magnetic field in the two hemispheres. In case of sunspot number Wang et al. (2009) reported that the Solar cycle - 24 started between March and April 2008 and its maxima should occur during May - October 2012 and it is nearly cleared from figure 3.1 (Upper Panel).

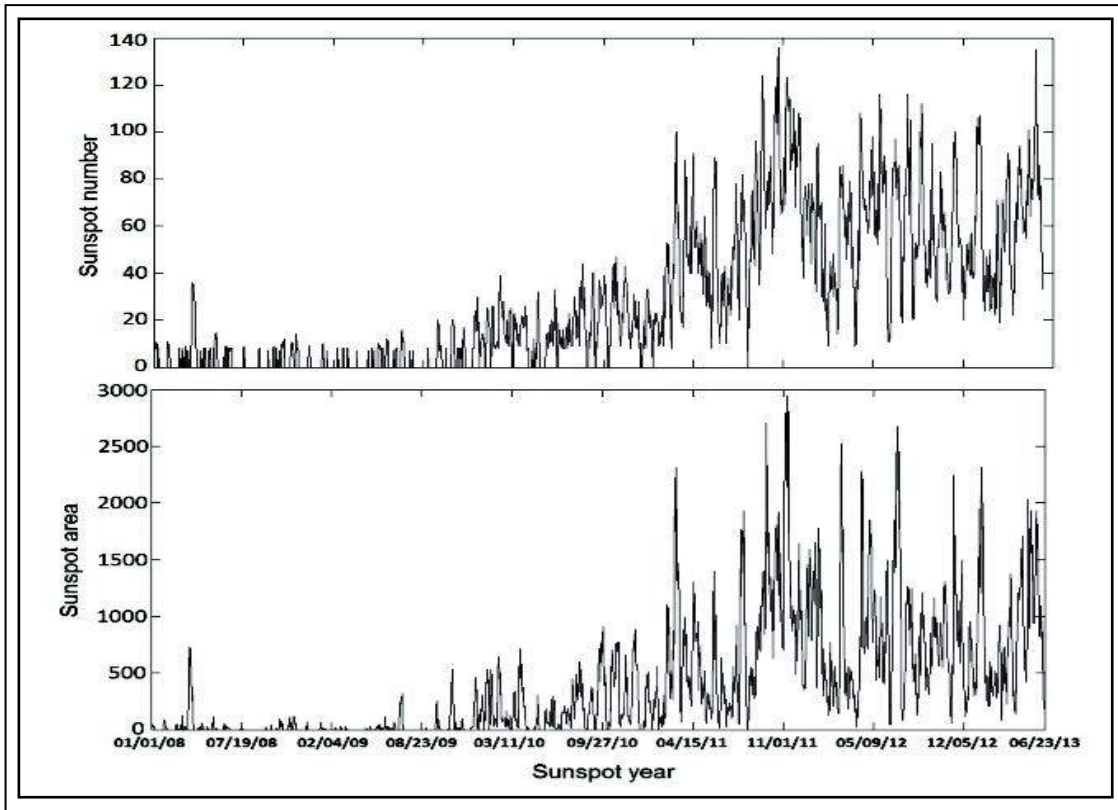


Figure - 2.1: Distribution of the sunspot number (upper panel) and sunspot area (bottom panel) for the time interval from January 2008 to May 2013

The wavelet power spectra for sunspot number (upper panel) and sunspot area (lower panel) are calculated and depicted in Figure 2.2 with a cone of avoidance and contours enclosing regions of 95% confidence level. The spectral power is relatively weak at the short periods or at high frequencies. Some distinct dual - patches of relatively higher contours around 16 to 64 days from September 2010 to May 2013 are found. The time flow of large variations has a periodicity of around 27 days for both sunspot number and the sunspot area. The rotational periodicity is the most dominant feature of the spectrum. It persists during the epochs of activity maximum, when identifiable solar active regions and their sunspots largely appear. The other

small peaks cannot be considered from coincidence due to multiple testing (Grinsted et al., 2004).

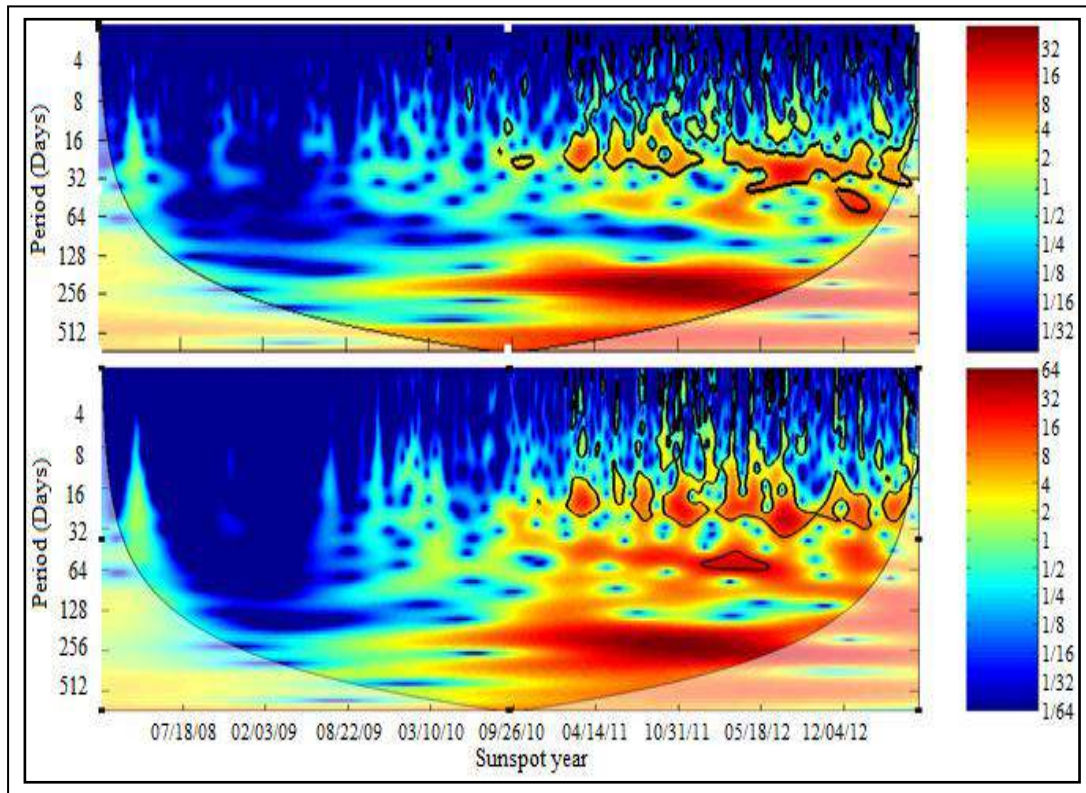


Figure - 2.2: Continuous wavelet transform (CWT): Daily sunspot number (upper panel) and sunspot area (bottom panel), with a cone of avoidance and enclosed regions of greater than 95 % confidence level (thick black solid line)

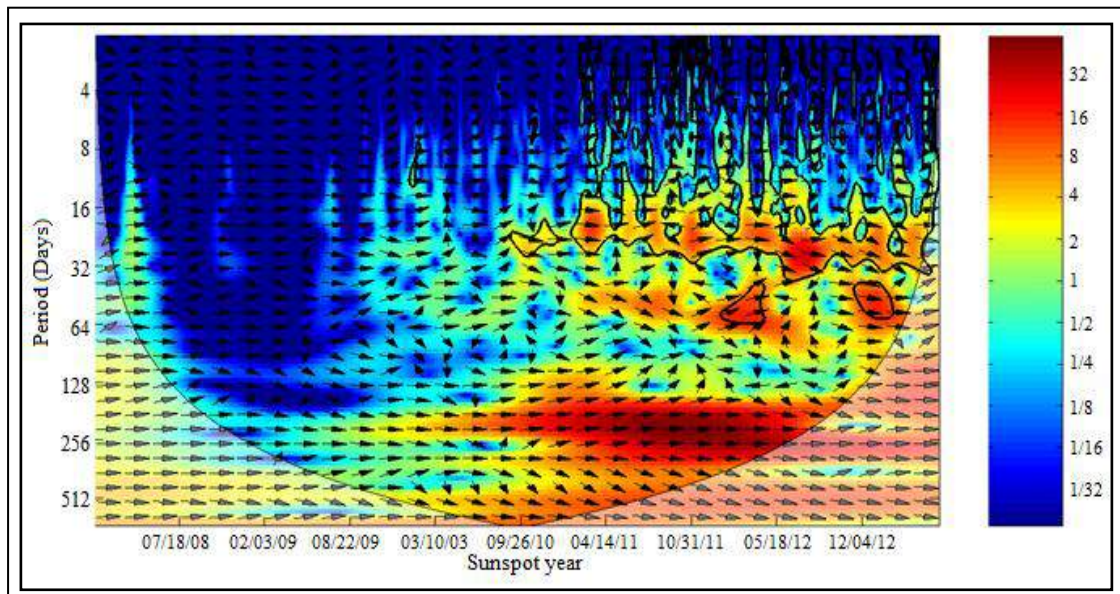


Figure - 2.3: Cross- wavelet spectra (XWT): Daily SSN and SSA with a cone of avoidance and enclosed regions of greater than 95 % confidence level (thick black solid line). The relative phase relationship is shown by arrows, with arrows pointing right for the in phase relationship, left for the anti-phase relationship, and straight up for the sunspot area leading the sunspot number by 90° .

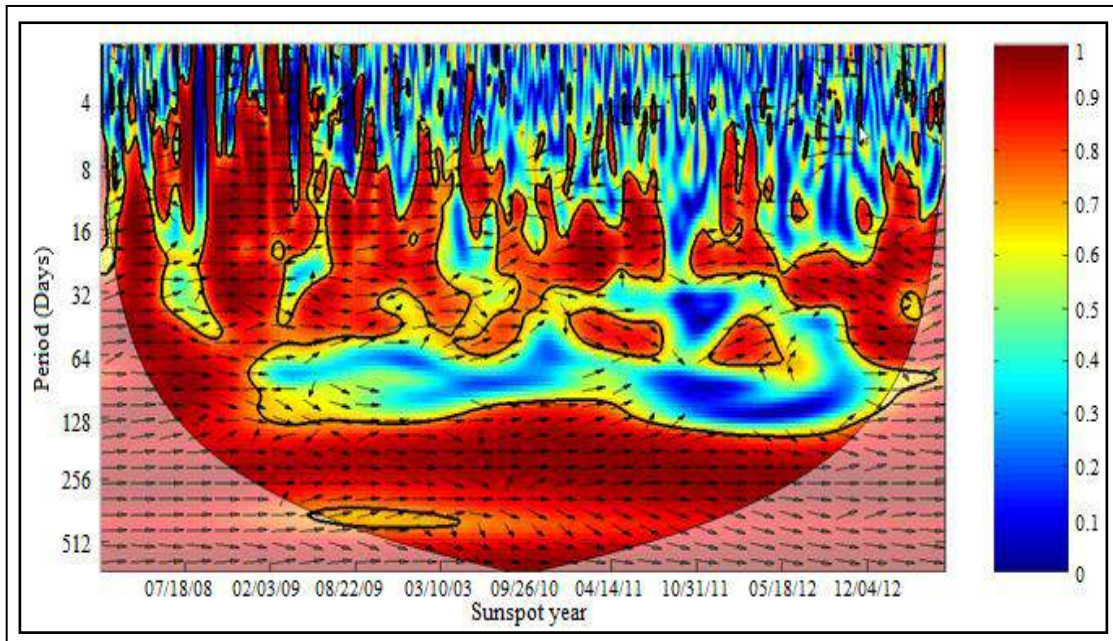


Figure - 2.4: Wavelet coherence of (WTC): Daily SSN and SSA with a cone of avoidance and enclosed regions of greater than 95 % confidence level (thick black solid line). The relative phase relationship is shown by arrows, with arrows pointing right for the in-phase relationship, left for the anti-phase relationship, and straight up for the sunspot area leading the sunspot number by 90° . (Above diagram presents the phase difference for sunspot number and sunspot area).

The XWT and WTC between the SSN and SSA were shown in Figure 2.3 and Figure 2.4 respectively. The XWT and WTC are rendering the regions with high common power and make known information about the phase relationship between two times series. Large contour on XWT shows phase relationship between SSA and SSN. The thin black contour (inside COI) demonstrates the periods above 95% confidence level (Torrence and Compo, 1998). In these figures, arrows point to the right when processes are in phase and to the left when they are in anti-phase. If an arrows points up (down), then the first process leads (lags) the second one. The thick black contour shown in figures designates the time series against red noise. The XWT shows that almost all arrows point to the right in the period scale of 27 day. The sunspot number and sunspot area are in phase in this area. Statistically, significant results are located within the cone of influence and the arrows beyond the cone of influence are not reliable. It was also noted that the arrows are fairly distributed in other periodic belts, implying strong phase mixing. The WTC (Figure 2.4) represents the strong phase mixing at period scale around the 32-128 days over the time period 2009-2012. However, the WTC indicates the

noisy behavior with strong phase mixing in the high frequency components of both the parameters SSN and SSA.

2.5 Conclusions

The present work used the wavelet cross-coherence to identify the quasi periodicities in the daily values of SSA and SSN during the period from January 2008 to May 2013 which includes rising phase of current Solar cycle 24. In the present study, we are interested in period related to the solar rotation and in their behavior with regard to the sunspot numbers and sunspot areas. The results of this work clearly demonstrated that there exists a strong correlation around the year 2012. We have found evidence for 27 day periodicity between the SSA and SSN during the ascending branch of Solar cycle 24 and a very weak evidence for the fundamental period reported by Ozguç, et al., (2002). This result is in agreement with the previous studies which show that at the beginning of the cycle the formation of sunspots start at higher latitude. In the successive stage the formation zone slowly moves towards the equator while appearing some saturation during the maximum activity years (Zharkov et al. 2007). This may arise because of different characteristics of the current cycle.

It was suggested that the variations in the rotation rate do indeed have an influence on the workings of the solar dynamo. This periodicity is enhanced during the period of maximum solar activity. However, this period varies from 16 - 64 days. CWT analysis shows that the 16 - 32 periodic range is statistically significant for short or mid - term periodicities. For the exact conclusion we have to wait until the end of cycle 24. The cross wavelet transform of the two time series shows that there is an area with high common spectral power located at the 16 - 64 periodic belts, where the two time series are in phase. The Cross Wavelet Transform (XWT) confirms the results given by wavelet coherence (WTC), which is found more suitable to find a coherent oscillation of the two time series than XWT.

This period is more stable than the other short-term periods and appeared from September 2010 to May 2013. Thus, we concluded that the Solar cycle 24 also includes the most remarkable period during the ascending

phase. Here many periodicities are not considered due to the fact that maximum peaks are below the significance level. Katsavrias et al. (2012) have identified the 27 days periodicity (with 13.5 days being its harmonic) in the dynamic parameters of the Solar wind, interplanetary magnetic field and the geomagnetic indices using wavelet analysis and the Lomb or Scargle periodogram.

The rotational periodicity of the Sun is expected to provide useful information about solar interior dynamics and mechanism of generation of the Solar magnetic field and its emergence on the Solar surface (Ichimoto et al., 1985; Sturrock and Bai, 1992). Bogart (1982) investigated autocorrelation functions of daily sunspot numbers for the period 1850 - 1977, obtaining a distinct period at 27 days. The 27 day Bartels rotation is very prominent period with respect to the occurrence of geomagnetic disturbances, and it is supposed to be relevant for the large scale Solar magnetic fields (Balthasar and Schussler 1984).

The 27 days orbital motion of the earth is a good indicator of the global pattern of heliospheric magnetic fields (Mavromichalaki et al., 2005). Chowdhury et al. (2011) proposed that 27 day periodicity is more stable than the other short - term periods and appeared in both rising and descending phases of Solar cycle 23. It is observed by many authors using different Solar activity parameters such as coronal index (CI), photospheric magnetic field, coronal mass ejections (CMEs), total Solar irradiance (TSI), and coronal Fe lines (Rusin et al., 1987; Knaack et al., 2005; Yin et al., 2007; Chowdhury et al., 2009b; Kilick 2009). Tong Xu et al. (2007) also predicted the values 112 of sunspot number for Solar cycle 24 prior to 2011 - 2012. Solar cycle 24 has the lower amplitude than that of cycles 21, 22 and 23 which is consistent with the results obtained by Duhau (2003) and Wang et al. (2002).

Analysis of Short Term Periodic Variation in Solar and Terrestrial Parameters

3.1 Introduction

The short term periodic variation of solar activity and its effect on terrestrial environment have been studied extensively from thousands of years. The terrestrial parameters respond to variation in solar surface associated with solar magnetic field and its periodic evolution. The geomagnetic Ap and AE indices shown the periodic variations in the range of a few day to centuries (Fraser-Smith, 1972, Courtillot et al. 1977, Donahue and Baliunas, 1992). The Solar parameter shows many types of interesting features associated with Solar cycle. These feature of solar plasma parameters carried out to the terrestrial environment which shows periodic variations due to the outflow of Solar wind. Solar wind plasma exhibits a wide variety of periodic variation.

The Solar wind is the charged atoms and sub-atomic particles (protons and electrons) at extremely high temperature flowing supersonically and helps the ionized plasma to overcome the Sun's gravitation field and emits as corpuscular radiation from outer part of Sun's Corona overcome the entire heliosphere. The speed and density of plasma depends on it generation condition and magnetic field of Sun. When it enters to the interplanetary space is termed as Interplanetary Magnetic Field (IMF). The magnitude and direction of IMF is depends on its interaction with slow and fast Solar wind originated from coronal holes and leads to create Co-rotating Interaction Regions (CIRs) (Akasofu, 1983; Shea et al., 1990; Kaushik et al., 2000).

The irregular behavior of IMF and Solar wind plasma emission associated with various solar phenomena are responsible for the generation of geomagnetic storms (Akasofu, 1983; Joselyn, et al., 1981). Geomagnetic

storms are associated with isolated disappearing filaments (Lakhina, 1994; Loewe et al., 1997; Gopalswamy et al., 2004; Turner et al., 2009). Lou et al. (2003) found Ap index periodicities of 187, 273 and 364 days in the 1999-2003 time interval. Short term periodicities of 275, 135, 9.1 and 6.8 days are identified in the Solar wind speed and IMF polarity it is due to the phenomena of solar rotation (Gonzalez and Gonzalez 1987; Clua de Gonzalez et al., 1993; Svalgaard and Wilcox, 1975; Fenimore et al., 1978; Sabhah and Kundela, 2011). Katsavrias et al., (2012) examined the periodicity in solar activity Solar wind plasma interplanetary magnetic field and geomagnetic activity during 1966 - 2000.

In this chapter short term periodicities and variations of various Solar activity parameters and geomagnetic indices have been done using the wavelet transform and global wavelet transform during the current solar cycle 24. Results of our analysis shows time localized spectral peaks, fluctuations in Solar wind parameters and geomagnetic indices. Some periodicities with specified intervals were also detected.

3.2 Prominent periodicities

The prominent periodic variations in solar wind plasma parameters and associated geomagnetic indices may vary from maximum to minimum in a characteristic way associated with the development of active regions on the solar surface during different solar cycles.

3.2.1 13.5 Day Period

The 13.5 day period is coupled with active longitudes and tilted dipole structure. It was observed in various solar wind parameters such solar wind, IMF, solar emissions, plages, sunspot area, sunspot number, emergence of solar magnetic flux, geomagnetic activity, ionospheric parameters etc. (Mursula and Zieger, 2000; Nayar et al., 2001; 2002; 2004). The 13.5 day periodicities are associated with both active longitudes and tilted dipole structure. Donnelly and Puga (1990) made widespread study of the 13.5 day periodicity at numerous wavelengths of solar radiation. They concluded that the power of the

13.5 day period is dependent on the wavelength or the source at the solar surface and does not behave as a sub-harmonic of the 27 day period.

3.2.2 27 Day Period

Bai (2003) studied longitudinal distributions of solar flares during the period of solar cycles 19 to 23 and identified active longitudes (hotspots), which causes flare periods ranging from 25 to 29 day. The 27 day solar rotation period was first observed in sunspot groups. The Carrington rotation period (27.275 day) specifies the solar rotation. Takalo and Mursula (2002) and Gosling et al. (1976) reported the 27 day periodicity in solar wind plasma and interplanetary magnetic field, Neugebauer (1999) observed it in IMF radial component, Olsen (1948) detected it in geomagnetic field and also in high speed streams by Snyder et al. (1963) and Gosling and Bame (1972). The uncertainty obtained in the 27 day periodicity suggests various mechanisms active on the solar surface, in addition to rotation. The active regions may emerge or disappear rapidly on the solar surface causing longitudinal shift in their position (Kane, 2003). The 27 day periodicity will be sharper in the spectrum of the considered parameter, if the active region structure is long lived. On the other hand if the two active regions are completely opposite, considered parameters reveal a periodicity less than 27 days. The distribution of magnetic structures and active regions on the solar surface, and the outflow of solar wind introduce a diversity of short period variations, with periods less than 27 days, in the interplanetary medium.

3.2.3 154 Day Period

The 154 day periodicity was first observed in occurrence rate of g-ray flares by the gamma-ray spectrometer onboard the Solar Maximum Mission satellite (Rieger et al., 1984). Further, it was found in various solar flare activities parameters such as solar wind velocity, IMF and geomagnetic activity around the solar maximum and have been comprehensively monitored using different wavelengths. The 154 day periodicity were associated preferentially with regions on the solar disk of compact magnetic field structures associated with sunspots rather than in the more dispersed weaker magnetic field and thus it may be confined to complex active regions containing large spots called

'super active regions. Evidence for a periodicity of 154 days has also been found in non-flare indices of solar activity as sunspot number, the Ottawa 10.7 quiet Sun flux etc. (Ichimoto et al., 1985).

3.2.4 11 Year Sunspot Cycle

11 years variations in sunspot number, geomagnetic as well as terrestrial climate parameters were known as Schwabe cycle (Schwabe 1844; Hathaway et al. 2002). Detail description is given in Chapter – 1.

3.2.5 22 Year Magnetic Cycle

The period of magnetic activity cycle is twice as that of sunspot cycle, about 22 years on average (Hale et al. 1919). Each solar cycle is unique in intensity, duration, and distribution of activity, which varies from 9.5 to 12.5 years. It also varies in both in cycle length and maximum amplitude. At the beginning of the sunspot cycle, the solar magnetic field is primarily dipolar associated with its rotation axis. The dipole strength vanishes around the solar maximum and reverses its polarity about one year after the maximum. In the declining phase, the dipole field is restored with polarity in the opposite direction. The dipole strength has a cyclic variation known as dipole cycle. The dipole cycle is more important in deciding the evolution of large scale solar magnetic field.

3.3 Method: Wavelet Transform

Grossman and Morlet (1984) developed the wavelet transform as a tool for advance signal processing. The wavelet transform can be used to analyze time series that contain non-stationary power at many different frequencies (Torrence & Compo, 1998), because the wavelet analysis maintains time and frequency localization in signal analysis by decomposing or transforming a one-dimensional time series into a two-dimensional time-frequency image simultaneously. It is possible to get information on both the amplitude of any “periodic” signals within the series, and how this amplitude varies with time.

The Morlet wavelet is the commonest function used in astrophysical signals expansion; this makes easier the comparison with previously published work (Torrence and Compo, 1998; Aydin and Markus, 2000). Furthermore, due to its Gaussian support, the Morlet wavelet expansion inherits optimally as regard as the uncertainty principle (Morlet et al., 1982). More detail about Morlet mother wavelet function given in Chapter 2. Technical details used in different mother wavelets can be seen in appropriate literature (Torrence and Compo, 1998).

The global wavelet spectra provide an unbiased and consistent estimation of the true power spectrum of the time series, and thus they are a simple and robust way to characterize the time series variability. Global wavelet spectra should be used to describe plasma parameters and geomagnetic indices variability in non-stationary. Global wavelet spectra are useful for summarizing a region's temporal variability and comparing it with geomagnetic indices in other regions. Analytically it is given by

$$(GWPS)_s(s) = \int_{-\infty}^{\infty} |W_x(\tau, s)|^2 \dots \dots \dots (3.1)$$

3.4 Data Set

In this work Solar wind parameters such as Solar wind speed V (km/s), proton density D (M/cm^3), temperature T (K), plasma pressure P (nPa), magnitude of average magnetic field vector also known as total magnetic field B_{total} or B (nT), interplanetary magnetic field (IMF) (*i.e.* B_x , B_y and B_z) and corresponding geomagnetic indices Dst have been analyzed. The Dst index is calculated by averaging the horizontal magnetic field from mid-latitude and equatorial magnetograms and represents the degree of equatorial magnetic field deviation specifying the magnitude of geo magnetic storms.

The A_p (linear version of K_p), and aurora electrojet index AE are the quantitative measure of the auroral zone magnetic activity produced by enhanced ionospheric currents below and within the auroral oval. All the dataset used in the work are available online at the OMNIweb data server (<http://omniweb.gsfc.nasa.gov/>). The data are measured at the distance of 1 AU

in daily values from January 2008 to December 2014 (that is time span of current Solar cycle 24).

3.5 Results

In this study we have analyzed the short term periodicity of Solar wind parameters during the current Solar cycle 24 and the resulting changes in geomagnetic indices (Dst, AE and Kp).

3.5.1 IMF Bx Component

Figure 3.1 depicts the variation in short term periodicity of IMF (B_x) during the period of 2008-2014. The wavelet power spectrum gives information on the relative power at a certain scale and a certain time. This analysis represents the actual oscillations of the individual wavelets rather than just their magnitude. The concentration of power can be easily identified in the frequency or time domain. We performed the Global wavelet spectrum (GWS) analysis to study the dominant periods of B_{ave} component for the different conditions during the period of analysis. The GWS provide an unbiased and consistent estimation of the true power spectrum of the time series, and thus they are a simple and robust way to characterize the time series variability. The results are shown in Figure 3.1(a) and Figure 3.1(b). In Figure 3.1(b) three relative maximum in cross-wavelet (14, 27, 60) was discovered. It is interesting to note that the relative maximum of 27 days may be associated with noise for the Solar cycles. In short periodic range the 27 day period is the most prominent one in all cycles

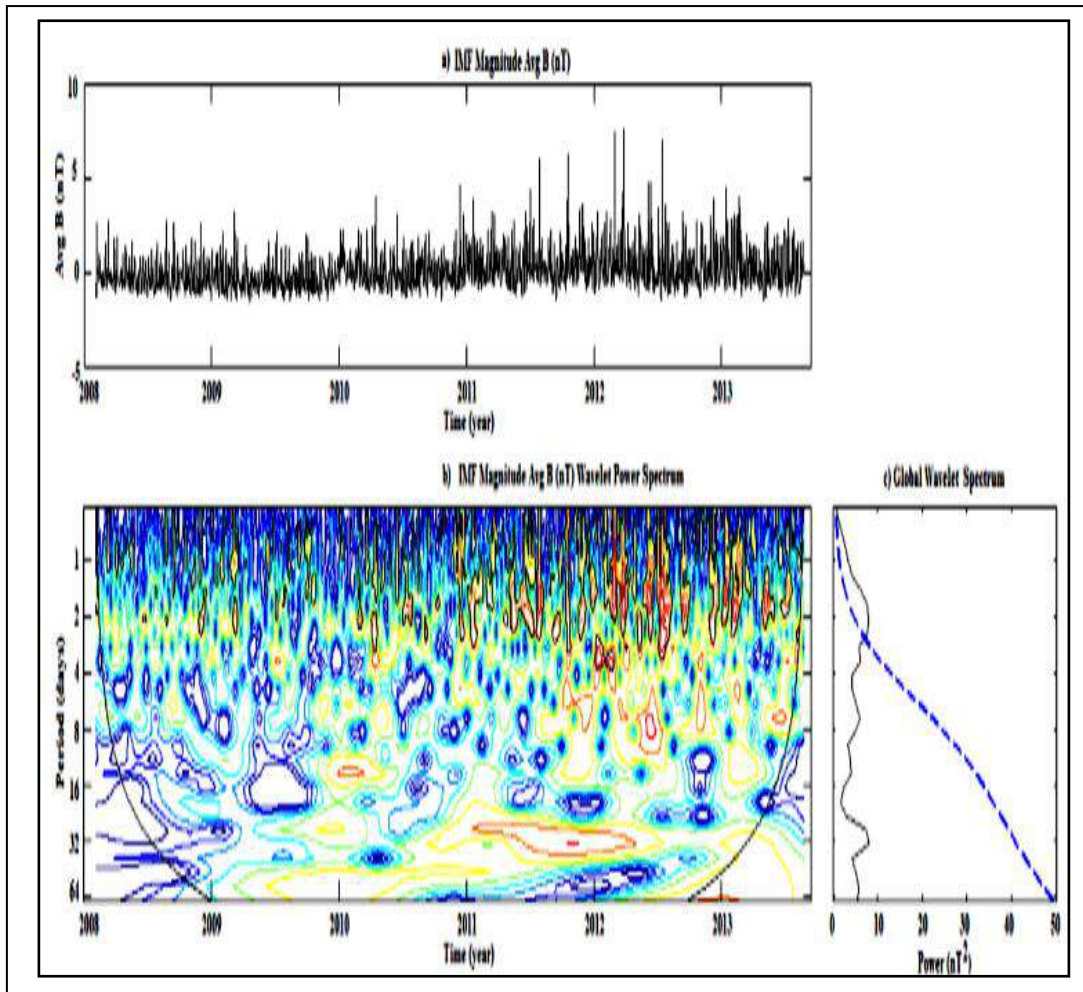


Figure - 3.1: Wavelet analysis of the original time series of magnitude of IMF a) The original IMF magnitude index b) The local wavelet power spectrum of the original IMF B_x magnitude index c) The global wavelet power spectrum of the original IMF B_x magnitude index

. In Figure 3.1(c) multiple peaks in the global spectra indicate that the IMF B_x signal is composed of oscillations with different time periods and magnitudes. In GWS spectral peaks are broader and many spectral peaks are vanished within the 90% confidence level.

3.5.2 IMF B_y Component

The wavelet power spectrum and global wavelet spectrum for IMF B_y is depicted in Figure 3.2. The most prominent periods for IMF B_y component are present in short period range of 9 day, 14 day and 27 days. Like IMF B_x these spectral peaks are also very sharp and highly significant. The spectral peaks around 27 day periods are very narrow and also many spectral peaks are vanished in GWS 90% confidence level.

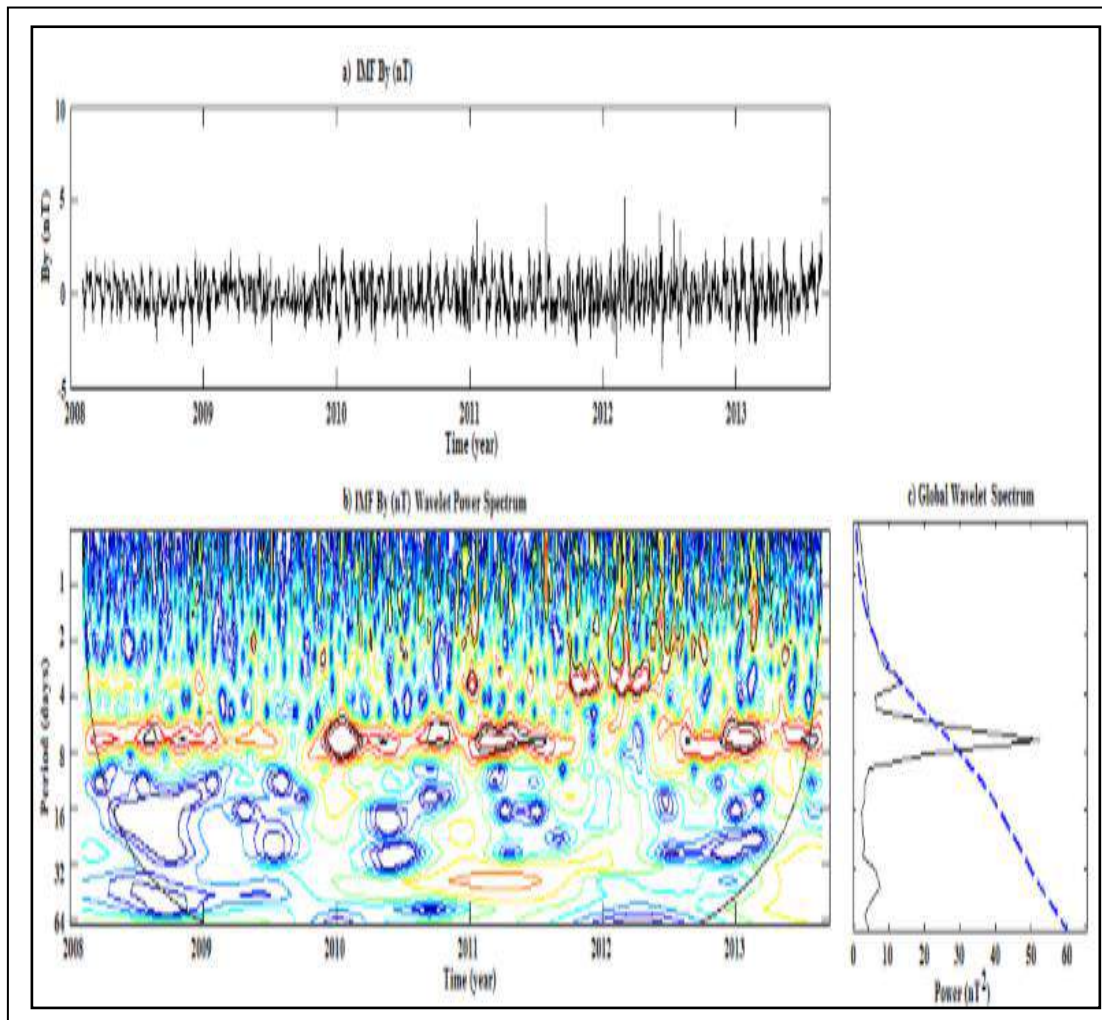


Figure - 3.2: Wavelet analysis of the original time series of IMF B_y a) The original IMF B_y index b) The local wavelet power spectrum of the original IMF B_y index c) The global wavelet power spectrum of the original IMF B_y index.

3.5.3 IMF B_z Component

Wavelet analysis of IMF B_z component was shown in Figure 3.3. It was noticed that wavelet power spectrum and global wavelet power spectrum are very complex and it is very difficult to identify the prominent periods present in the spectrum as compared to other interplanetary parameters. The B_z component shows a large number of periods between 4 to 64 day. In this period range most significant peak was observed at 14 day range. Periods are less prominent and immersed within noise. It was observed from GWS IMF B_z peaks are very low significance as most of the peaks below 90% significance level.

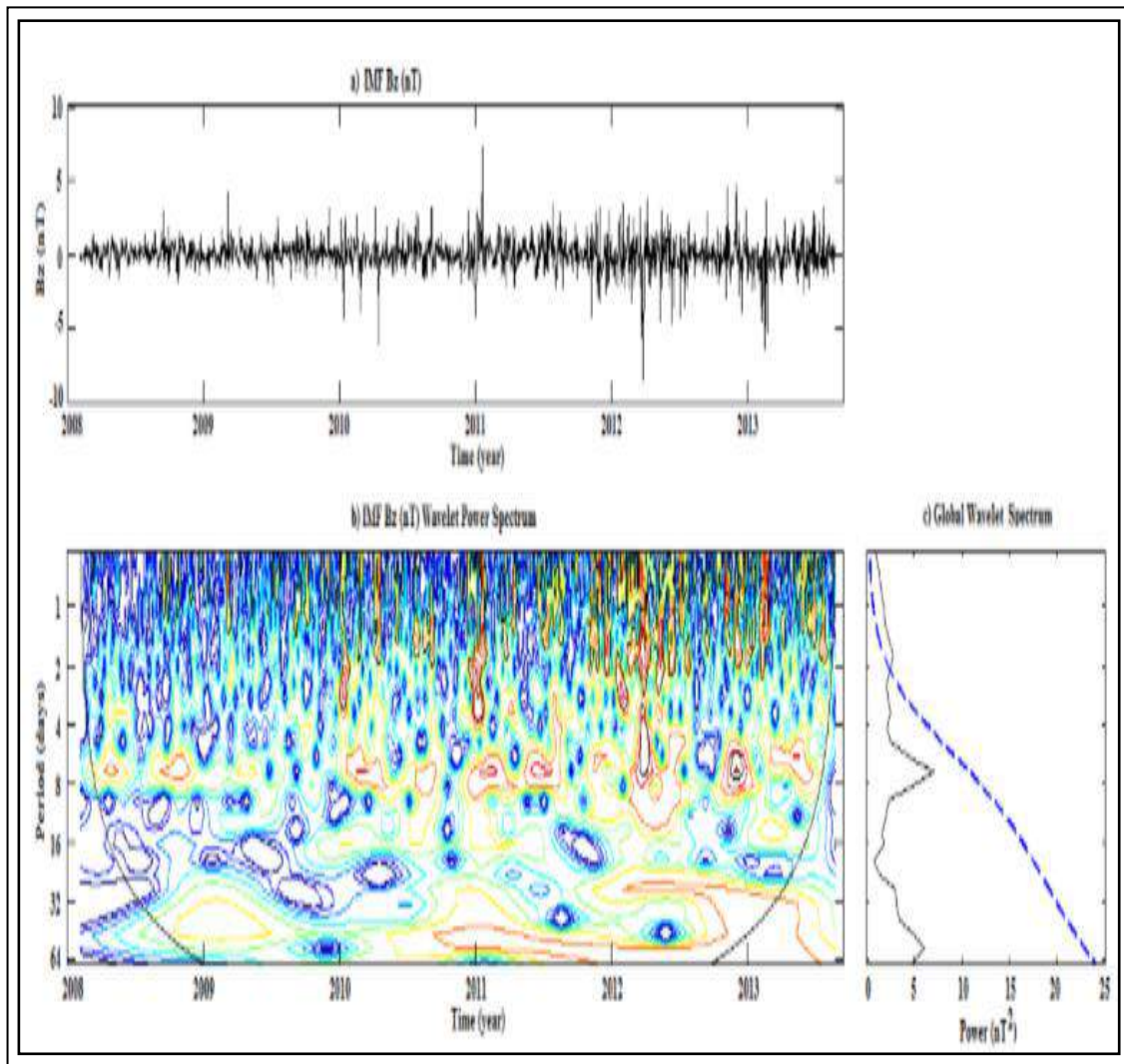


Figure - 3.3: Wavelet analysis of the original time series of IMF B_z a) The original IMF B_z index b) The local wavelet power spectrum of the original IMF B_z index c) The global wavelet power spectrum of the original IMF B_z index

3.5.4 Solar Wind Temperature

Wavelet analysis of Solar wind temperature was shown in Figure 3.4. The 14 and 27 days periodicities present in the spectrum with 90% confidence level in the overall. As seen from the figures for Solar wind temperature 14 day periods more prominent those 27 days. The Solar wind temperature shows a broad spectrum near the rotation period of 27 days.

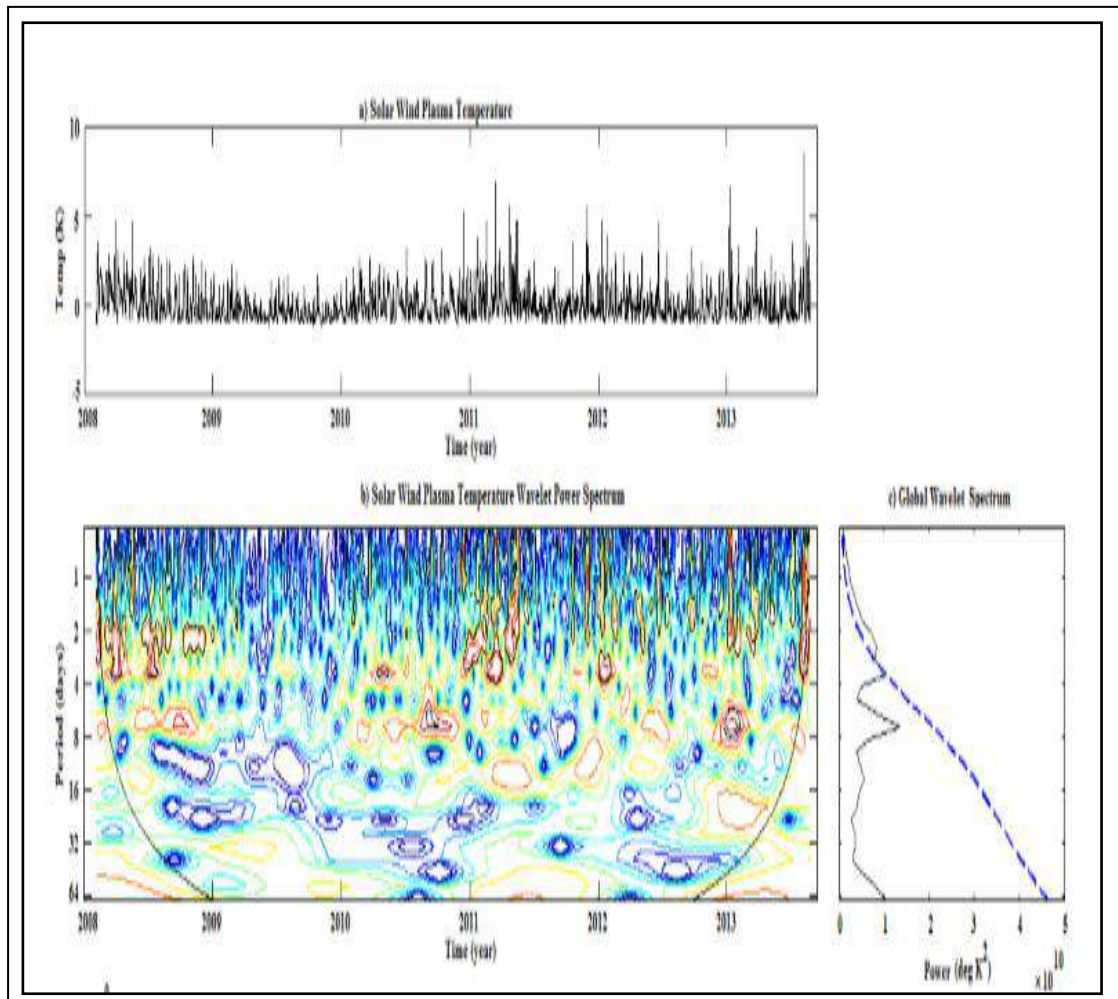


Figure - 3.4: Wavelet analysis of the original time series of Solar wind temperature a) The original Solar wind temperature time series b) The local wavelet power spectrum of the original Solar wind temperature time series c) The global wavelet power spectrum of the original Solar wind temperature time series

3.5.5 Solar Wind Plasma Density

Figure 3.5 shows the wavelet spectrum and global wavelet spectrum of Solar wind density calculated by the wavelet transform method during the year 2008-2015. The periodicities present in the spectrum with 90% confidence level in the overall data are 14 and 27 days. But 14 days periods found to be more prominent than 27 days. Other period occur randomly at different epochs, the spectral peaks are broader and many spectral peaks are vanished below 90% confidence level.

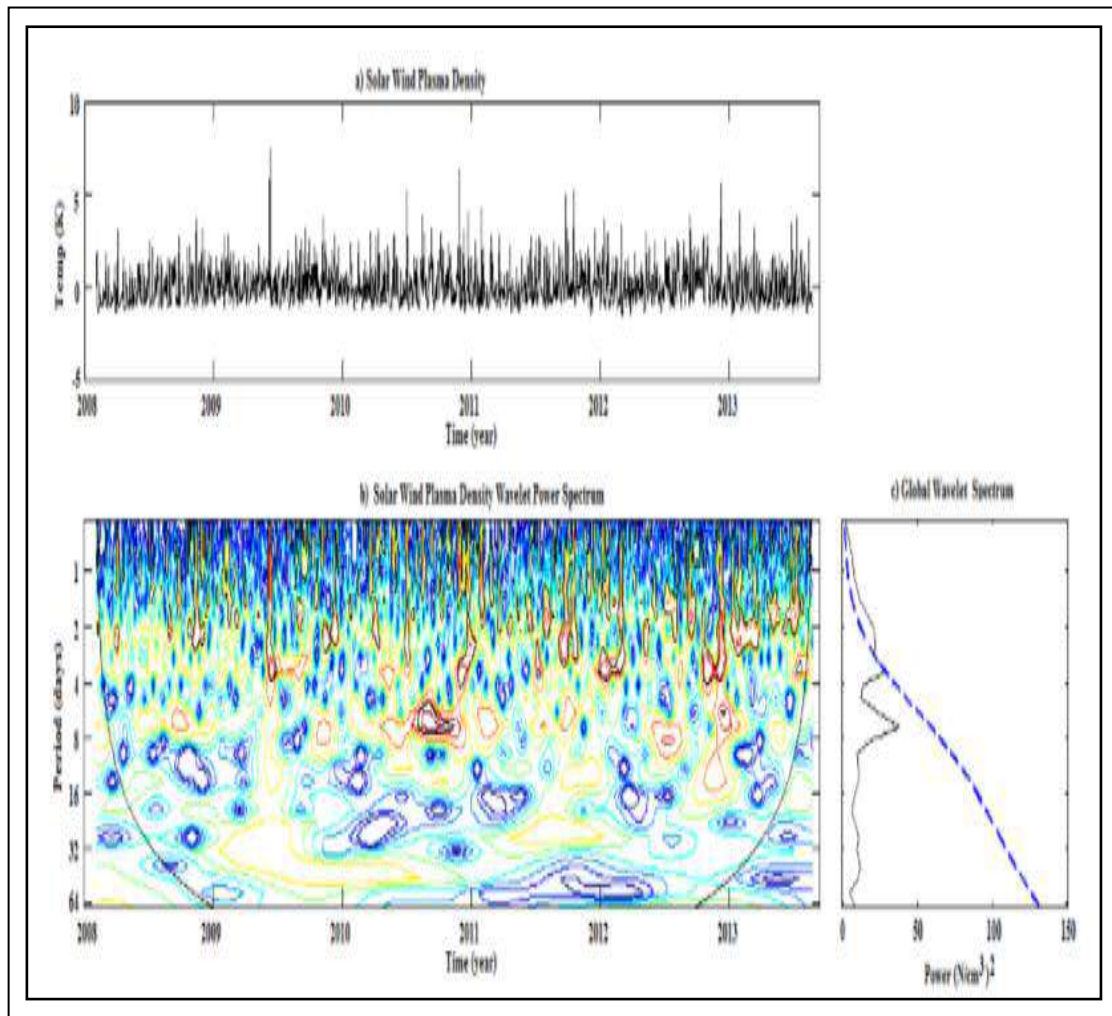


Figure - 3.5: Wavelet analysis of the original time series of Solar wind plasma density a) The original Solar wind plasma density time series b) The local wavelet power spectrum of the original Solar wind plasma density time series c) The global wavelet power spectrum of the original Solar wind plasma density time series

3.5.6 Solar Wind Plasma Speed

Figure 3.6 shows the wavelet based spectrum analysis of Solar wind plasma speed during the analysis period. It was noticed that the periods corresponding to 9 days and 14 are more prominent. The 9 day period is considerably more significant. Similarly 14 day period exhibits a variation in spectral power. Many other peaks are also present in the spectrum but they are vanished because they lie below 90% confidence level.

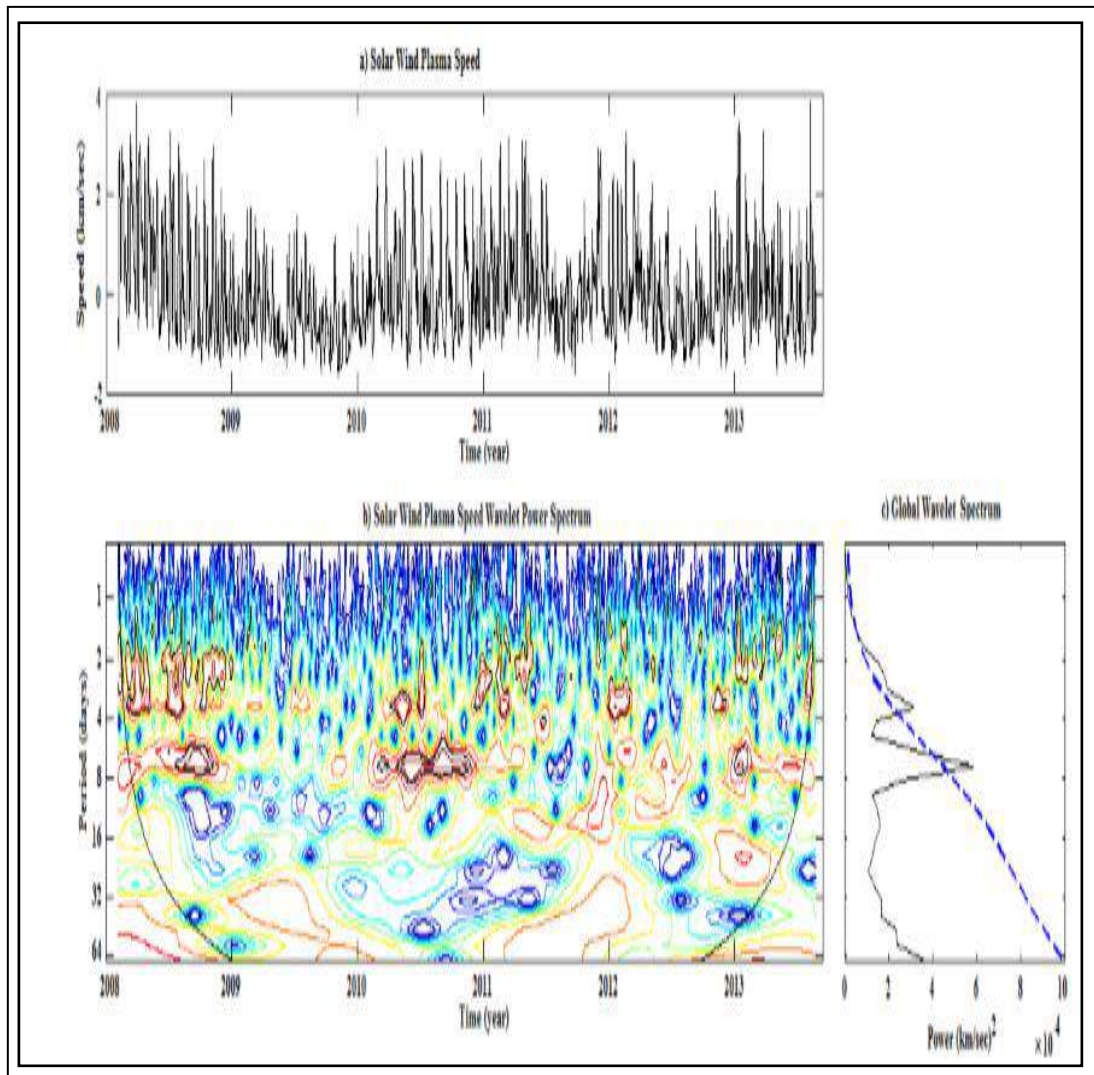


Figure - 3.6: Wavelet analysis of the original time series of Solar wind plasma speed a) The original Solar wind plasma speed time series b) The local wavelet power spectrum of the original Solar wind plasma speed time series c) The global wavelet power spectrum of the original Solar wind plasma speed time series

3.5.7 Geomagnetic Dst index

Figure 3.7 shows the wavelet spectrum and Global wavelet spectrum for geomagnetic Dst index. Most of the periodicities present in the both spectrum are highly significant with 90% confidence level. But short term periodicities of 22 to 30 days with 27.8 peaks appear intermittently and without any obvious pattern.

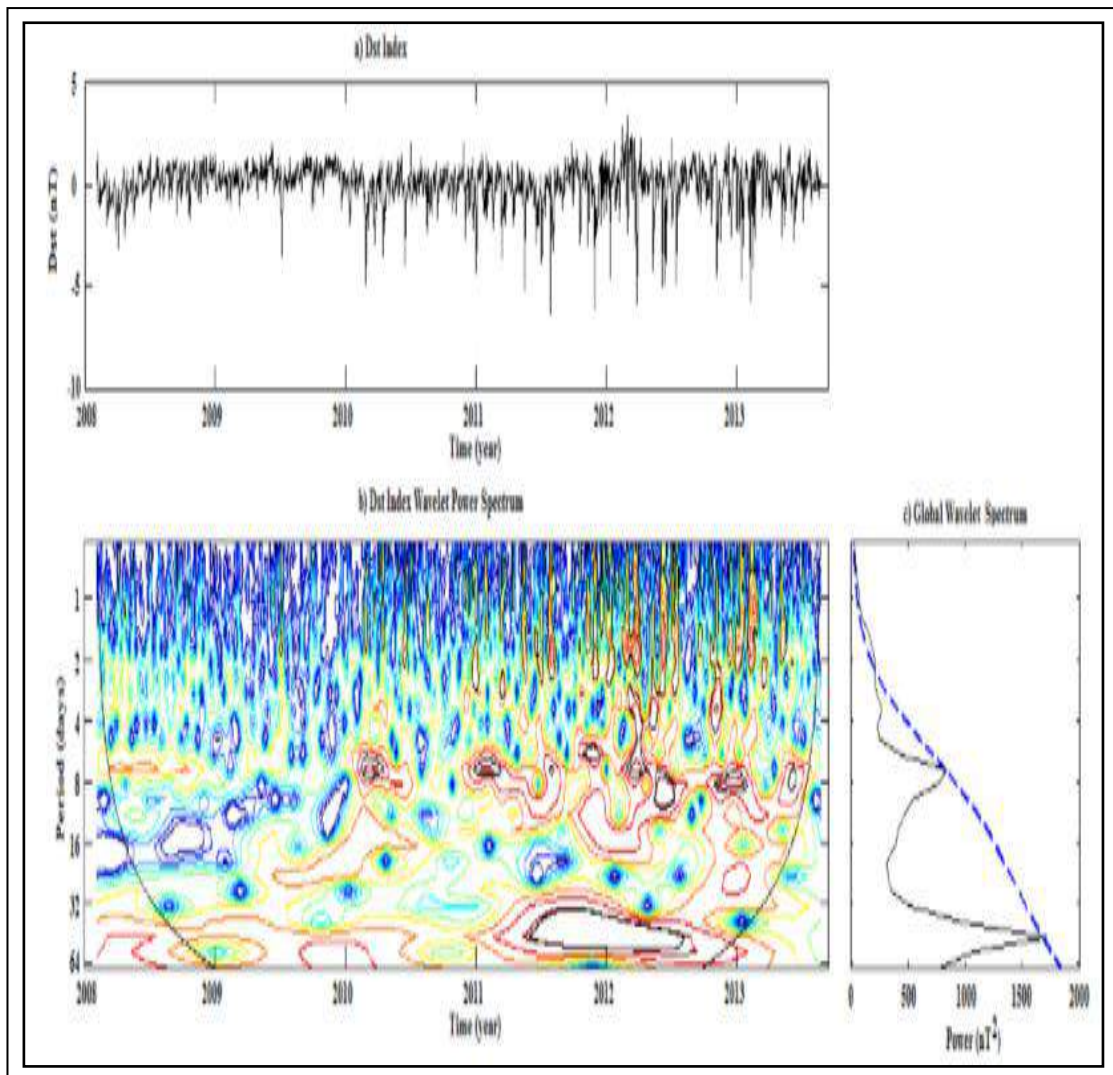


Figure - 3.7: Wavelet analysis of the original time series of Dst index a) The original Dst index time series b) The local wavelet power spectrum of the original Dst index time series c) The global wavelet power spectrum of the original Dst index time series

3.5.8 Geomagnetic Activity index A_p

Figure 3.8 shows the wavelet power and global wavelet power spectrum using wavelet analysis techniques. Most of the periodicities present in this spectrum are highly significant. The Solar rotation period of 27 days is highly diffused 9 day and 14 day periods are seen with greater significance. It was also noticed that 9 day and 14 day are very sharp and 9 day periodicity is more significant than 14 days period.

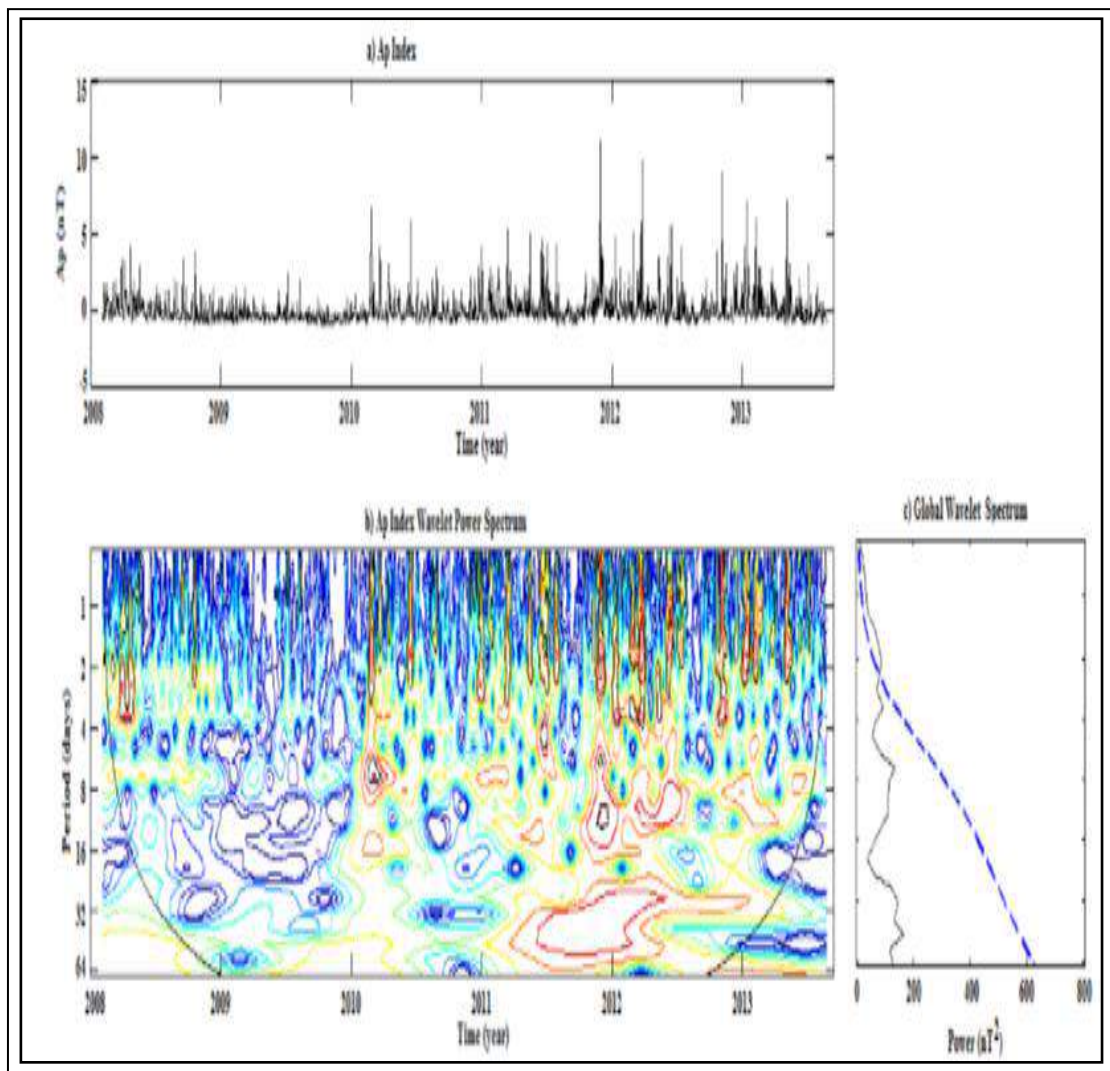


Figure - 3.8: wavelet analysis of the original time series of A_p index a) the original A_p index time series b) the local wavelet power spectrum of the original A_p index time series c) the global wavelet power spectrum of the original A_p index time series

3.5.9 Geomagnetic Activity index, AE

Figure 3.9 shows the wavelet analysis for geomagnetic AE index. The wavelet spectrum and global wavelet spectrum is very complex and it is very difficult to identify the prominent periods present in the 2 to 30 days period range. But 27 day periodicities appear sporadically throughout the analysis period.

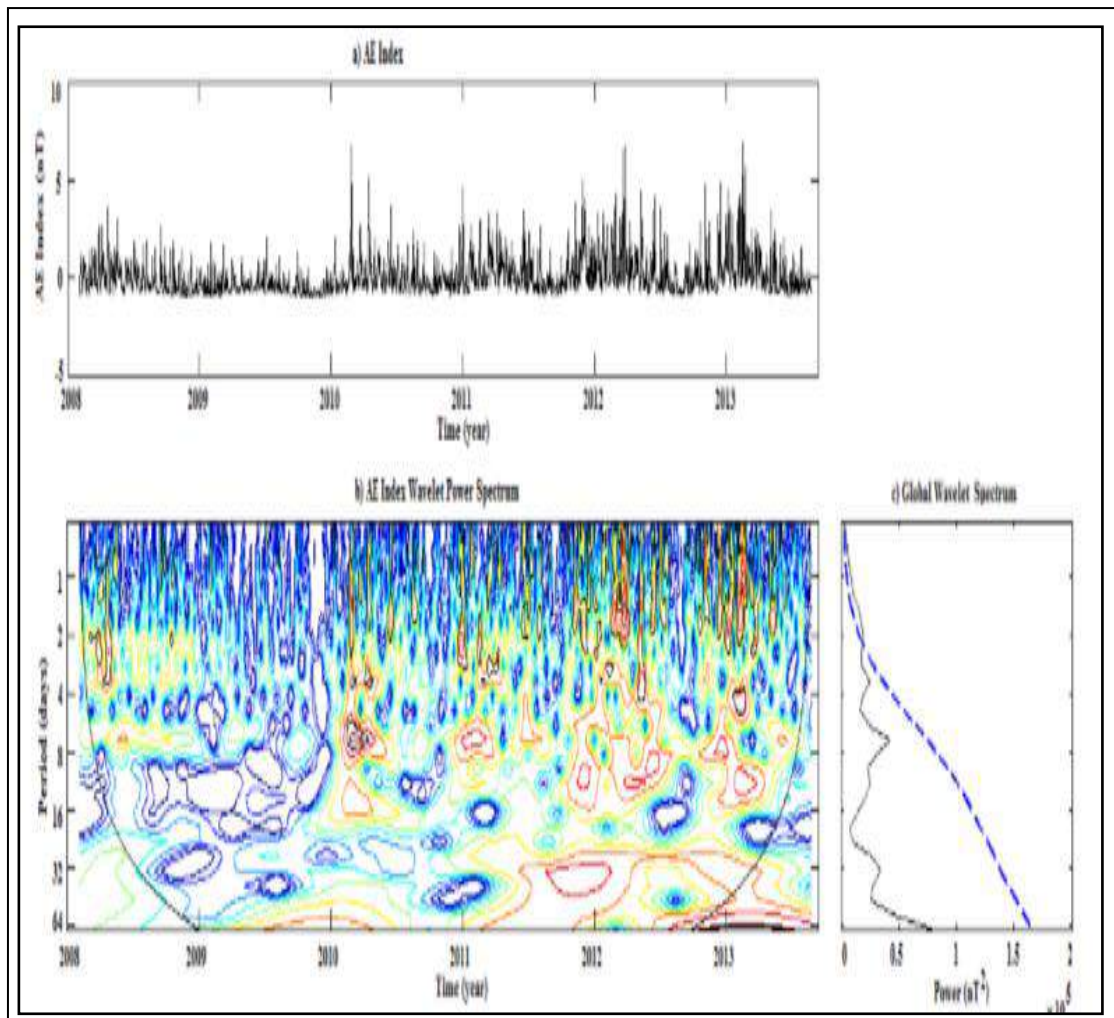


Figure - 3.9: Wavelet analysis of the original time series of AE index a) The original AE index time series b) The local wavelet power spectrum of the original AE index time series c) The global wavelet power spectrum of the original AE index time series

3.6 Conclusions

The short term periodicity of 14 days in the mean solar magnetic field was confirmed by Das and Nag (Das and Nag, 1999) using Fourier transform and autocorrelation techniques. The other periodicity of 26.7 days is due to the rotational modulation of the sun. The peak around the time period of 9 days might be due to the higher harmonics of the synodic rotational modulation of the sun. Bogart et al (1982) reported the existence periodicities for the solar rotation, solar activity cycle. The sunspot numbers show the same periodicities as it has been found for the mean solar magnetic field and the autocorrelation is very similar, it can be concluded that the mean magnetic field of the sun is mostly dominated by the effect coming from the active regions, due to which a 14 day periodicity is observed.

The periodic emergence of magnetic flux took place mainly within already developed sunspot groups, giving place to an enhancement of their magnetic complexity that triggered periodic energetic flares (Oliver et al. 1998; Ballester et al. 2002). This hypothesis was supported by the joint apparition of a strong periodicity in sunspot areas, and energetic flares, together with the absence of such periodicity in sunspot groups. Most of the periodic variations observed on the Sun are related to the dynamo region and its evolution. These periodic variations, though having their sources at entirely different solar active regions, are expected to have links between them. In this work, the characteristics of periodicities existing in the solar activity and interplanetary medium and their signature in the terrestrial environment are investigated. The amplitude of the periodicity depends on the parameter considered and each of them evolves differently.

In this chapter wavelet power spectrum and global wavelet spectrum methods are used to identify the short term periodicities of interplanetary magnetic field, Solar wind plasma parameters and terrestrial geomagnetic indices. Short term periodicities of 14 and 27 days were detected within the 90% confidence level in all parameters. These periods have different amplitude for different parameters. In case of Solar wind plasma density, B_z component of IMF and terrestrial geomagnetic indices short term periodicity of 14 day are more significant. Nayar et al., (2002) observed that periodicity in descending phases of Solar cycles 21, 22 and 23 on the other hand Jose Alver Bolzan et al., (2005a) report similar periodicity in speed and density. We also found periodicities of 9, 14 and 27 day using wavelet power and global wavelet spectrum. Mursula and Zieger (1996) proposed that periodicity of 13.5 day is due to the occurrence at 1AU of two high-speed streams per Solar rotation. Periodicity of 27 days with 90% confidence level is quite appeared for all Solar and terrestrial indices. This is probably due to fast stream from coronal holes overlaps with mass ejection from or near the active region resulting in a more or less random variation of measured Solar wind speed (Kotsavrias, 2012). Many researchers (Gonzalez and Gonzalez, 1987, Clua de Gonzalez et al. 1993; Svalgaard and Wilcox, 1975, Fenimore et al, 1978; Prabhakaran Nayar et al., 2002) identified the periodicities of 27.5, 13.5 - 9.1 and 6.8 days in

interplanetary magnetic field (IMF) for the time interval of 1964 - 2000. It was concluded that the wavelet power spectrum and Global wavelet spectrum have identified the 27 day periodicities (with 14 day being its harmonic) in the dynamic parameter of Solar wind, interplanetary magnetic field.

Study the Phase Relationship between Sunspot Number and F 10.7 cm Solar Radio Flux using Non-Linear Techniques

4.1 Introduction

The nature of solar activity is very complex and has become great practical and societal importance. The low energy phenomena (sunspots, 10.7 cm Solar radio flux and Ca K index) are related with lower atmospheric layers (photosphere, chromosphere and upper chromosphere respectively), while high energy phenomena (CMEs) are associated with higher atmospheric layers (Corona) and originate mostly from the Solar active regions (Gosling et al. 1976; Bachmann and White 1994; Feminella and Storini 1997; Sheeley et al. 1999). The larger eruptions like flares and coronal mass ejections (CMEs) are closely related to active regions (Harrison, 1990), which consist of one to dozens of sunspots. Sunspot is very useful parameter for the studies of terrestrial climate and space weather conditions (Eddy, 1976; Hoyt and Schatten, 1998; Hathaway et al., 2002). They are used as indicator for other solar activities such as active regions, plages, flares, prominences (Greenkorn, 2009). When temperature, density and magnetic fields are enhanced F10.7 radio flux is used to measure the general solar activity (Bruevich et al., 2012). The 10.7 cm radio flux emerges from high part of the chromosphere and low part of the corona. F10.7 radio flux emissions have two different sources: thermal bremsstrahlung and gyro - radiation. It is contributed for the undisturbed Solar surface and sunspots (Tapping, 1987). F10.7 radio flux is the surrogate indices for the combination of chromospheric transition region and coronal Solar EUV emissions modulated by bright solar active regions (Bruevich, et al., 2012). On the basis of characteristic time-scales F10.7 radio

flux emission is divided into three components: (i) transient events associated with flare and similar activity less than an hour; (ii) slow variations in intensity over hours to years designated as S-component; (iii) a minimum level component (*i.e.* when SSN is equal to zero as it was at the minimum of the cycle 24 and local magnetic fields are negligible) below which the intensity never falls- the "Quiet Sun Level" (Tapping and De Tracey, 1990). When the local magnetic fields grow to be strong at the rising phase of Solar cycle and Solar spots appear the gyro-radiation source of F10.7 radio flux begins to succeed over free - free radiation so transient's events and S - components begin to grow strongly.

The minimum level component is defined by free-free source. The S-component comprises the incorporated emission from all sources on Solar disc. It contains contribution from both free-free and gyroresonance processes and also some non-thermal emission Gaizauscas and Tapping (1988). Various studies show a good correlation between the F10.7 cm solar radio flux and Zurich sunspot relative number (Rz) (Foukal and Lean, 1990; Bouwer, 1992; Floyd et al., 2005; Tapping et al., 2007; Svalgaard and Hudson, 2010; Johnson, 2011; Tapping and Valdes, 2011; Zhang et al., 2012). Dodson et al. (1974) suggested that F10.7 solar flux lags behind sunspot numbers in Solar cycle 20. The mutual relationship between sunspot numbers and three Solar UV/EUV indices, the F10.7 radio flux and the Mg II core-to-wing ratio remained stable for 25 years until 2000 was pointed out by Floyd et al. (2005). Vitinsky et al. (1986) pointed out that correlation for relative sunspot numbers vs. radio flux F10.7 does not show the close linear connection during Solar cycles 18, 19 and 20. It is also established by Bruevich and Yakunina (2011) and Bruevich et al. (2012). The phase asynchrony between sunspot numbers and F10.7 solar radio flux is very significant for the study of climate of Sun and various space weather conditions.

The relation between solar activity and coronal index indicates that the ascending phase of the cycle may calibrate largely in terms of total energy released by flares. The daily values of coronal index allow the study of the wide range of variation in Sun. It is well known that synchronization of the Sun is one

key aspect for understanding the origin of evolution of active regions on Sun and their various manifestations in the Solar corona (Zolotova and Ponyavin, 2007).

Our efforts at the research presented were focused on revealing the phase asynchrony between sunspot activity and F10.7 cm solar radio flux using advanced non-linear techniques. Many authors used non-linear techniques for the study of phase relation between the two solar activity parameters. The performance of traditional linear approaches is compromised when dealing with real world data therefore nonlinear techniques are used in this work. There are many advanced nonlinear tools that can be used to examine the phase relationship between two time series (Marwan and Kurths, 2002, 2005). They are also used in numerous scientific researches, such as geophysics, astronomy, and other research fields in the last several decades (Li et al., 2008, 2009; 2010; Deng et al., 2012; Deng et al., 2013).

Currently, many nonlinear analysis approaches, such as those involving the continuous and discrete wavelet transform, the Cross Wavelet transform (XWT), Wavelet Transform Coherence (WTC), and Cross Recurrence Plots (CRPs) are widely used to study the nonlinear behavior of time series (Li 2008). Li et al. (2008) used CRPs and wavelet based techniques for the analysis of high-latitude solar activity (polar faculae) and found phase asynchrony between northern and southern hemisphere. Zolotova and Ponyavin (2007) found that phase synchronization was detected only in the low-frequency modes and the high-frequency component demonstrated a noisy behavior with amplitude synchronization and strong phase mixing. Chatterjee (2001) used an artificial neural network to predict the time series using the F10.7 cm radio flux as an index and concluded that it has a state space dimension of 11 and can be predicted one day in advance with reasonable accuracy.

4.2 Data Set

In this analysis data of daily sunspot numbers and the daily counts of solar radio flux at 10.7 cm are used. Exhaustive explanation of the calculation of the International Sunspot Numbers, which ensure the scaling with respect to

the Zurich Sunspot Numbers, is given in Cugnion (1997) and available online at <http://sidc.oma.be/index.php3>. Further, the sunspot number data are available online at the <http://www.ngdc.noaa.gov>.

4.3 Analysis With Various Techniques

In this work advanced non-linear techniques such as Cross Wavelet Transform (XWT), Wavelet Coherence (WTC) and Cross Recurrence Plots (CRPs) are used to study the phase asynchrony between sunspot activity and F10.7 cm solar radio flux. To maintain the continuity of the paper short description of methods are given in further sub sections.

4.3.1 Mutual Information and Embedding Dimension

The complex nonlinear system attracts to a stable periodic orbit or fixed point, when the maximal Lyapunov exponent is not larger than zero. The modulus of the exponent shows the level of the stabilization (Mininni et al. 2002). The dynamic system should be neutrally stable if the maximal Lyapunov exponent is equal to zero. Moreover, if the Lyapunov exponent is larger than zero, then we can define this system to be chaotic or unstable. The maximal Lyapunov exponent can be considered as the most important Lyapunov exponent because it can be used to define the dynamic properties of a certain system (Rosenstein et al., 1993).

The embedding dimension of a time series can be calculated by Cao algorithm (Kennel et al., 1992). For the time series $x(t)$, we should choose a proper embedding dimension m after selecting the suitable time delay τ .

4.3.2 Cross Recurrence Plots (CRPs)

To measure the phase difference between sunspot number and solar radio flux (F10.7 cm) the Cross-Recurrence Plot (CRPs) method has been used in this work (Marwan et al. 2007). Recurrence plots visualize the recurrence of states of dynamical system in phase space with an arbitrary number of dimensions (Eckmann et al., 1985, 1987). The method of recurrence plots is extended to the cross recurrence plots (CRP), which among other enables the

study of synchronization or time differences in two time series Zbilut et al. (1998). In the cross recurrence plots, the line of synchronization (LOS) is emphasized in a distorted main diagonal. Analytically it is given by

$$CR_{ij}^{m,\varepsilon_i} = \Theta(\varepsilon_i - \|\vec{x}_i - \vec{y}_i\|), \quad \dots\dots\dots (4.1)$$

where $x_i, y_i \in R_m$ ($i = 1, \dots, N_x, j = 1, \dots, N_y$, with N_x and N_y corresponding to the number of days, x_i and y_i are the variables. In this case for the sunspot number and Solar radio flux, ε_i is the threshold distance, $\|\cdot\|$ is the norm (e. g. the Euclidian norm) and Θ is the Heaviside function depends on the difference between the distance of two points and the preferred cut-off distance. Visualization of the CRP is a graphical pattern of the matrix $N_x \times N_y$ and all elements ($CR_{i,j}$) of which are either zero or one. The CRP of the two corresponding time series will not contain a main diagonal, but if the two are similar, a fluctuated line is the CRP linking a distorted main diagonal can occur. This line is called the Line of Synchronization (LOS). In the more common non-stationary case, an off – set of the LOS away from the main diagonal is an indication of a phase shift or a time delay between the two considered time series (Marwan et al., 2004).

4.3.3 Advanced Wavelet Techniques

Detailed discussions of wavelet analysis technique have been given in Chapter 2.

4.4 Results and Discussion

In this study advance non-linear approaches CRP, XWT and WTC are used to investigate the phase asynchrony between solar radio flux and sunspot activity. Figure 4.1, shows the daily counts of solar radio flux (F10.7) (upper panel) and sunspot number (bottom panel) in the time interval from January, 1996 to December, 2013. It was noticed that the daily Solar activity seems to have good phase synchronization at the ascending and descending phase of the Solar cycle 23 and ascending phase of Solar cycle 24. It was noticed that

the solar activity maxima occur at least during a cycle first near the end of the ascending activity phase and then in the early years of descending phase.

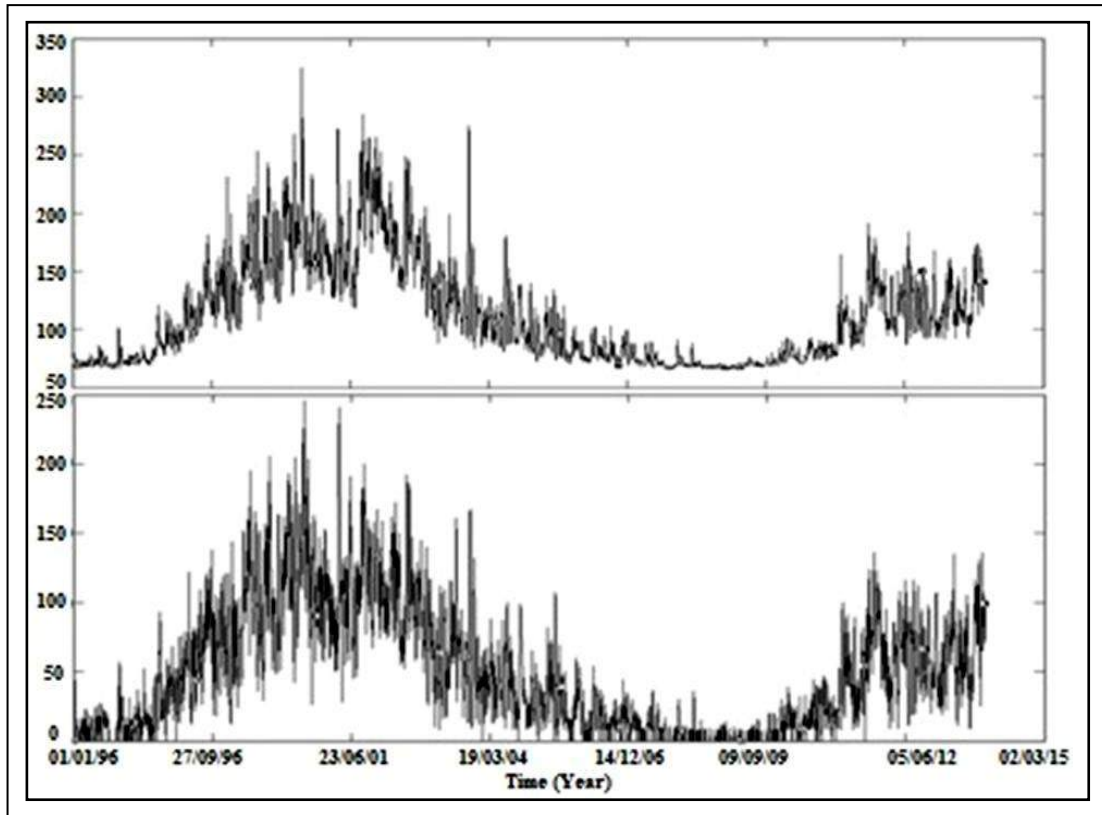


Figure - 4.1: Plots of daily counts of Solar radio (F10.7cm) flux (upper panel), and sunspot numbers (lower panel).

Figure 4.2 (upper panel) and (lower panel) show the graph of mutual information of Solar radio flux and sunspot numbers as a function of time delay. Fraser and Swinney (1986) suggested that the value of the time delay is the value when the mutual information exhibits a marked first minimum. The value of time lag for sunspot numbers and solar radio flux are 35 and 27 respectively. Mathematical algorithm written by Cao (1997) used to estimate the embedding dimension of solar radio flux and sunspot number and the result are displayed in Figure 4.3 (upper panel) and (lower panel). It was noticed that the value of E_1 is almost constant from 13 to 35 therefore the value of the embedding dimension of sunspot numbers is equal to 13 and for Solar radio flux is 10. The sunspot numbers and Solar radio flux time series is a fixed signal, but according to figure E_2 does not always equal to 1, which implies that the scalar Solar activity exhibits the dynamical properties of a low dimensional data deterministic chaos.

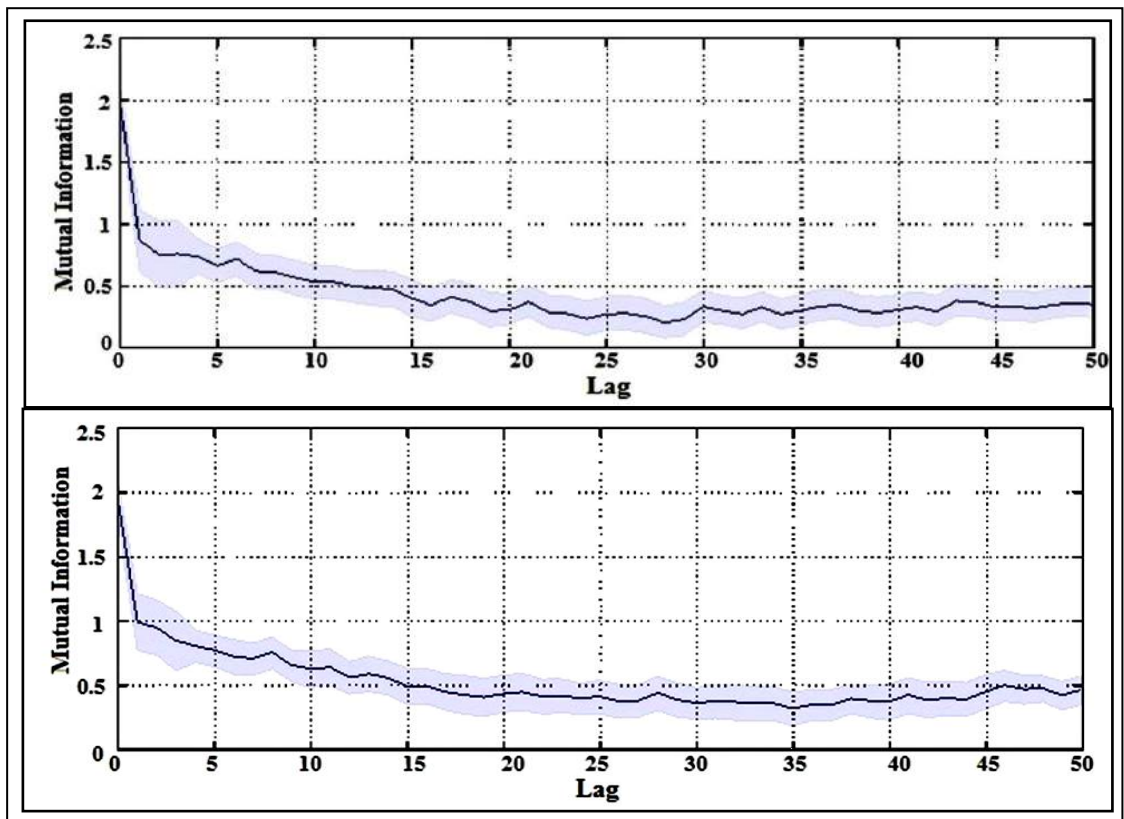


Figure - 4.2: Plots of Mutual information as a function of Time Lag for Solar radio flux (upper panel) and sunspot numbers (lower panel)

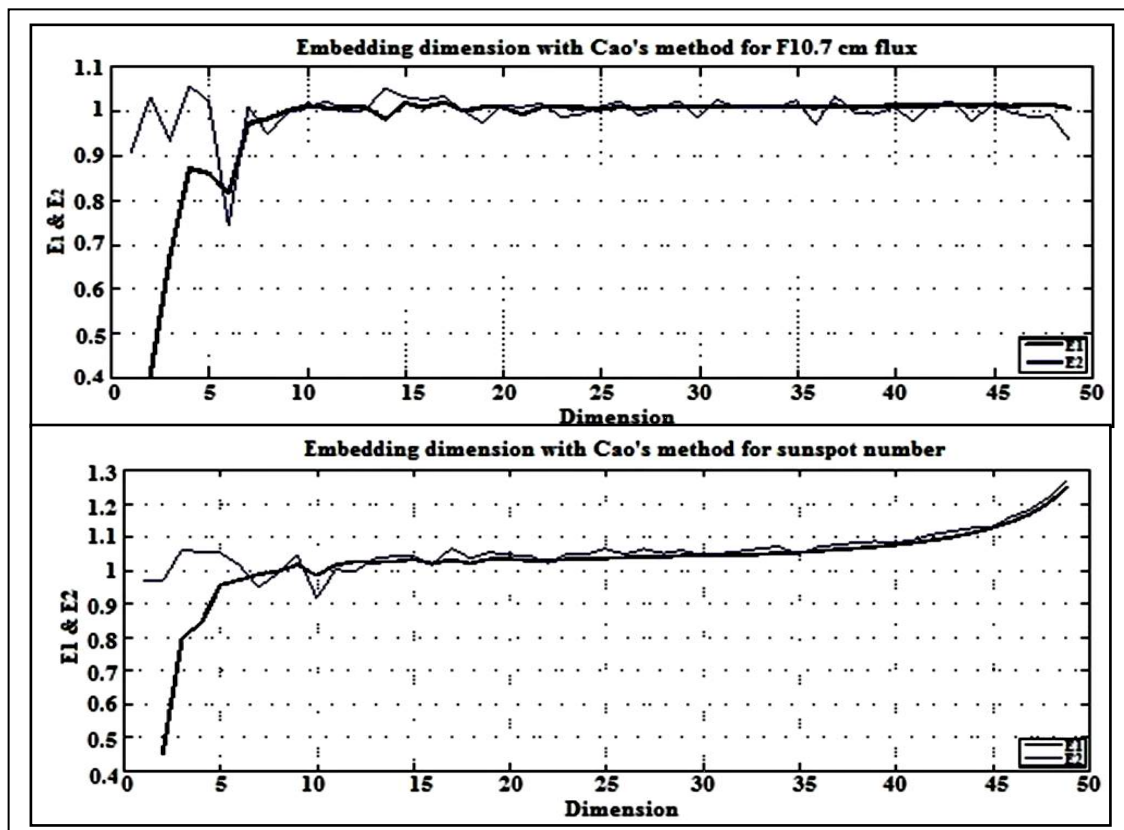


Figure - 4.3: Variables of E_1 and E_2 as a function of Dimension for Solar radio flux (upper panel) and sunspot numbers (lower panel)

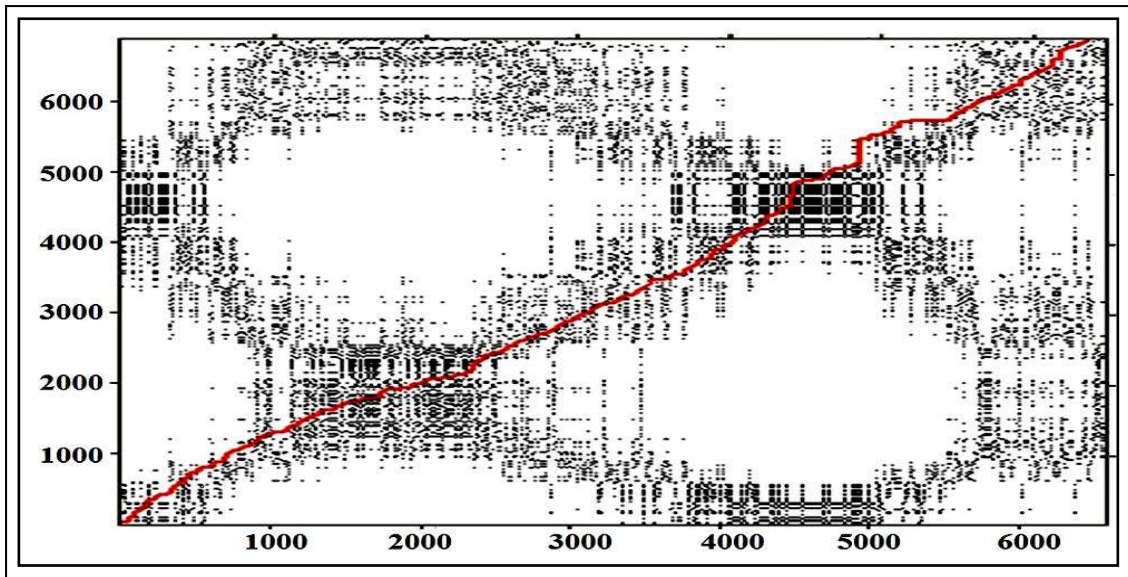


Figure - 4.4: Cross recurrence plot (CRP) of Sunspot number and Solar radio flux with the characteristics of Dimension: 1, Delay: 1, Threshold: 10% (fixed neighbors amount). Both axes are time axis day of year (DOY) from January 1, 1996 to December 3, 2013. Red line shows the Line of Synchronization (LOS)

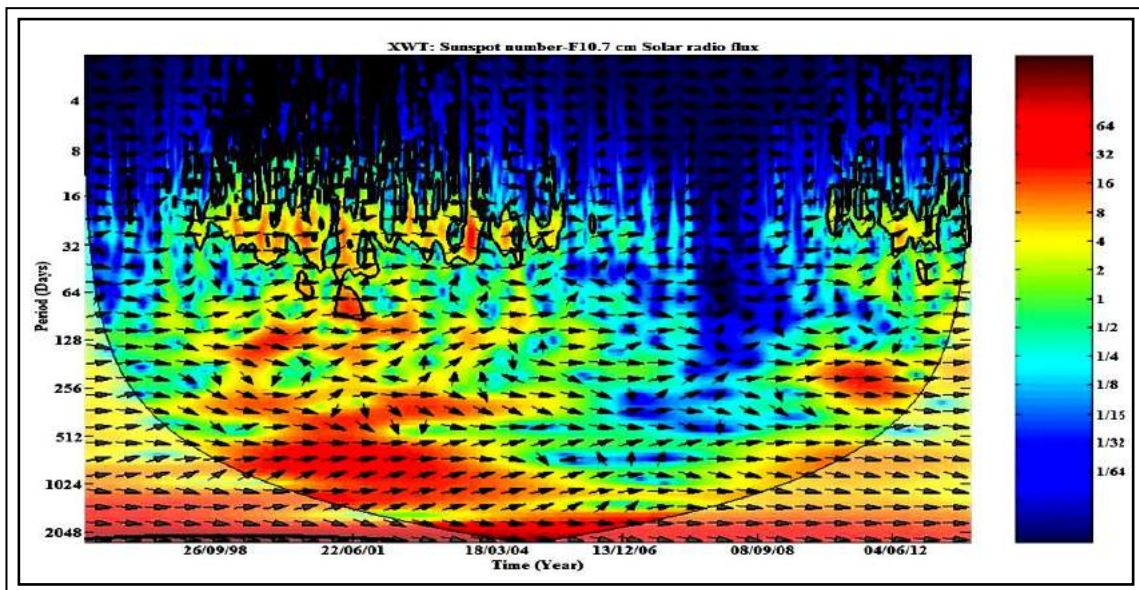


Figure - 4.5: Cross-wavelet transform (XWT) of Sunspot number and solar radio flux. The black contour indicates the 5% significance level. The cone of influence, which indicates the region affected by edge effects, is shown with a thin black line. The color code for power ranges from blue (low power) to red (high power)

Figure 4.4, shows the CRPs between daily counts of sunspot number and solar radio flux (F10.7cm). In figure black dots mark a recurrence and both axes are time axes. The regions around the days of activity (points) 2000 and 5000 (i.e. Days of years 2001 and 2008) corresponds to the period of high Solar activity. At 2000 point (cycle 23), the recurrences (black dots) are nearly equal, but around 5000 black dots evidence the difference in time when the

maximum of activity is reached. Also deviation of line of synchronization (LOS) slightly from the main diagonal (it related to the frequencies and phases of the systems considered) shows the level of synchronization (or time difference in two time series) between Solar radio flux and sunspot numbers at the maximum and declining phase of Solar cycle 23 (years 2001 and 2008 i.e. around the points 2000, 4000 - 5500). Dispersive points show the close correlation to the maximum phase.

Figure 4.5, displayed the XWT between the daily counts of sunspot number and Solar radio flux. Arrows represents the phase relation in time frequency space. Arrows point to the right when the two processes are in phase and to the left when they are in out of phase. If an arrow points up, then the first process lags behind the second one. From a statistical point of view, the reliable results are located within the cone of influence and the arrows beyond the cone of influence are not reliable (Torrence and Compo, 1998; Moortel, et al., 2004). The thin black curve (inside COI) demonstrates the periods above 95% confidence level (Torrence and Compo, 1998).

It is found that almost all of the arrows are horizontal and point to the right in the low frequency ranges, which suggested that Solar radio flux (F10.7) and sunspot numbers are in phase around the periodic scales of about 512 - 1024 days (*i.e.* 1.4 year - 2.8 year). However, there still have small phase deviations within these areas, the arrows subtend a small angle with the horizontal upward direction, which implies that F10.7 cm flux slightly lags behind the sunspot numbers. The Solar activities indicators show the asynchronous behavior during the year 2008 - 2009 at higher frequency band (see Figure 4.5). In the higher frequency bands (less than 256 days), all the significance levels (small black contours) inside the cone of influence (COI) represents the periodicity around 27 day (the Sun's rotational period around the equatorial) from 1996 to 2013. This result is in agreement with the previous study done by many researchers with the different solar parameters (Ness and Wilcox, 1964; Willson et al., 1999; Yin et al., 2007; Kilcik et al., 2010).

On the other side, lower frequency band (512-1024 days) shows the phase asynchronization during the time interval of 2000 - 2005, which is

considered as maximum phase and highly disturbed period of the Solar cycle 23. It was also noticed that Solar parameters shows day - to - day periodic variation it was due to the fact that radio flux (F10.7) originates from upper atmospheric layers of Sun's chromosphere and lower in its corona, changes steadily in response to the number of spot groups on the Solar disk. Bachmann and White (1994) reported that the phase shifts exhibit an odd-even pattern (there is no time lag or lead for cycles 20 and 21; there is one month time lag for cycles 22 and 23).

The cross wavelet transform and wavelet coherence (Figures 4.3 and 4.4) reveals the strong phase mixing in the high frequency component sunspot number and solar radio flux. Zhang et al. (2012) suggested that it may explain the various properties of the photosphere and corona on a short time scale. The wavelet coherence and phase difference for two frequency bands (namely 3.5 - 7 and 7 - 14 year bands) are shown in Figure 4.6 (b) and 4.6 (c).

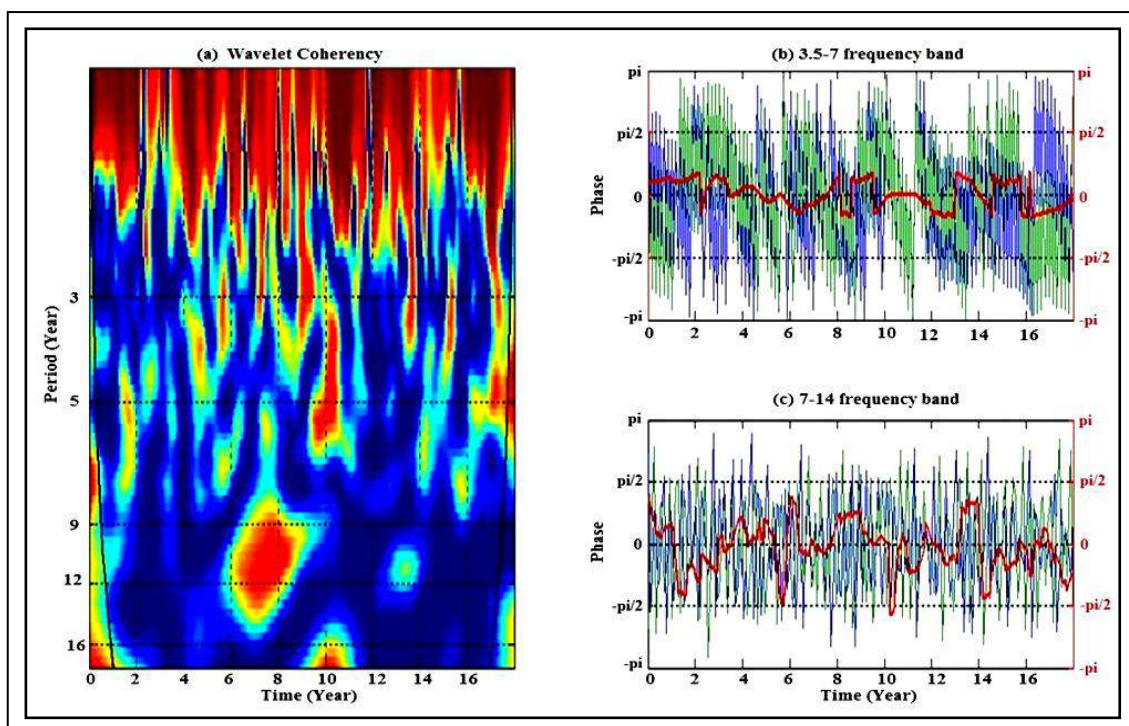


Figure - 4.6: (a) Wavelet coherence (WTC) between monthly counts of Sunspot number and solar radio flux (F10.7) from the period of 1996 to 2013. The cone of influence is shown with a thick black line. Coherency ranges from blue (low coherency) to red (high coherency). Figures (b) and (c) represents phase difference between monthly values of Sunspot number and solar radio flux (F10.7) with different frequency bands. Red line in figures (b) and (c) represents the phase difference between sunspot number and solar radio flux. The blue line represents sunspot number phase and green line represents solar radio flux phase

The wavelet coherency is essentially useful in highlighting the time and frequency interval where two phenomena have a strong phase interaction (Perez - Peraza, 2008). When a particular Solar cycle is strong, the value of the phase difference becomes in phase and vice versa. It was found that F10.7 cm flux lagging behind the sunspot numbers. The phase difference fluctuate violently at 7 - 14 frequency band (period scale around the 11 year Schwabe cycle) than 3.5 - 7 frequency band during the minimum and maximum phases of the cycle, which shows non-linear behavior in both the frequency bands. In Figure 4.6 (b), during the ascending phase (i.e. 0 - 2 years) of Solar cycle 23 the sunspot number leads by 90° to the Solar radio flux and at the declining phase (8.5 - 12.5 years) the Solar radio flux leads by 90° to sunspot number. Nearly strong correlation between the F10.7 cm radio flux and the sunspot number show an origin of weak magnetic fields. Both the Solar activity parameters viz. sunspot number and solar radio flux shows highly turbulent during the maximum phase of Solar cycle 23. Figure 4.6(c) displayed the phase difference of the solar activity parameters at 7-14 year frequency band. It is concluded that odd Solar cycle 23 is highly disturbed in comparison to even cycle 24. During the Solar cycles 23 and 24 sunspot number and solar radio flux have phase difference of one month. This result is an agreement with that of Bachmann and White (1994).

These analyses present that the different characteristics of sunspot number to the F10.7 cm radio flux at the lower and higher frequency band and it is verifying that sunspot number lead (0 to $\pi/2$) to the F10.7 cm radio flux during the initial (0-2 year band), maximum (3-5 year band) and in the declining phase (7-9 year band) of the Solar cycle 23. The initial phase (11 - 14 year band) of cycle 24 sunspot number leading but at the maximum phase of Solar cycle 24, F10.7 cm radio flux leading to the sunspot number. The Figures 4.7 and 4.8 illustrate the cross wavelet and wavelet coherence of sunspot number and solar radio flux respectively. The cross wavelet transforms reveals the ~ 28 days periodicity same as the wavelet coherence.

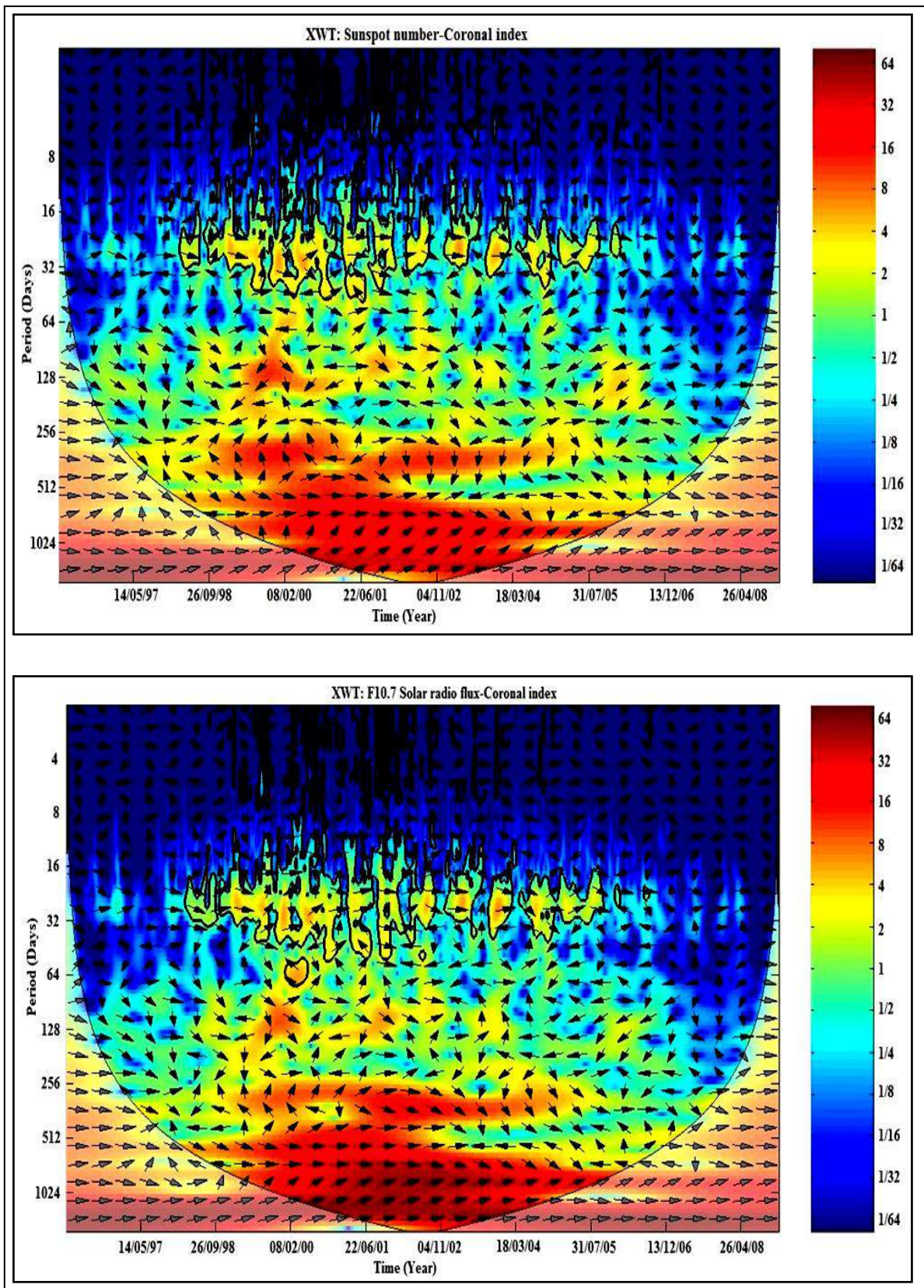


Figure - 4.7: Cross-wavelet transform (XWT) of daily counts of Sunspot number and coronal index, Time ranging from 1996 to 2008 (Solar cycle 23). The black thick contour indicates the 5% significance level. The cone of influence, which indicates the region affected by edge effects, is shown with a thin black line. The color code for power ranges from blue (low power) to red (high power)

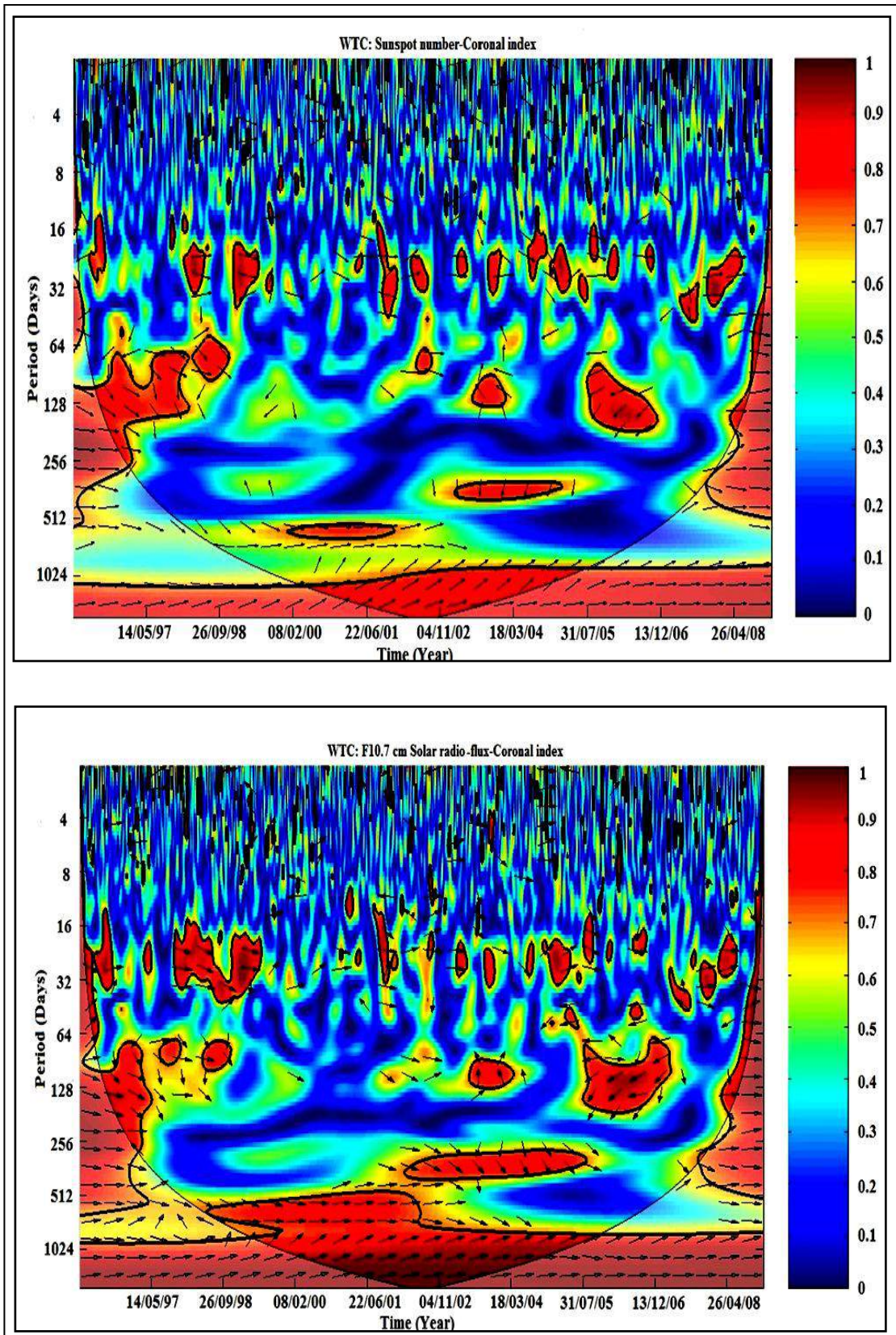


Figure - 4.8: Wavelet coherence (WTC) between daily counts of Solar radio flux and Coronal index (upper panel), Sunspot number and coronal (lower panel) index from the period of 1996 to 2008 (Solar cycle 23). The cone of influence is shown with a thick black line. Coherency ranges from blue (low coherency) to red (high coherency)

4.5 Conclusions

In this chapter, we studied the phase relation between sunspot number and radio flux at 10.7 cm using various non-linear techniques. To confirm our result we calculate the wavelet cross correlation and wavelet coherence of sunspot number and solar radio flux with the coronal index (CI) respectively. The quantitative CI represents the total energy emitted by the sun's outermost atmosphere at the wavelength of 530.3 nm. Cross wavelet Transform (see Figure 4.5) between sunspot numbers and Solar radio flux (F10.7cm solar radio flux) shows that the power is mainly concentrated at ~ 27 days, where as for sunspot numbers and coronal index (CI) as well as F10.7 cm radio flux and CI it is also concentrated around 27 days (See in Figures; 4.7 and 4.8).

The rotational characteristic manifests a strong phase asynchrony with respect to the solar equator. Therefore, there should certainly exist difference between the two caused by their different definitions. The relationship between the CI and SNs is not precisely linear some time it is not correlated with SNs (Deng et al. 2012). Different value of time lag for sunspot numbers and Solar radio flux shows that they are originated from different layers of Solar disc (i.e. photosphere and chromosphere) Sunspot activity is affected by the convection zone and the inner layer of the chromosphere. However, the Solar radio flux affected by the outer layer of the chromosphere and inner corona. These phenomena may responsible for the phase relationship (Zhang et al., 2012). Zhang et al., (2012), established the phase relationship between smoothed monthly mean sunspot number and F10.7 cm flux. They shows Schwabe cycle belt sitting across the region of high spectral power. A relation exists between the 2800 MHz (10.7 cm) solar radio flux observed by ground stations and the sunspot number as defined by Wolf (Covington, 1969 and Hathaway et al., 2002).

Our results are in agreement with Wilson et al., (1987) they found also near Solar maximum the F10.7 cm radio flux follows more closely the observed number of sunspots than the Zurich sunspot number, which is more strongly influenced by the number of sunspot groups. Deng et al. 2013 also reported that F10.7 cm radio flux lags behind SNs during most parts of time series from

period of 1950 to 2010 and their relative phase difference vary from -4 to 3 months with a mean value of -1.5 months. He concluded that these activity indicators are more asynchronous about the minimum and maximum of a Solar cycle as compared to ascending and descending phases of the cycle.

The phase relationship between them is not only time-dependent but frequency dependent also. The maximum of F10.7 cm solar radio flux occurs about 1.5 years after the maximum of sunspot numbers in Solar cycles 20 and 21, while there is no lag between them in Solar cycles 18 and 19 (Wilson et al., 1987). Cliver and Ling, (2001) proposed that the cosmic-ray cycle appears to lag behind the sunspot cycle by about one year for odd-numbered cycles (as 19 and 21) while even numbered cycle keep in phase. Therefore, these analyses may also conclude that the odd-even numbered cycles (as 23 and 24) essentially not in phase. Fligge and Solanki (1997) show good agreement between the inter - cycle variations of 10.7 cm radio flux relative to Zurich sunspot relative number and sunspot area over cycles 18 to 20 which are no longer true for Solar cycles 21 and 22.

The numbers of soft X-ray flares and H α flares have an obvious time lag in the odd-numbered Solar cycles and no time lag in the even-numbered Solar cycles with respect to sunspot number for the entire Sun and both hemispheres (Temmer et al., 2003). Yan et al. (2012) also found that smoothed monthly solar radio flux at 2800 MHz has a time lag for cycles 22 and 23 and no time lag for cycles 20 and 21 with respect to the smoothed monthly sunspot number. Finally, we conclude that the cross recurrence plots of sunspot number and solar radio flux have information about the synchronous behavior of data series. We found that phase synchronization only in the initial and at maximum phase of cycles 23 and its component demonstrated a noisy behavior at the declining phase of cycle 24.

This result suggests that their non-linear features as the sunspots group reveals on the photosphere and the radiation affected by number of sunspots decreasing. The cross wavelet transform shows the strong phase interaction at the maximum phase of cycles and has the periodicity of 27 day associated with the average solar rotation period for active regions. Mavromichalaki, et al

(2005) also suggested that the 27 days synodic repetition is a good indicator of the global sectorial pattern of heliospheric magnetic fields. This periodicity suggest that the formation of sunspots start from higher latitudes and in advancement stage formation zone slowly moves towards the equator approaching some saturation during the maximum activity years. These findings suggest that the magnetic field system originating on the photosphere in form of active regions (sunspot numbers or areas) and their evolutions in the course of the Solar cycle are inadequately coupled.

Multifractal Analysis of Sunspot Number Time Series

5.1 Introduction

Solar activities are related with the magnetic field of Sun. Its strength at a typical point on the solar surface is a few gauss. However significant variation in this value and there are localized regions known as sunspots, in which the field can much higher (Bray *et al.*, 1979). The sunspots are formed above the surface of Sun and extended out into the Sun's Corona. Due to symmetry of twisted magnetic lines as the origin of sunspot, they are generally seen in pairs or in groups of pairs at both sides of the solar equator. As the sunspot cycle progresses, spots appear closer to sun's equator giving rise to the so called "butterfly diagram" in the time latitude distribution (Petrovaye, 2000). The twisted magnetic fields above sunspots are sites where Solar flares are observed. It has been found that chromospheric flares show a very close statistical relationship with sunspots (Bray *et al.*, 1979).

The number of sunspots continuously changing in time in a random fashion and constitutes a typically random time series. Time series analysis approach for analyzing and understanding real world problems such as climatic and financial data is quite popular in the scientific world (Addison (2002), Feder(1988), Kumar and Foufoula (1993a), Kumar and Foufoula (1997), Lafreniere and Sharp (2003), Mandelbrot and Hudson (2004), Meyer (1998), Rangarajan and Sant (2004). Till a decade ago, statistical and Fourier analysis methods were quite popular for studying the behavior of real world data. However, recently wavelet and fractal methods are applied for a better understanding of the behavior of such series Addison (2002), Arneodo *et al.* (2003), Hu and Nitta (1996), Kulkarni (2000), Kumar and Foufoula (1993b, 1993c), Mallat (1999), Rangarajan and Sant (2004), Turiel *et al.* (2006).

Fractal and multifractal algorithms have been applied broadly to photospheric magnetic field data. Sunspots remain the best known manifestation of solar magnetic activity and its cycle, and thus have been a subject of extensive research. Indeed, sunspots and related activities have been analyzed by various methods, including correlation analysis (Bogart, 1982; Temmer *et al.*, 2002), Chaos analysis (Veronig *et al.*, 2000; Jevtic *et al.*, 2001) and multifractal analysis (Abramenko, 2005; Movahed *et al.*, 2006; McAteer, *et al.*, 2007). Multifractal theory provides an elegant statistical characterization of many complex dynamical variations in nature and engineering (Gao, *et al.*, 2006; 2007). It is conceivable that it may enrich characterization of the sun's magnetic activity and its dynamical modeling (Howe *et al.*, 2000).

In recent times, a particularly noteworthy work has been reported by Movahed (Movahed *et al.*, 2006). Abramenko *et al.* (2002) found that the relative fraction of small scale fluctuation in the magnetic field contribute significantly more prior to flaring. Abramenko *et al.* (2005) found that active regions reach a critical state of intermittency prior to flaring. The multifractal scaling behaviors reported by Movahed *et al.*, (2006) are valid for timescales up to more than 50 years. Movahed *et al.*, (2006) raised the question; this inconsistency compels us to question the relevance of the reported multifractality to sunspots: is it a genuine property of the sunspots or is it an irrelevant feature simply introduced by the specific filtering technique employed.

5.2 Data Set

In this analysis we used the monthly counts of sunspot number for the multifractal analysis from the time span of 1964 to 2013. This period include complete Solar cycles 20 – 23 and ascending phase of Solar cycle 24. The data set are available online and downloaded from <http://www.ngdc.noaa.gov/stp/space-weather/Solar-data/Solar-indices/>.

5.3 Theoretical background

In this chapter we studied the multifractal characteristics of sunspot number using wavelet based multifractal analysis technique. We have also analyzed the regularity of sunspot data using wavelet based non-parametric approach.

5.3.1 The Discrete Wavelet Transform (DWT)

The detail information of this method was given in Chapter - 1.

5.3.2 Wavelet Based Multifractal Formalism

Anomalous variation in sunspot data creates large amplitude wavelet coefficients. The wavelet transform not only locates isolated anomalous events, but can also characterize more complex multifractal sunspot data having non isolated singularities. Multifractal objects cannot be completely described using a single fractal dimension (mono fractals). They have an infinite number of dimension measures associated with them. The wavelet transform takes advantage of multifractal self- similarities, in order to compute the distribution of their singularities. This singularity spectrum is used to analyze multifractal properties. The time series of sunspot numbers usually depict fractal or multifractal features. Time series are commonly called self- affine functions as their graphs are self-affine sets that are similar to themselves when transformed by anisotropic dilations.

Mathematically, if $f(x)$ is a self- affine function representing the sunspot data then, For $x_0 \in R, \exists H \in R$ such that for any $\lambda > 0$,

$$f(x_0 + \lambda x) - f(x_0) \cong \lambda^H (f(x_0 + x) - f(x_0)) \quad \dots \dots (5.1)$$

The exponent H here is called roughness or Hurst exponent. Note that if $H < 1$, then f is not differentiable and smaller the exponent H , the more singular is f .

Hurst exponent indication indicates that how globally the function $f(x)$ is regular. It relates fractal dimension D_F as $D_F = 2 - H$. Fractal functions can possess multi-affine properties in the sense that their roughness (or regularity) may fluctuate from point to point. To describe these multifractal functions, one thus needs to change slightly the definition of the Hurst regularity of f so that it becomes a local quantity

$$|f(x+l) - f(x)| \sim l^{h(x)} \quad \dots \dots (5.2)$$

The local Hurst exponent $h(x)$ is generally called Holder exponent of f at the point x . For sunspot data time series $f(t)$, a function $h(t)$, the Holder function of f , which measures the regularity of f at which point t is associated.

The point wise Holder h of f at point x_0 is defined as

$$h(x_0) = \lim_{\rho \rightarrow 0} \inf \{h: \exists c > 0, |f(x) - f(x_0)| \leq c|x - x_0|^h, |x - x_0| < \rho\} \dots \dots (5.3)$$

(Here h is an integer and f is non-differentiable).

One may also define local exponent $h_l(x_0)$ as

$$h_l(x_0) = \lim_{\rho \rightarrow 0} \sup \{h: \exists c > 0, |f(x) - f(y)| \leq c|x - y|^h, |x - x_0| < \rho, |y - x_0| < \rho\} \dots \dots (5.4)$$

Where h and h_l are different in general. For example

$$f(x) = |x|^h \sin \frac{1}{|x|^\beta}, h(0) = 0, \text{ while } h_l(0) = \frac{h}{1 + \beta} \quad \dots (5.5)$$

They have quite different properties. For instance h_l is stable through differentiation ($h_l(f', x_0) = h_l(f, x_0) - 1$), whereas h is not. The smaller $h(x)$ is, the more irregular the function f is at t .

5.3.3 Partition Function

It is not possible to calculate the Pointwise Lipschitz (Holder) regularity of a multifractal because its singularities are not isolated, and the finite numerical resolution sufficient to discriminate them. To overcome this difficulty Muzy et

al. (1994) have introduced the concept of wavelet transform modulus maxima using a global partition function (Arneodo *et al.*, 2003). Let Ψ be a wavelet with n vanishing moments. Mallat has shown that if f has a pointwise Holder (Lipschitz) regularity $\alpha_0 \leq n$ at v then the wavelet transform $T_\psi f(a, b)$ has a sequence of modulus maxima that converges towards v at fine scales. The set of maxima at the scale a can thus be interpreted as a covering of the singular support of f with wavelets of scale a . At these maxima locations

$$|T_\psi f(a, b)| \approx a^{\alpha_0+1/2} \dots \dots \dots (5.5)$$

Let $\{u_p(a)\}_{p \in \mathbb{Z}}$ be the position of all local maxima of $|T_\psi f(a, b)| \approx a^{\alpha_0+1/2}$ at a fixed scale a . The partition function Z measures the sum at a power q of all these wavelet modulus maxima

$$Z(q, a) = \sum_p |T_\psi f(a, u_p)|^q \dots \dots \dots (5.6)$$

For each $q \in \mathbb{R}$, the scaling exponent $\tau(q)$ measures the asymptotic decay of $Z(q, a)$ at fine scale a

$$\tau(q) = \liminf \frac{\log Z(q, a)}{\log a} \dots \dots \dots (5.7)$$

This typically means that $Z(q, a) \sim a^{\tau(q)}$.

5.4 Analysis

In this chapter we have analyzed the multifractal characteristics of sunspot number during the Solar Cycles 20 to 23 and current Solar Cycle 24 using wavelet based multifractal techniques.

5.4.1 Wavelet analysis of Sunspot Numbers

Wavelet analysis is a tool for analyzing localized variations of power within a time series (Lau and Wang, 1995; Torrence and Compo, 1998). In this section, a given data set is divided into components with different scales, which allows the investigation of each component with a resolution matched to its scale. This property is especially useful for signals that are non-stationary,

having short-lived transient components and have features at different scales or have singularities (Kumar and Foufoula-Georgiou, 1997). In the present analysis both Daubechies and Coifmann wavelets are used as mother wavelet to decompose considered time series and Morlet wavelets are used for Multifractal spectral analysis.

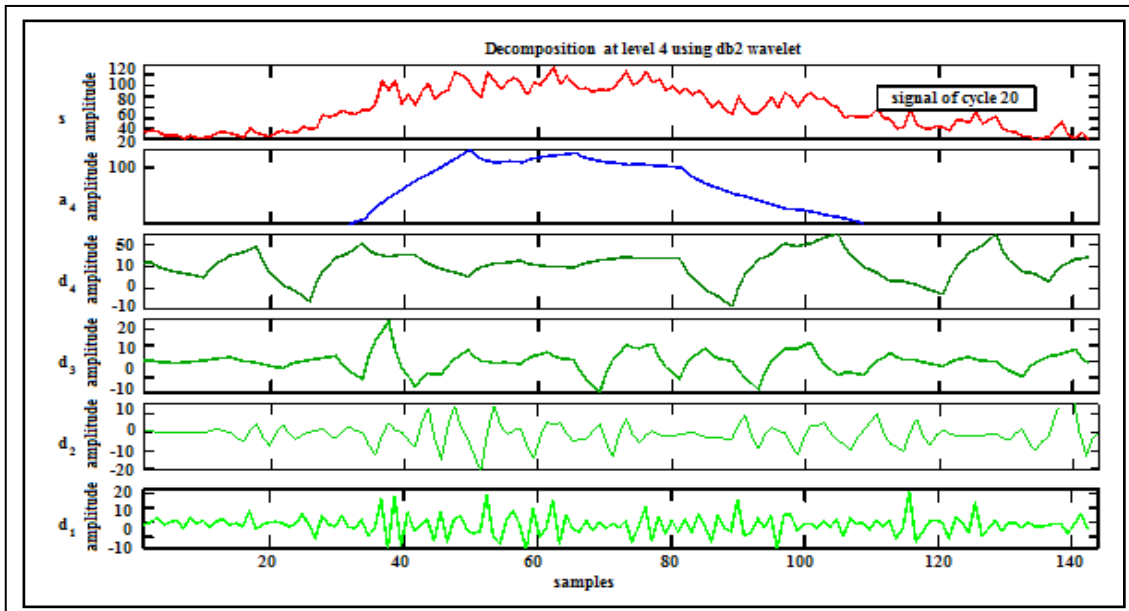


Figure - 5.1: DWT decompositions of Solar Cycle 20 using Daubechies2 wavelet. Anomalous variation should be found at 50 no. of samples (i.e. at the maximum phase of cycle)

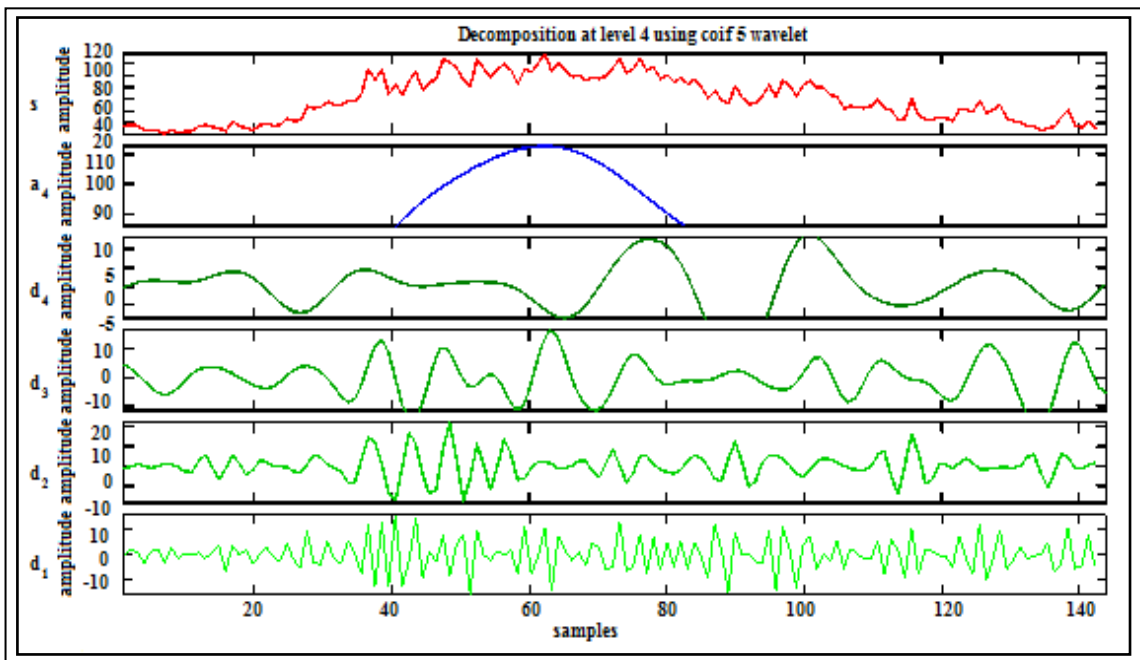


Figure - 5.2: DWT decomposition of Solar Cycle 20 using Coifman5 wavelet. Anomalous sharp variation should be found between 60 to 65 no. of samples (i.e. at the maximum phase of cycle)

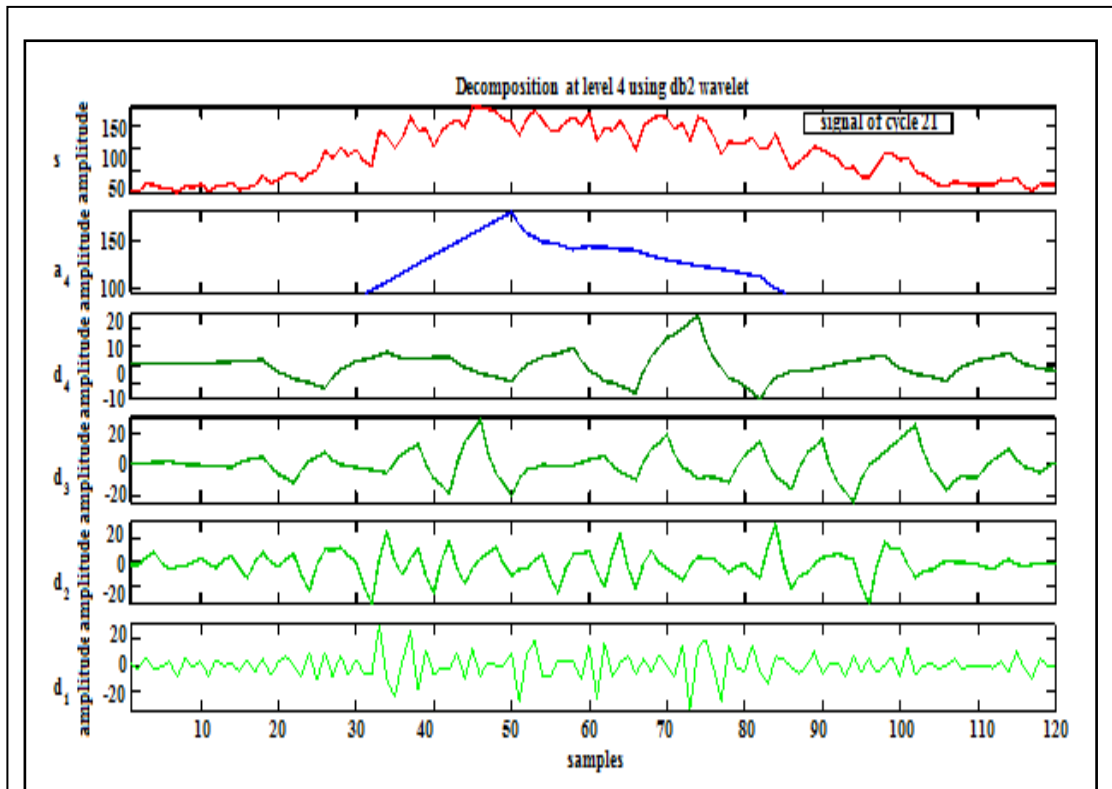


Figure - 5.3: DWT decompositions of Solar Cycle 21 using Daubechies2 wavelet. Anomalous sharp variation should be found at 50 no. of samples (i.e. at the maximum phase of cycle)

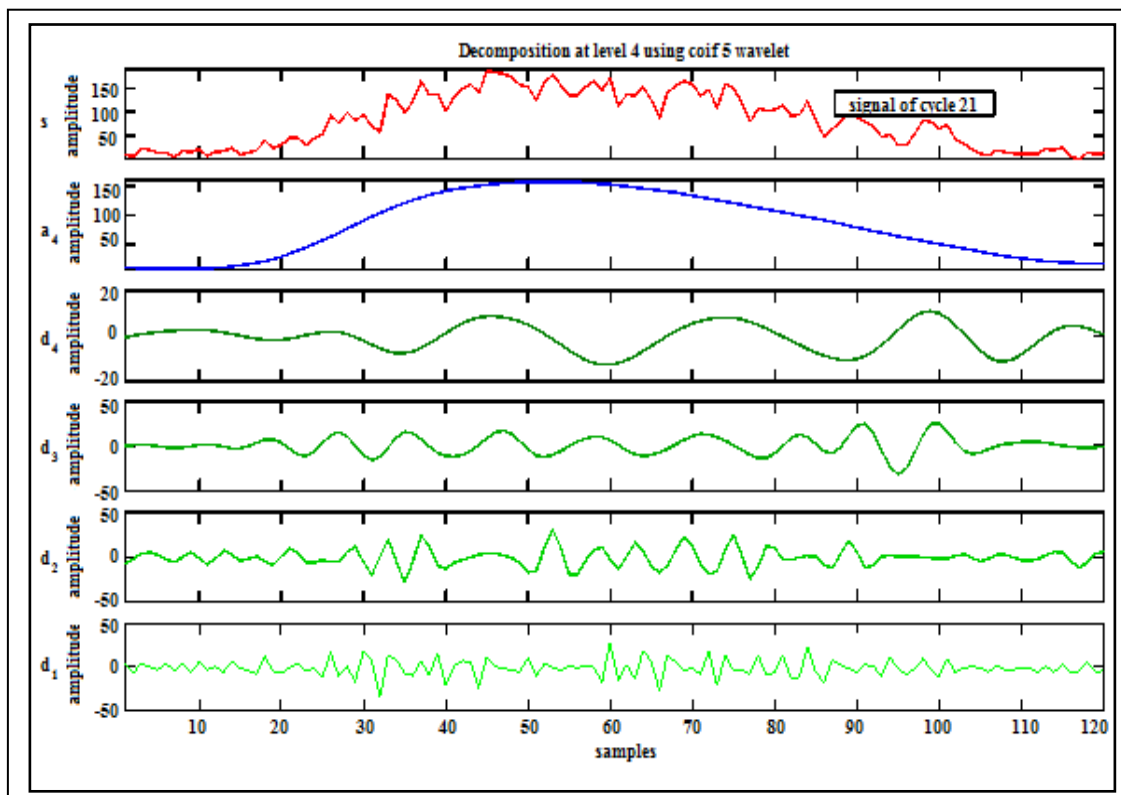


Figure - 5.4: DWT decompositions of Solar Cycle 21 using Coifman5 wavelet. Anomalous sharp variation should be found between 48 to 58 no. of samples (i.e. at the maximum phase of cycle)

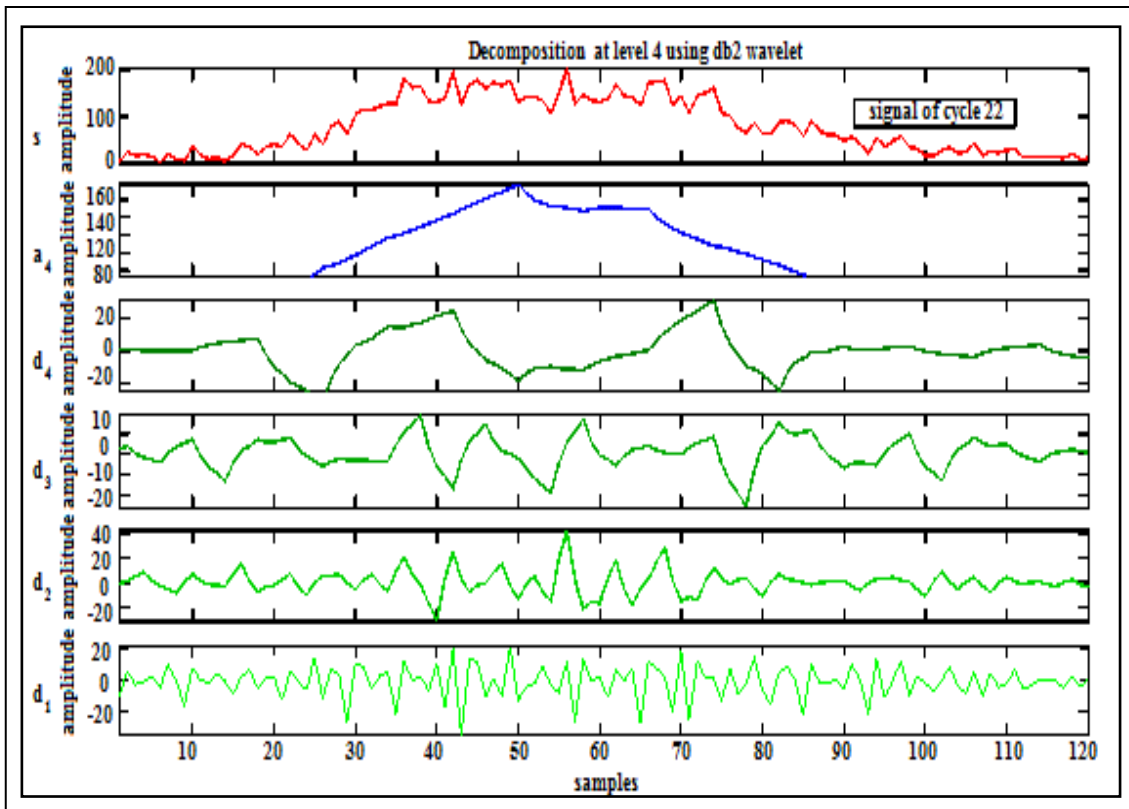


Figure - 5.5: DWT decompositions of Solar Cycle 22 using Daubechies2 wavelet. Anomalous variation should be found at 50 no. of samples (i.e. at the maximum phase of cycle)

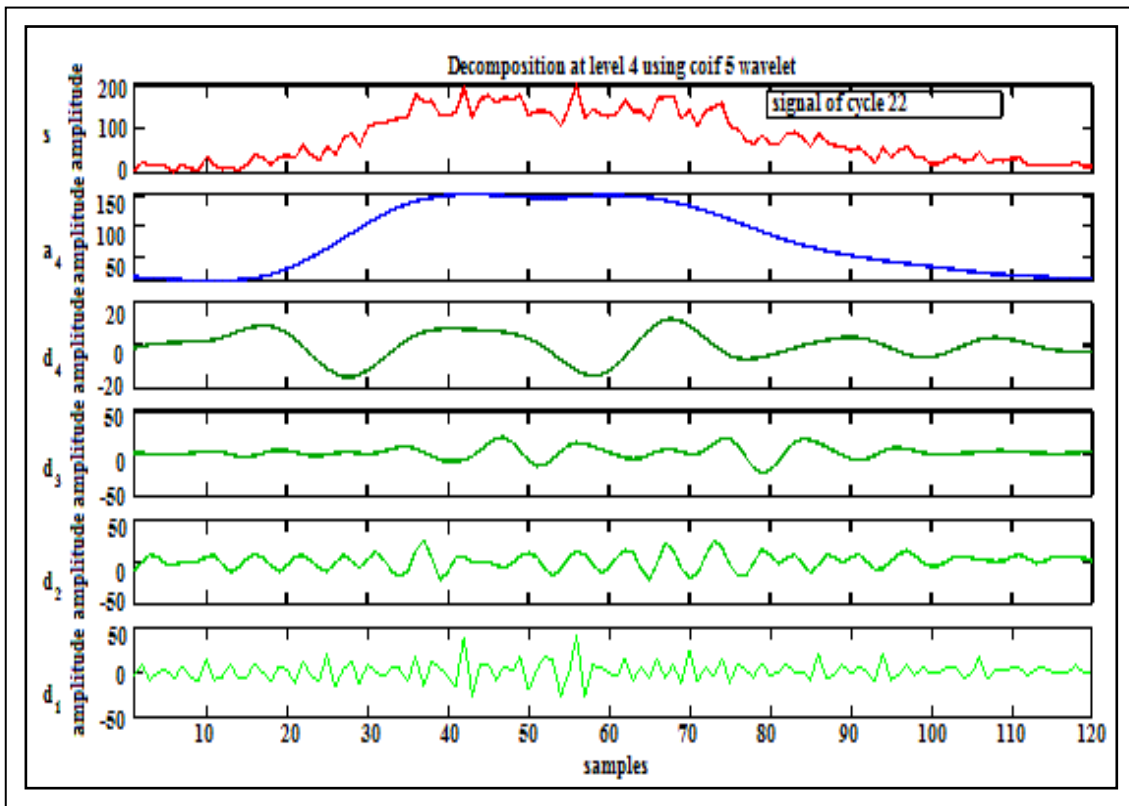


Figure - 5.6: DWT decompositions of Solar Cycle 22 using Coifman5 wavelet. Anomalous sharp variation should be found between 40 to 60 no. of samples (i.e. at the maximum phase of cycle)

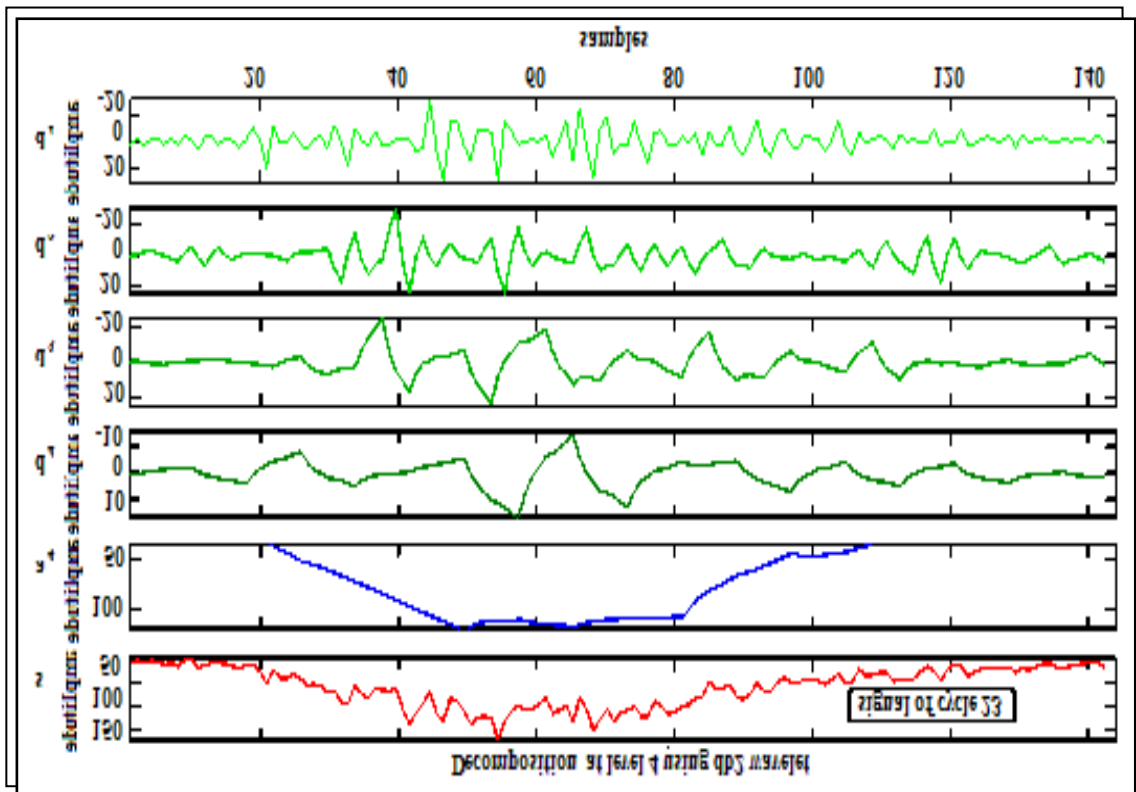


Figure - 5.7: DWT decompositions of Solar Cycle 23 using Daubechies 2 wavelet. Anomalous variations should be found between 45 to 80 no. of samples (i.e. at the maximum phase of cycle)

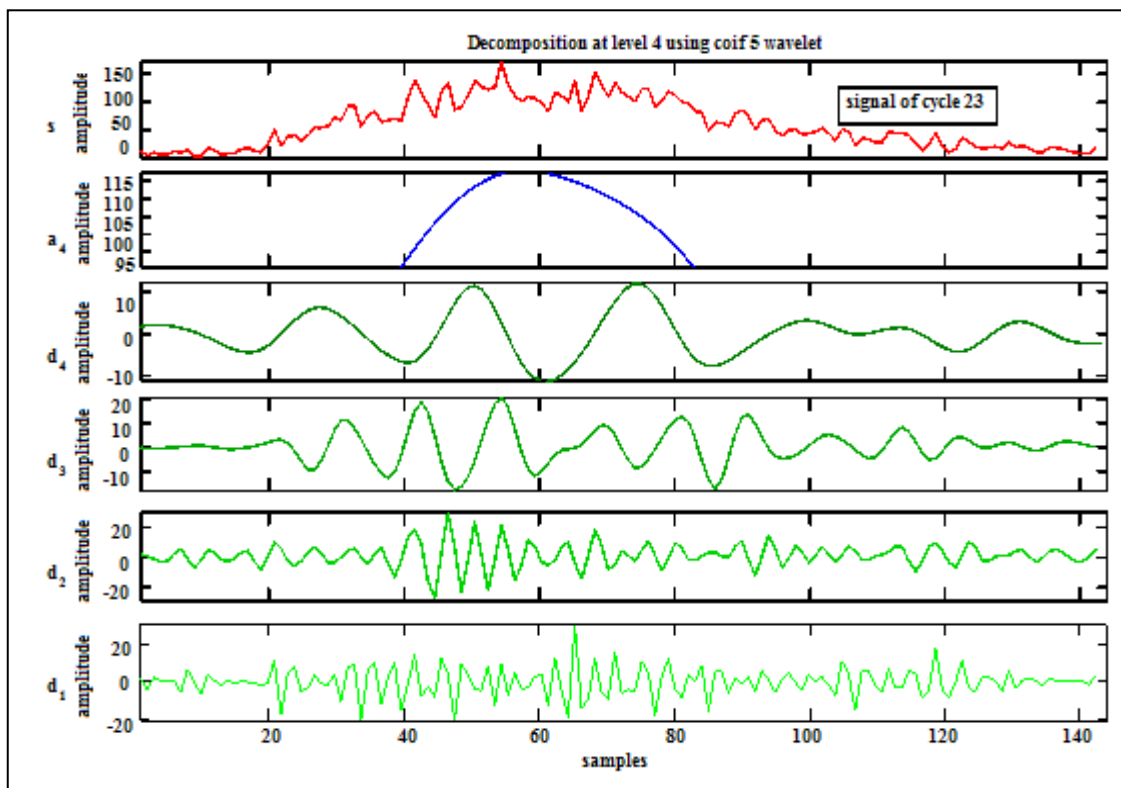


Figure - 5.8: DWT decompositions of Solar Cycle 23 using Coifman5 wavelet. Anomalous sharp variation should be found at 58 no. of samples (i.e. at the maximum phase of cycle)

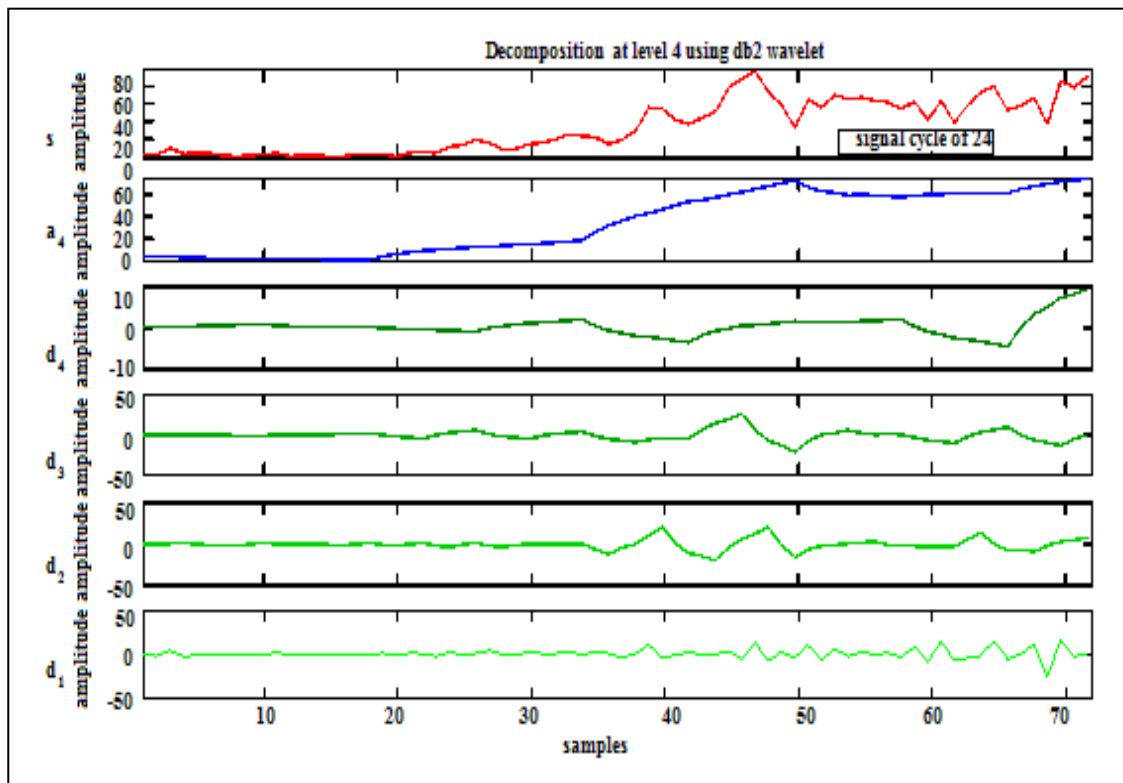


Figure - 5.9: DWT decompositions of Solar Cycle 24 using Daubechies2 wavelet. Anomalous variation found at 50 no. of samples (i.e. at the maximum phase of cycle)

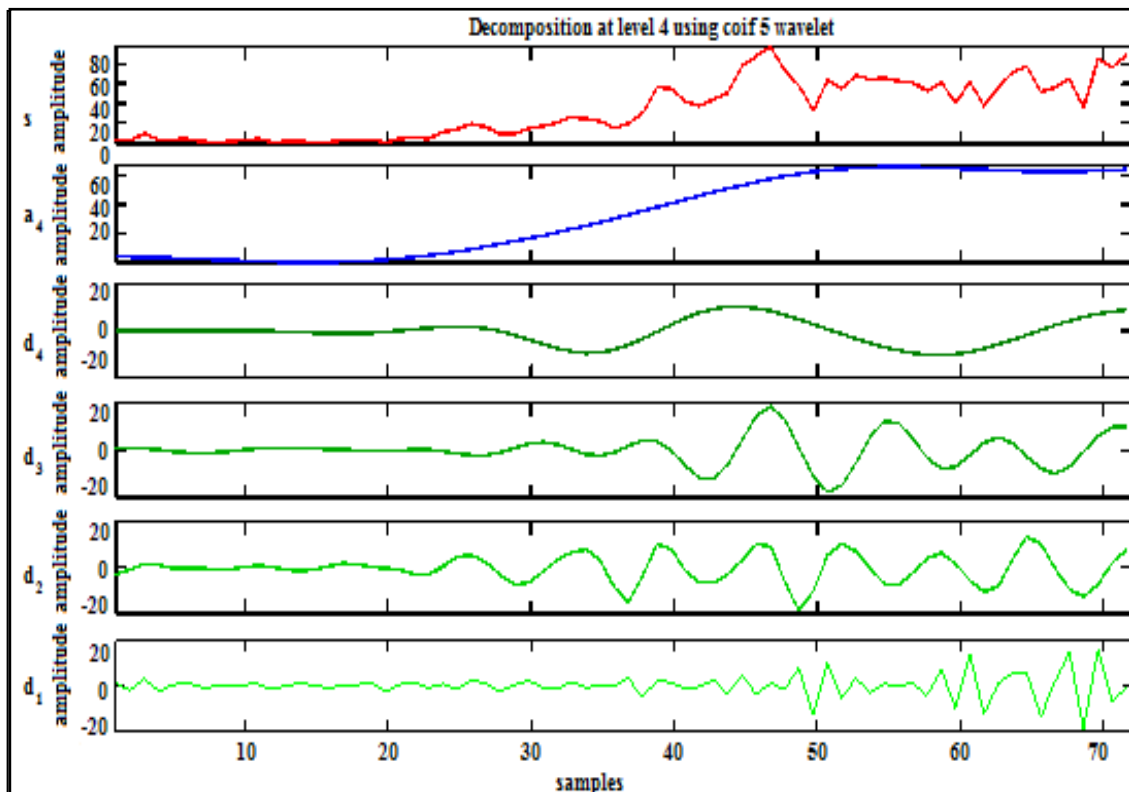


Figure - 5.10: DWT decompositions of Solar Cycle 24 using Coifman5 wavelet. Anomalous sharp variation should be found between 50 to 60 no. of samples (i.e. at the maximum phase of cycle)

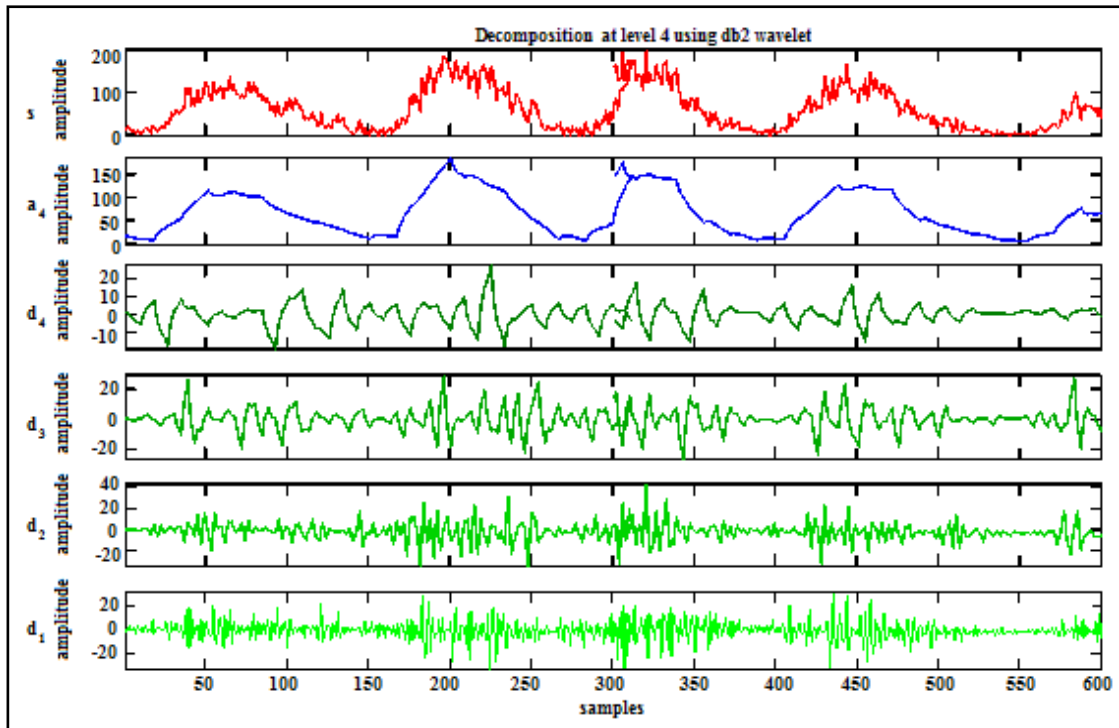


Figure -5.11: DWT decompositions of Solar cycle 20, 21, 22, 23 and 24 using Daubechies 2 wavelet. Anomalous variations should be found at the maximum phase of respective cycles.

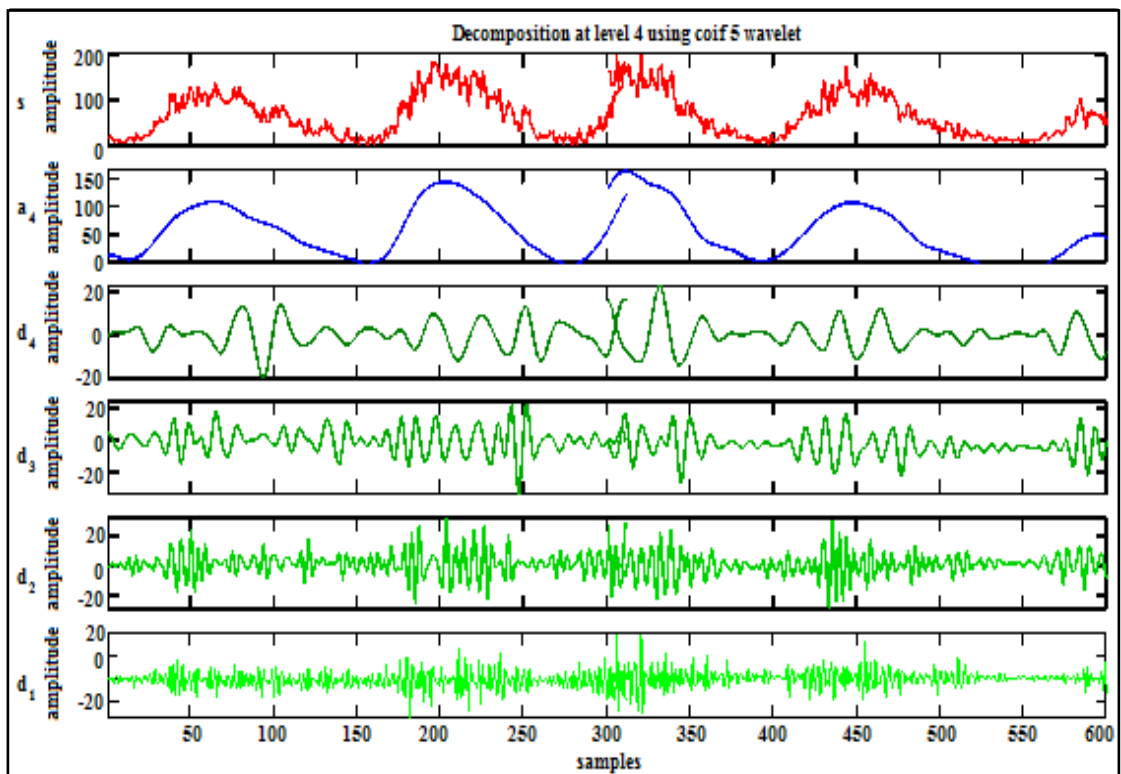


Figure- 5.12: DWT decompositions of Solar cycle 20, 21, 22, 23 and 24 using Coifman 5 wavelet. Anomalous sharp variations should be found at the maximum phase of respective cycles.

The DWT analysis of different Solar cycles as well as the whole Solar cycle's data is shown in Figures from 5.1 to 5.12. In these figures, the x-axis represents the time period of the data under consideration. In all figures first panel represents the variation in observed sunspot number time series. The second one gives the approximation " A_4 " which approximation part corresponds to the amplitude of the sunspot data for respective wavelets used at level 4. Approximation coefficient " A_4 " of all the figures separate the short term anomalous variation from the long term variations. On the other hand, other four parts D_1, D_2, D_3 and D_4 represent detail coefficients of the sunspot data.

The detail coefficients reveal that the sunspot magnetic field strength changes between positive and negative values. It indicates the existence of a strong and variable magnetic field on the Sun as sunspots. The detail coefficients of sunspot numbers show the high frequency components during the initial and main phase of the Solar cycle and their time evolution. However, it also displayed the result of cycles having high amplitudes in the period/sampling range.

It was found that very high frequency components present only during the main phase of the respective Solar cycles and they are very strong in amplitude and stable for higher level of decomposition. Even though there are some strong fluctuations in the main phase and recovery phase but they are not as persistent as that present during the initial phase and main phase of the cycles. Our analysis shows that multi-resolution analysis using wavelet detail and approximation coefficients allow analysis of local features of sunspot number time series.

5.4.2 Multifractal Analysis of Sunspot Numbers

We performed the multifractal analysis by calculating the Legendre spectra using FRACLAB software, developed at INRIA and available online at <http://www-rocq.inria.fr>. Since the sunspot data have some missing values we take the longest segments of sunspot data without any missing values. The length of each segment is about 120, thus permitting to obtain reliable estimates of the singularity spectrum and multifractal parameters. Figures 5.13

to 5.18 (Right upper panel) shows the singularity spectrum and (right lower panel) shows the singularity spectrum for the selected segments for each Solar cycle.

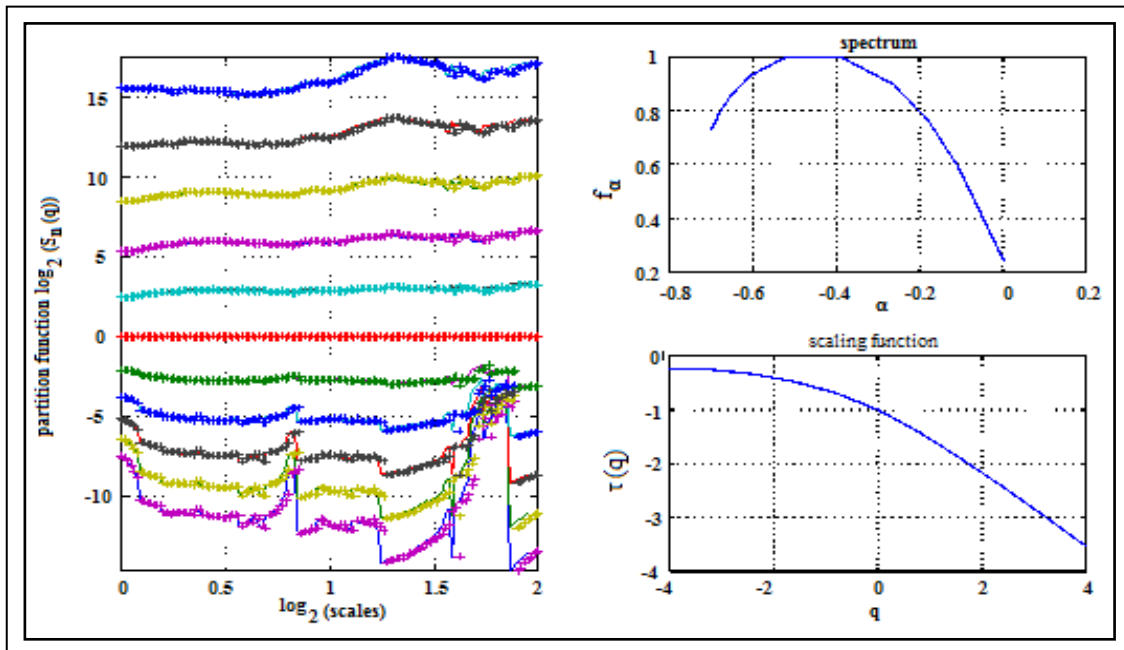


Figure - 5.13: Multifractal analysis of Solar Cycle 20 using CWT (Morlet wavelet of size 8 and 128 voices, LS regression and local maxima). In figure Left panel show the Legendre spectra and Right (upper) panel gives the singularity spectrum and Right (lower) panel for scaling function of the considered time series

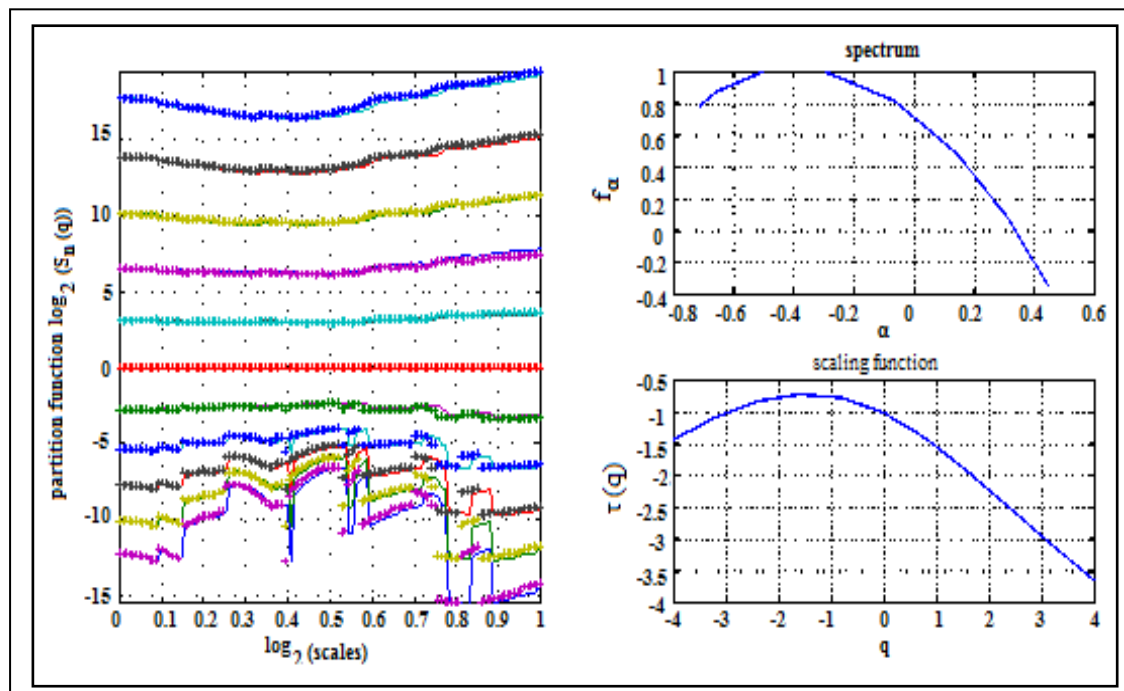


Figure - 5.14: Multifractal analysis of Solar Cycle 21 using CWT (Morlet wavelet of size 8 and 128 voices, LS regression and local maxima). In figure Left panel show the Legendre spectra and Right (upper) panel gives the singularity spectrum and Right (lower) panel for scaling function of the considered time series

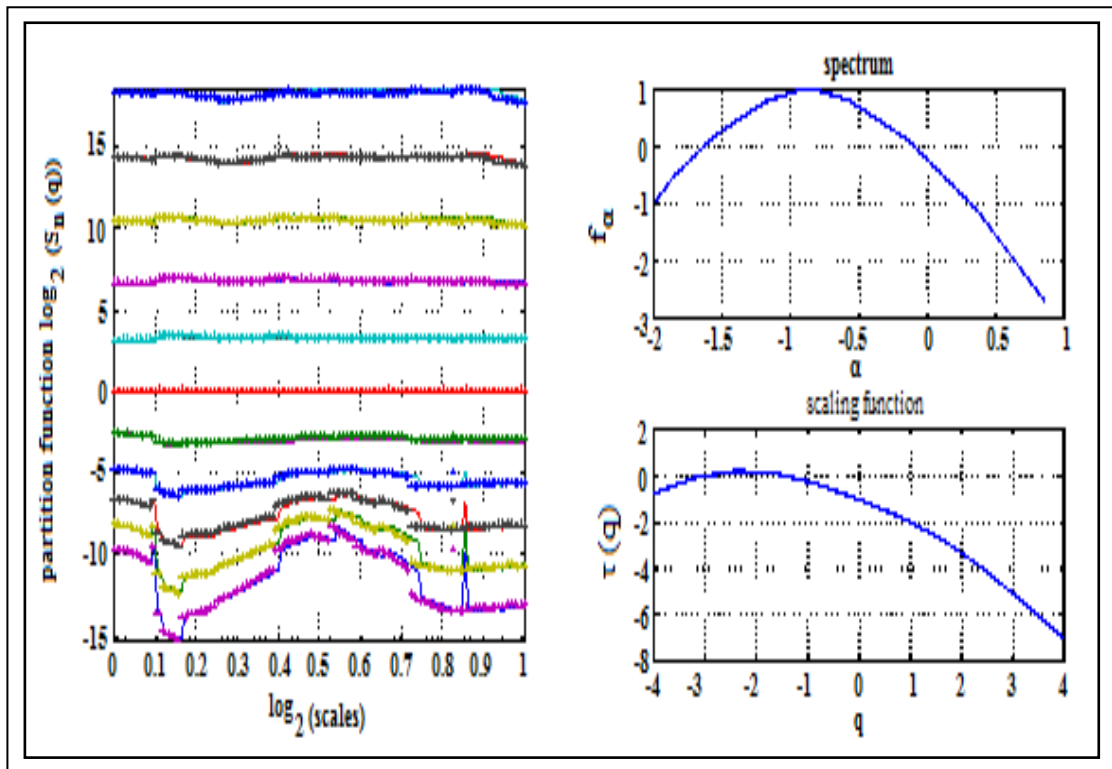


Figure - 5.15: Multifractal analysis of Solar Cycle 22 using CWT (Morlet wavelet of size 8 and 128 voices, LS regression and local maxima). In figure Left panel show the Legendre spectra and Right (upper) panel gives the singularity spectrum and Right (lower) panel for scaling function of the considered time series

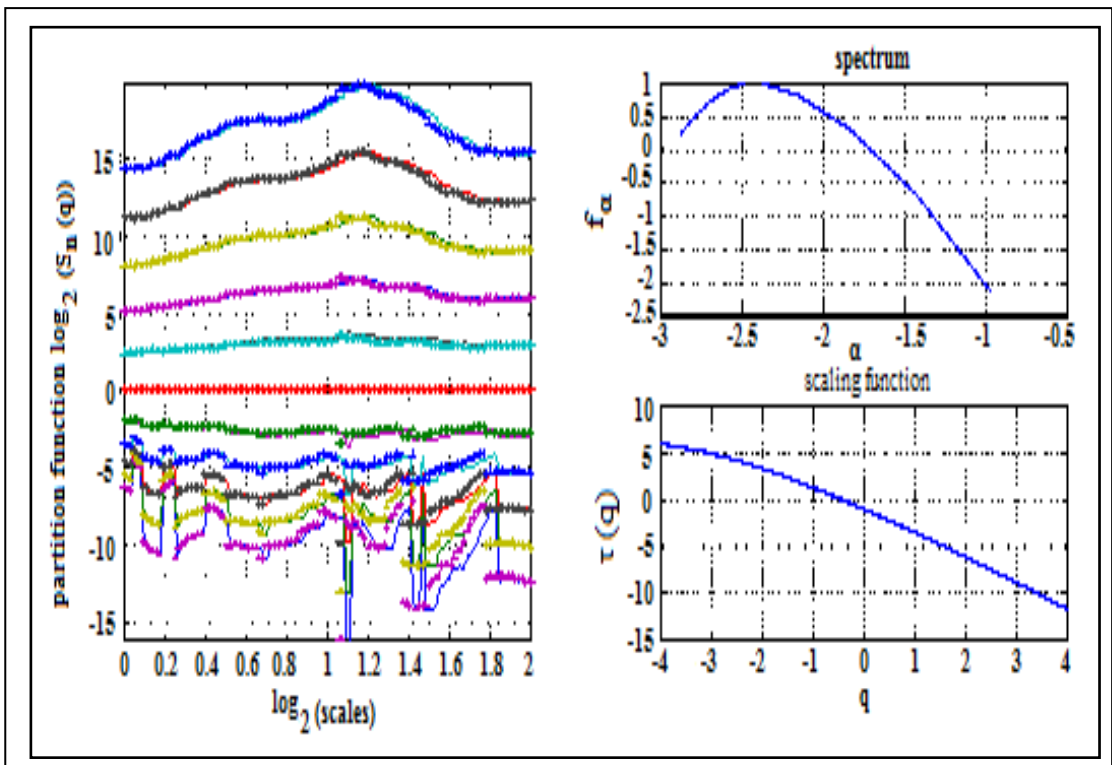


Figure - 5.16: Multifractal analysis of Solar Cycle 23 using CWT (Morlet wavelet of size 8 and 128 voices, LS regression and local maxima). In figure Left panel show the Legendre spectra and Right (upper) panel gives the singularity spectrum and Right (lower) panel for scaling function of the considered time series

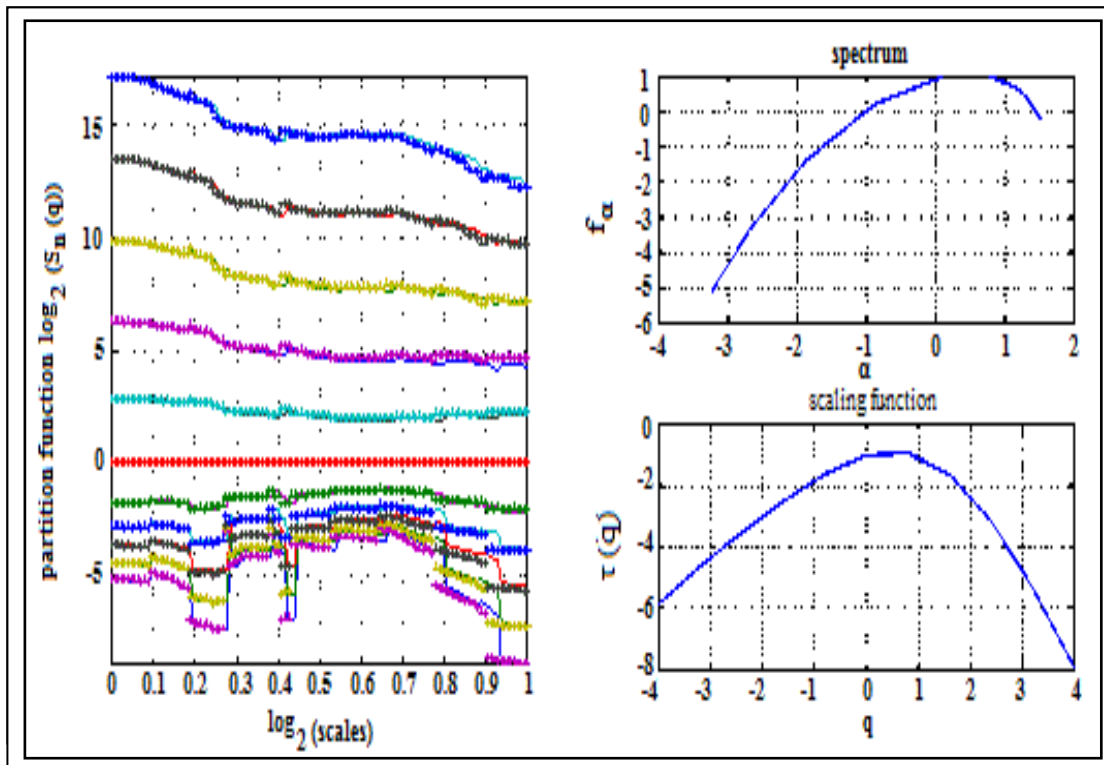


Figure - 5.17: Multifractal analysis of Solar Cycle 24 using CWT (Morlet wavelet of size 8 and 128 voices, LS regression and local maxima). In figure Left panel show the Legendre spectra and Right (upper) panel gives the singularity spectrum and Right (lower) panel for scaling function of the considered time series

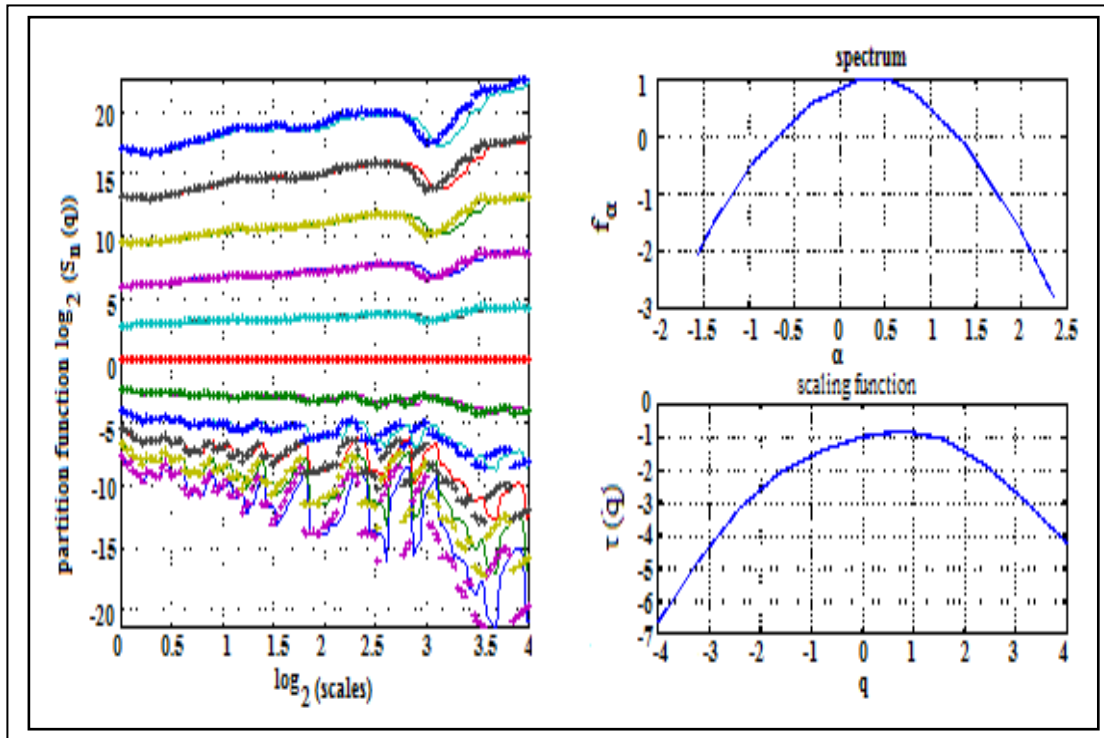


Figure - 5.18: Multifractal analysis of Solar cycles 20, 21, 22, 23 and 24 using CWT (Morlet wavelet of size 8 and 128 voices, LS regression and local maxima). In figure Left panel show the Legendre spectra and Right (upper) panel gives the singularity spectrum and Right (lower) panel for scaling function of the considered time series.

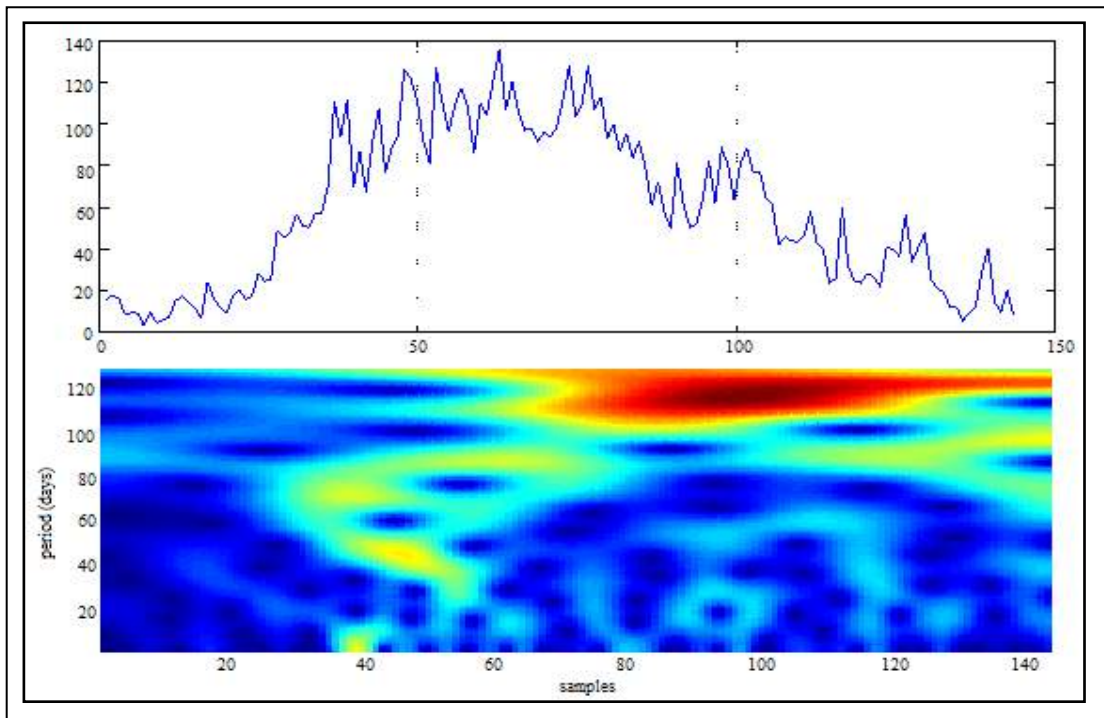


Figure - 5.19: CWT of Solar Cycle 20 using Morlet Wavelet of size 8 and 128 voices. In figure X axis represents the number of samples and Y axis represent scale. The upper panel shows the raw data of the time series and lower panel its continuous wavelet transform (CWT)

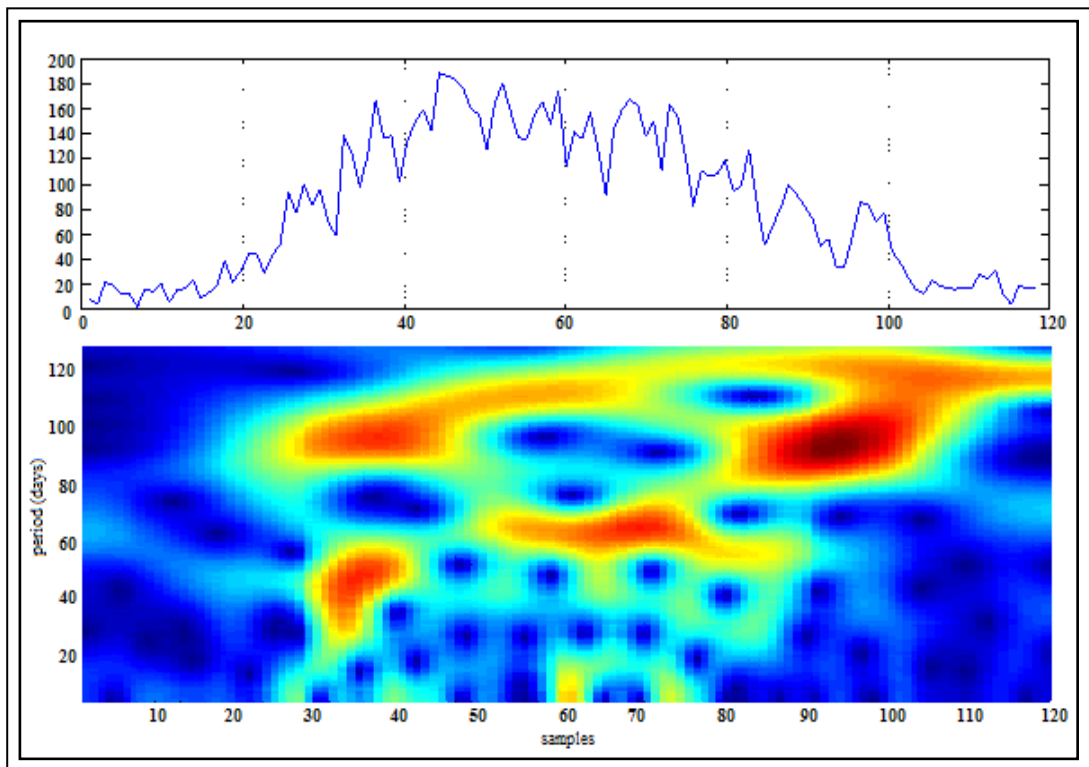


Figure - 5.20: CWT of Solar Cycle 21 using Morlet Wavelet of size 8 and 128 voices. In figure X axis represents the number of samples and Y axis represent scale. The upper panel shows the raw data of the time series and lower panel its continuous wavelet transform (CWT)

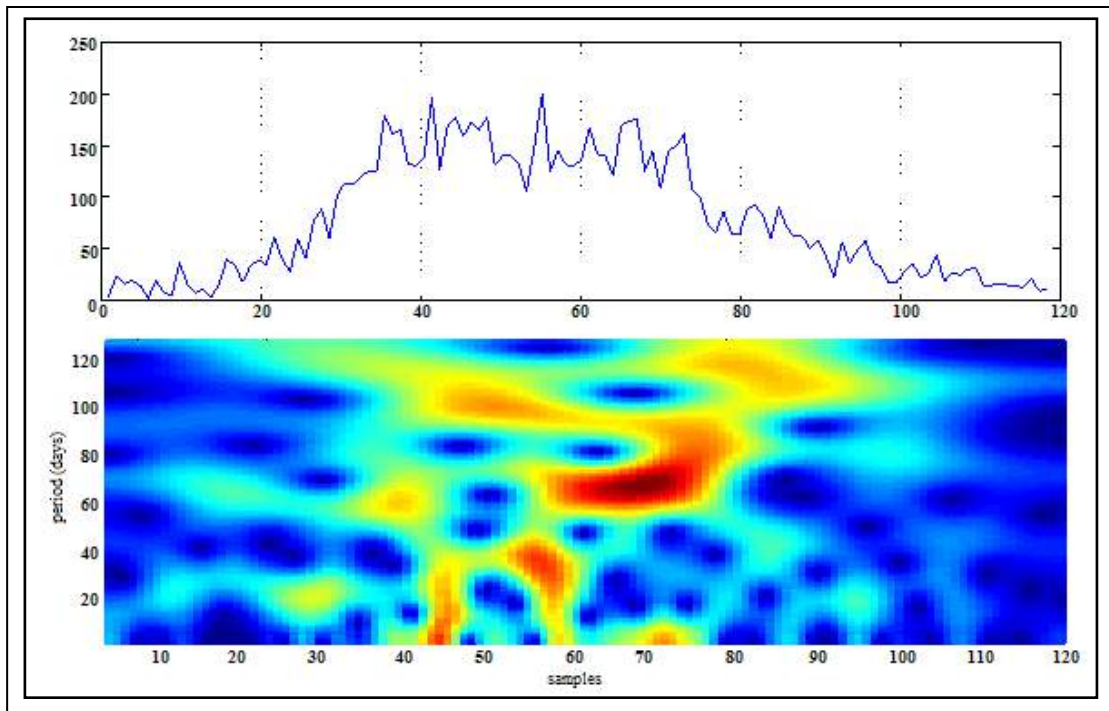


Figure - 5.21: CWT of Solar Cycle 22 using Morlet Wavelet of size 8 and 128 voices. In figure X axis represents the number of samples and Y axis represent scale. The upper panel shows the raw data of the time series and lower panel its continuous wavelet transform (CWT)

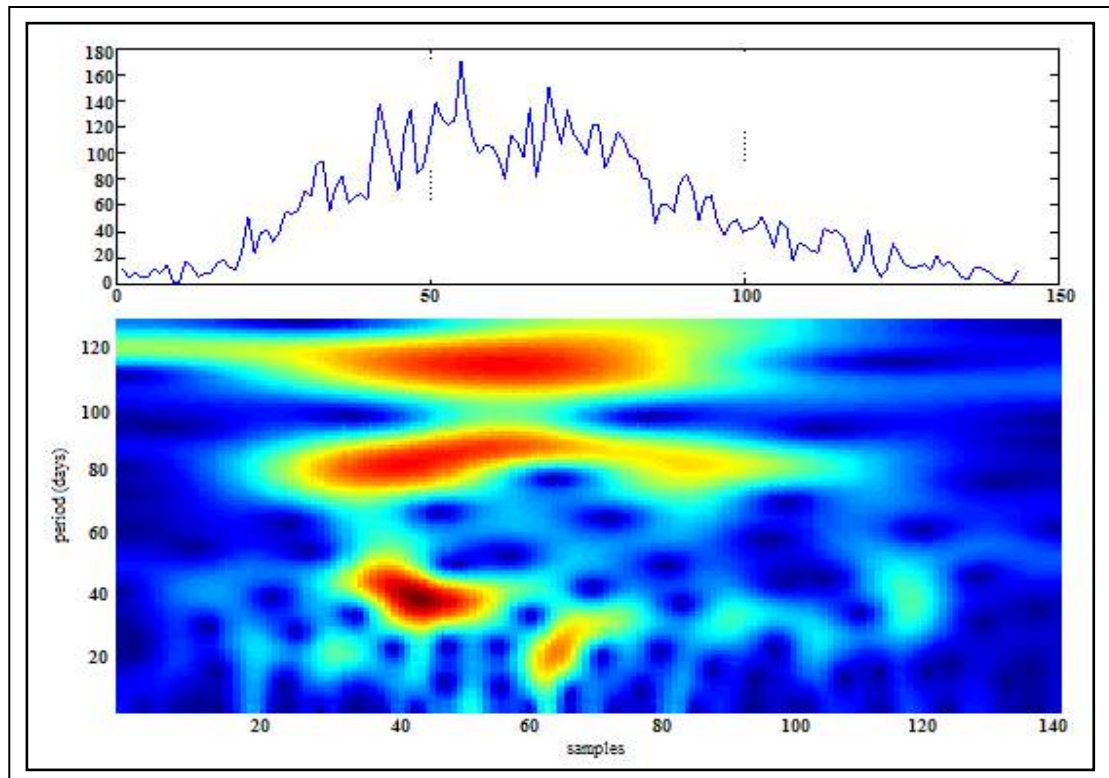


Figure - 5.22: CWT of Solar Cycle 23 using Morlet Wavelet of size 8 and 128 voices. In figure X axis represents the number of samples and Y axis represent scale. The upper panel shows the raw data of the time series and lower panel its continuous wavelet transform (CWT)

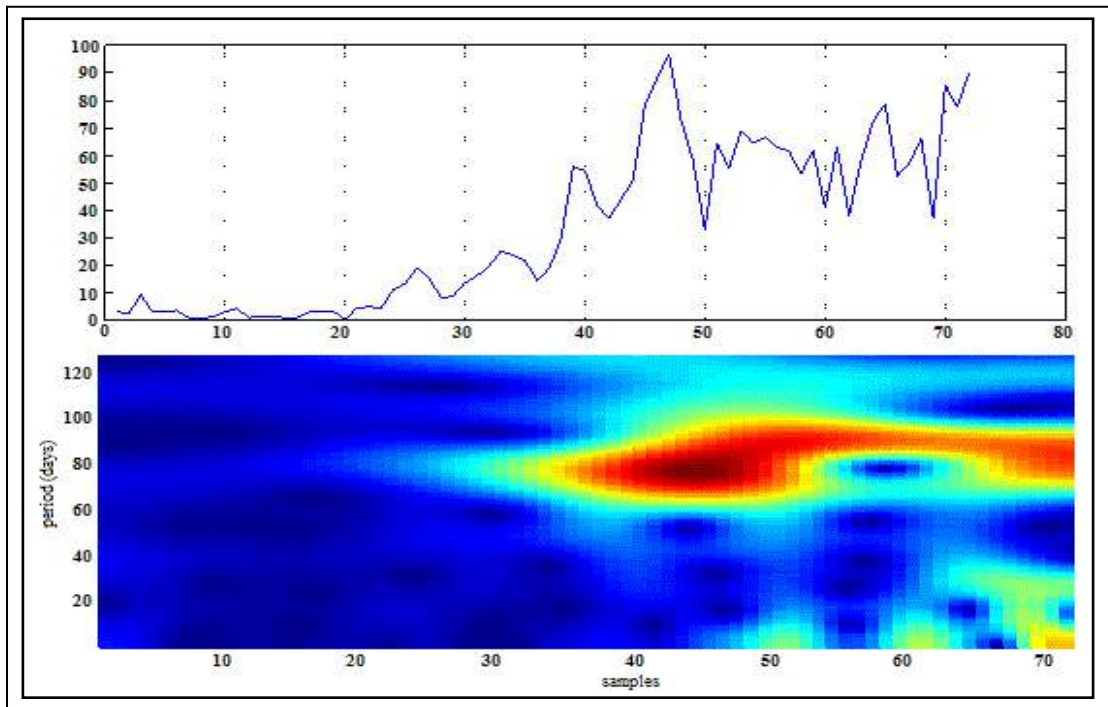


Figure - 5.23: CWT of Solar Cycle 24 using Morlet Wavelet of size 8 and 128 voices. In figure X axis represents the number of samples and Y axis represent scale. The upper panel shows the raw data of the time series and lower panel its continuous wavelet transform (CWT)

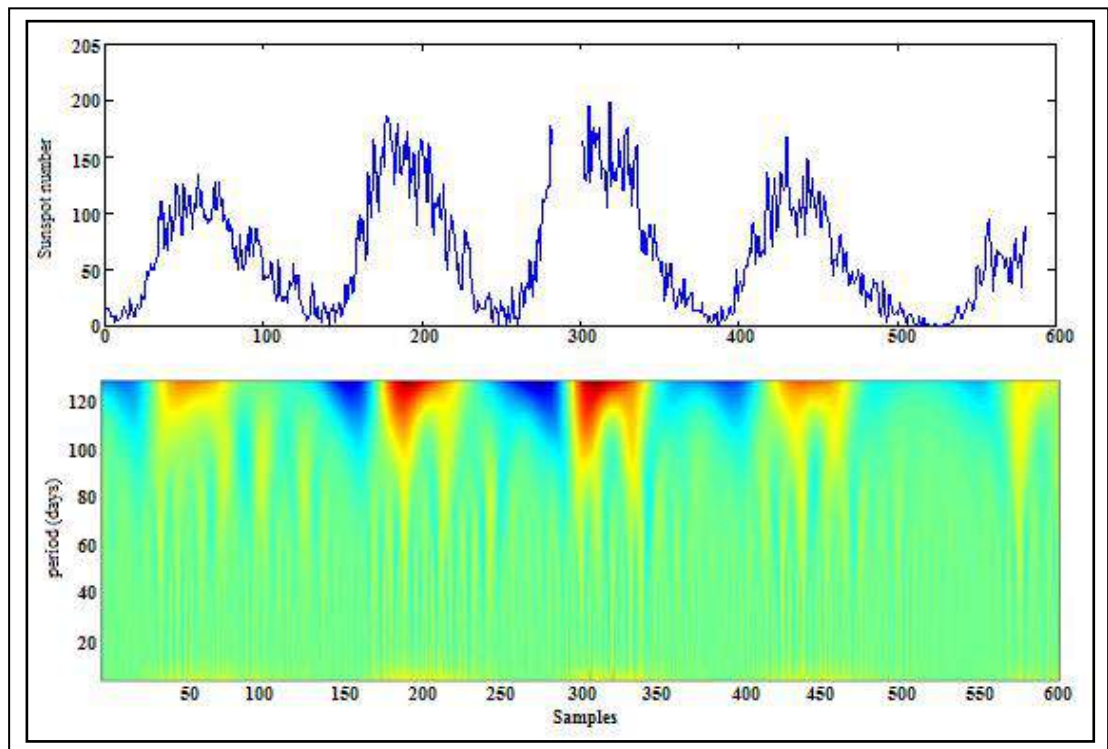


Figure - 5.24: CWT of Solar cycle 20, 21, 22, 23 and 24 using Morlet Wavelet of size 8 and 128 voices. In figure X axis represents the number of samples and Y axis represent scale. The upper panel shows the raw data of the time series and lower panel its continuous wavelet transform (CWT)

The entire spectrum presents the typical single - humped shape that characterizes multifractal nature of sunspot number. The spectra for each segments of sunspot time series, are not identical, although they are very similar to each other. The smaller values of α correspond to the burst of events, while higher values of α correspond to events occurring sparsely (Voros, 2000). The spectrum gives geometrical information pertaining to the dimension of sets of points in a signal having a given Holder exponent. This is the most precise spectrum from a mathematical point of view, but is also difficult one to estimate. Large deviation spectrum yields statistical information, related to the probability of finding a point with a given Holder exponent in the signal. More precisely, it measures how this probability behaves with the change in resolution.

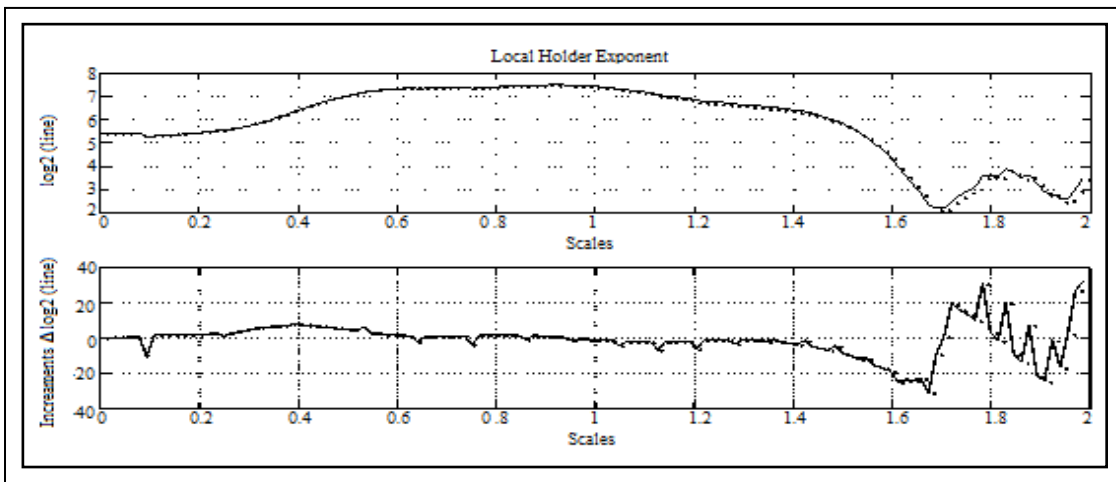


Figure - 5.25: Non-parametric point wise Holder regularity estimation using CWT with Morlet wavelet for the Solar Cycle 20

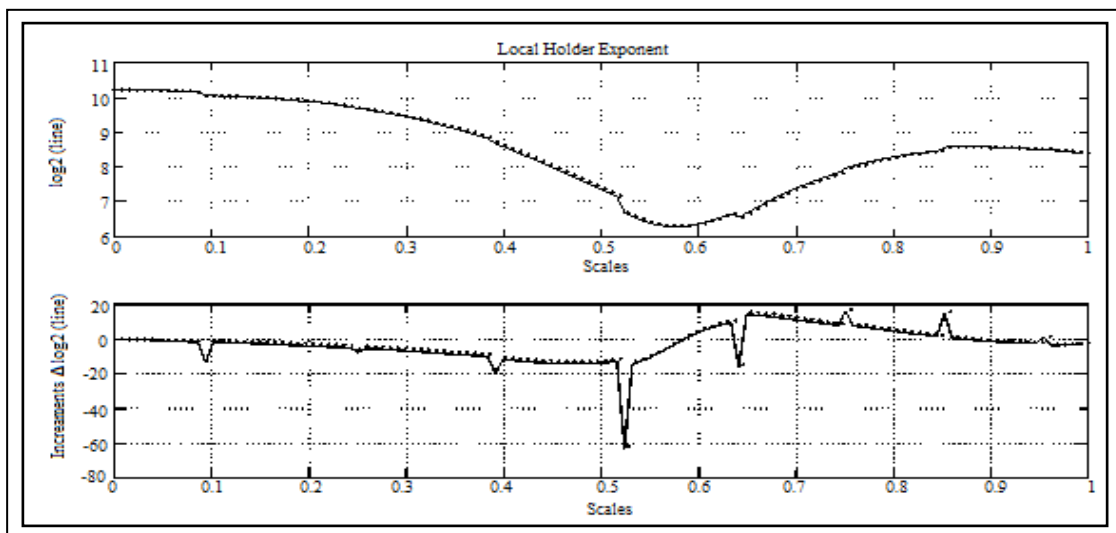


Figure - 5.26: Non-parametric point wise Holder regularity estimation using CWT with Morlet wavelet for the Solar Cycle 21

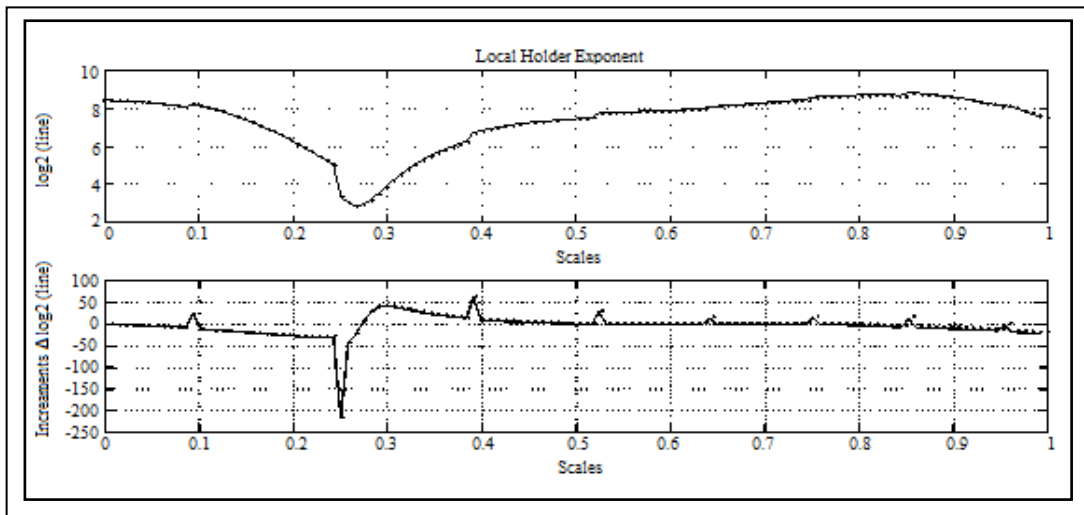


Figure - 5.27: Non-parametric point wise Holder regularity estimation using CWT with Morlet wavelet for the Solar Cycle 22

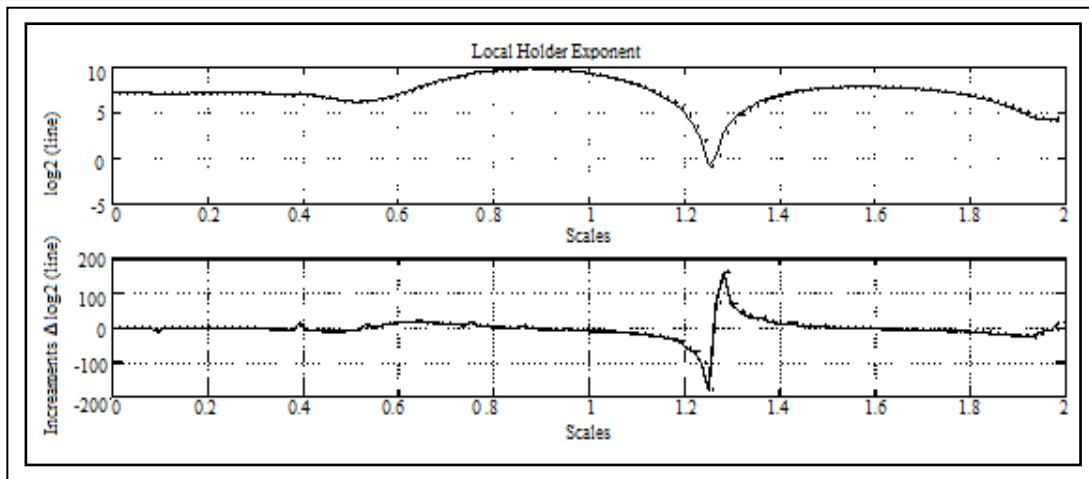


Figure - 5.28: Non-parametric point wise Holder regularity estimation using CWT with Morlet wavelet for the Solar Cycle 23

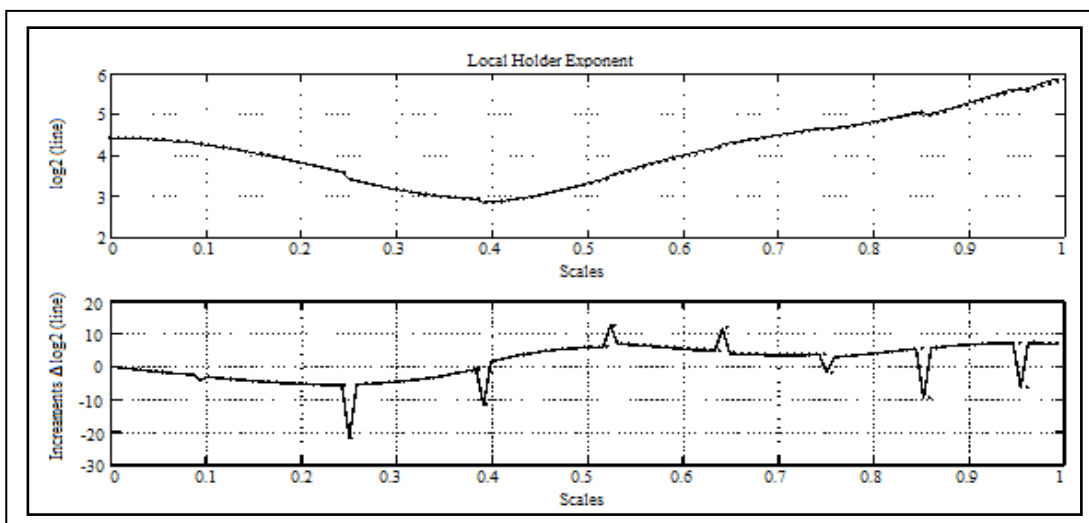


Figure - 5.29: Non-parametric point wise Holder regularity estimation using CWT with Morlet wavelet for the Solar Cycle 24

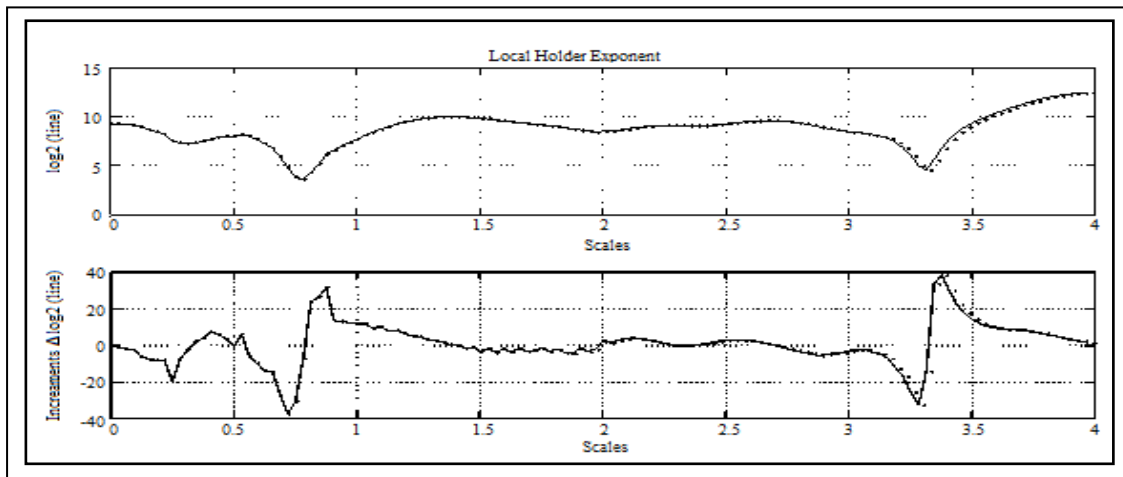


Figure - 5.30: Non-parametric point wise Holder regularity estimation using CWT with Morlet wavelet for the Solar Cycles 20 - 24

Legendre spectrum is a concave approximation to the large deviation spectrum. Its main purpose is to yield much more robust estimates, though at the expense of a loss of information. It could base on box method or CWT techniques. In the sequel we show some sample results for the spectra computed with the Legendre technique. Figures 5.13 to 5.18 (left panel) show the results of the CWT (Morlet wavelet) based estimation of the Legendre spectrum which represents an approximation of the spectrum for five different Solar cycles. Each of the Figures 5.14 to 5.22 consists of two parts. The first part on the top of each of these figures represents the signal or raw data. The second part of these figures shows the analyzed pattern with the application of Morlet wavelet of size 8 and 128 voices of five different Solar cycles. Figure 5.24 shows multifractal analysis of the whole Solar cycles. The Holder exponent characterizes the regularity of the magnetic field strength of sunspot under consideration either by point wise regularity or local regularity. The non-parametric point wise Holder regularity approach used with CWT with Morlet wavelet for the Solar Cycle 20 - 24 also for whole Cycles (i.e. 20 – 23 and ascending phase of Solar Cycle 24) was shown in Figure 5.25 to 5.30. It clearly shows that the exponent that arise sharply in the multifractal analysis asses the regularity of sunspot time series.

5.5 Conclusions

In the Present study wavelet transform techniques was employed to decompose the time series of sunspot numbers into different scales. Wavelet

analysis is particularly suited to decomposition and detect the multiple signal (time series) and follow the time evolution of the frequency distribution of a given time series (Ivanov *et al.*, 2001; Kovacs *et al.*, 2001; Lui, 2002; Mendes *et al.*, 2005; Manda and Balasis, 2006; Zaourar *et al.*, 2006; Gaci *et al.*, 2010). This property is important particularly when one considers non-stationary processes. In addition, wavelet analysis is a powerful multistage resolution technique to deeply understanding the complex features of real world processes different kinds of multifractality, long-range dependence (LRD), non-stationary, oscillatory behaviour and trends. Wavelet-based estimators used successfully for estimating scaling behaviour and applied to time series (Balasis *et al.*, 2006).

Various phenomena related to sun and space weather conditions show fractal and multifractal behavior when plotted against time. Multifractals have infinite number of dimensions associated with them. Solar activity data which are multifractal, are singular (i.e. changes abruptly) at almost every point. There exist three main multifractal spectra, viz. the Hausdroff, large deviation and Legendre spectra. The multifractal spectra provide a useful substitute of the build-up of magnetic energy for solar active regions. The scaling of magnetic structures is associated with the regime of fully developed turbulence at high Reynolds number. It is also based on the close analytical connection between fractal geometry and turbulence in magnetized plasmas (McAteer, Gallagher and Conlon, 2010; McAteer, 2013). Basically, any of these three spectra provides information as to which singularities occur in the data, and which are dominant: a spectrum is a one dimensional curve where abscissa represents the Holder exponents actually present in the data, and ordinates are related to the amount of points where we encounter a given singularity. Wavelet analysis provided visualization of the sunspot number data at different levels. The results of this work provide a general view of the pattern of sunspot number data of different Solar cycles along with the whole cycles. However, recent studies have shown that non-gaussian fluctuation is responsible for the presence of extreme events in space plasmas.

Multifractal Detrended Fluctuation Analysis (MF-DFA) of Solar Wind Plasma Parameters during Solar Cycle 23

6.1 Introduction

Precise study of solar wind plasma parameters is very important in context of solar terrestrial plasma relation with magnetosphere. Solar wind consist of continuous extremely variable hot plasma that radially flows out from the corona, and moves with supersonic speeds, ranges from 300 km s^{-1} to about 2000 km s^{-1} during transient solar events. The solar winds are embedded with magnetic field of the Sun, as well as different structures, waves and turbulent fluctuations on a wide range of scales. There are two basic characteristic that represent the two states of flow of the solar wind: fast streams and slow streams. These states can be differentiated by kinetic parameters such as speed, kinetic temperature and more precisely by the elemental and charge state composition (Feldman et al., 2005). That compositional difference between the fast and slow solar wind arises due to their different origins in the corona. Solar wind plasma parameters (*i.e* speed, density and temperature) are continuously measured by many satellites. Many processes like adiabatic cooling, heating due to stream interactions and shocks, dissipation of waves, and transfer of energy from pickup protons to the thermal protons affect the temperature as the solar wind moves outward.

Several publications discuss the variation in Solar wind parameters which have durations of hours and boundary widths of tens of minutes. These variations in the Solar wind parameter can also lead to better understanding of the nature and properties of the Solar wind plasma, the stability (or lack thereof)

of these structures and the character of plasma instabilities. An analysis of the properties and features of large changes of the Solar wind ion flux was presented by Riazantseva et al. (2003). Now a day in Solar wind parameters are well investigated even though some indistinct problems are still exist (Schwenn and Marsch, 1990; Burlaga, et al., 2005). It is because the origin of the Solar wind is complex and the region of Solar wind acceleration has not been probed properly. Also most of the phenomena related with solar wind plasma are non-linear. These are generally characterized by multifractality and intermittence phenomena.

The magnetohydrodynamic (MHD) description of nonlinearity in solar wind plasma induces dynamical scenario of nonlinear partial differential equations. The variation in dynamical profile of the solutions due to control parameter can diverge from simple self-organized states, such as limit cycles or torus, to strange attractors and multifractal spatiotemporal patterns. Also, the nonlinearity in solar wind plasma generate the intermittent turbulence with the representative characteristics of the anomalous diffusion process and strange topologies of stochastic scalar wind velocity and magnetic fields are caused by the strange dynamics and strange kinetics. Many scientists worked on understanding the solar wind plasma dynamics using complexity theory approach. Burlaga et al. used concept of self-organization and low-dimensional chaotic process for solar wind and space plasmas (Burlaga 1987, 1991a,b,c, 1992, 1993, Burlaga and Forman 2002, Burlaga et al. 2003) and Pavlos et al. (1991v). Moreover Pavlos et al. (Pavlos, 2011; 2012) presents the multiscale and multifractal and non-Gaussian character of the solar wind medium introducing the intermittent turbulence theory for the explanation of solar wind dynamics.

The concept of multifractality was used in the context of scaling properties of intermittent turbulence in Solar wind plasma (e.g., Marsch and Tu, 1997; Bruno et al., 2001). Many authors propose the observed scaling exponents, using simple and advanced models of the turbulence based on distribution of the energy flux between cascading eddies on various scales. Burlaga (1991) has been investigated the multifractal spectrum of magnetic

field data using Voyager in the outer heliosphere and using Helios (plasma) data in the inner heliosphere (Marsch et al., 1996).

The standard multifractal analysis techniques have been developed for the multifractal characterisation of normalized time series. This techniques does not give correct results for non-stationary time series, such as solar wind plasma, which are affected by trends. In order to quantify the multifractality in Solar wind plasma parameters such as solar wind temperature, proton density and solar wind speed multifractal detrended fluctuation analysis (MFDFA) method (Oswiecimkaa, 2005; Drozd, et al., 2009; Gyuchang, et al., 2007; Norouzzadeh, et al., 2006; Zhou, 2009; Yuan, 2009; Gu, et al., 2007; Wang, et al., 2009; Oswiecimka, et al., 2008) has been used in this work. Multifractal detrended fluctuation analysis (MFDFA), is a generalisation of the standard detrended fluctuation analysis (DFA), it is based on the identification of the scaling of the q^{th} -order moments of non-stationary time series (Kantelhardt et al., 2002).

In recent years the detrended fluctuation analysis (DFA) method has become a widely-used technique for the determination of (mono) fractal scaling properties and the detection of long-range correlations in noisy, non-stationary time series. It has successfully been applied to diverse fields such as DNA sequences (Peng et al., 1994, Buldyrev et al., 1998), heart rate dynamics (Bunde et al., 2000, Peng et al., 2001), neuron spiking (Blesic et al., 2001), human gait (Hausdroff et al., 1997), long-time weather records (Koscielny-Bunde et al., 1998), cloud structure (Ivanova et al., 2000), geology (Malamud et al., 1999), ethnology (Alados et al., 2000), economics time series (Mantegna et al., 1999), and solid state physics (Kantelhardt et al., 1999). Yu et al. (2012) examined the multifractal properties of the daily solar X-ray brightness, X_I (i.e., 1 - 8 °A X - rays (Wattsm^{-2})) and X_s (i.e., 0.5 - 4 Å X - rays (Wattsm^{-2})), during the period from 1 January 1986 to 31 December 2007, including two solar cycles (Solar Cycles 22 and 23 respectively), using the universal multifractal approach (Schertzer and Lovejoy 1987) and MFDFA (Kantelhardt et al. 2002). The MF-DFA method shows that the multifractality of the time series in cycle 23 is weaker than that in cycle 22.

6.2 Data Source

The data used for this study are the daily counts of Solar wind plasma parameters as temperature, density and speed from January 1996 to December 2006 it is nearly the time span of Solar Cycle 23. The dataset used in the work was available online at the OMNIweb data explorer (at <http://omniweb.gsfc.nasa.gov/>). The data were analyzed using the multifractal detrended fluctuation analysis technique in order to characterize the intrinsic scaling property of Solar wind plasma parameters.

6.3 Multifractal Detrended Fluctuation Analysis (MF-DFA)

The Wavelet Transform Modulus Maxima (WTMM) method and Multifractal Detrended Fluctuation Analysis (MF-DFA) method are used to find the multifractal spectrum of non-stationary time series. If true fractal structure of data is unknown MF-DFA gives more accurate result as compare to WTMM method. It shows less bias and being less likely to give a false positive result. Due to the fact MF-DFA is used in this work to analyze the Solar wind plasma parameter. MF-DFA is well suited for analysis of Solar wind data because it is designed for data of a finite length N , without requiring an $N \rightarrow \infty$ approximation for validity. In this method Solar wind data is treated as a one-dimensional line and assigns new values to each portion of data. It deals with the data having direction-dependent scaling properties and the non - equivalence of the time and value axes. The assigned values are then assessed for multifractality.

The generalized multifractal DFA (MFDFA) for Solar wind data can be described as follows. Suppose that X_j be a Solar wind plasma parameter time series of length N , with compact support, i.e. $X_j = 0$ for an insignificant fraction of the values only. The profile at location i , $Y(i)$ is defined by taking the sum of deviation from the mean value and analytically given by (Kantelhardt et al., 2002; Telesca et al., 2004),

$$Y(i) = \sum_{k=1}^i \{X_j - \bar{X}\}, \quad i = 1, \dots, N. \quad \dots \dots \dots (6.1)$$

Subtraction of the mean \bar{X} is not compulsory, because it would be eliminated in the preceding step.

The profile $Y(i)$ is divided into $Ns \equiv \text{int}(N/s)$ non-overlapping segments of equal size s . Since the length N of the series may not be multiple of the considered time scale s , an unequal and short part ($< s$) of the profile may left at the end. In order not to disregard this part of the series, the same procedure is repeated starting from the opposite end. Thus, $2Ns$ segments are obtained altogether. Then local trend for each of the $2Ns$ segments is calculated by a least-square fit of the series.

The variance between the series $Y(i)$ and the ordinate of the fitted polynomial $[y_v(i)]$ is calculated as

$$F^2(s, v) = \frac{1}{s} \sum_{i=1}^s \{Y[(v-1)s + i] - y_v(i)\}^2 \quad \dots \dots (6.2)$$

Where indices i and v correspond to the original data points and the segment of size s respectively.

- The fluctuation function can be extended to include higher order moments (say q values) to analyze the scaling property of different ranges of fluctuations, and also the detrending polynomial, y_v can take any order n (linear, quadratic, cubic, etc.). The generalized fluctuation function, $F_q(s)$ is thus defined by averaging over all segments to obtain the q th order fluctuation function as

$$F_q(s) = \left\{ \frac{1}{2Ns} \sum_{v=1}^{2Ns} [F(s, v)]^{\frac{q}{2}} \right\}^{1/q} \quad \dots \dots (6.3)$$

where the index variable q can take any real value except zero. In case $q = 0$, the fluctuation function cannot be determined directly from equation (6.3) because of diverging exponent. Thus, $F_0(s)$ is approximated by taking the logarithmic average as,

$$F_0(s) = \left\{ \exp \frac{1}{4N_s} \sum_{v=1}^{2N_s} \ln[F(s, v)] \right\} \dots \dots (6.4)$$

- To develop the relation between segment length q and fluctuation functions $Fq(s)$ above procedure was repeating several times for different values of segment length. Typically $F(q)s$ will increase with increasing s .
- The scaling behavior of the fluctuation functions was determined by analyzing log-log plots $Fq(s)$ versus s for each value of q . If the series X_j has long-range power-law correlated, $Fq(s)$ increases, for large values of s , as a power-law,

$$F_q(s) \propto s^{h(q)} \dots \dots (6.5)$$

The exponent $h(q)$ may depend on q and known as generalized Hurst exponent. For $q = 2$, $h(q)$ is identical to the well-known Hurst exponent H and provide information about the average fluctuation of the series. For positive values of q , $h(q)$ describes the scaling behavior of the segments with large fluctuations. The large fluctuations are characterized by a smaller scaling exponent $h(q)$ for multifractal series. On the other hand, for negative values of q , $h(q)$ describes the scaling behavior of the segments with small fluctuations, characterized by a larger scaling exponent.

- The simplest way to analyze the Solar wind plasma is to link the generalized fluctuation function and the standard box counting formalism of multifractal analysis. For original data X_j , the mass distribution probability in the v th segment of size s unit, $P_s(v)$ is written as,

$$P_s(v) = \sum_{k=(v-1)s+1}^{vs} X_j = Y(vs) - Y[(v-1)s] \dots \dots (6.6)$$

- The mass scaling function, $\tau(q)$ is then defined by partition function $\mu(q, s)$ as,

$$\mu(q, s) = \sum_{v=1}^{N/s} |P_s(s)|^q \propto \dots \dots (6.7)$$

- The mass scaling function is related to the generalized Hurst scaling function, $h(q)$ as Yu et al. (2011)

$$\tau(q) = qh(q) - 1 - qH' \dots \dots (6.8)$$

where $H' = h(1) - 1$ is called the non conservation parameter and proceed to the $f(\alpha)$ spectrum by the Legendre transforms:

$$\alpha(q) = \frac{d\tau(q)}{dq}$$

$$f(\alpha(q)) = \alpha(q)q - \tau(q) \dots \dots (6.9)$$

A plot of $f(\alpha)$ and α is the multifractal spectrum for the Solar wind data. Here α is the singularity strength or Holder exponent, while $f(\alpha)$ denotes the dimension of the subset of the series that is characterized by α . We can directly relate α and $f(\alpha)$ to $h(q)$,

$$\alpha = h(q) + qh'(q) \text{ and } f(\alpha) = q[\alpha - h(q)] + 1 \dots \dots (6.10)$$

Non - stationarity is a frequent characteristic of composite variability and associated with various trends in the data patches having different local statistical properties (Kantelhardt et al., 2001). The DFA method reduces the effect of non - stationarities on scaling property of data. The reason for detrending analysis is to remove the undue influence of larger scale on the statistics of Solar wind plasma data at the scale. The MF-DFA method allows the detection of scaling property of a physical variable embedded in noisy data that can disguise true fluctuations of the series Biswaset al. (2012).

6.4 Results and discussion

The Multifractal Detrended Fluctuation Analysis (MFDFA) method allows a reliable multifractal characterization of multifractal non - stationary time series of Solar wind plasma parameters. The variation of Solar wind plasma

parameters as temperature (upper panel), density (middle panel) and speed (lower panel) for solar cycle 23 are presented in Figure 6.1. We have analyzed the Solar wind temperature, proton density and Solar wind speed data using multifractal detrended fluctuation analysis technique.

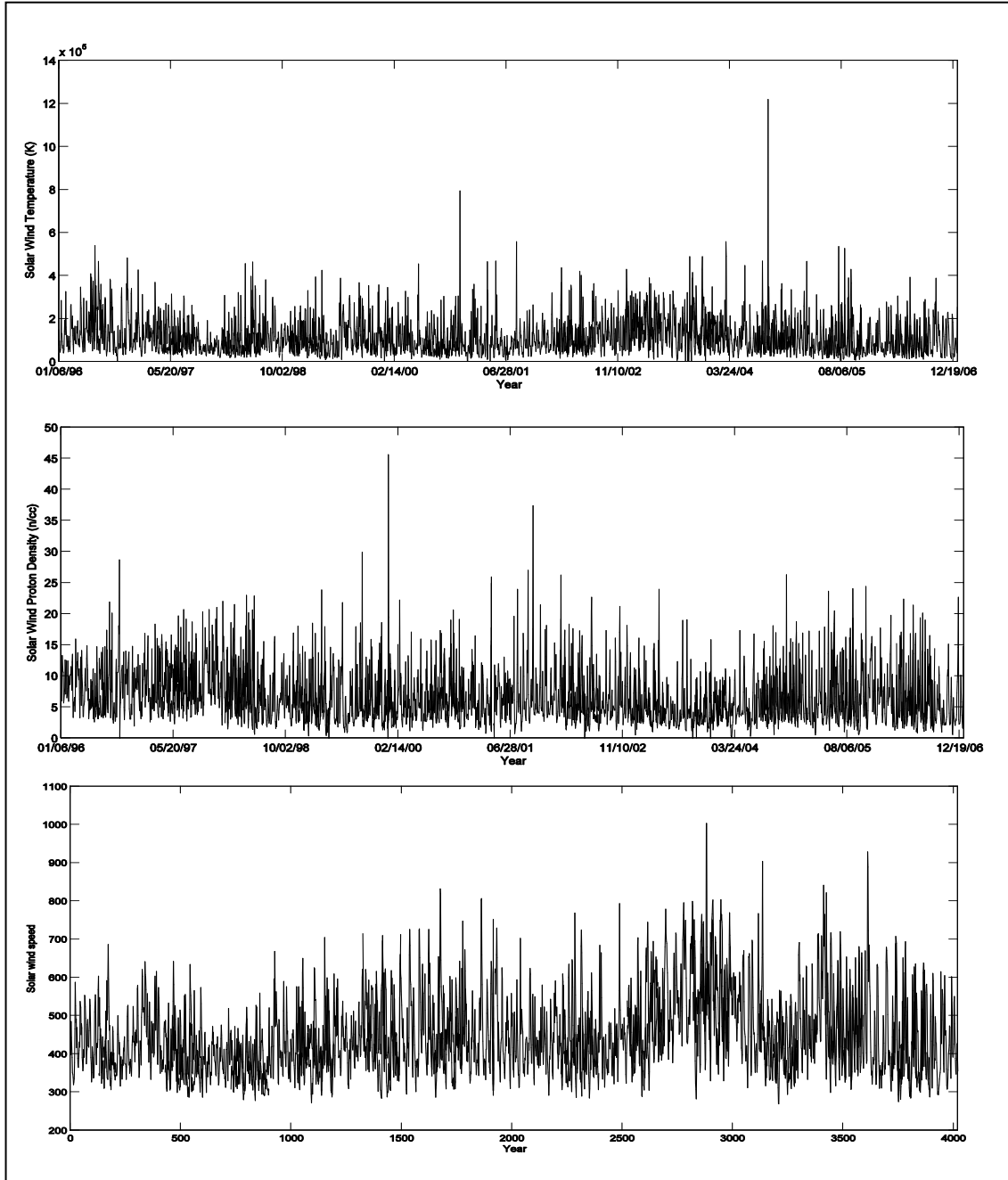


Figure - 6.1 Variations in solar plasma parameters as solar wind temperature (upper panel) /proton density (middle panel) and solar wind speed (Lower panel) during Solar cycle 23

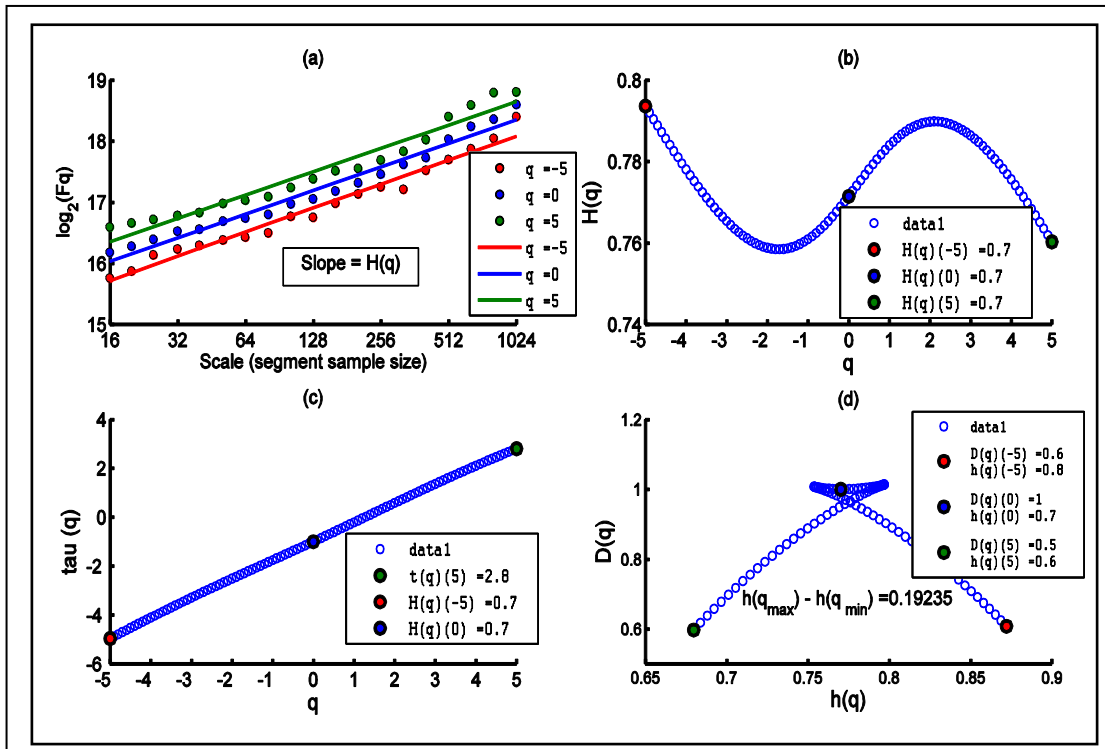


Figure - 6.2 (a) q -order Hurst exponent (b) Generalized Hurst exponent q -order mass exponent (c) Mass exponent function (d) Singularity spectrum $D(q)$ as function $h(q)$ for Solar wind temperature for Solar Cycle 23.

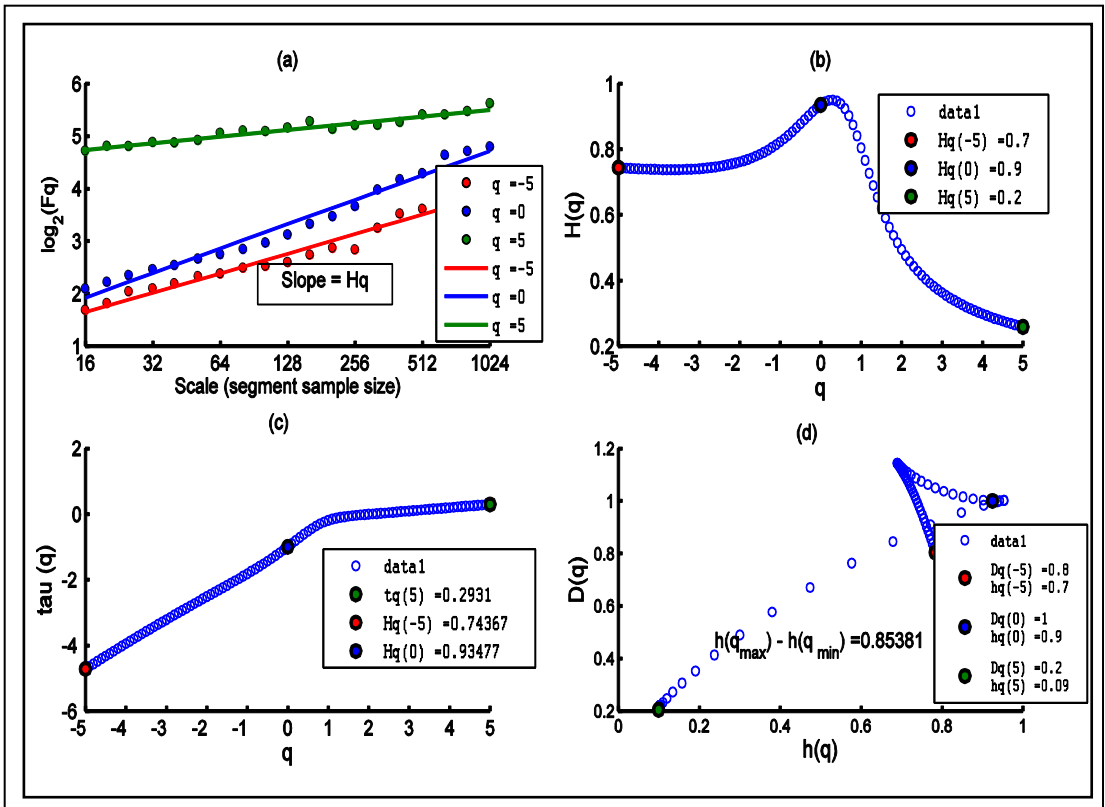


Figure - 6.3 (a) q -order Hurst exponent (b) Generalized Hurst exponent q -order mass exponent (c) Mass exponent function (d) Singularity spectrum $D(q)$ as function $h(q)$ for Solar wind density for Solar Cycle 23

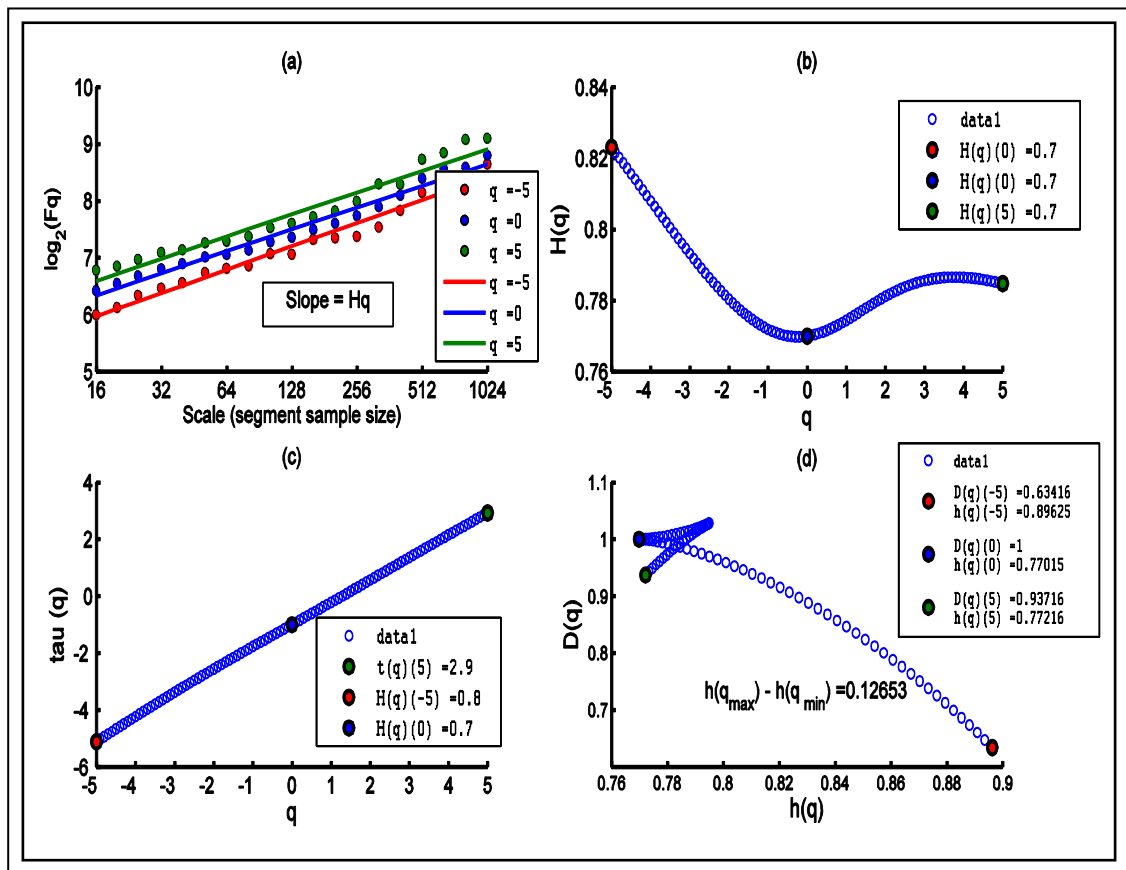


Figure- 6.4 (a) q -order Hurst exponent (b) Generalized Hurst exponent q -order mass exponent (c) Mass exponent function (d) Singularity spectrum $D(q)$ as function $h(q)$ for Solar wind speed for Solar Cycle 23

Figures 6.2 (a), 6.3 (a) and 6.4 (a) represents the q -order Hurst exponent that slope gives the generalized Hurst exponent, which are shown in Figure 6.2 (b), Figure 6.3 (b) and Figure 6.4 (b), for temperature, density and speed respectively an in all figures q ranging from - 5 to 5. For monofractal time series characterized by a single exponent over all time scales, $h(q)$ is independent of q . For multifractal time series, $h(q)$ varies with q . The different scaling of small and large fluctuation will yield a significant dependence of $h(q)$ on q . Therefore, for positive value of q , $h(q)$ describes the scaling behavior of the segments with large fluctuations; and for negative q values, the scaling exponent $h(q)$ describes the scaling behavior of segments with small fluctuations. Taking $h(q) = - 5$ the boundary, the generalized Hurst exponents $h(q)$ for all the parameters decreases as the value of q increases for $q=0$ the value of $h(q) = 0.7$ for Solar wind temperature $h(q) = 0.9$ for proton density and $h(q) = 0.7$ for Solar wind speed after that value of $h(q)$ decreases with the value of q in positive phase of wavelike structure. This indicates that small variations of all

parameters are persistent and the value of $h(q)$ gets closer to 0 with the increase in q , whereas the large variation of temperature display anti-persistent properties. It was concluded that Solar wind proton density possesses the multifractal features. On the other hand Solar wind plasma temperature and speed extremely show multifractality nature.

Figures 6.2 (c), 6.3 (c) and 6.4(c) show the dependence of $\tau(q)$ and q . It was found that the entire plot shows non-linear behavior. The non - linear $\tau(q)$ means multiple scaling and degree of non - linearity of the $\tau(q)$. The slopes of $\tau(q)$ for all the parameters are similar indicating a similar degree of multifractality. The distinct value of $\tau(q)$ given in figures, for various parameters of Solar wind parameter suggested the highest degree of multifractality in these parameters. Figures 6.2 (d), 6.3 (d) and 6.4 (d) shows the singularity spectra for all Solar wind parameter under studied. The width of the fractal spectrum shows the distinction between the maximum probability and the minimum probability (i.e. $\Delta h = h(q_{max}) - h(q_{min})$). The widths of spectrum (degree of multifractality) are 0.19235, 0.85381 and 0.12653 for temperature, density and speed respectively suggesting that the strength and complexity of Solar wind parameters fluctuations. Also all of them exhibit the shape of parabolic curve, indicating the multifractal structure of Solar wind parameters. The singularity spectrums of Solar wind have left truncation for Solar wind temperature and speed whereas the singularity spectrum has right truncation for proton density. This is because proton density has multifractal structure that is sensitive to large magnitude of local fluctuation.

6.5 Conclusions

In this chapter, we attempted to demonstrate the multifractal properties of Solar wind plasma parameter, (i.e. Solar wind temperature, proton density and Solar wind speed) using Multifractal Deterended Fluctuation Analysis (MFDFA). The multifractal property of Solar wind parameters is the key significance in studying Solar wind plasma turbulence for a symmetric scaling. The concept of multifractality of solar wind plasma can be used to increase deeper insight into the various processes occurring in non-linear dissipative

dynamical systems such as magnetized plasma in the solar atmosphere. The plot of the generalized Hurst exponents is a distinctive fingerprint of the presence of multifractality. One more reason to include multifractality is the existence of a highly intermittent character of solar wind plasma that arises in the evolution of the dynamic systems, where dissipative processes may not be neglected. This finding suggests that monofractal models like fractional Brownian motion are not sufficient to capture the inherent richness of the time series properties of the Solar wind plasma parameters. Furthermore, the values of the generalized Hurst exponents suggest that small fluctuations in the analyzed time series are persistent.

The fluctuations in Solar wind speed are not quite of a random nature but result from deterministic non-linear dynamic. It can be described by a small number of parameter, most likely by a strange attractor with multifractal structure (Macek, 2006). The multifractality in our analysis characterized the impulsive and intermittent phase of solar wind parameters. Intermittency implies a tendency of a certain quantity to concentrate into small-scale features of high intensity surrounded by extended areas of much lower fluctuations (Monin & Yaglom 1975). Intermittency manifests itself via the burst-like behavior in temporal and spatial domains.

Non-Gaussian fluctuations can be incorporated by using the non-extensive approach (Tsallis, 1988) as in Bolzan et al. (2005b). Gotoh and Kraichnan (2004) concluded that any non-extensive representation of turbulence phenomena requires significant assessment of the turbulent plasma environment. Recently it was found that non-gaussian fluctuation is responsible for the presence of extreme events in solar wind plasma parameters. Using a non-extensive approach, Balasis et al. (2008) suggested the emergence of two distinct phases: (i) the phase where the intense magnetic storms cause a higher degree of magnetic field organization, which is associated with the presence of various kinds of large scale coherent structures Chang et al. (2006) and (ii) the phase which characterizes the normal periods with lower magnetic field coherence.

Thus we concluded that, a theoretical framework is required to developed for examine the nature of the higher solution observations of the solar wind plasma fluctuations. Our results provide direct supporting evidence the Solar wind plasma parameter is likely to have multifractal structure. It is worth pointing that multifractality of solar wind plasma is an important finding, which open the possibility of approximately predicting the behavior of the Solar wind plasma. We hope that analysis of multifractality of Solar wind plasma could to a deeper understanding of their nature and may be even to predict there seemingly unpredictable behavior.

Bibliography

- ❖ Abramenko, V.I., Yurchshyn, V.B., Wang, H., Spirock, T.J., Goode, P.R.: Scaling Behavior of Structure Functions of the Longitudinal Magnetic Field in Active Regions on the Sun, *Astrophysical Journal*, 577, 1, 487-495, 2002.
- ❖ *Abramenko, V.I.: Multifractal Analysis of Solar magnetograms, Sol. Phys.* 228, 29 - 42, 2005.
- ❖ Abramneko, V.I., Longcope, D.W.: Distribution of the Magnetic Flux in Elements of the Magnetic Field in Active Regions, *The Astrophysical Journal*, 619, 2, 1160-1166, 2005.
- ❖ Addison, P.S.: The Illustrated Wavelet Transform Handbook: Introductory Theory and Applications in Science Engineering, *Medicine and Finance (Bristol: Institute of Physics Publishing)*, 2002.
- ❖ Aguiar-Conraria, L., Azevedo, N., Soares, M.J.: Business cycle synchronization and the Euro: a wavelet analysis, *Journal of Macroeconomics forthcoming*, 2011b.
- ❖ Aguiar-Conraria, L., Azevedo, N., Soares, M.J.: Oil and the macroeconomy: using wavelet to analyze old issues, *Empirical Economics forthcoming*, 2011a. doi: 10.1007/500181-010-0371-x
- ❖ Aguiar-Conraria, L., Azevedo, N., Soares, M.J.: Using Wavelets to Decompose the Time-Frequency Effects of Monetary Policy, *Physica A: Statistical Mechanics and its Applications*, 387, 2863 - 2878, 2008.
- ❖ Akasofu, S.I.: Solar-wind disturbances and the solar wind-magnetosphere energy coupling function, *Space Sci. Rev.*, 34, 173 - 183, 1983.

- ❖ Alados, C.L., Huffman, M.A.: Detrended fluctuation analysis of the Ornstein-Uhlenbeck process: Stationarity versus nonstationarity, *Ethnology* 106, 105, 2000.
- ❖ Angelopoulos, V.: The THEMIS Mission, *Space Science Reviews*, 141 (5), 1 - 4, 2008.
- ❖ Arneodo, A., Decoster, N., Kestener, P., Roux, S.G.: A wavelet-based method for multifractal image analysis: From theoretical concepts to experimental applications, *Adv. Imaging. Electr. Phys.*, 126, 1 – 92, 2003.
- ❖ Aydin, N., Markus, H.S.: Directional wavelet transform in the context of complex quadrature Doppler signals, *IEEE Signal Processing Letters*, 7, 10, 278-280, 2000.
- ❖ Babcock, H.W.: The Topology of the Sun's Magnetic Field and the 22-YEAR Cycle, *Astrophysical Journal*, 133, 572, 1961.
- ❖ Bachmann, K.T., White, O.R.: Observations of hysteresis in solar cycle variations among seven solar activity indicators, *Solar Phys.*, 150, 347, 1994.
- ❖ Bai, T., Sturrock, P.A.: The 152-day periodicity of the solar flare occurrence rate, *Nature* (ISSN 0028 - 0836), 327, 601 - 604, 1987.
- ❖ Bai, T.: Periodicities in Solar Flare Occurrence: Analysis of Cycles 19 - 23, *The Astrophysical Journal*, 591, 1, 406 - 415, 2003.
- ❖ Bai, T.: The 77 day periodicity in the flare rate of cycle 22, *Astrophysical Journal*, Part 2 - Letters (ISSN 0004-637X), 388, L69 - L72, 1992.
- ❖ Baker, D.N.: The occurrence of operational anomalies in spacecraft and their relationship to space weather, *IEEE Trans. Plasma Sci.*, 28 (6), 2007 - 2016, 2000.
- ❖ Balasis, G., Daglis, I. A., Papadimitriou, C., Kalimeri, M.: Anastasiadis, A., Eftaxias, K.: Dynamical complexity in Dst time series using non-extensive Tsallis entropy, *Geophys. Res. Lett.*, 35, L14102, 2008.

- ❖ Balasis, G., Daglis, I., Kapis, P., Manda, M., Vassiliadis, D., Eftaxias, K.: From pre-storm activity to magnetic storms: A transition described in terms of fractal dynamics, *Ann. Geophys.*, 24, 3557 - 3567, 2006.
- ❖ Ballester, J.L., Oliver, R., Baudin, F.: Discovery of the near 158 day periodicity in group sunspot numbers during the eighteenth century, *ApJ*, 522, L153, 1999.
- ❖ Ballester, J.L., Oliver, R., Carbonell, M.: The Near 160 Day Periodicity in the Photospheric Magnetic Flux, *The Astrophysical Journal*, 566, 1, 505 - 511, 2002.
- ❖ Ballester, J.L., Oliver, R., Carbonell, M.M.: The periodic variation of the North-South asymmetry of sunspot areas revisited, *Astron. Astrophys.* 431, L5, 2005.
- ❖ Balthasar, H., Scussler, M.: Evidence for the 22-YEAR-CYCLE in the Longitudinal Distribution of Sunspots, *Solar Physics*, 93, 1, 177 - 179, 1984.
- ❖ Bower, S.D.: Periodicity of solar irradiance and solar activity indices: II, *Sol. Phys.*, 142, 365 - 389, 1992. doi:10.1007/BF00151460.
- ❖ Bing, G., Ya-Xian, F., Jing, C., Hui-Tian, W., Jun, H., Wei, J.: Z-scan theory of two-photon absorption saturation and experimental evidence, *Journal of Applied Physics*, 102, 8, 083101-083101-5, 2007.
- ❖ Biswas, T., Gerwick, Erik., Koivisto, T., Mazumdar, A.: Towards Singularity- and Ghost-Free Theories of Gravity, *Physical Review Letters*, 108, 3, 2012.
- ❖ Blesic, B.: Protura and Diplura (Insecta: Apteygota) of the Republic of Macedonia 75 years, Macedonian Museum of Natural History, *Skopje*, 157-162.
- ❖ Bogart R.S.: Recurrence of solar activity: Evidence for active longitudes, *Sol. Phys.* 76, 155, 1982.

- ❖ Bogart, R.S., Noerdlinger, P.D.: On the distribution of orbits among long-period comets, *Astronomical Journal*, 87, 911 - 917, 1982.
- ❖ Bolzan, M. J. A., Sahai, Y., Fagundes, P. R., Rosa, R. R., Ramos, F. M., and Abalde, J. R.: Intermittency analysis of geomagnetic storm time-series observed in Brazil, *J. Atmos. Solar-Terr. Phys.*, 67, 1365 – 1372, 2005a.
- ❖ Bolzan, M., Sahai, Y., Fagundes, P., Rosa, R., Ramos, Fernando M., Abalde, J.: Intermittency analysis of geomagnetic storm time-series observed in Brazil, *Journal of Atmospheric and Solar-Terrestrial Physics*, 67, 14, 1365 - 1372, 2005.
- ❖ Boteler, D.H., Pirjola, R., Nevanlinna, H.: The effects of geomagnetic disturbances on electrical systems at the earth's surface, *Adv. Space Res. J.*, 22 (1), 17 - 27, 1998.
- ❖ Bothmer, V.: The solar and interplanetary causes of space storms in solar cycle 23, *IEEE Trans. Plasma Sci.*, 32 (4), 1411 - 1414, 2004.
- ❖ Baubeau, P., Cazelles, B.: French economic cycles: a wavelet analysis of French retro-spective GNP series, *Clometrica* 3, 275 – 300, 2009.
- ❖ Bray R.J., Loughhead, R.E.: Sunspots, *Dover Publications*, New York, 1979.
- ❖ Bruevich, E.A., Yakunina, G.V.: Solar Activity Indices in the Cycles, *Astrophysics.*, 50, 187, 2011.
- ❖ Bruevich, E.A., Yakunina, G.V.: The study of time series of monthly averaged values of F10.7 from 1950 to 2010, *Sun and Geosphere*, 7 (1), 65 - 70, 2012.
- ❖ Bruno, R., Carbone, V., Veltri, P., Pietropaolo, E., and Bavassano, B.: Identifying intermittent events in the solar wind, *Planet. Space Sci.*, 49, 1201–1210, 2001.
- ❖ Bruno, R., Carbone, V., Veltri, P., Pietropaplo, E., Bavassano, B.: Identifying intermittency events in the solar wind, *Planetary and Space Science*, 49, 12, 1201-1210, 2001.

- ❖ Burlaga, L.F., Wang, C., Richardson, J.D., Ness, N.F.: Evolution of Magnetic Fields in Corotating Interaction Regions from 1 to 95 AU: Order to Chaos, *Astrophysical Journal*, 590, 1, 554 - 566, 2003.
- ❖ Buldyrev, S.V., Dokholyan, N.V., Goldberger, A.L., Havlin, S., Peng, C.K., Stanley, H.E., and Viswanathan, G.M.: Analysis of DNA sequences using methods of statistical physics, *Physica, A* 249, 430 - 438, 1998.
- ❖ Bunde, A., Havlin, S., Kantelhardt, J.W., Penzel, T., Peter, J.H., Voigt, K.: Correlated and uncorrelated regions in heart-rate fluctuations during sleep, *Phys. Rev. Lett.* 85, 3736 - 9, 2000.
- ❖ Burlaga, L.F., Behannon, K.W., Klein, L.W.: Compound streams, magnetic clouds, and major geomagnetic storms, *Journal of Geophysical Research*, 92, 1987, 5725 - 5734, 1987.
- ❖ Burlaga, L.F., Forman, Miriam, A.: Large-scale speed fluctuations at 1 AU on scales from 1 hour to ≈ 1 year: 1999 and 1995, *Journal of Geophysical Research (Space Physics)*, 107 (A11), SSH 18 -1, 2002.
- ❖ Burlaga, L.F., Intermittent turbulence in the solar wind, *J. Geophys. Res.*, 96, 5847-5851, 1991c.
- ❖ Burlaga, L.F., Multifractal structure of speed fluctuations in recurrent streams at 1 AU and near 6 AU, *Geophys. Res. Lett.*, 18, 1651 - 1654, 1991b.
- ❖ Burlaga, L.F., Multifractal structure of the interplanetary magnetic field: Voyager 2 observations near 25 AU, 1987 – 1988, *Geophys. Res. Lett.*, 18, 69 - 72, 1991a.
- ❖ Burlaga, L.F., Ness, N.F., Acuna, M.H., Lepping, R.P., Connerney, J.E.P., Stone, E.C., McDonald, F.B.: Crossing the Termination Shock into the Heliosheath: Magnetic Fields, *Science*, 309, 5743, 2027 - 2029, 2005.

- ❖ Burlaga, L.F.: Multifractal structure of the magnetic field and plasma in recurrent streams at 1 AU, *Journal of Geophysical Research*, 97, 4283 - 4293, 1992.
- ❖ Burlaga, L.F.: Intermittent turbulence in large-scale velocity fluctuations at 1 AU near solar maximum, *Journal of Geophysical Research*, 98, 17467 - 17474, 1993.
- ❖ Cane, H.V., Richardson, I.G., Roseninge, T.T.: Interplanetary magnetic field periodicity of 153 days, *G Geophys. Res. Lett.*, 25, 4437, 1998.
- ❖ Cao, L.Y.: Practical method for determining the minimum embedding dimension of a scalar time series, *Physica D: Nonlinear Phenomena*, 110 (43), 1997.
- ❖ Carbonell, M., Ballester, J.L.: A short-term periodicity near 155 day in sunspot areas, *A&A*, 238, 377 - 381, 1990.
- ❖ Carlowicz, M.J., Lopez, R.E.: Storms from the Sun: The Emerging Science of Space Weather, *Joseph Henry Press*, 2002
- ❖ Chang, T.: Self-organized criticality, multifractal spectra, sporadic localized reconnections and intermittent turbulence in the magnetotail, *Phys. Plasmas*, 6, 4137 - 4145, 1999.
- ❖ Chatterjee, T. N.: On the application of information theory to the optimum state-space reconstruction of the short-term solar radio flux (10.7cm), and its prediction via a neural network, *Mon. Not. Roy. Astron. Soc.* 323 (1), 101 - 108, 2001.
- ❖ Chou, C.M.: Applying multi resolution analysis to differential hydrological grey models with dual series. *J. Hydrol.* 332 (1 - 2), 174 – 186, 2007.
- ❖ Chou, C.M.: Wavelet-based multi-scale entropy analysis of complex rainfall time series. *Entropy*, 13 (1), 241 – 253, 2011.

- ❖ Chowdhury, P., Dwivedi, B.N.: Periodicities of Sunspot Number and Coronal Index Time Series During solar Cycle 23, *Solar Physics*, 270, 365 - 383, 2011.
- ❖ Chowdhury, P., Khan, M., Ray, P.C.: Evaluation of the intermediate-term periodicities in solar and cosmic ray activities during cycle 23, *Astrophys. Space Sci.* 326, 191 - 201, 2010a.
- ❖ Chowdhury, P., Khan, M., Ray, P.C.: Intermediate-term periodicities in sunspot areas during solar cycles 22 and 23, *Mon. Not. Roy. Astron. Soc.* 392, 1159 - 1180, 2009b.
- ❖ Christopher, T., Gilbert, P.C.: A practical guide to wavelet analysis, *Bull AmerMeteorolSoc*, 79, 61 - 68, 1998.
- ❖ Clark D.H., Stephenson F.R.: An interpretation of the pre-telescopic sunspot records from the orient, *Q.J. Roy. Astron. Soc.* 19, 387 - 410, 1978.
- ❖ Cliver, E.W., Ling, A.G.: 22 Year Patterns in the Relationship of Sunspot Number and Tilt Angle to Cosmic-Ray Intensity, *Astrophys. J. Lett.*, 551, 189, 2001.
- ❖ Clua de Gonzalez, Alicia I., Gonzalez, Walter D., Dutra, Severino L. G., Tsuritani, Bruce T.: Periodic variation in the geomagnetic activity: A study based on the Ap index, *Journal of Geophysical Research*, 98, A6, 9215-9232, 1993.
- ❖ Connor, J., Rossiter, R. Wavelet Transforms and Commodity Prices, *Studies in Nonlinear Dynamics & Econometrics*, 9 (1). 6, 20, 2005.
- ❖ Consolini, G., De Michelis, P., Tozzi, R.: On the earth's magnetospheric dynamics evolution and the fluctuation theorem, *J. Geophysics. Res.*, 113, A08222, 2008.
- ❖ Covington, A.E.: Solar radio emission at 10.7cm, *Roy J. Astron. Soc. Can.*, 63, 125, 1969.

- ❖ Crowley, P., Mayes, D.: How fused is the euro area core? An evaluation of growth cycle co movement and synchronization using wavelet analysis, *Journal of Business Cycle Measurement and Analysis*, 4, 63 - 95, 2008.
- ❖ Crowley, T.J., Berner, R.A.: CO₂ and climate change, *Science* 292, 870 – 872, 2001.
- ❖ Daglis, I.A., Baker, D.N., Galperin, Y., Kappenman, J.G., Lanzerotti, L.J.: Technological impacts of space storms: Outstanding issues, *Eos, Transactions American Geophysical Union*, Volume 82, Issue 48, p. 585-585, 2001.
- ❖ Daglis, I.A., Delcourt, D., Metallinou, F.A., Kamide, Y.: Particle acceleration in the frame of the storm-substorm relation, *IEEE Trans. Plasma Sci.*, 32 (4 - 1), 1449 - 1454, 2004.
- ❖ Das, T.K., Nag, T.K.: A 14 - day periodicity in the mean solar magnetic field, *Solar Physics*, 187, 1, 177 - 184, 1999.
- ❖ de Artigas, M.Z., Elias, A.G., de Campra, P.F.: Discrete wavelet analysis to assess long-term trends in geomagnetic activity, *Phys. Chem. Earth*, 31 (1-3), 77 - 80, 2006.
- ❖ De Pater, I., Lissauer, Jack J.: *Planetary Sciences, Planetary Sciences*, by Imke de Pater and Jack J. Lissauer, 544, 2001.
- ❖ Defise, J.M. et al., SWAP and LYRA: space weather from a small spacecraft, *2nd Int. Conf. on Recent Advances on Space Technologies 2005 (RAST2005)*, 9 - 11th June, 2005.
- ❖ Delache, P.H., Laclare, F., Sadsoud, H.: Long period oscillations in solar diameter measurements, *Nature*, 317, 416 - 418, 1985.
- ❖ Deng, L.H., Li B., Zheng Y.F., Cheng X.M.: Relative phase analyses of 10.7 cm flux with sunspot numbers. *New astronomy*, 23 - 24, 1 - 5, 2013.

- ❖ Deng, L.H., Qu, Z.Q., Wang K.R., et al.: Phase asynchrony between coronal index and sunspot numbers, *Adv Space Res*, 50, 1425 - 1433, 2012.
- ❖ Deng, L.H., Qu, Z.Q., Yan X.L., et al.: Phase analysis of sunspot group numbers on both solar hemispheres, *Res AstronAstr*, 13, 104 - 114, 2013.
- ❖ Dennis, B.R.: Solar Hard X-Ray Bursts, *Solar Phys.*, 100, 465 – 490, 1985.
- ❖ Dodson, R., Hedeman, E.R., Mohler, O.C.: Comparison of activity in solar cycles 18,19 and 20, *Res. Astron. Geophys.Space Phys.*, 12, 329, 1974.
- ❖ Donnelly, R. F., and L. C. Puga.: Thirteen-day periodicity and the center-to-limb dependence of UV, EUV, and X-ray emission of solar activity, *Sol. Phys.*, 130, 369 - 390, 1990.
- ❖ Dorman, L.I.: Forecasting of great radiation hazard: estimation of particle acceleration and propagation parameters by possible measurements of gamma rays generated in interactions of sep with upper corona and solar wind matter, *2nd Online Proceeding on European Space Weather Week*, ESA-ESTEC, Noordwijk, Netherland, 14 - 18th November, 2005.
- ❖ Droge, W., Gibbs, K., Grunsfeld, J.M., Meyer, P., Newport, B.J.: A 153 day periodicity in the occurrence of solar flares producing energetic interplanetary electrons, *ApJS*, 73, 279, 1990.
- ❖ Drozd, S., Kwapien, J., Oswiecimka, P., Rak, R.: Quantitative features of multifractal subtleties in time series, *EPL (Europhysics Letters)*, 88, 6, 60003, 2009.
- ❖ Duhau, S.: Wavelet analysis of solar activity recorded by sunspot groups, *Solar Phys.*, 213: 203 – 212, 2003.
- ❖ Eckmann, J.P., Kamphorst, S.O., Ruelle, D.: Recurrence plots of dynamical systems, *Europhysics Letters*, 5, 973 – 977, 1987.
- ❖ Eckmann, J.P., Ruelle, D.: Ergodic theory of chaos and strange attractors, *Review of Modern Physics*, 57 (3), 617 – 656, 1985.

- ❖ Eddy, J.A.: The Maunder Minimum, *Science*, 192, 1189 - 1202, 1976.
- ❖ Farge, M.: Wavelet transforms and their applications to turbulence, *Ann. Rev. Fluid Mech.* 24, 395 – 457, 1992.
- ❖ Feder J.: *Fractals*, Plenum Press, New York, 1988.
- ❖ Feminella, F., Storini, M.: Large-scale dynamical phenomena during solar activity cycles, *Astronomy and Astrophysics*, 322, 311 - 319, 1997.
- ❖ Fenimore, E.E., Cannon, T.M.: Coded aperture imaging with uniformly redundant arrays, *Applied Optics*, 17, 337 - 347, 1978.
- ❖ Fenimore, E. E., Cannon, T. M.: Coded aperture imaging with uniformly redundant arrays, *Applied Optics*, 17, 337 - 347, 1978.
- ❖ Floyd, L., Newmark, J., Cook, J., Herring, McMullin, D.: Solar EUV and UV spectral irradiances and solar indices, *J. Atmos. Sol. Terr. Phys.*, 67, 3 - 15, 2005. doi: 10.1086/521592.
- ❖ Foukal, P., Lean.: An empirical model of total solar irradiance variation between 1874 and 1988, *J. Science*, 247, 556 - 558, 1990.
- ❖ Fraser-Smith, A.C.: Spectrum of the geomagnetic activity index Ap, *Journal of Geophysical Research*, 77, 22, 4209, 1972.
- ❖ Freeman, J.W.: *Storms in Space*, Cambridge University Press, 2001.
- ❖ Fugal, D.L.: *Conceptual wavelets in Digital Signal Processing. An in-depth, Practical Approach for the Non-mathematician, first ed. Space & Signals Technologies LLC*, 2009.
- ❖ Gaci, S., Zaourar, N., Hamoudi, M., Holschneider, M.: Local regularity analysis of strata heterogeneities from sonic logs, *Nonlinear Processes in Geophysics*, 17, 5, 2010, 455 - 466, 2010.
- ❖ Gaizauskas, V., Tapping, K.F.: Compact sites at 2.8 cm wavelength of microwave emission inside solar active regions, *AJ*, 325, 912, 1988.

- ❖ Gallegati, M., Gallegati, M.: Wavelet variance analysis of output in g-7 countries', *Studies in Nonlinear Dynamics & Econometrics*, 11(3), 2007.
- ❖ Galsgaard, K., Longbottom, A.W.: Formation of Solar Prominences by Flux Convergence, *APJ*, 510, 444 – 459, 1999.
- ❖ Galsgaard, K., Longbottom, A.W.: Formation of Solar Prominences by Flux Convergence, *ApJ*, 510, 444 - 459, 1999.
- ❖ Gao, J.B., Cao, Y.H., Tung, W.W., Hu, J.: *Multiscale Analysis of Complex Time Series - Integration of Chaos and Random Fractal Theory, and Beyond*, New York: Wiley - Interscience, 2007.
- ❖ Gao, J.B., Hu, J., Tung, W.W., Cao, Y.H., Sarshar, N., Roy, chowdhury, V.P.: Assessment of long range correlation in time series: How to avoid pitfalls, *Phys. Rev. E*, 73 016117, 2006.
- ❖ Garrett, H.B., Hoffman, A.R.: Comparison of spacecraft charging environments at the Earth, Jupiter, and Saturn, *IEEE Trans. Plasma Sci.*, 28(6), 2048 - 2057, 2000.
- ❖ Gencay, R., Selcuk, F., Whitcher, B.: Multiscale Systematic Risk, *Journal of International Money and Finance*, 24(1), 55 - 70, 2005.
- ❖ Gencay, R., Selcuk, F., Whitcher, B.: Scaling properties of foreign exchange volatility, *Physica A*, 289, 249 - 266, 2001a.
- ❖ Gonzalez, A. L. C., Gonzalez, W. D.: Periodicities in the interplanetary magnetic field polarity, *J. Geophys. Res.*, 92, 4357, 1987.
- ❖ Gopalswamy, N.: American institute of Physics conference proceedings proc, 11th *International Astrophysical conference*, edited by Q.Ho, G.P.Zank, G.Fry, X.Ao and J. Adams, 2012.
- ❖ Gopalswamy, Nat.: Halo coronal mass ejections and geomagnetic storms, *Earth, Planets and Space*, 61, 595-597, 2009.

- ❖ Gosling, J.T., Asbridge, J.R., Bame, S.J., Felman, W.C.: Solar wind speed variations – 1962 - 1974, *Journal of Geophysical Research*, 81, 5061 - 5070, 1976.
- ❖ Gosling, J.T., Bame, S.J.: Solar-wind speed variations 1964 - 1967: An autocorrelation analysis, *Journal of Geophysical Research*, 77, 1, 12, 1972.
- ❖ Gosling, J. T., Hildner, E., MacQueen, R. M., Munro, R. H., Poland, A. I., Ros, C. L.: The speeds of coronal mass ejection events, *Solar Physics*, 48, 389 - 397, 1976.
- ❖ Gotoh. T., Kraichnan, R.: Turbulence and Tsallis statistics, *Physica D: Nonlinear Phenomena*, 193, 231 - 244, 2004.
- ❖ Graps, A.: An introduction to wavelets, *IEEE Comp. Sci. Engng*, 2 (2), 50 – 61, 1995.
- ❖ Greenkorn, R.A.: Analysis of sunspot activity cycles *Solar Phys*, 255, 301-323, 2009.
- ❖ Greenkorn, Robert A.: Analysis of Sunspot Activity Cycles, *Sol. Phys.*, 255, 2, 301 - 323, 2009.
- ❖ Grinsted, A., Moore, J.C., Jevrejeva, S.: Application of the cross wavelet transform and wavelet coherence to geophysical time series, *Nonlinear Proc Geophys*, 11, 561 – 566, 2004.
- ❖ Gu, R.B., Chen, H.T., Wang, Y.D.: Multifractal analysis on international crude oil markets based on the multifractal detrended fluctuation analysis, *Physica A* 389, 2805 – 2815, 2010.
- ❖ Hale George E.: On the Nature of Sun-Spots, *Proceedings of the Royal Society of London. Series A, Containing Papers of a Mathematical and Physical Character*, 95, 668, 234 - 236, 1919.
- ❖ Hale, G.E., Ellerman, F., Nicholson, S.B., Joy, A.H.: The Magnetic Polarity of Sun - Spots, *Astrophysical Journal*, 49, 153, 1919.

- ❖ Harrison, R.A.: The source regions of solar coronal mass ejections, *Solar Phys*, 126, 185 – 193, 1990.
- ❖ Harvey, J.H. (1996). *Embracing their memory: Loss and the social psychology of story-telling*. Needham Heights, MA: Allyn & Bacon.
- ❖ Hathaway, D.H., Wilson, R.M., Reichmann, E.J.: Group sunspot numbers; Sunspot Cycle Characteristics, *Solar Phys.*, 211, 357 – 370, 2002.
- ❖ Hathaway D.H.: The solar cycle, *Living reviews in Solar Physics*, 7, 1 - 65, 2010.
- ❖ Hathaway, D.H., Wilson, R.M., Riechmann, E.J.: Group Sunspot Numbers: Sunspot Cycle Characteristics, *Sol. Phy.*, 211, 1, 357-370, 2002.
- ❖ Hausdorff, J.M., Mitchell, S.L., Firtion, R., Peng, C.K., Cudkowicz, M.E., Wei, J.Y., Goldberger, A.L.: Altered fractal dynamics of gait: reduced stride-interval correlations with aging and Huntington's disease, *J. Appl. Physiology* 82, 262, 1997.
- ❖ Hill, F., Erdwurm, W.D., Branston, McGraw, R.: The National Solar Observatory Digital Library - a resource for space weather studies, *J. Atmos. Sol. Terr. Phys.*, 62, 1257 - 1264, 2000.
- ❖ Howe, R., Christensen-Dalsgaard, J., Hill, F., Komm, R.W., Larsen, R.M., Schou, J., Thompson, M.J., Toomre, J.: Dynamic Variations at the Base of the Solar Convection Zone, *Science*, 287, 2456, 2000.
- ❖ Hoyt, D.V., Schatten, K.H.: Group Sunspot Numbers: A New Solar Activity Reconstruction, *Solar Phys.*, 179, 189 - 219, 1998.
- ❖ Hoyt, D.V., Schatten, K.H.: Group Sunspot Numbers: A New Solar Activity Reconstruction, *Solar Phys.*, 179, 189, 1998a.
- ❖ Hoyt, D.V., Schatten, K.H.: Group Sunspot Numbers: A New Solar Activity Reconstruction, *Solar Phys.*, 181, 491 - 512, 1998b.

- ❖ Hu, Z.Z., Nitta, T.: Wavelet analysis of summer rainfall over North China and India and SOI using 1891-1992 data, *J. Meteorol. Soc., Japan*, 74, 833 - 844, 1996.
- ❖ Hurst, H.: Long term storage capacity of reservoirs, *Transactions of the American Society of Engineers*, 116, 770 – 799, 1951.
- ❖ Ichimoto, K., Kubota, J., Suzuki, M., Tohmura, I., Kurokawa, H.: Periodic behaviour of solar flare activity, *Nature*, 316, 422 - 424, 1985.
- ❖ Illing, R.M.E., Hundhausen, A.J.: Disruption of a coronal streamer by an eruptive prominence and coronal mass ejection, *J. Geophys. Res.* 91,10951 - 10960, 1986.
- ❖ Ivanova, K., Ausloos, M., Clothiaux, E.E., Ackerman, T.P.: Break-up of stratus cloud structure predicted from non-Brownian motion liquid water and brightness temperature fluctuations, *Europhys. Lett.* 52, 40 2000.
- ❖ Jevtic, N., Schweitzer. J.S., Cellucci, C.J.: Nonlinear time series analysis of northern and southern solar hemisphere daily sunspot numbers in search of short-term chaotic behavior, *Astron. Astrophys.*, 379, 611 - 615, 2001.
- ❖ Johnson, R.W.: Power law relating 10.7 cm flux to sunspot number, *Astrophys. Space Sci.*, 332, 73 - 79, 2011.
- ❖ Jokiahho, O.P.: Impact of space weather on satellite operations and terrestrial systems, *55th Int. Astronautical Congress of the International Astronautical Federation, the International Academy of Astronautics, and the International Institute of Space Law*, Vancouver, Canada, 4 - 8th October, 2004.
- ❖ Joselyn, J.A., McIntosh, P.S.: Disappearing solar filaments: A useful predictor of geomagnetic activity, *J. Geophys. Res.*, 86, 4555, 1981.
- ❖ Jury, M.R., Enfield, D.B., Mèlice, J.: Tropical monsoons around Africa: stability of E1 Niño-Southern oscillation associations and links with continental climate, *J. Geophys. Res.*, 107(C10), 3151 – 3167, 2002.

- ❖ Kamide, Y., Yokoyama, N., Gonzalez, W.D., Tsurutani, B.T., Daglis, I.A., Brekke, A., Masuda, S.: Two-step development of geomagnetic storms, *J. Geophys. Res.*, 103, 6917 - 6921, 1998a.
- ❖ Kane, R.P.: Periodicities of a few months in solar indices, *Journal of Atmospheric and Solar-Terrestrial Physics*, 65, 8, 979 - 986, 2003.
- ❖ Kantelhardt, J.W., Berkovits, R., Havlin, S., Bunde, A.: Are the phases in the Anderson model long-range correlated? *Physica A*, 266, 461 - 464, 1999.
- ❖ Kantelhardt, J.W., Zschiegner, S.A., Koscielny-Bunde, E., Havlin, S., Bunde, A., Stanley, H.E.: Multifractal detrended fluctuation analysis of nonstationary time series, *Physica A: Statistical Mechanics and its Applications*, 316, 1, 87 - 114, 2002.
- ❖ Kantelhardt, J.W., Zschiegner, S.A., Koscielny-Bunde, E., Havlin, S., Bunde, A., Stanley, H.E.: Multifractal detrended fluctuation analysis of nonstationary time series, *Physica A: Statistical Mechanics and its Applications*, 316, 1, 87 - 114, 2002.
- ❖ Kantelhardt, J.W., Koscielny-Bunde, E., Rego, H.H.A., Havlin, S., Bunde, A.: *Detecting long-range correlations with detrended fluctuation analysis*, *Physica A* 295, 441 – 454, 2001.
- ❖ Kappenman, J.G.: Geomagnetic storm and power system impacts: advanced storm forecasting for transmission system operations, *Power Engineering Society Summer Meeting*, 18 - 22th July, 1999.
- ❖ Katsavrias, C. Preka-Papadema, P., Mossas, X.: Wavelet Analysis on solar Wind Parameters and Geomagnetic Indices, *Solar Phys.*, 2012. DOI 10.1007/s1 1207-012-0078-6.
- ❖ Kaushik, S.C., Shrivastava, P.K.: Influence of magnetic clouds on interplanetary features, *Indian Journal of Physics*, 74 B (2), 159 – 162, 2000.
- ❖ Kennel, Mathew B., Brown, Reggie., Abarbanel, Henry, D.I.: Determining embedding dimension for phase-space reconstruction using a geometrical

- construction, *Physical Review A (Atomic, Molecular, and Optical Physics)*, 45, 6, 3403 - 3411, 1992.
- ❖ Kikuchi, T.: Space weather hazards to communication satellites and the space weather forecast system, *21st Int. Communications Satellite Systems Conference and Exhibit, Yokohama, Japan, 15 - 19th April, 2003*.
 - ❖ Kilcik, A., Ozguc, A., Rozelot, J.P., Atac, T.: Periodicities in Solar Flare Index for Cycles 21 - 23 Revisited, *Sol. Phys.*, 264, 255 - 268, 2010.
 - ❖ Kile, J.N., Cliver, E.W.: A search for the 154 day periodicity in the occurrence rate of solar flares using Ottawa 2.8 GHz burst data. *ApJ*, 370, 442, 1991.
 - ❖ Kilic, H.: Midrange periodicities in sunspot numbers and flare index during solar cycle 23, *Astron. Astrophys.*, 481, 235 - 238, 2008.
 - ❖ Kilic, H.: Short-Term Periodicities in Sunspot Activity and Flare Index Data during Solar Cycle 23, *Sol. Phys.* 255, 155 - 162, 2009.
 - ❖ Kiplinger, A.L., Dennis, B.R., Orwig, L.E.: Detection of a 158 Day periodicity in the Solar hard X-Ray Flare Rate, *BAAS*, 16, 891, 1984.
 - ❖ Knaack, R., Stenflo, J.O., Berdyugina, S.V.: Evolution and rotation of large-scale photospheric magnetic fields of the Sun during cycles 21-23. Periodicities, north-south asymmetries and r-mode signatures, *Astron. Astrophys.* 438, 1067 - 1082, 2005.
 - ❖ Koscielny-Bunde, E., Bunde, A., Havlin, S., Roman, H. E., Goldreich, Y., and Schellnhuber, H. J.: Indication of a universal persistence law governing atmospheric variability, *Phys. Rev. Lett.*, 81, 729 - 732, 1998.
 - ❖ Kovacs, P., Carbone, V., Voros, Z.: Wavelet-based filtering of intermittent events from geomagnetic time series, *Planetary and Space Science*, 49, 1219 - 1231, 2001.

- ❖ Krivova, N.A., Solanki, S.K.: The 1.3-year and 156-day periodicities in sunspot data: Wavelet analysis suggests a common origin, *Astron. Astrophys.*, 394, 701 - 706, 2002.
- ❖ Kulkarni, J.R.: Wavelet analysis of the association between the Southern Oscillation and the Indian summer monsoon. *Int. J. Climatol.*, 20 (1), 89 – 104, 2000.
- ❖ Kumar, P., Foufoula-Georgiou, E.: A new look at rainfall fluctuations and scaling properties of spatial rainfall using orthogonal wavelets, *J. Appl. Meteorol.*, 32, 209 – 222, 1993c.
- ❖ Kumar, P., Foufoula-Georgiou, E.: Wavelet Analysis for Geophysical Applications, *Reviews of Geophysics*, 35(4), 385 – 412, 1997.
- ❖ Kumar, P., Foufoula-Georgiou, E.: A multicomponent decomposition of spatial rainfall fields, 1, Segregation of large- and small - scale features using wavelet transforms, *Water Resour. Res.*, 29 (8), 2515 – 2532, 1993a.
- ❖ Kumar, P., Foufoula-Georgiou, E.: A multicomponent decomposition of spatial rainfall fields, 2, Self-similarity in fluctuations, *Water Resour. Res.*, 29(8), 2533 - 2544, 1993b.
- ❖ L. Gyuchang, Kim, S. Y., Lee, H., Kim, K., and Lee, D. I.: Multifractal detrended fluctuation analysis of derivative and spot markets, *Physica A*, 386, 1, 259–266, 2007.
- ❖ Label, K.A., Barth, J.L.: Radiation effects on emerging technologies—implications of space weather risk management, *AIAA Space 2000 Conference and Exposition, Long Beach, CA*, 19 - 21th September, 2000.
- ❖ Lai, S.T., DSCS satellite dielectric charging correlation with magnetic activity, *IEEE Int. Conf. Plasma Sci. (ICOPS'99)*, 20 - 24th June, 1999.
- ❖ Lai, S.T., What measurements in space weather are needed for predicting spacecraft charging?, *IEEE Int. Conf. Plasma Sci.*, 3 - 5th June, 1996.

- ❖ Lakhina G.S.: Solar wind-magnetosphere-ionosphere coupling and chaotic dynamics, *Surveys in Geophysics*, 15 (6), 703 - 754, 1994.
- ❖ Lau, K.M., Weng, H.: Climate Signal Detection Using Wavelet Transform: How to Make a Time Series Sing, *Bulletin of the American Meteorological Society*, 76, 12, 2391-2402, 1995.
- ❖ Le, G.M.: Wavelet analysis of the schwabe cycle properties in solar activity, *Chin J Astron Astrophys.*, 4, 578 – 582, 2004.
- ❖ Lean, J.L., Brueckner, G.E.: Intermediate-term solar periodicities: 100-500 days, *Astrophys. J.*, 337, 568, 1989.
- ❖ Lean, J.L., Rind, D.H.: How natural and anthropogenic influences alter global and regional surface temperatures: 1889 to 2006, *Geophys. Res. Lett.*, 35, L18701, 2008.
- ❖ Lean, J.L.: Evolution of the 155 day periodicity in sunspot areas during solar cycles 12 to 21, *Astrophys. J.* 363, 718, 1990.
- ❖ Li, K.J., Gao, P.X., Zhan, L.S., et al.: On the Synchronization of hemispheric high-latitude solar activity, *Mon. Not. Roy. AstronSoc.*, 391, L34 - L38, 2008.
- ❖ Li, K.J., Gao, P.X., Zhan, L.S., et al.: Relative phase analyses of long-term hemispheric solar flare activity, *Mon. Not. Roy. AstronSoc.*, 401, 342 – 346, 2010.
- ❖ Li, K.J., Gao, P.X., Zhan, L.S.: Synchronization of hemispheric sunspot activity revisited: Wavelet transform analyses, *Astrophys J*, 691, 537 – 546, 2009.
- ❖ Li, Q.X.: Periodicity and hemispheric phase relationship in high-latitude solar activity, *Sol. Phys.*, 249, 135 - 145, 2008
- ❖ Li, X., Yao, X., Jefferys, J.G.R., Fox. J.: Computational neuronal oscillation with morlet wavelet transform, *Proceedings of 27th annual international conference of the IEEE engineering in medicine and biology Society, Shanghai, SEP., IEEE Press*, 1 - 4, 2005.

- ❖ Li, Z., Lu, X.: Cross-correlations between agricultural commodity futures markets in the US and China, *Physica A*, 391, 3930 – 3941, 2012.
- ❖ Li, Z., Lu, X.: Multifractal analysis of China's agricultural commodity futures markets, *Energy Procedia*, 5, 1920 – 1926, 2011.
- ❖ Lockwood, M.: Reconstruction and Prediction of Variations in the Open Solar Magnetic Flux and Interplanetary Conditions, *Living Reviews in Solar Physics*, 10, 1, 4, 88, 2013.
- ❖ Loewe, C.A., Prolss, G.W.: Classification and mean behavior of magnetic storms, *J. Geophys. Res.*, 102, 14209 - 14213, 1997.
- ❖ Lou, Yu-Qing; Wang, Yu-Ming; Fan, Zuhui; Wang, Shui; Wang, Jing Xiu.: Periodicities in solar coronal mass ejections, *Monthly Notices of the Royal Astronomical Society*, 345, 3, 809-818, 2003.
- ❖ Love, D.P., Toomb, D.S., Wilkinson, D.C., Parkinson, J.B.: Penetrating electron fluctuations associated with GEO spacecraft anomalies, *IEEE Trans. Plasma Sci.*, 28(6), 2075 - 2084, 2000.
- ❖ Lui, A.T.Y.: Multiscale phenomena in the near-Earth magnetosphere, *J. Atmos. Sol. Terr. Phys.*, 64, 125 - 143, 2002.
- ❖ Macek, W.M.: Modeling Multifractality of the Solar Wind, *Space Science Reviews*, 122, 1 - 4, 329 - 337, 2006.
- ❖ Malamud, B.D., Turcotte, D.L.: Self-affine time series: measures of weak and strong persistence, *J. Stat. Plan. Infer.*, 80 (1 -2), 173 - 196, 1999.
- ❖ Mallat, E., Klotz, A., Brecht, A., Gauglitz, G., Barcelo, D.: River Analyzer for Chlorotriazines with a Direct Optical Immunosensor, *Environmental Science & Technology*, 33, 6, 965-971, 1999.
- ❖ Manda, M., Balasis, G.: FAST TRACK PAPER: The SGR 1806-20 magnetar signature on the Earth's magnetic field, *Geophysical Journal*, 167, 2, 586-591, 2006.

- ❖ Mandelbrot, B.: The Fractal Geometry of Nature, *Freeman, New York*, 1983.
- ❖ Mandelbrot, B.B., Hudson, R.: The (mis)behaviour of markets, *Perseus Books, Cambridge MA*, 2004.
- ❖ Mantegna, R.N., Stanley, H.E.: Introduction to Econophysics, 158, Cambridge, UK: *Cambridge University Press*, 1999.
- ❖ Marsch, E., Tu, C. Y.: Intermittency, non-Gaussian statistics and fractal scaling of MHD fluctuations in the solar wind, *Nonlinear Processes in Geophysics*, 4,2, 101 - 124, 1997.
- ❖ Marwan, N., Kurths, J.: Cross recurrence plots and their applications, in *Mathematical Physics Research at the Cutting Edge*, C.V. Benton Editor, *Nova Science Publishers*, 101 - 139, 2004.
- ❖ Marwan, N., Kurths, J.: Line structures in recurrence plots, *Phys. Lett. A*, 336 (4 - 5), 349 - 357, 2005.
- ❖ Marwan, N., Kurths, J.: Nonlinear analysis of bivariate data with cross recurrence plots, *Physics letters A*, 302, 299 - 307, 2002.
- ❖ Marwan, N., Romano, M.C., Thiel, M., Kurths, J.: Recurrence plots for the analysis of complex systems, *Phys. Rep.*, 438 (5 – 6), 237 - 329, 2007.
- ❖ Marwan, N., Thiel, M., Nowaczyk, N.R.: Cross recurrence plot based synchronization of time series, *Nonlin. Processes Geophys.*, 9, 325 - 331, 2002a.
- ❖ Mavromichalaki, H., Petropoulos, B., Plainaki, C., Dionatos, C., Zouganelis, I., Coronal index as a solar activity index applied to space weather, *Advances in Space Research*, 35, 410 – 415, 2005.
- ❖ McAteer R.T.J., Young, C.A., Ireland, J. Gallagher, P.T.: The Bursty Nature of Solar Flare X-Ray Emission , *Astrophys. J.*, 662 (1), 691 - 700, 2007.

- ❖ Mendes, A.C.R., Neves, C., Oliveira, W., Takakura, F.I.: Supersymmetrization of radiation damping, *Journal of Physics A: Mathematical and Theoretical*, 38, 42, 9387-9394, 2005.
- ❖ Meyer, F., Averbuch, A., Stromberg, J.O.: Fast wavelet packet image compression, *In IEEE data compression conference-DCC'98*, 1998.
- ❖ Milan, S.E., Lester, M., Cowley, S.W.H., Brittnacher, M.: Convection and auroral response to a southward turning of the IMF: Polar UVI, CUTLASS, and IMAGE signatures of transient magnetic flux transfer at the magnetopause, *Journal of Geophysical Research*, 105, A7, 15741-15756, 2000.
- ❖ Mininni, P.D., Gomez, D.O., Mindlin, G.B.: Biorthogonal decomposition techniques unveil the nature of the irregularities observed in the solar cycle, *Physical Review Letters*, 89, 061101, 2002.
- ❖ Morlet, J., Arens, G. et al.: Wave propagation and sampling theory, *Geophysics*, 47, 203 – 236, 1982.
- ❖ Movahed, M.S., Jafari, G.R., Ghasemi, F., Rahvar. S., Tabar, M.R.R.: Multifractal detrended fluctuation analysis of sunspot time series, *J. Stat. Mech.*, P02003, 2006.
- ❖ Mursula, K., Zieger, B.: The 1.3-Year Variation in Solar Wind Speed and Geomagnetic Activity, *Advances in Space Research*, 25, 9, 1939 - 1942, 2000.
- ❖ Mursula, K., Zieger, B.: The 13.5-day periodicity in the Sun, solar wind, and geomagnetic activity: The last three solar cycles, *Journal of Geophysical Research*, 101, A12, 27077-27090, 1996.
- ❖ Muzy, J.F., Bacry, E and Arneodo, A.: The multifractal formalism revisited with wavelets, *Int. J. Bifurc. Chaos* 4, 245 - 302, 1994.
- ❖ Nayar, S.R.P., Nair, V.S., Radhika, V.N., Revathy, K.: Short period features of the interplanetary plasma and their evolution, *Sol. Phys.*, 201, 405, 2001.

- ❖ Nayar, S.R.P., Radhika, V.N., Revathy, K., Ramadas, V.: Wavelet analysis of solar wind and geomagnetic parameter, *Sol. Phys.*, 208, 359, 2002.
- ❖ Ness, N.F., Wilcox, J.M.: Solar origin of the interplanetary magnetic field, *Phys. Rev. Letters*, 13, 46, 1964.
- ❖ Neugebauer, M.: The three-dimensional solar wind at solar activity minimum, *Reviews of Geophysics*, 37, 1, 107 - 126, 1999.
- ❖ Norouzzadeh, P., Rahmani, B.: A multifractal detrended fluctuation description of Iranian rialUS dollar exchange rate, *Physica A*, 367, 328 – 337, 2006.
- ❖ Oliver, R., Ballester, J.L., Baudin, F.: Emergence of magnetic flux on the Sun as the cause of a 154-day periodicity in sunspot areas, *Nature*, 394, 552, 1998.
- ❖ Oliver, R., Ballester, J.L., Baudin, F.: Emergence of magnetic flux on the Sun as the cause of a 158-day periodicity in sunspot areas, *Nature*, 394, 6693, 552 - 553, 1998.
- ❖ Oslen, J.: Persistent Solar Rotation-Period of 26 7/8 Days and Solar-Diurnal Variation in Terrestrial Magnetism, *Terrestrial Magnetism and Atmospheric Electricity (Journal of Geophysical Research)*, 53, 2, 123-134, 1948.
- ❖ Oswiecimka, P., Kwapien, J., Drozd, S.: Multifractality in the stock market: price increments versus waiting times, *Physica A: Statistical Mechanics and its Applications*, 347, 626 - 638, 2005.
- ❖ Oswiecimka, P., Kwapien, J., Gorski, A.Z., Drozd, S., Rak, R.: Different Fractal Properties of Positive and Negative Returns, *Acta Physica Polonica A*, 114, 3, 547, 2008.
- ❖ Özgüç, A., Ataç, T., Rybák, J.: Flare index variability in the ascending branch of solar cycle 23, *J. Geophys. Res.* 107, 2002. 10.1029/2001JA009080.

- ❖ Özgüç, A., Atac, T.: Periodic behavior of solar flare index during solar cycles 20 and 21, *Solar Phys.*, 123, 357, 1989.
- ❖ Pap, J., Tobiska, W.K., Bouwer, S.D.: Periodicity of solar irradiance and solar activity indices, I, *Solar Phys.*, 129, 165, 1990.
- ❖ Pavlos et al., Chaotic dynamics in Astrophysics and Space Physics, Proc. 1st General Conference of the Balkan Physical Union, Thessaloniki, 1991.
- ❖ Pavlos G.P., et al., First and second order non-equilibrium phase transition and evidence for non-extensive *Tsallis statistics in Earth's magnetosphere*, *Physica A*, 390, 2819 - 2839, 2011.
- ❖ Pavlos G.P., et al., Tsallis statistics and magnetospheric self-organization, *Physica A*, 391, 3069 - 3080, 2012.
- ❖ Peng, C.K., Buldyrev, S.V., Havlin, S., Simons, M., Stanley, H.E., Goldberger, A.L.: Mosaic organization of DNA nucleotides, *Phys. Rev. E* 49, 1685 - 1689, 1994.
- ❖ Peng, Q., Vienne, A., Shen, K.X.: VizieR Online Data Catalog: Saturnian Satellites positions (1996-2000), VizieR On-line Data Catalog: J/A+A/383/296, 2001.
- ❖ Perez-Peraza J., Velasco V., Kavlakov, S.: Wavelet coherence analysis of atlantichurricanes and cosmic rays, *Geofisica International*, 47 (3), 231 - 244, 2008.
- ❖ Pettauer, T., Brandt, P.N.: On Novel Methods to Determine Areas of Sunspots from Photoheliograms, *Sol. Phys.*, 175, 197 - 203, 1997.
- ❖ Pirjola, R., Viljanen, A., Amm, O., Pulkkinen, A.: Power and pipelines (ground systems), *the Proceeding of the ESA Workshop on Space Weather, ESTEC, Noordwijk, Netherlands*, 11 - 13th November, 1998.
- ❖ Pirjola, R.: Space weather and risk management, *54th Int. Astronomical Congress of the International Astronautical Federation, the International*

Academy of Astronautics, and the International Institute of Space Law, Bremen, 29 - 3rd September, 2003

- ❖ Plunkett, S.P., Vourlidas, A., Simberova, S., Karlicky, M., Kotrc, P., Heinzel, P., Kupryakov, Y.A., Guo, W.P., Wu, S.T.: Simultaneous SOHO and Ground-Based Observations of a Large Eruptive Prominence and Coronal Mass Ejection, *Sol. Phys.* 194, 371 - 391, 2000.
- ❖ Podobnik, B., Horvatic, D., Petersen, A.M., Stanley, H.E.: Cross-correlations between volume change and price change, *Proceedings of the National Academy of Sciences of the United States of America* 106, 22079 – 22084, 2009.
- ❖ Podobnik, B., Stanley, H.E.: Detrended cross-correlation analysis: a new method for analyzing two nonstationary time series, *Physical Review Letters*, 100, 084102, 2008.
- ❖ Popivanov, I., Miller, R.J.: Similarity search over time-series data using wavelets, *In Proceedings of the 18th International Conference on Data Engineering (ICDE)*, 2002.
- ❖ Prabhakaran Nayar, S. R., Radhika, V. N., Revathy, K. and Ramadas, V.: Wavelet analysis of periodicities in interplanetary medium, *Solar Phys.*, 212, 207-211, 2002.
- ❖ Prabhakaran Nayar, S. R., Radhika, V. N., Revathy, K., Ramadas, V.: Wavelet Analysis of solar, solar wind and geomagnetic parameters, *Solar Physics*, 208, 2, 359-373, 2002.
- ❖ Prialnik, D.: An Introduction to the Theory of Stellar Structure and Evolution, *2nd edition, Cambridge University Press, ISBN 0-521-86604-9*, 2000.
- ❖ Pulkkinen, A., Piriola, R., Viljanen, A.: Determination of ground conductivity and system parameters for optimal modeling of geomagnetically induced current flow in technological systems, *Earth, Planets and Space*, 59, 999-1006, 2007.

- ❖ Pulkkinen, Tujja.: Space Weather: Terrestrial Perspective, *Living Reviews in Solar Physics*, 4, 1, 1, 60, 2007.
- ❖ Raihan, Wen, Zeng.: Wavelet: a new tool for business cycle analysis, *Working paper 2005 - 050 A, Fedral Reserve Bank of St. Louis*, 2005.
- ❖ Ramsay, J.O., Ramsey, J.B.: Functional data analysis of the dynamics of the monthly index of nondurable goods production, *Journ. of Econometrics*, 107, 327 - 344, 2002.
- ❖ Ramsey, J.B., Lampart, C.: The Decomposition of Economic Relationship by Time Scale Using Wavelets: Expenditure and Income, *Studies in Nonlinear Dynamics and Econometrics*, 3 (1), 23 – 42, 1998b.
- ❖ Ramsey, J.B., XLampart, D.C.: Decomposition of Economic Relationship by Time Scales Using Wavelets, *Macroeconomic Dynamics*, 2(1), 49 – 71, 1998a.
- ❖ Ramsey, J.B.: The contribution of wavelets to the analysis of economic and financial data, *Phil. Trans. R. Soc.Lond.A*, 357, 2593 – 2606, 1999; reprinted in *Wavelets*, ed. Silverman, B.W., Vassilicos, J.C.: *Oxford Univ. Press, Oxford*, Chapter 12, 221 - 236, 1999.
- ❖ Rangarajan, G., Sant, D.A.: Fractal dimensional analysis of Indian climatic dynamics, *Chaos, Solitons and Fractals* 19, 285 – 291, 2004.
- ❖ Riazantseva, M.O., Dalin, P.A., Zastenker, G.N., Richardson, J.: Orientation of Sharp Fronts of the Solar Wind Plasma, *Cosmic Research*, 41, 4, 382-391, 2003.
- ❖ Ribes, E., Merlin, Ph., Ribes, J.C., Barthlot, R.: Absolute periodicities in the solar diameter, derived from historical and modern data, *Annales Geophysicae*, 7, 321 - 329, 1987.
- ❖ Rieger, E., Kanbach, G., Reppin, C., Share, G. H., Forrest, D.J., Chupp, E. L.: A 154-day periodicity in the occurrence of hard solar flares?, *Nature*, 312, 1984, 623 - 625, 1984.

- ❖ Rieger, E., Share, G.H., Forrest, D.J., Kambach, G., Reppin, C., Chupp, E.L.: A 154-day periodicity in the occurrence of hard solar flares?, *Nature*, 312, 623 - 625, 1984.
- ❖ Rishbeth, H.: History and Evolution of the world data centre system, *J. Geomagn. Geoelectr. Suppl.*, 43, 921, 1991.
- ❖ Rosenstein, Michael T., Collins, James J., De Luca, Carlo J.: A practical method for calculating largest Lyapunov exponents from small data sets, *Physica D: Nonlinear Phenomena*, 65, 1-2, 117-134, 1993.
- ❖ Rostoker, G., Filthammer, C.G.: Relationship between changes in the interplanetary magnetic field and variations in the magnetic field at the Earth's surface, *J. Geophys. Res.*, 72, 5853, 1967.
- ❖ Royar, D.L.: CO₂ forced climate threshold during the Phanerozoic, *Geochim Cosmochim Acta* 70, 5665 – 5675, 2006.
- ❖ Rua, A., Nunes, L.C.: International co-movement of stock market returns: A wavelet analysis, *Journal of Empirical Finance* 16, 632 – 639, 2009.
- ❖ Rua, A.: Measuring co-movement in the time - frequency space, *Journal of macroeconomics* 32, 685 – 691, 2010.
- ❖ Rusin, V., Rybansky, M., Zverko, J.: Rotation and short periodicities of the green corona derived from a coronal index for cycle 20 ,*Bull. Astron. Inst. Czechoslov.*, 38, 181 - 184, 1987.
- ❖ Russell, C.T., McPherron, R.L., Burton, R.K.: Reply [to “Comment on ‘Semiannual variation of geomagnetic activity’ by C. T. Russell and R. L. McPherron”], *Journal of Geophysical Research*, 79, 1132 – 1133, 1974.
- ❖ Ruttenberg, T., Rishbeth, H.: World Data Centres — past, present and future, *J. Atm. Solar Terr. Phys.*, 56, 865 – 870, 1994.
- ❖ Schertzer, D., Lovejoy, S.: Physical modeling and analysis of rain and clouds by anisotropic scaling multiplicative processes, *Journal of Geophysical Research: Atmospheres*, 92, D8, 9693 - 9714, 1987.

- ❖ Schmidt, M.W., Ruedenberg, K.: Effective convergence to complete orbital bases and to the atomic Hartree-Fock limit through systematic sequences of Gaussian primitives, *Journal of Chemical Physics*, 71, 10, 3951 - 3962, 1979.
- ❖ Schou, J., Anita, H.M.: Helioseismic Studies of Differential Rotation in the Solar Envelope by the Solar Oscillations Investigation Using the Michelson Doppler Imager, *The Astrophysical Journal*, 505 (1), 390 - 417, 1998.
- ❖ Schwabe, M.: Sonnenbeobachtungen im Jahre 1843. Von Herrn Hofrath Schwabe in Dessau, *Astronomische Nachrichten*, 21, 233, 1844.
- ❖ Schwenn, R., Marsch, E.: Physics of the Inner Heliosphere I. Large-Scale Phenomena, Physics of the Inner Heliosphere I. *Springer-Verlag Berlin Heidelberg New York*, 20, 282, 1990.
- ❖ Shaviv, N.J., Veizer, J.: Celestial driver of Phanerozoic climate?, *GSA Today* 13, 4 - 10, 2003.
- ❖ Shea, M.A., Smart, D.F.: A summary of major solar events, *Sol. Phys.*, 127, 297 - 320, 1990.
- ❖ Sheeley, N.R., Walters, J.H., Wang, Y.M., Howard, R.A.: Continuous tracking of coronal outflows: Two kinds of coronal mass ejections, *Journal of Geophysical Research*, 104, A11, 24739 - 24768, 1999.
- ❖ Sibeck, D.G., Lopez, R.E., Roel of, E.C.: Solar wind control of the magnetopause shape, location, and motion, *Journal of Geophysical Research*, 96, 1991, 5489-5495.
- ❖ Smith, L.C., Turcotte, D.L., Isacks, B.L.: Stream flow characterization and feature detection using a discrete wavelet transform, *Hydrol. Processes* 12, 233 - 249, 1998.
- ❖ Spiegel, E.A., Weiss, N.O.: Magnetic activity and variations in solar luminosity, *Nature*, 287, 616 – 617, 1980.

- ❖ Sturrock, P.A., Bai, T.: Search for evidence of a clock related to the solar 154 day complex of periodicities, *Apj*, 397, 337, 1992.
- ❖ Sugiura, M.: Data Center for Geomagnetism (WDC-C2) in Kyoto, swdcwww.kugi.kyoto-u.ac.jp/dstdir, 1991.
- ❖ Sugiura, M.: Hourly values of equatorial Dst for the IGY, *Ann Int Geophys Year (US)*, 35, 9 - 45, 1964.
- ❖ Svalgaard, L., Hudson, H.S.: The Solar Microwave Flux and the Sunspot Number, SOHO-23: Understanding a Peculiar Solar Minimum ASP Conference Series, 428, 325, San Francisco: Astronomical Society of the Pacific, 2010.
- ❖ Svalgaard, L., Wilcox, J.M.: Long-term evolution of solar sector structure, *Sol. Phys.*, 41, 461-475, 1975.
- ❖ Synder, C.W., Neugebauer, M., Rao, U.R.: The Solar Wind Velocity and Its Correlation with Cosmic-Ray Variations and with Solar and Geomagnetic Activity, *Journal of Geophysical Research*, 68, 6361, 1963.
- ❖ Takalo, J., Mursula, K.: Annual and solar rotation periodicities in IMF components: Evidence for phase/frequency modulation, *Geophysical Research Letters*, 29, 9, 31 -1, 2002.
- ❖ Tanaka, H., Castelli, J.P., Covington, A. E., Kruger, A., Landecker, T. L., Tlamicha, A.: Absolute calibration of solar flux density in the microwave region, *Sol. Phys.*, 29, 243 – 262, 1973.
- ❖ Tapping, K. F.: Recent solar radio astronomy at centimeter wavelengths: The variability of the 10.7 cm flux, *J. Geophys. Res.*, 92, 829 - 838, 1987.
- ❖ Tapping, K.F., Boteler, D., Charbonneau, P., Crouch, A., Manson, A., Paquette, H.: Solar magnetic activity and total irradiance since the Maunder Minimum, *Sol. Phys.*, 246, 309 - 326, 2007. doi: 10.1007/s11207-007-9047.

- ❖ Tapping, K.F., Cameron, H.T., Willis, A.G.: S-Component Sources at 21 cm Wavelength in the Rising Phase of Cycle 23, *Solar Phys.* 215, 357 - 383, 2003.
- ❖ Tapping, K.F., Charrios, D.P.: Limits of the accuracy of the 10.7 CM flux, *Solar Physics*, vol. 150, no. 1-2, p. 305-315, 1994.
- ❖ Tapping, K.F., DeTracey, B.: The origin of the 10.7 cm flux, *Sol. Phys.*, 127, 321 - 332, 1990.
- ❖ Tapping, K.F., Valdes, J.J.: Did the Sun change its behavior during the decline of cycle 23 and into cycle 24?, *Sol. Phys.*, 272, 337 - 350, 2011.
- ❖ Telesca, L., Lapenna, V., Macchiato, M.: Detrended fluctuation analysis of the spatial variability of the temporal distribution of southern California Seismicity. *Chaos Solitons of Fractals*, 21,2, 335-342, 2004.
- ❖ Temmer, M., Veronig, A., Hanslmeier, A.: Does solar flare activity lag behind sunspot activity?, *Sol. Phys.*, 215, 111 - 126, 2003.
- ❖ Thompson, D.J., Bertsch, D.L., et al., Supplement to the Second EGRET Catalog of High-Energy Gamma-Ray Sources, *Astrophysical Journal Supplement* 107, 227, 1996.
- ❖ Thompson, M.J., Toomre, J and 24 coauthors.: Differential Rotation and Dynamics of the Solar Interior, *Science*, 272, 5266, 1300-1305, 1996.
- ❖ Thompson, T. A., Burrows, A; Pinto, Philip A.: hock Breakout in Core-Collapse Supernovae and Its Neutrino Signature, *The Astrophysical Journal*, 592, 1, 434-456, 2003.
- ❖ Tong, Xu., Jian, Wu., Zhen-Sen, Wu., Qiang, Li., Long - Term Sunspot Number Prediction based on EMD Analysis and AR Model, *Chin. J. Astron. Astrophys*, 8 (3), 337 - 342, 2007.
- ❖ Torrence, C., and Webster, P.J.: The annual cycle of persistence in the El Niño–Southern Oscillation. *Quart. J. Roy. Meteor. Soc.*, in press, 1998.

- ❖ Torrence, C., Compo, G.P.: A practical guide to wavelet analysis, *Bull. Am. Meteorol. Soc.*, 79, 61 - 78, 1998.
- ❖ Torrence, C., Webster, P.: International changes in the ENSO-Monsoon System, *J. Clim.*, 12, 2679 – 2690, 1999.
- ❖ Touminen, J.: On Stellar Envelopes, *Annals of the New York Academy of Sciences*, 41, 1 The Internal , 61-76, 1941.
- ❖ Tsallis, C.: Possible generalization of Boltzmann-Gibbs statistics, *Journal of Statistical Physics*, 52, 1-2, 479-487, 1988.
- ❖ Tsurutani Bruce T., Gonzalez, W.D.: The efficiency of 'viscous interaction' between the solar wind and the magnetosphere during intense northward IMF events, *Geophysical Research Letters (ISSN 0094-8276)*, 22, 6, 663-666, 1995.
- ❖ Tsurutani, B.T., Gonzalez, W. W.: Magnetic Storms, *Geophys. Monogr. Ser.*, 98, 77-89, 1997.
- ❖ Tsurutani, B.T., Lee, Y.T., Gonzalez, W.D., Tang, F.: Great magnetic storms, *Geophysical Research Letters*, 19, 73 – 76, 1992.
- ❖ Turiel, A., Perez-Vicente, C.J., Grazzini, J.: Numerical methods for the estimation of multifractal singularity spectra on sampled data: A comparative study, *Journal of Computational Physics*, 216, 1, 362-390, 2006.
- ❖ Turner, N.E., Cramer, W.D., Earles, S.K., et al.: Geoefficiency and energy partitioning in CIR-driven and CME-driven storms, *Journal of Atmospheric and Solar Terrestrial Physics*, 71 (10-11), 1023 – 1031, 2009.
- ❖ Turner, R.: Solar particle events from a risk management perspective, *IEEE Trans. Plasma Sci.*, 28 (6), 2103 - 2113, 2000.
- ❖ Uritsky, V.M., Klimas, A.J., Vassiliadis, D.: Comparative study of dynamical critical scaling in the auroralelectrojet index versus solar wind fluctuations, *Geophys. Res. Lett.*, 28, 3809 - 3812, 2001.

- ❖ Usoskin, I.G., Kromer, B., Ludlow, F., Beer, J., Friedrich, M., Kovaltsov, G.A., Solanki, S.K., Wacker, L.: The AD775 cosmic event revisited: the Sun is to blame, *Astron. Astrophys.*, 552, L3, 2013. Vassenius, B. 1733, *Phil. Trans. Roy. Soc. London*, 38, 134.
- ❖ Vassenius, B.: Observatio Eclipsis Solis Totalis Cum Mora Facta Gothoburgi Sveciae, Sub Elev. Poli 57 degrees 40 $^{\prime}$ 54 $^{\prime}$ d. 2 Maij, Stylo, *Phil. Trans. Roy. Soc. London*, 38, 134 – 135, 1733.
- ❖ Verma, V.K., Joshi, G.C., Paliwal, D.C.: Study of periodicities of solar Nuclear Gamma Ray Flares and Sunspots, *Sol. Phys.*, 138, 205 – 208, 1992.
- ❖ Veronig , A, Messerotti, M., Hanslmeier, A.: Determination of fractal dimensions of solar radio bursts, *Astron. Astrophys.*, 357, 337 - 350, 2000.
- ❖ Vitinsky, Yu.I., Kopecky, M., Kuklin, G.B.: The sunspot solar activity statistics of the Generating Activity of the Sun, *Nauka, Moscow*, 1986.
- ❖ Vonesch, C., Blu, T., Unser, M.: Generalized Daubechies Wavelet families, *IEEE Trans. Signal Process*, 55 (9), 4415 – 4429, 2007.
- ❖ Voros, Z.: Onmultifractality of high-latitude geomagnetic fluctuations, *Ann. Geophysicae*, 18, 1273 – 1282, 2000.
- ❖ Waldmeier, M.: The sunspot activity in the years 1618-1960, *Zurich: Schulthess and co.*, 1961.
- ❖ Wang, J.L., Gong, J.C., Liu, S.Q., et al.: The prediction of maximum amplitudes of solar cycles and the maximum amplitude of solar cycle 24, *Chin. J. Astron. and Astrophys*, 2 (6), 557 – 562, 2002.
- ❖ Wang, J.L., Zong, W.G., Le, G.M., Zhao, H.J., Tang, Y.Q., Zhang, Y.: Predicting the start and maxima amplitude of solar cycle 24 using similar phases and a cycle grouping, *Res. Astron. Astrophys.*, 9, 133 – 136, 2009.

- ❖ Wang, Y.D., Liu, L.: Is WTI crude oil market becoming weakly efficient over time? New evidence from multiscale analysis based on detrended fluctuation analysis. *Energy Economics* 32, 987 – 992, 2010.
- ❖ Wanliss, J.: Fractal properties of SYM-H during quiet and active times, *Journal of Geophysical Research: Space Physics*, 110, A3, 2005.
- ❖ Wanliss, J.A., Dobias, P.: Space storm as a phase transition, *Journal of Atmospheric and Solar-Terrestrial Physics*, 69, 6, 675-684, 2007.
- ❖ Willson, Richard C., Mordvinov, Alexander V.: Time-frequency analysis of total solar irradiance variations, *Geophysical Research Letters*, 26, 24, 3613-3616, 1999.
- ❖ Wilson, R.M., Rabin, D., Moore, R.L.: 10.7-cm Solar radio flux and the magnetic complexity of active regions, *Sol. Phys.*, 111, 279 - 285, 1987.
- ❖ Yan, X.L., Deng, L.H., Qu, Z.Q., Xu, C.L., Kong, D.F.: Phase Relationship Between Sunspot Number, Flare Index and Solar Radio Flux, *J. Astrophys. Astr.* 33, 387 – 397, 2012.
- ❖ Yin, Z.Q., Han, Y.B., Ma, L.H., Le, G.M., Han Y.G.: Short-Term Period Variation of Relative Sunspot Numbers, *Chin. J. Astron. Astrophys.*, 7, 823, 2007.
- ❖ Yuan, Y., Zhuang, X.T., Jin, X.: Measuring multifractality of stock price fluctuation using multifractal detrended fluctuation analysis, *Physica A*, 388, 2189 - 2197, 2009.
- ❖ Zaourar, N., Hamoudi, M., Briqueu, I.: Détection des transitions lithologiques par l'analyse de la composante fractale des diagraphies par transformée continue en ondelettes, *Comptes rendus - Géoscience*, 338, 8, 514-520, 2006.
- ❖ Zbilut, J.P., Giuliani, A., Webber Jr., C.L.: Detecting deterministic signals in exceptionally noisy environments using cross-recurrence quantification, *Physics Letters, A* 246 (1-2), 122 – 128, 1998.

- ❖ Zhang, Xue Feng, L.E. Gui-Ming, Zhang. Yan-Xia.: Phase relationship between the relative sunspot number and solar 10.7 cm flux. Chinese science Bulletin, *Sun & Solar system*, 57 (17), 2078 - 2082, 2012.
- ❖ Zharkov, S.I., Gavryuseva, E.V., Zharkova, V.V.: The latitudinal distributions of sunspot areas and magnetic fields and their correlation with the background solar magnetic field in the cycle 23, *Preprint submitted to Elsevier science*, 2007.
- ❖ Zhou, S.: How to make thermodynamic perturbation theory to be suitable for low temperature? *Journal of Chemical Physics*, 130, 5, 054103-054103-11, 2009.
- ❖ Zhou, Wei-Xing.: Multifractal detrended cross-correlation analysis for two non-stationary signals, *Physical Review E*, 77, 6, 2008.
- ❖ Zolotova, N.V., Ponyavin, D.I.: Synchronization in sunspot indices in the two hemispheres, *Solar Phys*, 243, 193, 2007.
- ❖ Zririn, H.: Book-Review - Astrophysics of the Sun, KNUDSEN, *Science*, 242, 4885/DEC16, 1586, 1988.



Study of Sunspot Time Series Using Wavelet-based Multifractal Analysis during Solar Cycle 23 and Ascending Phase of Cycle 24

S. K. Kasde^{1*}, D. K. Sondhiya² and A. K. Gwal³

¹Space Science Research Laboratory, Department of Physics and Electronics, Barkatullah University, Bhopal 462 026, India.

²Department of Education in Science and Mathematics, Regional Institute of Education, Shyamla Hills, Bhopal 462013, India.

³AISECT University, Chiklod Road, Raisen, 464993, India.

Authors' contributions

This work was carried out in collaboration between all authors. Authors SKK and DKS designed the study, performed the statistical analysis, wrote the protocol, wrote the first draft of the manuscript and managed the analyses of the study. Author AKG managed the literature searches. All authors read and approved the final manuscript.

Article Information

DOI: 10.9734/PSIJ/2017/30319

Editor(s):

(1) Kazuharu Bamba, Division of Human Support System, Faculty of Symbiotic Systems Science, Fukushima University, Japan.

(2) Stefano Moretti, School of Physics & Astronomy, University of Southampton, UK.

Reviewers:

(1) Jagdish Prakash, University of Botswana, Botswana.

(2) Samsul Ariffin Bin Abdul Karim, Universiti Teknologi Petronas, Malaysia.

(3) Loukas Zachilas, University of Thessaly, Greece.

Complete Peer review History: <http://www.sciencedomain.org/review-history/18059>

Original Research Article

Received 2nd November 2016

Accepted 24th February 2017

Published 6th March 2017

ABSTRACT

Wavelet based Multifractal analysis techniques provides a sophisticated statistical characterization of many complex dynamical phenomena related with Sun and its environment. In this work multifractal property of the Sunspot number time series, has been analyzed during Solar cycle 23 and ascending phase of Solar cycle 24 using Wavelet transform and wavelet based multifractal approach. Present analysis has been performed using the software FRACLAB, developed at INRIA and available online at <http://www-rocq.inria.fr>. It was found that the singularities spectrum for sunspot time series was well Gaussian in shape suggesting the multifractal characteristics of time series. Thus we conclude that the multifractal based approach provide the local and adaptive description of dynamical processes related with Sun and its climate and can be applied effectively in the study of solar activity.

*Corresponding author: E-mail: sbskasde@gmail.com;

Keywords: Sunspot number; magnetic field; multifractal analysis and wavelet transform technique.

1. INTRODUCTION

The significant feature of the Sun's outer regions is the existence of a reasonably strong magnetic field which governs all solar activities inside the Sun and its atmosphere. According to the lowest order of approximation, the magnetic field of the Sun is dipolar and axisymmetric in nature. In some localized regions known as sunspot the value of magnetic field are much higher [1]. Sunspots are generally seen in pairs or in groups of pairs at both sides of the solar equator. According to Petrovaye [2] as the sunspot cycle progresses, spots appear closer to sun's equator giving rise to the so called "butterfly diagram" in the time latitude distribution. The twisted magnetic fields above sunspots are sites where solar flares are observed. Bray [1] has been found that chromospheric flares show a very close statistical relationship with sunspots. The number of sunspots continuously changing in time in a random fashion and constitutes a typically random time series [3]. The newly corrected sunspot time series [4-7] progressively indicates the declination in solar activity before the commencement of the Maunder Minimum, while the slow rising drifts in activity after the Maunder Minimum. It shows that by the mid 18th century, solar activity returned to levels corresponding to those observed in current solar cycles. Also Gkana and Zachilas [8] analyze Sunspot number version 2.0 data and claim that prolonged solar activity minimum is probable occur, lasting up to the year ≈ 2100 .

Analysis of sunspot could lead significant improvement in the measurement of solar activity [9]. Recently sunspots and related activities have been analyzed by various methods, including correlation analysis [10], Chaos analysis [11,12] and multifractal analysis [13-15]. Schatten [16] used SODA index (Solar Dynamo Amplitude) for understanding of the Sun's dynamo processes to explain the connection between how the Sun's fields are generated and how the Sun broadcasts its future activity levels to Earth. Zachilas and Gkana [17] analyze the yearly data of mean sunspot-number during the period of 1700 to 2012 and concluded that the yearly sunspot number is a low-dimensional deterministic chaotic system. Tarbell et al. [18] used the fractal analysis technique in the context of solar magnetic field to find a fractal dimension. Many authors [18-20] used fractal analysis technique to study the photospheric magnetic structure

[18,20]. Tao et al. [21] applied numerical simulate distribution for the multifractal analysis of surface magnetic field. Later, numerical simulations of multifractality and intermittency of the solar structure were performed by so many researchers [22-26]. Multifractal theory provides an elegant statistical characterization of many complex dynamical variations in nature and engineering [27,28]. It is conceivable that it may enrich characterization of the sun's magnetic activity and its dynamical modeling [29-30]. The relative fraction of small scale fluctuation in the magnetic field contributes significantly and reach a critical state of intermittency more prior to flaring [26]. It was found that active regions reach a critical state of intermittency prior to flaring [26]. The multifractal scaling behaviors reported by Movahed [31] are valid for timescales up to more than 50 years. McAteer [32] found analytical connection between multifractal formalism and the set of 3D equations that govern the small-scale and large-scale magnetic structure on the Sun [33,34]. Recently, Georgoulis [35] and McAteer [32] achieved a contrary conclusion that studies of multifractals do not provide a predictive ability for the onset of solar flares. In this paper we have used the multifractal techniques and noticed the presence of multifractality in sunspot number time series during the Solar Cycle 23 and ascending phase of Solar Cycle 24.

2. DATA SET

In this analysis we used the monthly counts of sunspot number for the multifractal analysis for the time span of 1996 to 2016. This period includes complete Solar Cycles of 23 and ascending and maximum phase of current Solar Cycle 24. The dataset available online and downloaded from <http://www.sidc.be/silso/datafiles>. The Sunspot Index and Long Term Solar Observatory (SILSO) is the World Data Center for the production, preservation and dissemination of the international sunspot number.

3. THEORETICAL BACKGROUND

3.1 Wavelet Transforms

Wavelet transform is an ideal technique for the analysis of real world signals that contain sharp changes and localized discontinuities [36]. The

wavelet transform use different window sizes, which are able to compress and stretch wavelets in different scales or widths; these are then used to decompose a time series [37] and decompose a one-dimensional signal into two-dimensional time–frequency domains at the same time [38]. Wavelet transform can be performed using two approaches: Continuous Wavelet Transform (CWT) and Discrete Wavelet Transform (DWT). The CWT introduces a very redundant and finely detailed description of time series in terms of both time and frequency. It is particularly helpful in resolving problems involving signal detection and identification of hidden transients such as hard to detect, short – lived elements of a time series. The scales and locations used in DWT are normally based on a dyadic arrangement (i.e. integer powers of two) [39]. DWT is especially useful for time series containing sharp jumps or shifts [40].

3.2 Time Series Decomposition via the Discrete Wavelet Transform (DWT)

The DWT is usually based on the dyadic calculation of position and scale of a signal [39]. The DWT is excellent for denoising the signals [41]. The DWT of a vector is the outcome of a linear transformation resulting in a new vector that has equal dimensions to those of the initial vector [42]. The discretization of wavelet functions is accomplished using a logarithmic uniform spacing that has a coarser resolution at higher scales [43,44]. In this study all the time series (for the Solar Cycles 23 and ascending phase of current Cycle 24) were decomposed using the Daubechies (db2) and Coifman (coif5) wavelets. Daubechies and Coifman (coif5) wavelets provide compact support, which indicate that the wavelets have non-zero basis functions over a finite interval, as well as full scale and translational orthonormality properties [45,46]. These features are very important for localizing events in the time-dependent signals [46].

3.3 Wavelet Based Multifractal Formalism

The wavelet transform not only locates isolated anomalous events, but can also characterize more complex multifractal sunspot data having non isolated singularities. Multifractal objects cannot be completely described using a single fractal dimension (mono fractals). They have an infinite number of dimension measures

associated with them. The wavelet transform takes advantage of multifractal self-similarities, in order to compute the distribution of their singularities. This singularity spectrum is used to analyze multifractal properties. The concepts of fractals and multifractals and their relevance to the real world data were introduced by Mandelbrot [47]. The time series of sunspot numbers usually depict fractal or multifractal features. Time series are commonly called self-affine functions as their graphs are self-affine sets that are similar to themselves when transformed by anisotropic dilations.

Mathematically, if $f(x)$ is a self- affine function representing the sunspot number then

For $x_0 \in R, \exists H \in R$ such that for any $\lambda > 0$,

$$f(x_0 + \lambda x) - f(x_0) \cong \lambda^H (f(x_0 + x) - f(x_0)) \quad (1)$$

Here exponent H is known as roughness or Hurst exponent. Note that if $H < 1$, then f is not differentiable and smaller the exponent H, the more singular is f .

For sunspot number $f(x)$, a function $h(x)$, the Holder function of f , which measures the regularity of f at which point t is associated.

The point wise Holder h of f at point x_0 is defined as:

$$h(x_0) = \lim \sup \{h: \exists c > 0, |f(x) - f(x_0)| \leq c|x - x_0|^h, |x - x_0| < \rho\} \quad (2)$$

(Here h is an integer and f is non- differential).

One may also define local exponent $h_l(x_0)$ as:

$$h_l(x_0) = \lim \sup \{h: \exists c > 0, |f(x) - f(y)| \leq c|x - y|^h, |x - x_0| < \rho, |y - x_0| < \rho\} \quad (3)$$

Where h_l and h are different in general. For example for

$$f(x) = |x|^h \sin \frac{1}{|x|^\beta}, h(0) = 0, \text{ while } h_l(0) = \frac{h}{1+\beta} \quad (4)$$

They have quite different properties. For instance h_l is stable through differentiation ($h_l(f, x_0) = h_l(f, x_0) - 1$), whereas h is not. The smaller $h(x)$ is, the more irregular the function f is at t .

3.4 Partition Function

Calculation of Pointwise Lipschitz (Holder) regularity of multifractal is not possible because its singularities are not isolated and the finite numerical resolution sufficient to discriminate them. To overcome this difficulty Muzy [48] have introduced the concept of wavelet transform modulus maxima using a global partition function [49]. Let Ψ be a wavelet with n vanishing moments. Mallat [43] has shown that if f has a pointwise Holder (Lipschitz) regularity $\alpha_0 \leq n$ at v then the wavelet transform $T_\psi f(a, b)$ has a sequence of modulus maxima that converges towards v at fine scales. The set of maxima at the scale a can thus be interpreted as a covering of the singular support of f with wavelets of scale a . At these maxima locations

$$|T_\psi f(a, b)| \approx a^{\alpha_0+1/2} \quad (5)$$

Let $\{u_p(a)\}_{p \in \mathbb{Z}}$ be the position of all local maxima of $|T_\psi f(a, b)| \approx a^{\alpha_0+1/2}$ at a fixed scale a . The partition function Z measures the sum at a power q of all these wavelet modulus maxima:

$$Z(q, a) = \sum_p |T_\psi f(a, u_p)|^q \quad (6)$$

For each $q \in \mathbb{R}$, the scaling exponent $\tau(q)$ measures the asymptotic decay of $Z(q, a)$ at fine scale a :

$$\tau(q) = \liminf \frac{\log Z(q, a)}{\log a} \quad (7)$$

This typically means that $Z(q, a) \sim a^{\tau(q)}$.

4. RESULTS AND ANALYSIS

In this study we have analyzed the multifractal characteristics of sunspot number during the Solar Cycle 23 and current Cycle 24 using wavelet based multifractal techniques. Sunspot numbers (SNs) are widely and frequently used in astronomy to reflect long term variations of solar activity, which has served as the primary time series to define solar activity [50-53].

4.1 Wavelet Analysis of Sunspot Numbers

In this section DWT of the sunspot numbers for Solar Cycle 23 and 24 were carried out in terms of approximations and details coefficients using Daubechies and Coifmann mother wavelets. These wavelets have fractal structure and include both highly localized wavelets and highly smooth wavelets [54]. The sunspot time series (s) is decomposed into two orthonormal components, frequency (details) and approximations component. The approximations represent the long term of data which is almost identified to original time series and the detail coefficients represent the short period fluctuations in given period range. The result of analysis was shown in Figs. 1 – 4. In figures, the X-axis represents the time period of the sunspot time series. In all figures first panel represents the variation in sunspot number time series. The second panel gives the approximation coefficient “ a_4 ” of all the figures. It separates the short term anomalous variation from the long term variations.

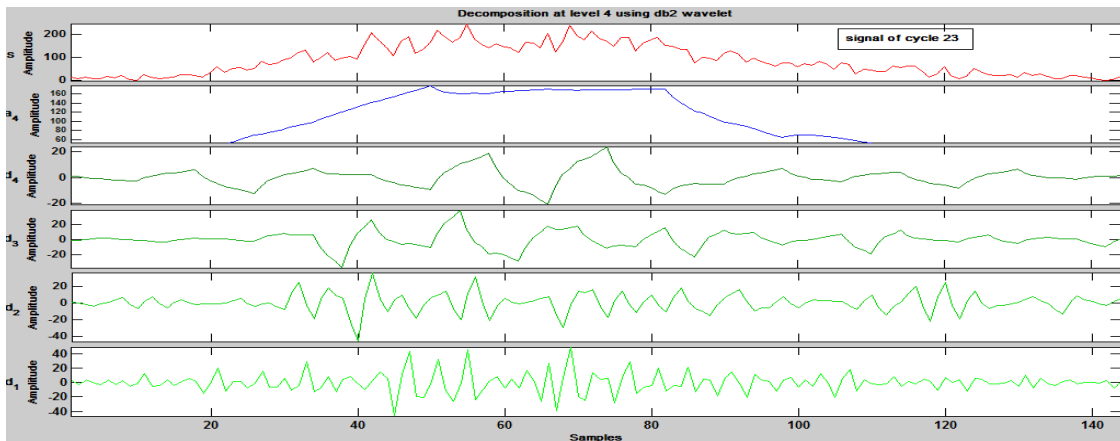


Fig. 1. DWT decompositions of Solar Cycle 23 using Daubechies 2 wavelet. Anomalous variations found between 45-60 no. of samples (i.e. at the maximum phase of cycle)

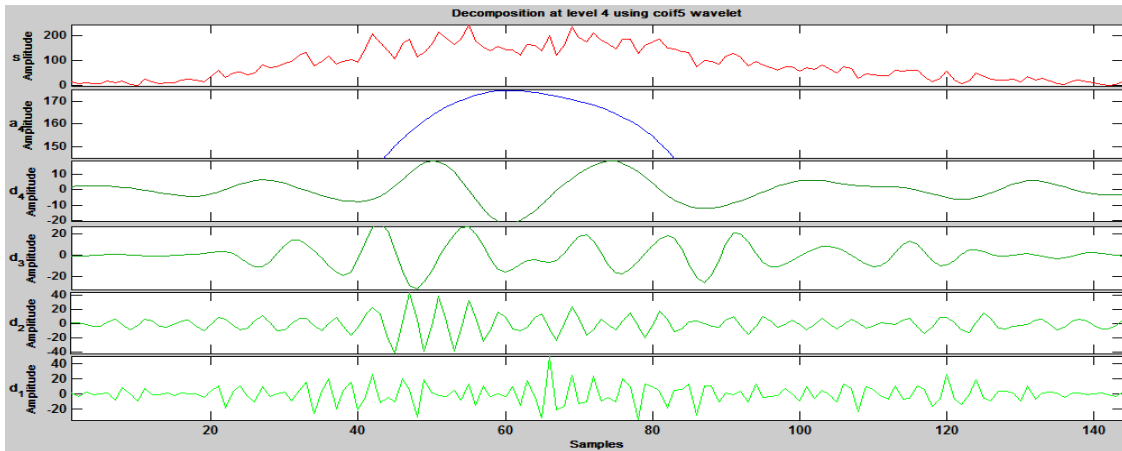


Fig. 2. DWT decompositions of Solar Cycle 23 using Coifman 5 wavelet. Anomalous sharp variations found between 40-60 no. of samples (i.e. at the maximum phase of cycle)

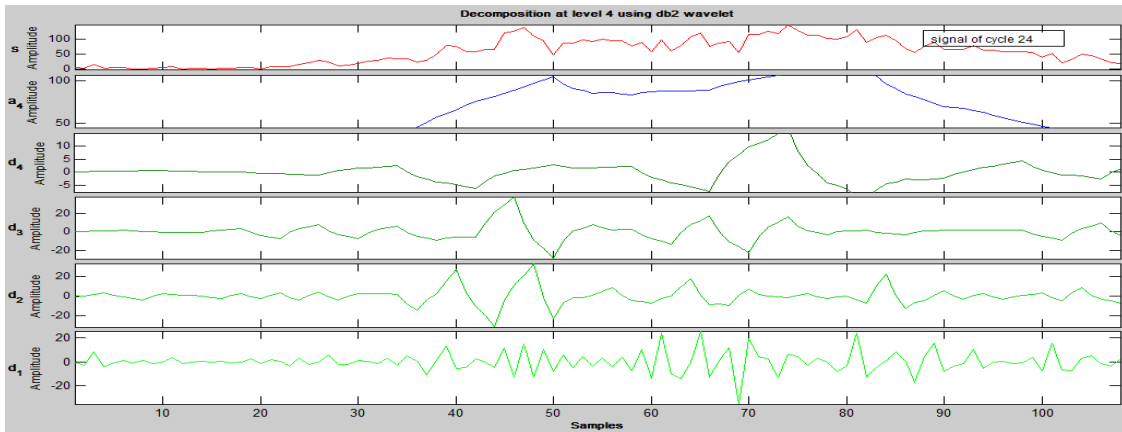


Fig. 3. DWT decompositions of Solar Cycle 24 using Daubechies 2 wavelet. Anomalous variations showing between 40 to 50 no. of samples (i.e. at the maximum phase of cycle)

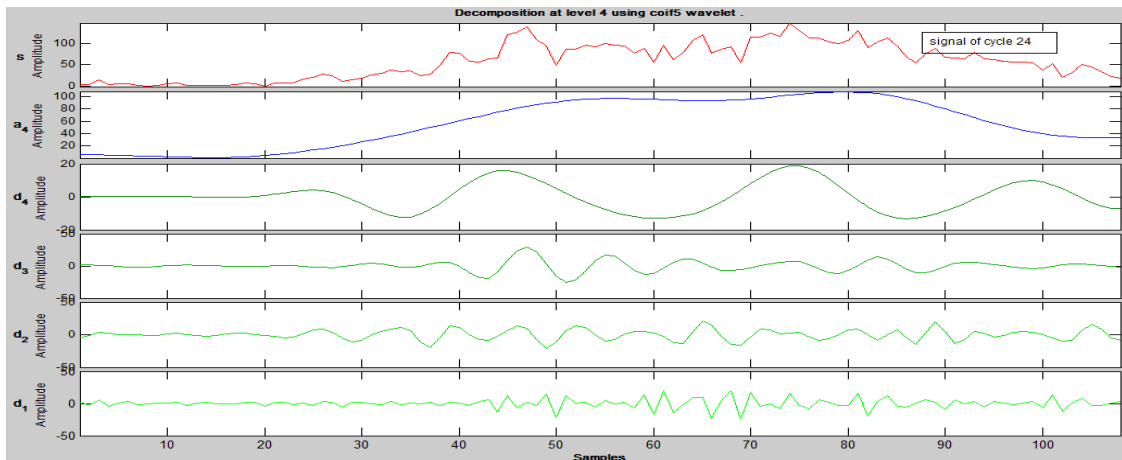


Fig. 4. DWT decompositions of Solar Cycle 24 using Coifman 5 wavelet. Anomalous sharp variations found between 40 to 50 no. of samples (i.e. at the maximum phase of cycle)

On the other hand, other four parts d_1, d_2, d_3 and d_4 represent detail coefficients of the sunspot time series. The detail coefficients reveal that the field strength changes between positive and negative values. This indicates the existence of a strong and variable magnetic field on the Sun as sunspots. The detail coefficients of sunspot numbers show that high frequency components during the initial and main phase of the solar cycle and their time evolution. It was noticed that very high frequency components present only during the main phase of the respective solar cycles and they are very strong in amplitude and stable for higher level of decomposition. Even though there are some strong fluctuations in the main phase and recovery phase but they are not as persistent as that present during the initial phase and main phase of the cycles.

4.2 Multifractal Analysis of Sunspot Numbers

In this section, we have done multifractal analysis of sunspot numbers time series [26,27].

The Legendre spectrum was calculated by FRACLAB software, developed at INRIA and available online at <http://www-rocq.inria.fr>. Since

the sunspot data have some missing values we take the longest segments of sunspot data without any missing values. The order of the magnitude of the length of each segment is about 120, thus permitting to obtain reliable estimates of the singularity spectrum and multifractal parameters. Figs. 5 and 7 (Right panel) shows the Legendre spectra for the selected segments for both solar cycle. All the spectra present the typical single-humped shape that characterizes multifractal nature of sunspot number. The spectra of the segments for each sunspot time series, calculated for different time intervals are not identical. Nonlinear fluctuations are possibly due to the presence of multifractal processes. The smaller values of α correspond to the burst of events, while higher values of α correspond to events occurring sparsely [55]. The spectrum gives geometrical information pertaining to the dimension of sets of points in a signal having a given Holder exponent. This is the most precise spectrum from a mathematical point of view, but is also difficult one to estimate. Large deviation spectrum yields statistical information, related to the probability of finding a point with a given Holder exponent in the signal. More precisely, it measures how this probability behaves with the change in resolution.

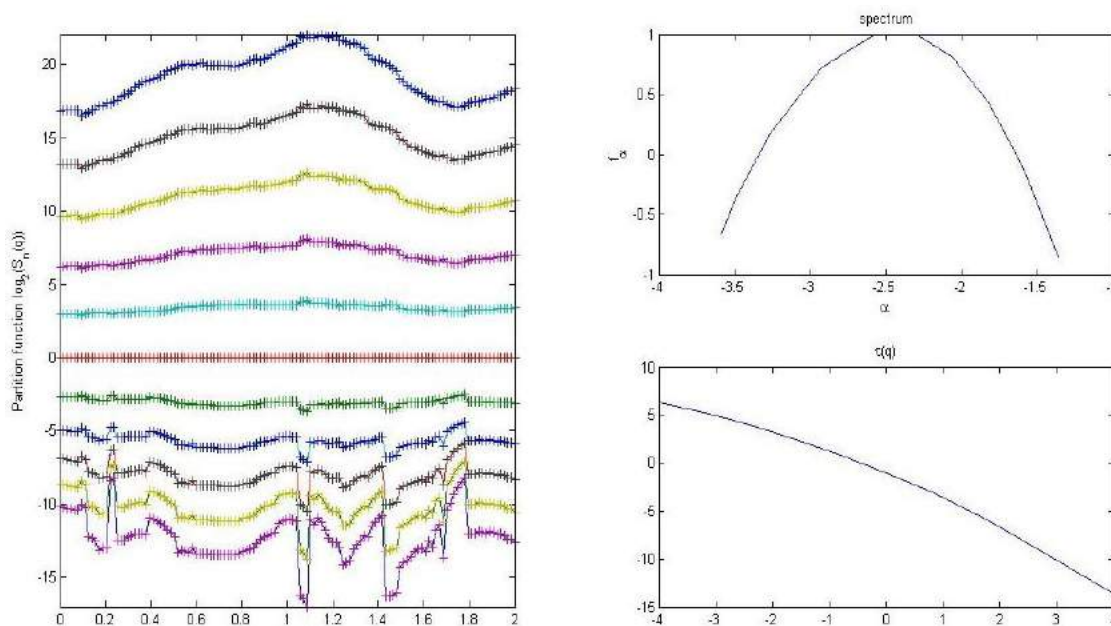


Fig. 5. Multifractal analysis of Solar Cycle 23 using CWT (Morlet wavelet of size 8 and 128 voices, LS regression and local maxima). In figure Left panel show the Legendre spectra and Right (upper) panel gives the singularity spectrum and Right (lower) panel for scaling function of the considered time series

Legendre spectrum is a concave approximation to the large deviation spectrum. Its main purpose is to yield much more robust estimates, though at the expense of a loss of information. It could base on box method or CWT techniques. In the sequel we show some sample results for the spectra computed with the Legendre technique. Figs. 6 and 8 show the results of the CWT (Morlet wavelet) based estimation of the Legendre spectrum which represents an approximation of the spectrum for two different Solar Cycles. Each figures consist of two parts in which the first part on the top of each figure

represents the signal or raw data. The second part of figure shows the analyzed pattern with the application of Morlet wavelet of size 8 and 128 voices of different Solar Cycles. The non-parametric point wise Holder regularity approach based on CWT with Morlet wavelet for the Solar Cycle 23 and ascending phase of Cycle 24 was shown in Figs. 9 and 10. The Holder exponent is used for the study that characterizes the regularity of the measure (function) of the magnetic field strength of sunspot under consideration at either pointwise regularity or local regularity.

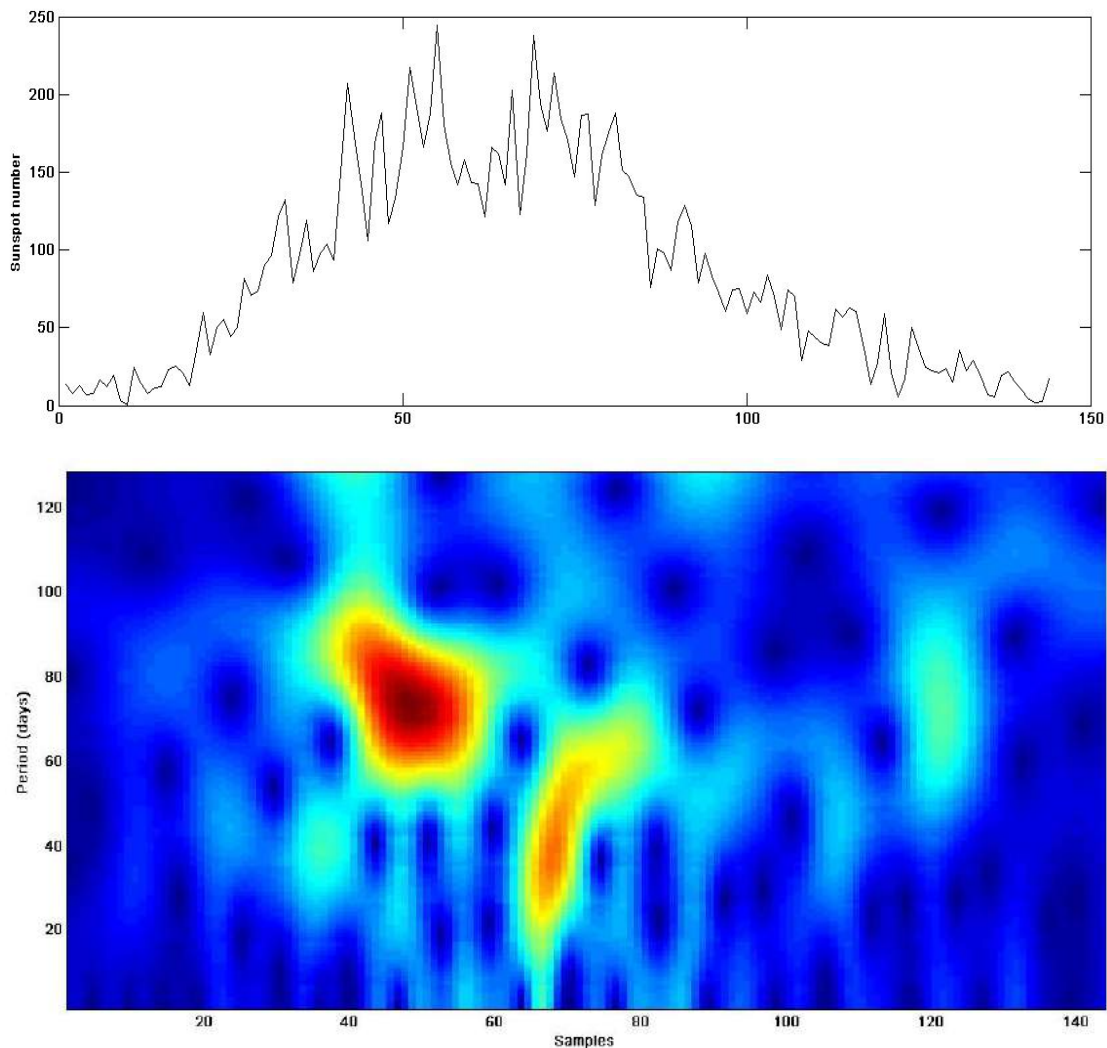


Fig. 6. CWT of Solar Cycle 23 using a Morlet wavelet of size 8 and 128 voices. In figure X axis represents the number of samples and Y axis represents scale. The upper panel shows the raw data of the time series and lower panel its continuous wavelet transform (CWT)

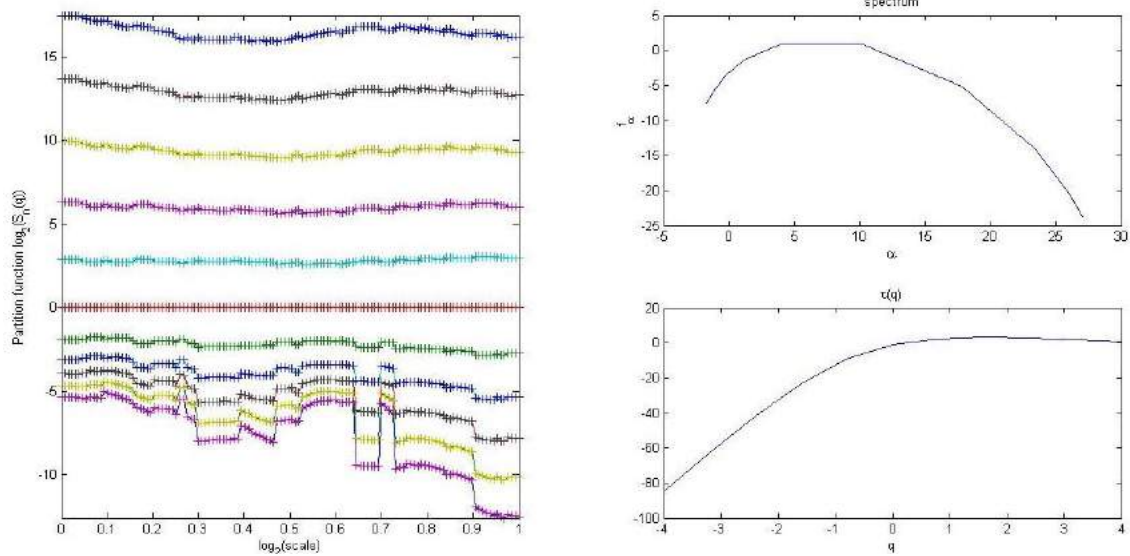


Fig. 7. Multifractal analysis of Solar Cycle 24 using CWT (Morlet wavelet of size 8 and 128 voices, LS regression and local maxima). In figure Left panel show the Legendre spectra and Right (upper) panel gives the singularity spectrum and Right (lower) panel for scaling function of the considered time series

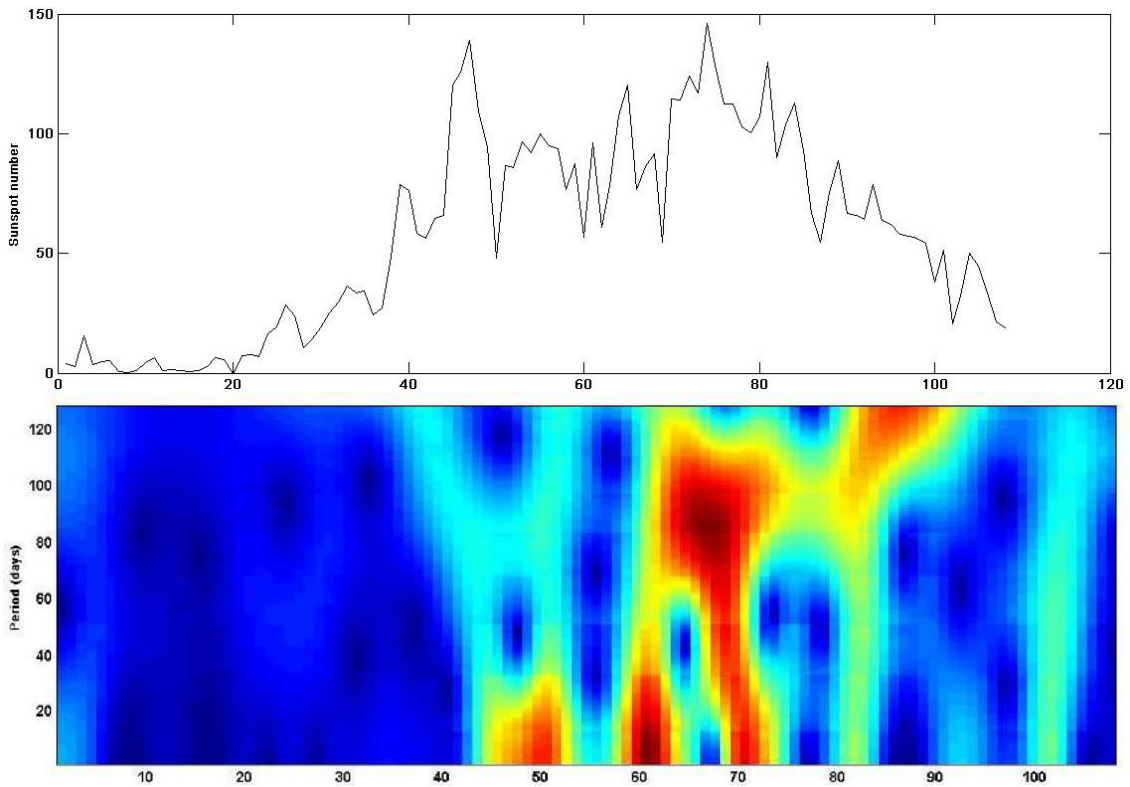


Fig. 8. CWT of Solar Cycle 24 using a Morlet Wavelet of size 8 and 128 voices. In figure X axis represents the number of samples and Y axis represents scale. The upper panel shows the raw data of the time series and lower panel its continuous wavelet transform (CWT)

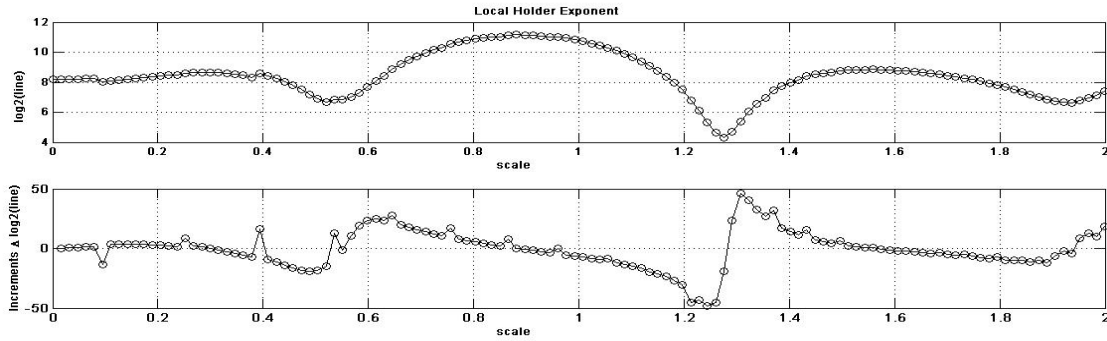


Fig. 9. Non-parametric point wise Holder regularity estimation using CWT with Morlet wavelet for the Solar Cycle 23

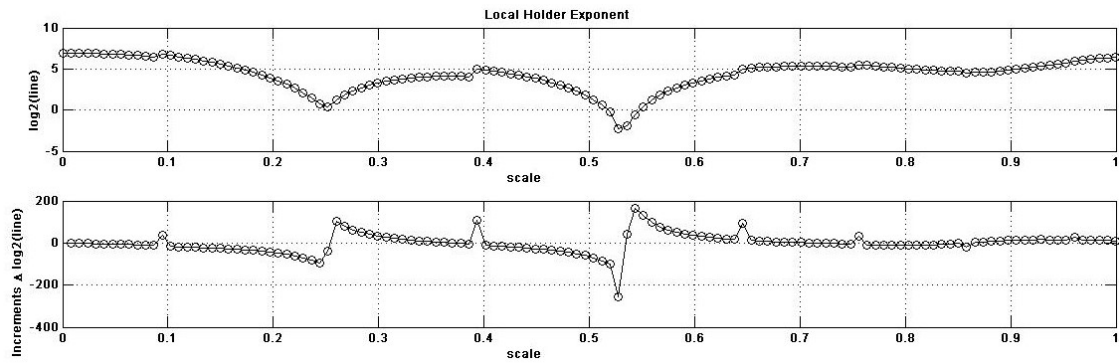


Fig. 10. Non-parametric point wise Holder regularity estimation using CWT with Morlet wavelet for the Solar Cycle 24

5. CONCLUSION

Wavelet based multifractal analysis is a useful way to characterize the multifractality in time series. The result of our analysis shows that sunspot time series reveal multifractal character during Solar Cycle 23 and ascending phase of Solar Cycle 24. The DWT (Figs. 1 - 4) of Sunspot time series shows the phenomenological difference between Solar Cycle 23 and Cycle 24. It present Solar Cycle 23 has large range fluctuation due to the contribution of highly magnitude solar activities whereas during the Cycle 24 it is not noticed hence it is a quite Cycle except during the maximum phase reveals the large fluctuations. The wavelet spectrum depicts in Figs. 6 and 8 reveals the time at which large variations in time series occur, which is more important for the investigation of multifractality. Various phenomenon related to Sun such as solar flares, sunspot, coronal mass ejection (CME) etc. Three main multifractal spectra viz. the Housdorff, large deviation and Legendre spectra (see Figs. 5 and 7) provides information

as to which singularities occur in sunspot time series and which are dominant. Multifractal analysis provided both a local and a global description of the singularities of a signal. Recent studies have shown that non-Gaussian fluctuation is responsible for the presence of extreme events in space plasmas. Recently, using a non-extensive approach Balasis et al. [56] suggested emergence of two distinct phases: (i) the phase where the intense magnetic storms cause a higher degree of magnetic field organization, and (ii) the phase which characterizes the normal periods with lower magnetic field coherence. The phase (i) may be associated with the presence of different kinds of large scale coherent structures, also pointed out by Chang et al. [57]. The wavelet spectrum displayed in Figs. 6 and 8 reveals the time at which large variations occur which is very important in the investigation of multifractality. Thus, we conclude that Solar Cycle 23 commonly shows the multiracial nature around the initial maximum and declining phase of cycle rather than Solar Cycle 24. It was not effective

during the initial phase of cycle. Solar Cycle 24 has more fractal nature at the maximum phase and we wait for more result till complete the ongoing cycle.

ACKNOWLEDGEMENT

A Matlab software package being used by the authors for performing XWT and WTC can be found at <http://www.pol.ac.uk/home/research/wavelet-coherence/>. One of us (S. K. Kasde) is thankful to University Grants Commission, New Delhi (India) for financial assistance under the scheme of RGNF.

COMPETING INTERESTS

Authors have declared that no competing interests exist.

REFERENCES

1. Bray RJ, Loughhead RE. Sunspots Dover Publications, New York; 1979.
2. Petrovay K. What makes the Sin tick? The origin of the solar cycles. *ESA Publ.* 2000;SP-463:3-14.
3. Fanchiotti H, Sciutto SJ, Garcia CA, Hojvat C. Analysis of sunspot number fluctuations. *Fractals.* 2004;12(04):405-411.
4. Clette F, Svalgaard L, Vaquero JM, Cliver EW. Revisiting the sunspot number. A 400-year perspective on the solar cycle. *Space Sci. Rev.* 2014;186:35.
5. Svalgaard L, Updating the historical sunspot record, in SOHO-23: Understanding a peculiar solar minimum. Proceedings of a workshop held 21–25 September in Northeast Harbor, Maine, USA, ed. by SR Cranmer, JT Hoeksema, JL Kohl. ASP Conference Series, (Astronomical Society of the Pacific, San Francisco, 2010). 2009;428:297.
6. Vaquero JM, Vázquez M. The sun recorded through history. *Astrophysics and Space Science Library*, Springer, Berlin. 2009;361:382.
7. Cliver EW. Carrington, Schwabe and the gold medal. *Eos. Trans. Am. Geophys. Union.* 2005;86:413–418.
8. Gkana A, Zachilas L, Re-evaluation of predictive models in light of new data: Sunspot number version 2.0. *Sol. Phys.* 2016;291(8):2457–2472. DOI: 10.1007/s11207-016-0965-3
9. Hoyt DV, Schatten KH. A new look at Wolf sunspot numbers in the late 1700's. *Solar Phys.* 1992;138:387.
10. Temmer M, Veronig A, Hanslmeier A. Hemispheric sunspot numbers R_n and R_s : Catalogue and N-S asymmetry analysis. *Astronomy and Astrophys.* 2002;390:707.
11. Veronig A, Messerotti M, Hanslmeier A. Determination of fractal dimensions of solar radio bursts. *Astronomy and Astrophys.* 2000;357:337-350.
12. Jevtic N, Schwetzer JS, Cellucci CJ. Nonlinear time series analysis of northern and southern solar hemisphere daily sunspot numbers in search of short-term chaotic behavior. *Astron Astrophys.* 2001;379:611-615.
13. Abramenko VI. Multifractal analysis of solar magnetograms. *Sol. Phys.* 2005;228:29–42.
14. Movahed MS, Jafari GR, Ghasemi F, Rahvar S, Tabar MRR. Multifractal detrended fluctuation analysis of sunspot time series. *J. Stat. Mech.* 2006;P02003.
15. McAteer RTJ, Young CA, Ireland J, Gallagher PT. The bursty nature of solar flare X-ray emission. *Astrophys. J.* 2007;662:691.
16. Schatten KH. Solar activity and the solar cycle. *Adv. Space Res.* 2003;32:451.
17. Zachilas L, Gkana A. On the verge of a grand solar minimum: A second maunder minimum? *Sol. Phys.* 2015;290(5):1457–1477. DOI: 10.1007/s11207-015-0684-1
18. Tarbell T, Ferguson S, Frank Z, Shine R, Title A, Topka K, Scharmer G. Solar photosphere: Structure, convection, and magnetic fields. In Stenflo JO, (ed.), (by the IAU 138), 147; 1990.
19. Gallagher PT, Phillips KJH, Harra-Murnion LK, Keenan FP. Properties of quiet sun EUV network. *Astron. Astrophys.* 1998; 335:733-745.
20. Balke AC, Schrijver CJ, Zwaan C, Tarbell TD. Percolation theory and the geometry of photospheric magnetic flux concentrations. *Solar Physics.* 1993;143:215-227.
21. Tao L, Du Y, Rosner R, Cattaneo F. On the spatial distribution of magnetic fields on the solar surface. *Astrophys. J.* 1995;443: 199-211.
22. Cadavid AC, Lawrence JK, Ruzmaikin AA, Kayleng-Knight A. Multifractal models of small-scale solar magnetic fields. *Astrophys. J.* 1994;429:391-399.

23. Georgoulis M, Velli M, Einaudi G. Statistical properties of magnetic activity in the solar corona. *Astrophys. J.* 1998;497: 957.
24. Dmitruk P, Comez DO, DeLuca EE. Magnetohydrodynamic turbulence of coronal active regions and the distribution of nanoflares. *Astrophys. J.* 1998;505:974.
25. Janssen K, Vogler A, Kneer F. On the fractal dimension of small-scale magnetic structures in the Sun. *Astronomy and Astrophysics.* 2003;409:1127-1134.
26. Gao JB, Hu J, Tung WW, Cao YH, Sarshar N, Roy Chowdhury VP. Assessment of long range correlation in time series: How to avoid pitfalls. *Phys. Rev.* 2006;E73: 016117.
27. Gao JB, Cao YH, Tung WW, Hu J. Multiscale analysis of complex time series—Integration of chaos and random fractal theory and beyond. New York: Wiley–Interscience; 2007.
28. Howe R, Christensen-Dalsgaard J, Hill F, Komm RW, Larsen RM, Schou J, Thompson MJ, Toomre J. Dynamic variations at the base of the solar convection zone. *Science.* 2000;287:2456-2460.
29. Movahed MS, Jafari GR, Ghasemi F, Rahvar S, Tabar MRR. Multifractal detrended fluctuation analysis of sunspot time series. *J. Stat. Mech.* 2006;P02003.
30. Abramenko VI, Yurchyshyn VB, Wang H, Spirock TJ, Goode PR. Scaling behaviour of structure functions of the longitudinal magnetic field in active region on the sun. *Astrophys. J.* 2002;577:487.
31. Movahed MS, Jafari GR, Ghasemi F, Rahvar S, Tabar MRR. Multifractal detrended fluctuation analysis of sunspot time series. *J. Stat. Mech.* 2006;P02003.
32. McAteer RTJ. Frozen-in fractals all around: Inferring the large scale effects of small-scale magnetic structure. *SOLA: Arxiv* 1506.07914v1. 2015;1-13.
33. McAteer RTJ, Gallagher PT, Conlon PA. Turbulence, complexity, and solar flares. *Adv. Sp. Res.* 2010;45:1067.
34. McAteer RTJ. SOC and fractal geometry. In *Self Organized Criticality Systems*. Ashwanden MA, (ed). 2013;73.
35. Georgoulis MK. Toward an efficient prediction of solar flares: Which parameters, and how? *Entropy.* 2013;15: 5022.
36. Quiroz R, Yarlequé C, Posadas A, Mares V, Immerzeel WW. Improving daily rainfall estimation from NDVI using a wavelet transforms. *Environ. Modell. Softw.* 2011;26(2):201–209.
37. Santos CAG, Galvão CO, Suzuki K, Trigo RM. Matsuyama city rainfall data analysis using wavelet transform. *Ann. J. Hydraul. Engng. ISCE.* 2001;45:211-216.
38. Adamowski K, Prokoph A, Adamowski J. Development of a new method of wavelet aided trend detection and estimation. *Hydrol. Process.* 2009;23(18):2686–2696.
39. Chou CM. Applying multi-resolution analysis to differential hydrological grey models with dual series. *J. Hydrol.* 2007;332(1–2):174–186.
40. Partal T, Kuçuk M. Long-term trend analysis using discrete wavelet components of annual precipitations measurements in Marmara region (Turkey). *Phys. Chem. Earth.* 2006;31(18): 1189–1200.
41. Fugal DL. Conceptual wavelets in digital signal processing: An in-depth, practical approach for the non-mathematician. Firsted. Space & Signals Technologies LLC; 2009.
42. Chou CM. Wavelet-based multi-scale entropy analysis of complex rainfall time series. *Entropy.* 2011;13(1):241–253.
43. Mallat SG. A theory for multiresolution signal decomposition: The wavelet representation. *IEEE Trans. Pattern Anal. Mach. Intell.* 1989;11(7):674–693.
44. Daubechies I. The wavelets transform time-frequency localization and signal analysis. *IEEE transformation and Information Theory.* 1990;36:961-1005.
45. Vonesch C, Blu T, Unser M. Generalized Daubechies wavelet families. *IEEE Trans. Signal Process.* 2007;55(9):4415–4429.
46. Popivanov I, Miller RJ. Similarity search over time-series data using wavelets. In *Proceedings 18th International Conference on Data Engineering.* 2002;212–221.
47. Mandelbrot BB, Hudson R. The (mis) behaviour of markets. Perseus Books, Cambridge MA; 2004.
48. Muzy JF, Bacry E, Arneodo A. The multifractal formalism revisited with wavelets. *Int. J. Bifurc. Chaos.* 1994;4:245–302.
49. Arneodo A, Decoster N, Kestener P, Roux SG. A wavelet-based method for multifractal image analysis: From theoretical concepts to experimental applications. *Adv. Imaging Electr. Phys.* 2003;126:1–92.

50. Hoyt DV, Schatten KH. Group sunspot numbers: A new solar activity reconstruction. *Solar Phys.* 1998a;179: 189-219.
DOI: 10.1023/A:1005007527816
51. Hoyt DV, Schatten KH. Group sunspot numbers: A new solar activity reconstruction. *Solar Phys.* 1998b;181: 491-512.
DOI: 10.1023/ A:1005056326158
52. Hathaway DH, Wilson RM, Reichmann EJ. Group sunspot numbers: Sunspot cycle characteristics. *Solar Phys.* 2002;211:357–370. [ADS] (Cited on pages 10, 11, 31, 34, and 42).
53. Hathaway DH. The solar cycle. *Living Rev. Solar Phys.* 2010;7(1).
DOI: 10.12942/lrsp-2010-1
54. Mallat SG. A wavelet tour of signal processing. 3rd Edition from Stephane Mallat. ISBN-9780123743701, Printbook, Release Date; 2008.
55. Voros Z. On multifractality of high-latitude geomagnetic fluctuations. *Ann. Geophysicae.* 2000;18:1273–1282.
56. Balasis G, Daglis IA, Papadimitriou C, Kalimeri M, Anastasiadis A, Eftaxias K. Dynamical complexity in Dst time series using non-extensive Tsallis entropy. *Geophys. Res. Lett.* 2008;35:L14102.
DOI: 10.1029/2008GL034743
57. Chang K, Constantinescu G, Park SO. Analysis of the flow and mass transfer process for the incompressible flow past an open cavity with a laminar and a fully turbulent incoming boundary layer. *J. Fluid Mech.* 2006;561:113–14.

© 2017 Kasde et al.; This is an Open Access article distributed under the terms of the Creative Commons Attribution License (<http://creativecommons.org/licenses/by/4.0>), which permits unrestricted use, distribution, and reproduction in any medium, provided the original work is properly cited.

Peer-review history:
The peer review history for this paper can be accessed here:
<http://sciencedomain.org/review-history/18059>

Analysis of Sunspot Time Series During the Ascending Phase of Solar Cycle 24 Using the Wavelet Transform

Satish Kumar Kasde^{1,*}, Deepak Kumar Sondhiya², Ashok Kumar Gwal¹

¹Space Science Research Laboratory, Department of Physics and Electronics, Barkatullah University, Bhopal, India

²Department of Physics, LNCT Group of Colleges, Bhopal, India

Email address:

sbskasde@gmail.com (S. K. Kasde), deepsondhiya@gmail.com (D. K. Sondhiya), ashok.gwal@gmail.com (A. K. Gwal)

*Corresponding author

To cite this article:

Satish Kumar Kasde, Deepak Kumar Sondhiya, Ashok Kumar Gwal. Analysis of Sunspot Time Series During the Ascending Phase of Solar Cycle 24 Using the Wavelet Transform. *American Journal of Modern Physics*. Vol. 5, No. 5, 2016, pp. 79-86.

doi: 10.11648/j.ajmp.20160505.11

Received: July 6, 2016; Accepted: July 18, 2016; Published: August 17, 2016

Abstract: The sunspots are widely used to measure the rotational rate of solar surface. We are interested in analysis of the temporal evaluation of the short-term period present in sunspot time series (*i.e.* sunspot number and area) during the ascending phase of Solar Cycle 24. For the better understanding of variation in solar activity originated at different layers of the solar atmosphere with respect to sunspot cycles, we study the phase relation between sunspot numbers and sunspot areas using cross correlation analysis techniques based on extended wavelet based approaches such as continuous wavelet transform, cross-wavelet transform, and wavelet coherence. In this study we found the short-term periodicity “27 days-rotational rate of Sun” for current solar cycle 24 (January 2008-May 2013), which suggested that the Solar Cycle 24 has minimum solar activity. We have also investigated the correlation between both parameters and identify the unusual conditions in space weather.

Keywords: Sunspots, Rotational Rate of Sun, Solar Cycle, Solar Activity, Wavelet Analysis

1. Introduction

The helioseismic revealed that the solar magnetic field is created at the base of convection zone (tachocline) through a dynamo mechanism. Because of buoyancy, this magnetic field rises in the upward direction and appears on the solar surface as sunspots, plages, and networks. In the long-term period, the Sun exhibits an early 11-year sunspot cycle (Schwabe Cycle) and for short-term periods the 27-day periodicity is the most prominent [1], [2]. The 27 day periodicity revealed in the interval 1994-2000 by [3]. The corresponding rotation period of the Sun found by [4] in their study of solar wind parameters of the interplanetary magnetic field (IMF). Several authors investigated the “midterm” periodicities of the sunspot data during Solar Cycles 12 through 23 [5]-[12]. Sunspot numbers and sunspot areas are historically used to describe the long-term, mid-term and short-term quasi periodicities. Mid-term quasi-periodicities (one to several months or longer) was used in the diagnostics of various solar flare activities and sunspot numbers or areas

etc. [13]-[21], [5], [22], [5], [23]-[29]. The relation between total corrected sunspot area A (in millionths of the visible solar hemisphere) and sunspot number R is not particularly good for daily values, although it has often been stated that the relationship becomes better when using monthly or yearly averages.

This study aims to enhance the possibilities for detection and quantification of relationships between sunspot number and sunspot areas with wide stratigraphic uncertainties. Previous studies on this topic relied on basic statistical techniques such as cross-spectral analysis, regression, or correlation techniques. In addition, visual assessment of plots of such records is frequently used and extensively accepted [30]-[32]. Statistical methods and trend analysis are able to determine the significance of relationships between non-stationary time-series. However, performance of these methods compromised if time-series analyzed are same (*i.e.* having same wavelength) and phase shifted. Linear analysis approaches such as using the Fourier transform, may generate artifacts when they are applied to analysis of real world process. Currently, many advanced

analysis approaches, such as the cross wavelet transform (XWT), wavelet coherence (WTC) and cross-recurrence plot (CRPs) are widely used to study the nonlinear behavior of time series [33].

Cross-wavelet analysis permits detection, extraction and reconstruction of relationships between two non-stationary signals simultaneously in frequency (or scale) and time (or location) [34]. Cross-spectral analysis is a bivariate version of spectral analysis for comparison of two data sets [35]. Similarly, cross-wavelet transform (XWT) can be considered as a bivariate extension to wavelet transform (WT), which has been developed as a tool to filter, examine, and extract non-stationary signals in time-series and images [36]. A range of analysis approaches, namely continuous wavelet, cross wavelet, and wavelet coherence analyses, are employed to clarify the phase relationship between the smoothed monthly mean sunspot number and solar 10.7cm flux (F10.7) [37]. Analysis shows that the rise region of high spectral power sits across the Schwabe Cycle belt, where the two time series are in phase [38]. However, analysis of the cross-wavelet transform and wavelet coherence unveils asynchronous behavior featured with phase mixing in the high-frequency components of sunspot activity and solar F10.7, which may explain the different activity properties of the photosphere and corona on a short time scale. The comprehensive explanations of wavelet squared coherency and cross-wavelet phase angle using Morlet wavelet based on continuous cross-wavelet transform are given in [39] and [34] and references therein. The main concern of this paper is to apply the advanced wavelet based technique for the analysis of sunspot area and sunspot data. This paper is subdivided into section 2: includes the observation data and method of analysis; through section 3: we have interpreted the results and finally in the section 4: conclusion.

2. Observational Data and Method of Analysis

2.1. Data Set

The daily values of sunspot number of the whole solar disk, northern and southern hemispheres of the Sun are published by the ‘‘Solar Influences Data Analysis Centre’’ (<http://sidc.oma.be/sunspot-data/>), a solar physics research division of the Royal Observatory of Belgium.

We have used the daily and total (both the Northern and Southern hemisphere) values of sunspot number and area (expressed in units of millionths of the solar hemisphere) time series prior to January 2008 to May 2013, covering the ascending and maximum phase of Solar Cycle 24. The sunspot area data, beginning in May 9, 1874 were compiled at Royal Greenwich Observatory from a small network of observatories and available online at <http://www.solarscience.msfc.nasa.gov>.

2.2. Wavelet Transform Technique

We studied the relative behavior of sunspot area and

sunspot number using wavelet based cross correlation techniques. Wavelet analysis is a tool for analyzing localized variations of power spectra within a time series [40], [34]. The wavelet technique decomposes a one-dimensional time series into a two-dimensional time-frequency space. Therefore, this method determines not only the periodicities of the dominant modes of variability, but also shows how the modes vary in time. Moreover, the wavelet technique is suitable to detect a signal which is relatively weak and intermittent in nature [40], [41]. To take into account describe wavelet in following ways:

2.2.1. Continuous Wavelet Transform

Wavelet analysis involves a transform from a one dimensional time series to a diffuse two-dimensional time-frequency image for detecting the localized and quasi-periodic fluctuations by using the limited time span of the data [40], [42]. The CWT has edge artifacts because the wavelet is not completely localized in time. It is therefore useful to introduce a cone of influence (COI) in which edge effects cannot be ignored. Here we take the COI as the area in which the wavelet power caused by a discontinuity at the edge has dropped to e^{-2} of the value of edge. It is used to satisfy the admissibility condition [43], [40], [34], [42]. The continuous wavelet transform of the time series is given by

$$W_{\Psi}(s, t) = \frac{1}{\sqrt{s}} \int_{-\infty}^{\infty} f(t) \Psi^* \left(\frac{t-x}{s} \right) dt, \quad (1)$$

Where $f(t)$ is the time series of the sunspot data, Ψ^* is the complex conjugate of continuous wavelet function Ψ , $s > 0$ the scaling factor controlling the dilation of the mother wavelet and a is the translation parameter determining the shift of the mother wavelet. It is common to use the Morlet wavelet, which consists of a complex exponential, where, t is the time, s is the wavelet scale and ω_0 is the non-dimension frequency function. It is given by function [43] as

$$\Psi(t) = \pi^{-\frac{1}{4}} e^{i\omega_0 t} e^{-\frac{\eta^2}{2}} \quad (2)$$

Where η is the frequency parameter that allows one to shift the frequency range for the investigation. When using wavelets for feature extraction purposes the Morlet wavelet (with $\omega_0 = 6.6$) is a good choice, since it provides a good balance between time and frequency localization. Fig.2 shows the continuous wavelet spectra of the daily sunspot number and area. There evidently are common features in the wavelet power of the time series of high power above the 95% confidence level. Both have a small scale periodicity (range from 16-32 days) about 27 days as the rotational rate of Sun. We therefore, restrict our further treatment to this wavelet, although the methods we present are generally applicable [44]. The idea behind the CWT is to apply as a bandpass filter to the time series. The wavelet stretched in time by varying its scale (s), so that $\eta = s \cdot t$, and normalizing it to have unit energy. Detailed technical information about the Morlet wavelet is available at the website

<http://atoc.colorado.edu/research/wavelets/wavelet2.html>.

2.2.2. Cross Wavelet Transform

Cross-wavelet transform (XWT) is an extension of wavelet transform to expose their common power and relative phase in time-frequency space between two time series [42]. The XWT of two time series x and y is defined as $W^{xy} = W^X W^y$, where $*$ denotes complex conjugation. We further the cross-wavelet power as $|W^{XY}|$. The complex argument $\arg(W^{XY})$ can be interpreted as the local relative phase between x and y in time frequency space. The cross wavelet transform exposes regions with high common power and further reveals information about the phase relationship. If the two series are physically related we would expect a consistent or slowly varying phase lag that can be tested against mechanistic models of the physical process. The univariate wavelet power spectrum can be extended to compare sunspot area $x(s)$ and sunspot number $y(s)$. One can define the wavelet cross spectrum as the expectation value of the product of the corresponding

$$W_{xy}(s, t) = W_x(s, t) W_y^*(s, t) \tag{3}$$

Where $*$ denotes the complex conjugate and $W_x(s, t)$, $W_x(s, t)$ and $W_y(s, t)$ are the wavelet transform of $x(s)$ and $y(s)$ respectively. It not only determines the periodicities of the dominant modes of variability, but also shows how the modes vary in time. In contrast to the WPS, the WCS are complex valued. In order to get the phase relationship, we employed the codes provided by [34], which is displayed in Fig. 3. Furthermore, XWT shows that the two time series are in phase in the area, namely about 27 days periodic scale, with significant common features found in Fig. 2 with their confidence level is above 95%. However, during the maximum (i.e from year 2011 to 2013) phase arrows are pointing in the right direction and it shows that both time series are synchrony. The high frequency components range from 4 to 8 days scale demonstrates the strong phase mixing because arrows at high frequencies are randomly distributed. [45] found via cross-recurrence plots the high frequency components in hemispheric sunspot activity are not responsible for the strong phase synchronization.

2.2.3. Wavelet Coherence

The wavelet coherence (WTC) another useful measure, which can show coherent cross-wavelet transform, is in time-frequency space. WTC is necessary because the cross-wavelet spectrum appears to be unsuitable for significant testing the interrelation between two processes [46]. Wavelet coherence is defined between two CWTs to find significant coherent even though the common power is low and WTC closely resembles a localized correlation coefficient in time frequency space [34]. The WTC between two time series x and y is defined as [34].

$$R_{ns}^2(s) = \frac{\left| S \left(s^{-1} W_n^{xy}(s) \right) \right|^2}{S \left(s^{-1} \left| W_n^x \right|^2 \right) * S \left(s^{-1} \left| W_n^y \right|^2 \right)} \tag{4}$$

where S_{scale} is smoothing operator. The wavelet coherence can be taken as a correlation coefficient to show the localization of time frequency, as the definition and the traditional correlation coefficient are very smaller. In this context, the smoothing operator S is

$$S(W) = S_{scale} \left(S_{time} (W_n(S)) \right), \tag{5}$$

where S_{time} denotes smoothing along the wavelet scale axis, and S_{scale} smoothing along the time axis. In the context of the Morlet wavelet, the smoothing operators given as [31]

$$S_{time}(W)|_s = \left(W_n(S) * C_1 \frac{t^2}{2s^2} \right)_s, \tag{6}$$

$$S_{scale} W|_s = (W_n(S) * c_2 \Pi(0.6s))|_n \tag{7}$$

where c_1 and c_2 are normalization constant and Π is a rectangle function. The factor 0.6 is a scale decorrelation length determined empirically for the Morlet wavelet [47]. Both convolutions are discrete. As a result, the normalization coefficients have to be determined numerically [34]. Fig. 4 displayed the result of the XWT between the SSA and SSN. The WTC represents the strong phase mixing at period scale around the 32-128 days over the time period 2009-2012. However, the WTC indicates the noisy behavior with strong phase mixing in the high frequency components of both the SSN and SSA.

3. Results and Discussion

It is started by applying the well known wavelet tools, developed by [40], on the daily grouped sunspot number and sunspot area data from January 2008 May 2013. The current Solar Cycle 24 rises at a lower level of activity during the ascending phase. Fig. 1 shows the variations in both the parameters. From the Fig.1 it is cleared that (i) SSN and SSA solar indices never peak at the same time, and the SSN peaks earlier than the SSA; (ii) however, the SSA and SSN develops with the same magnetic field variations on the photosphere of the Sun and the magnetic field strength increases according to the ascending epochs. An understanding of complexity in the periodicities of the SSA and SSN may provide insight into the complex dynamics of the solar magnetic field in the two hemispheres.

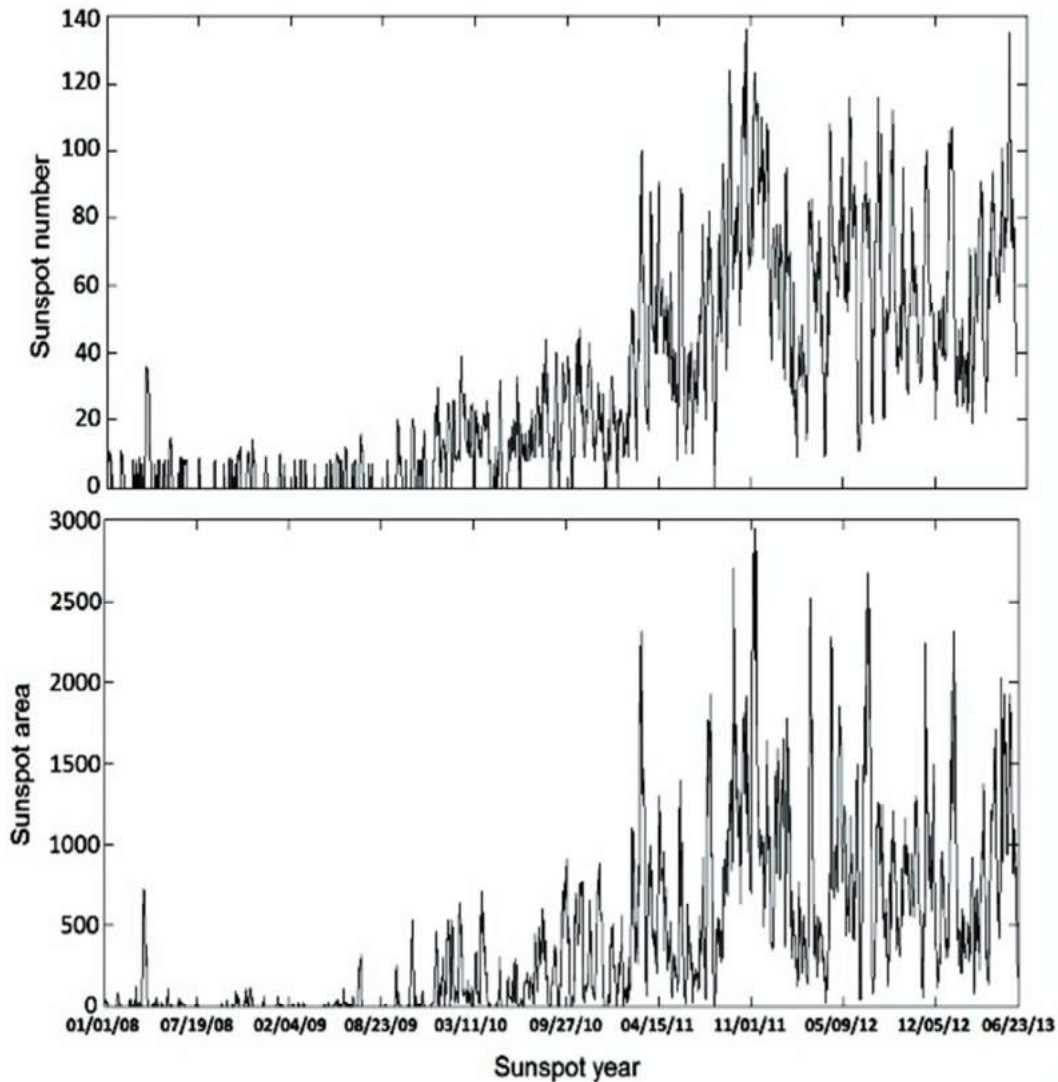


Fig. 1. The distribution of the sunspot number (upper panel) and sunspot area (bottom panel) for the time interval 2008 January to 2013 May.

The wavelet power spectra for sunspot area and sunspot number are calculated and shown in Fig. 2 with a cone of avoidance and contours enclosing regions of greater than 95% confidence level. It was noticed that the spectral power is relatively weak at the short periods or at high frequencies. However, it is not difficult to locate some distinct dual-patches of relatively higher contours at around scale factor (i.e. periods) of around 16 to 64 days from September 2010 to May 2013. It is found that large variations at the time flow have a periodicity of around 27 day for both sunspot number and the sunspot area. The other small peaks cannot be considered from coincidence due to multiple testing [34].

The XWT and WTC are rendering the regions with high common power and make known information about the phase relationship between two time series. The WTC between SSN and SSA are shown in Fig. 4. Compared with the XWT a larger black contour stands out as being significant and all these area show phase relationship between SSA and SSN. The XWT and WTC have edge artifacts because the wavelet is not completely localized in

time. It is therefore necessary to introduce a cone of influence (COI) in which the transformation suffers from these edge effects. The COI is defined so that the wavelet power for a discontinuity at the edges decreases by a factor e^{-2} [34]. The thin black contour (inside COI) demonstrates the periods above 95% confidence level [40]. In these figures, arrows point to the right when processes are in phase and to the left when they are in anti-phase. If an arrows points up (down), then the first process leads (lags) these con done. The statistical significance of wavelet power can be assessed relative to the null hypothesis that the signal is generated by a stationary process with a given background power spectrum. The thick contour shown in figure designates the time series against red noise.

The XWT shows that almost all arrows point to the right and indicate 27 day periodic time in the period-scale. It means the sunspot number and sunspot area are in phase in this area. Statistically it is found that the significant result that there liable results are located within the cone of influence and the arrows beyond the cone of influence are not

reliable. It is also noted that the arrows are fairly distributed in other periodic belts, implying strong phase mixing. The squared wavelet coherency is a measure of the intensity of the covariance of the two series in time-frequency space [40]. We have found that strong value of coherency in the period of 32-128 days of the epoch 2009-2012. All the sections show both the times series correlating to each other. By [48] shown that 27 days periodicity more pronounced during the descending phase than ascending phase of solar cycle. [49] have found the 27 days periodicity (with 13.5 days being its harmonic) in the dynamic parameters of the solar wind, B_x , B_y and the geomagnetic indices by both the wavelet analysis and the Lomb/Scargle periodogram. The rotational periodic of the Sun is expected to provide useful information about solar interior dynamics and mechanism of generation of the solar magnetic field and its emergence on the solar surface

[16], [50]. [51] also predicted the values 112 of sunspot number for solar cycle 24, prior to 2011-2012 which is displayed in Fig.1 (upper panel). Solar cycle 24 has the lower amplitude than that of cycles 21, 22 and 23 which is consistent with the results obtained by [52] and [53]. [54] found the short-term periodicities in the daily data of the sunspot numbers and areas are investigated separately for the full disk, northern, and southern hemispheres during Solar Cycle 23 for a time interval from 1 January 2003 to 30 November 2007 corresponding to the descending and minimum phase of the cycle. The wavelet power spectrum technique exhibited a number of quasi-periodic oscillations in all the datasets. In the high frequency range, we find a prominent period of interval 22–35 days in both sunspot indicators.

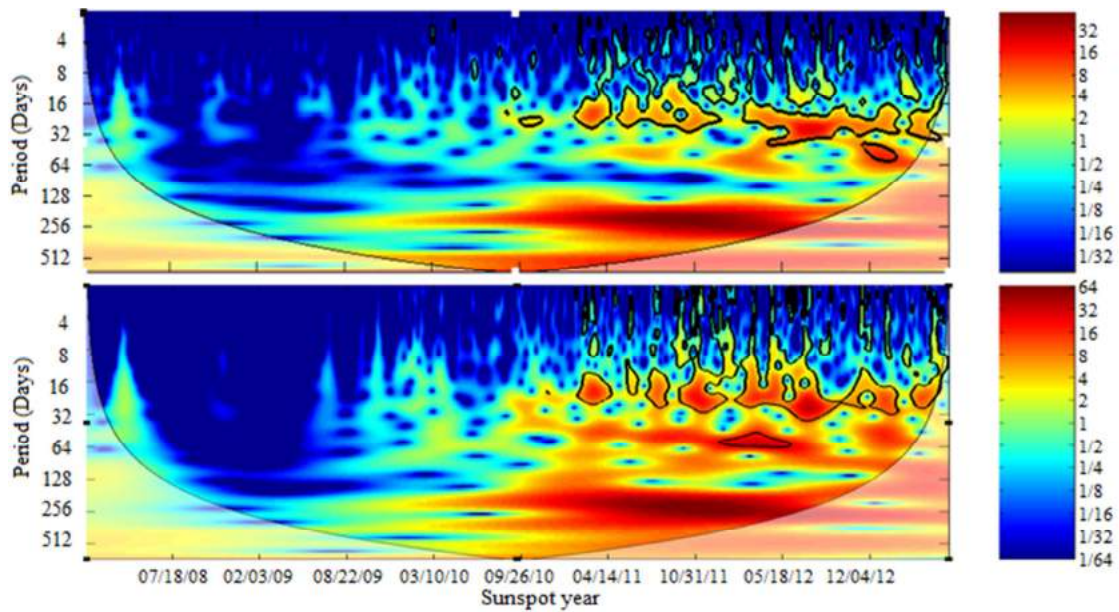


Fig. 2. Wavelet power spectra (WTC): Daily sunspot number (upper panel: fig.1) and sunspot area (bottom panel: fig. 1), with a cone of avoidance and enclosed regions of greater than 95% confidence level (thick black solid line).

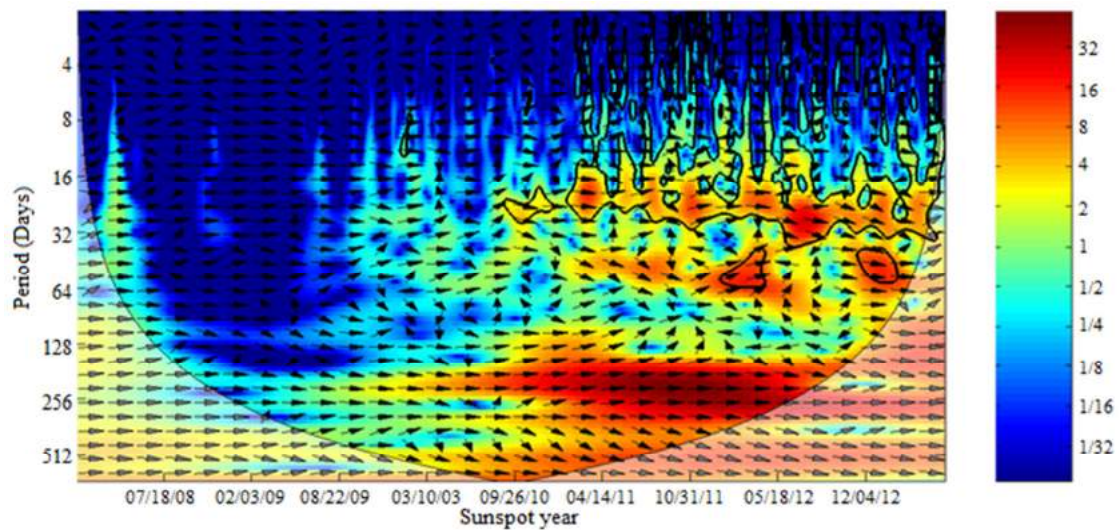


Fig. 3. Cross-wavelet spectra (XWT): Daily sunspot number and sunspot area with a cone of avoidance and enclosed regions of greater than 95% confidence level (thick black solid line).

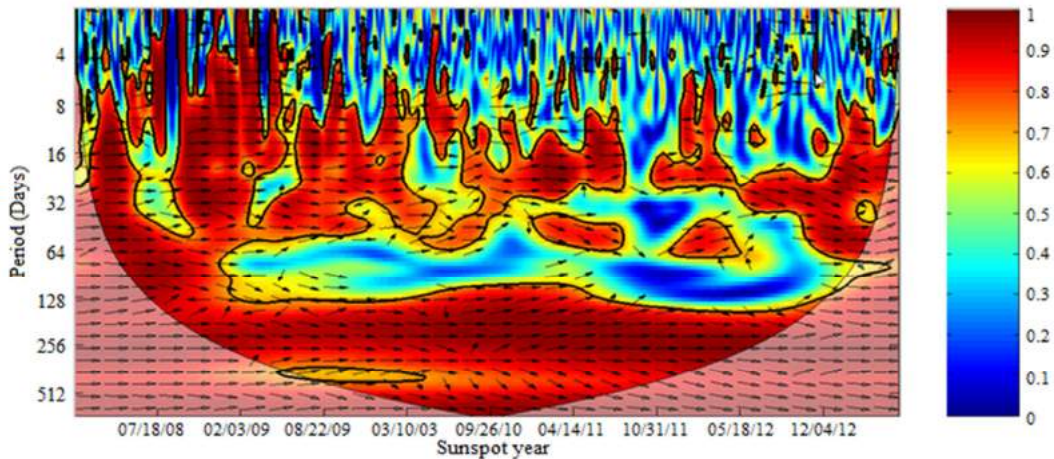


Fig. 4. Wavelet coherence of (WTC): Daily sunspot number and sunspot area with a cone of avoidance and enclosed regions of greater than 95% confidence level (thick black solid line).

4. Conclusions

This paper deals with the wavelet cross-correlation analysis of the daily values of SSA and SSN. Our study covers the entire maximum phase and a major portion of the minimum phase of Solar Cycle 24 (period from January 2008 to May 2013). For total sunspot number and sunspot area wavelet analysis detected a significant period of about 27 days (solar orbit rotation). However, this period varies from 16 to 64 days. This period is more stable than the other short-term periods and appeared from September 2010 to May 2013. With this periodicity, we have concluded that the solar cycle 24 also include the most remarkable period during the ascending phase. Here, the many periodicities are not considered due to the maximum peaks are below the significance level. Near 27 day periodicity is noticed in the sunspot number [55], [56], [57] and in the sunspot area [57]. It is also detected in the different following solar activities CaK plage area [58], globally averaged coronal radio fluxes [59], [60], [61] and in the coronal mass ejection (CME) activity during Solar Cycle 23 [62]. [63] revealed the 27 days periodicity is present almost in their analysis using the wavelet technique on the daily data of sunspot numbers covering the Solar Cycles 10-23.

The results of this work clearly demonstrate that there exists a strong correlation around the year 2012. In conclusion we have found evidence for a 27 day periodicity in both the sunspot area and sunspot number during the ascending branch of solar cycle 24 and a very weak evidence for the fundamental period reported by [48]. This may arise because of different characteristics of the current cycle. For the exact conclusion we have to wait until the end of cycle 24. However, the strong magnetic fields in sunspots are not necessarily unstable. It is worth noting that the same time interval similar periodicities exist in the SSA and SSN. The continuous wavelet transforms of the two time series show that the 16-32 periodic range are statistically significance for short-term periodicities. The cross wavelet transform of the

two time series shows that there is an area with high common spectral power, located at the 16-64 periodic belts, where the two time series are in phase. The cross wavelet transform (XWT) confirms the results given by wavelet coherence (WTC), but WTC is found more suitable to find a coherent oscillation of the two time series than XWT. This analysis reveals that the Solar Cycle 24 has only mid range periodicity which can predict that this cycle has minimum amplitude than others.

Acknowledgments

We thank to Solar Influence Data Analysis Center (SIDC) and NASA Solar Science Center for providing data. A Matlab software package being used by the authors for performing XWT and WTC can be found at <http://www.pol.ac.uk/home/research/waveletcoherence/>. One of us (SKK) is thankful to University Grants Commission, New Delhi (India) for financial assistance under the scheme of RGNF.

References

- [1] Bartels, J. (1934). *Terr. Magn. Atmos. Elec.*, 39, 201.
- [2] Watari, S. (1996). *Solar Phys.* 168, 413.
- [3] Polygiannakis, J., Preka-papadema, P., Petropoulos, B., Pothitakis, G., Moussas, X., pappas, G., Hilliaris, A. (2002). In: H. Swaya- Lacoste (ed.) SOLMAG2002. Proc. Magnetic Coupling of the Solar Atmosphere Euro conference, ESASP-505, 537.
- [4] Katsavrias, C., Preka Papadema, P., Moussas, X. (2012). Wavelet Analysis on Solar Wind Parameters and Geomagnetic Indices. *SolarPhys.* DOI10.1007/s11207-012-0078-6.
- [5] Lean, J. L., Brueckner, G. E. (1989). intermediate-term solar periodicities:100-500days, *ApJ*, 337, 568.
- [6] Lean, J. L. (1990). Evolution of the 155 day periodicity in sunspot areas during solar cycles 12 to 21, *Astrophys. J.* 363, 718.

- [7] Carbonell, M., Ballester, J. L. (1992). *Astron. Astrophys.* 255, 350.
- [8] Oliver, R., Carbonell, M. and Ballester, L. (1992). *Sol. Phys.*, 137, 141.
- [9] Krivova, N. A., Solanki, S. K. (2002). *Astron. Astrophys.* 394, 701.
- [10] Richardson, I. G. and Cane, H. V.: 2005, *Geophys. Res. Lett.*, 32, L02104.
- [11] Ataç, T., Özgüç, A., Rybák, J. (2006). *Solar Phys.* 237, 433.
- [12] Joshi, B., Pant, P., Manoharan, P. K. (2006). *Astron. Astrophys.* 452, 647.
- [13] Rieger, E., Share, G. H., Forrest, D. J., Kambach, G., Reppin, C., Chupp, E. L. (1984). *Nature*, 312, 623.
- [14] Kiplinger, A. L., Dennis, B. R., Orwig, L. E. (1984). *BAAS*, 16, 891.
- [15] Dennis, B. R. (1985). *Solar Phys.*, 100, 465.
- [16] Ichimoto, K., Kubota, J., Suzuki, M., Tohmura, I., Kurokawa, H. (1985). *Nature*, 316, 422.
- [17] Delache, P. H., Laclare, F., Sadsoud, H. (1985). *Nature*, 317, 416.
- [18] Bogart, R. S., Bai, T. (1985). *ApJ*, 299, L51.
- [19] Bai, T., and Sturrock P. A. (1987). The 152 day periodicity of the solar flare occurrence rate, *Nature*, 327, 601-604.
- [20] Ribes, E., Merlin, Ph., Ribes, J. C., Bartholot, R. (1987), *Annales Geophysicae* 7, 321.
- [21] Lean, J. L., Bruckner, G. E. (1989). Intermediate-term solar periodicities: 100-500 days, *APJ*, 337, 568.
- [22] Özgüç, A., Ataç, T. (1989). *Solar Phys.*, 123, 357.
- [23] Carbonell, M., Ballester, J. L. (1990). *A&A*, 238, 377.
- [24] Droge, W., Gibbs, K., Grunsfeld, J. M., Meyer, P., Newport, B. J. (1990). *ApJS*, 73, 279.
- [25] Pap, J., Tobiska, W. K., Bouwer, S. D. (1990). *Solar Phys.*, 129, 165.
- [26] Kile, J. N., Cliver, E. W. (1991). *ApJ*, 370, 442.
- [27] Verma, V. K., Joshi, G. C. and Paliwal, D. C. (1992). *Solar Phys.*, 138, 205.
- [28] Cane, H. V., Richardson, I. G., von Roseninge, T. T. (1998). *Geophys. Res. Lett.*, 25, 4437.
- [29] Ballester, J. L., Oliver, R., Baudin, F. (1999). *ApJ*, 522, L153.
- [30] Crowley, T. J., Berner, R. A. (2001). *CO₂ and climate change. Science* 292, 870-872.
- [31] Shaviv, N. J., Veizer, J. (2003). Celestial driver of Phanerozoic climate? *GSA Today* 13: 4-10.
- [32] Royar, D. L. (2006). *CO₂ forced climate threshold during the Phanerozoic. Geochim Cosmochim Acta* 70:5665-5675.
- [33] Li, Q. X. (2008). Periodicity and hemispheric phase relationship in high-latitude solar activity. *Sol. Phys.* 249, 135.
- [34] Grinsted, A., Moore J. C., Jevrejeva. S. (2004). Application of the cross wavelet transform and wavelet coherence to geophysical time series. *Nonlinear Proc. Geophys.*, 11, 561-566.
- [35] Davis, J. C. (2002). *Statistics and data analysis I geology*, 3rd edn. Wiley, New York, p 637.
- [36] Morlet, J., Arens, G., Fourgean, E. and Giard, D. (1982). Wavepropagation and sampling theory, part1; complex signal and scattering in multi layer media. *Journal of Geophys.* 47:203-221.
- [37] Zhang, Xue Feng, GuiMing, Le. And Zhang, Yan. Xia. (2012). *Chinese Science Bulletin*, Vol. 57, No. 2078-2082.
- [38] Le, G. M. (2004). Wavelet analysis of the schwabe cycle properties in solar activity. *Chin J Astron Astrophys*, 4:578-582.
- [39] Torrence, C. and Webster, P. (1999). International changes in the ENSO-Monsoon System, *J. Clim.*, 12, 2679-2690.
- [40] Torrence, C. and Compo, G. P. (1998). A practical guide to wavelet analysis, *Bull. Am. Meteorol. Soc.*, 79, 61-78.
- [41] Knaack, R., Stenflo, J. O., S. V., Berdyugina: 2005, *Astron. Astrophys.* 438, 1067.
- [42] Li, K. J., Gao, P. X., & Su, T. W. (2005). *Sol. Phys.*, 229, 181.
- [43] Farge, M. (1992). *Ann. Rev. Fluid Mech.* 24, 395.
- [44] Foufoula-Georgiou, E. and Kumar. P., (1995). *Wavelet in Geophysics*, Academic Press, 373.
- [45] Zolotova, N. V., & Ponyavin, D. I. (2006), *A & A*, 449, L1.
- [46] Maraun, D., Kurths, J. (2004). *Nonlinearproc. Geophys.*, 11, 505.
- [47] Christopher, T., Gilbert, P. C. (1998). A practical guide to wavelet analysis. *Bullamer Meteorolog Soc*, 79, 61-68.
- [48] Özgüç, A., Ataç, T. and Rybák, J. (2002) *J. Geophys. Res.* 107, 10. 1029/2001JA009080.
- [49] Katsavrias, Ch., Preka-Papadema, P., Moussas, X. (2012). astro-ph. SR, arXiv:1205.2229v1.
- [50] Sturrock, P. A., Bai, T. (1992). *Apj*, 397, 337.
- [51] Tong, Xu., Jian, Wu., Zhen-Sen, Wu., and Qiang, Li. (2007). *Chin. J. Astron. Astrophys.* Vol. 8, No. 3, 337-342.
- [52] Duhau, S. (2003). Wavelet analysis of solar activity recorded by sunspot groups. *Solar Phys.* 213:203-212.
- [53] Wang, J. L., Gong, J. C., Liu, S. Q., et al. (2002). The prediction of maximum amplitudes of solar cycles and the maximum amplitude of solar cycle 24. *Chin. J. Astron. And Astrophys*, 2 (6): 557-562.
- [54] Chowdhury Parth. (2010). Short Term Periodicities in Sunspot Activities During the Descending Phase of Solar Cycle 23. *Solar Phys* 261:173-191. DOI10.1007/s11207-009-9478-7.
- [55] Lean, J. L. (1991). *Rev. Geophys.*, 29, 4, 505.
- [56] Balthasar, H. (2007). *A & A*, 471, 281.
- [57] Kilick, H. (2009). *Sol. Phys.*, 253, 281.
- [58] Singh, Jand Prabhu T. P. (1985). *Sol. Phys.*, 97, 203.

- [59] Kane, R. P., Vats, H. O. and Sawant, H. S. (2001). *Sol. Phys.*, 2011, 181.
- [60] Kane, R. P. (2002). *Sol. Phys.* 205, 351.
- [61] Hiremath, K. M. (2002). In *Proc. IAU Coll 188, (ESASP.505)*. P. 425.
- [62] Lara, A, Borgazci, A, Mendas, Odim, Jr., Rosa, R. R., Dominguer, M. O. (2008). *Solar Phys*, 248, 155.
- [63] Yin, Z. Q., Han, Y. B., Ma, L. H., Le, G. M., Han, Y. G. (2007). *Chin. J. Astron. Astrophys.* 7, 823.

Fine Structure Analysis of Very Low Frequency (VLF) Signal Transients using Wavelet Transform Modulus Maxima (WTMM) Technique

D.K. Sondhiya, S.K. Kasde, Rahul Shrivastava, Monu Raghuvanshi and A.K. Gwal

*Space Science Laboratory, Department of Physics and Electronics,
Barkatullah University, Bhopal – 462026, India
Email – deepsondhiya@gmail.com
Contact No: +91755-4202785, +91-9981400802*

Abstract

Very Low Frequency (VLF) disturbances like whistlers and hiss are non-stationary in nature. They are the points of sharp variation such as singularities in VLF signal, which usually carry the most important information about these disturbances. The qualitative analysis of the various transients in VLF signals helps us to detect and characterize the nature of these transients and related phenomenon. For the analysis of these disturbances, we have tried to detect the irregularity in the signal using the wavelet transform modulus maxima (WTMM) algorithm as it gives a reliable multistage representation of the signal. The results show that WTMM method is very efficient and suitable for detection of occurrence time of VLF signal disturbances and extraction of the characteristic points of the VLF signal for the identification of many important signatures present in VLF signal.

Keywords – VLF transients, Wavelet Transform Modulus Maxima, Noise Suppression.

I. INTRODUCTION

VLF transients like whistlers and Hiss are considered to be very effective tools for the analysis of various phenomena related to magnetosphere and plasmasphere [1-4]. Whistler mode waves play significant role in precipitation of energetic particles in connection with auroral pulsations [5]. Whistlers are capable of attenuating some portion of naturally occurring noises [6]. Interaction between energetic electrons and whistlers-mode waves, in particular, had been suggested as being a primary indicator in determining the morphology of radiation belts [7]. The frequency spectrum of hiss

emissions is irregular in structure and intensity. Thus, a detailed understanding of the generation, propagation and maintenance of modulating hiss emissions is important problem in magnetospheric physics.

For the spectral analysis of such types of emissions Fast Fourier Transform (FFT) based spectrograms are commonly used. Spectrograms are unable to detect accurately the onset and end of sustained events like points of sharp disturbances or singularities generated by various geophysical processes [8]. Therefore it becomes mandatory to define a representation that can be adopted to extract the characteristic features of these disturbances.

Singularities detection by the WTMM representation has proved to be very beneficial in the last few decades [9 – 12]. The core theme of this work is to discuss the theoretical formulation of the WTMM technique and present some results related with whistlers and Hiss observed by onboard DEMETER satellite

II. THEORETICAL FRAMEWAORK

The wavelet transform of VLF transients $f(t)$ associated to the mother wavelet is defined as

$$Wf(x, s) = \frac{1}{\sqrt{s}} \int_{-\infty}^{+\infty} f(t) \varphi^* \left(\frac{t-x}{s} \right) dx \quad (1)$$

The wavelet transform $Wf(x, s)$ is a function of the scale s and position (time) x . It measures the variation $f(t)$ in in the neighborhood of position, whose size is proportional to the scale factor > 0 . The point is defined to be a modulus maxima, if $|Wf(x, s)|$ is a local maximum .i.e. if

$$\frac{\partial Wf(x_0, s_0)}{\partial x} = 0 \quad (2)$$

and if $Wf(x_0, s_0)$ is strictly increasing to left of x_0 or strictly decreasing to right of x_0 . A connected curve γ in the scale space plane is called a ‘‘Maxima Line’’ if $(x, s) \in \gamma$ implies (x, s) is a modulus maximum. For each Modulus maxima there is at least one curve that locally intersects the points (x_0, s_0) . In order to estimate the time at which the singularity occurs, the following equation has been defined

$$g(\gamma, n) = \frac{\sum_{i=1}^n \gamma_i}{n} \quad (3)$$

The calculated value of $g(\gamma, n)$ corresponds to the approximate time of disturbances occurrence. Some time these values are affected by overall trends and by noise introduced by the high frequency components of the signals [13]. The final result of analysis is a characteristics vector of the same length as the original signal. The resulting characteristics vector indicates the time when a singularity was detected and its weight defined by propagation of the corresponding maxima line

III. RESULTS AND ANALYSIS

The block diagram depicted in Fig. 1 is proposed to study the VLF disturbances. VLF transients analyzed in this work are observed by DEMETER satellite during February, 2009 Indonesia earthquake. The waveforms and spectrograms of transients (Hiss and Whistlers) are illustrated in Fig. 2 and Fig. 3. Transients are normalized by using appropriate wavelet filter. They are then denoised and reconstructed using WTMM. To denoise the signal appropriate threshold level is achieved by modified version of Universal threshold [14] stated as:

$$Thresh = \sigma \sqrt{\log(n)} \quad (4)$$

Where n is the number of sample and σ is calculated by median mirror filter.

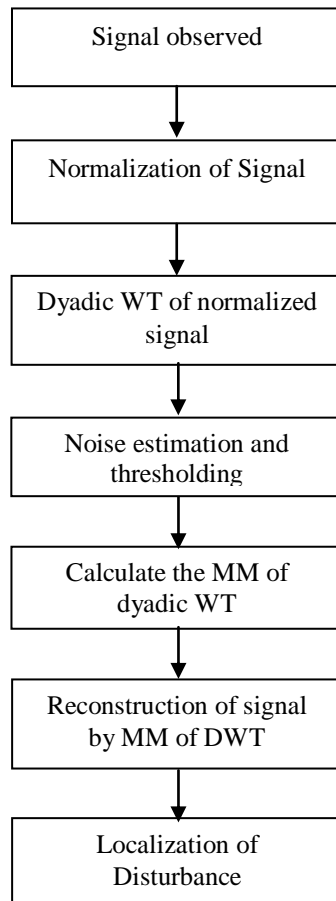


Fig. 2 Block diagram of the proposed method for the identification and localization of the VLF signal disturbance

For detecting the exact location of disturbance, the reconstructed signal is decomposed by the Multi Stage Decomposition (MSD) algorithm [15]. The spectral frequency band of MSD detail coefficients at various levels of decomposition for

sampling frequency $f_s = 40 \text{ kHz}$ is given in table 1.

Table – 1

SN	Detail coefficient	Frequency bands (in kHz)
1.	d_1	(40-20)
2.	d_2	(20-10)
3.	d_3	(10-5)
4.	d_4	(5-2.5)
5.	d_5	(2.5-1.25)
6.	d_6	(1.25-0.625)

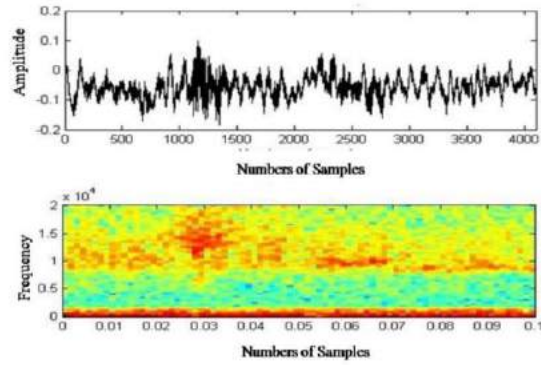


Fig.2 Waveform of VLF Hiss emission observed by DEMETER satellite (Upper panel) and its spectrogram (Lower panel).

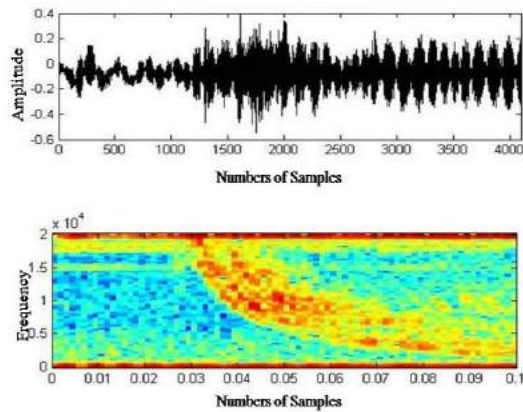


Fig.3 Waveform of VLF Whistler emission observed by DEMETER satellite (Upper panel) and its spectrogram (Lower panel)

A. *VLF signal with Hiss emission*

Hiss emission is a special kind of disturbance produced in the VLF signal generated as a result of lighting, tornado and sometimes also due to earthquakes and volcanic eruptions. It is considered to be random and turbulent in nature. The ground and

satellite ELF/VLF measurements indicate that the chorus is frequently accompanied by a back ground of hiss [16 – 18]. In Fig. 4, WTMM spectrum of VLF Hiss with the maxima curve is shown. Presence of large numbers of maxima curves indicates the highly turbulent nature of hiss and also the presence of unwanted noises of less physical importance.

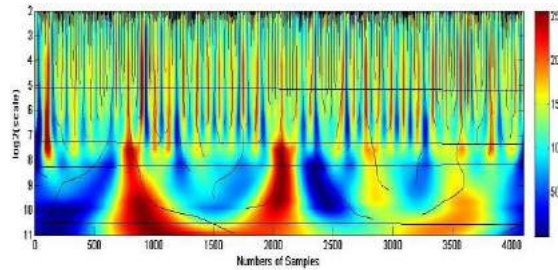


Fig. 4 WTMM curve of VLF Hiss.

The waveform of reconstructed hiss along with modulus maxima curves is given in Fig. 5. It shows less noise as compare to signal observed. Hence the signal disturbances can easily be identified. It is observed that the signal is highly disturbed between the ranges 1200-1400, which in turn is the most evident region of signal disturbances.

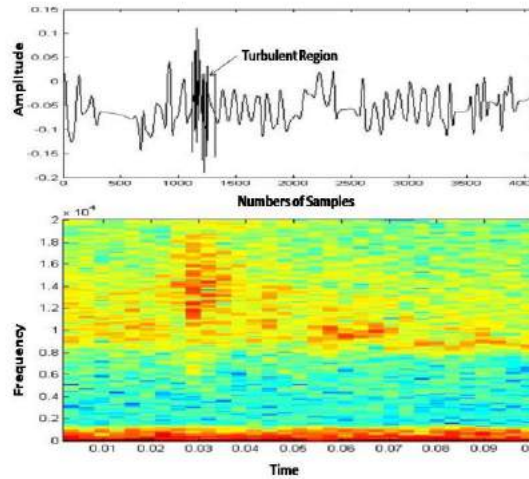


Fig. 5 Waveform of VLF Hiss emission reconstructed by WTMM method (Upper panel) and its WTMM curve (Lower panel)

Thus it can be concluded that the some part of the hiss signal is highly turbulent and incoherent, whereas some parts indicate the presence of monochromatic wave. Many authors have also confirmed this result with the fine resolution spectral analysis [18 – 19]. They have found that some parts of hiss are highly incoherent; on the other hand some indicate the presence of wavelets or monochromatic wave

components with considerable duration near the upper edge of the hiss band. Hattori [21] proposes that if the intensity and duration of the wavelet is sufficiently large, they produce chorus type noise. It is very important for the modeling of chorus events.

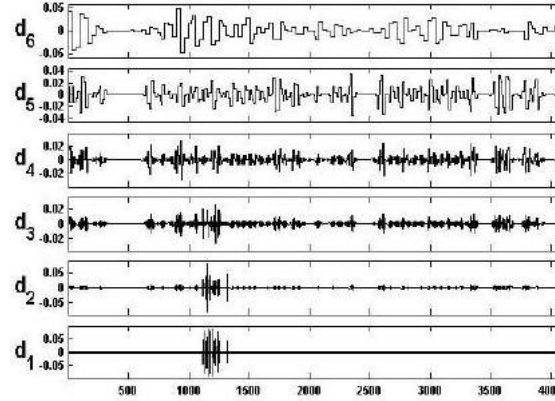


Fig. 6 Identification and localization of disturbance in VLF Hiss emission using Haar wavelet at Level 6.

Discrete Wavelet Transform (DWT) is used to detect the exact location of disturbances in VLF signal (Fig. 6). It contains the wavelet coefficients of various sub bands. Wavelet coefficients with high values indicate the VLF disturbance events. The wavelet detail coefficient shows the exact location of disturbance and its amplitude. The small magnitude coefficients line at position 1400 indicates a small change in amplitude before and after this position and at position 1200 the coefficient line has large magnitude, indicates rapid changes in the VLF signal amplitude. It can be evidently seen that the signal is highly disturbed in the frequency range of 20-10 kHz. The other points of coefficient D_1 are smooth thus indicating that the signal follows some regular pattern in those periods without having noise.

B. VLF whistler emission

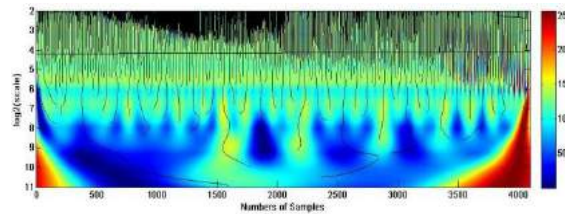


Fig. 7 WTMM curve of VLF Whistlers

Whistlers are electromagnetic impulses generated by lightning that have their frequency time spectrum modified as a result of dispersive propagation over very long path [22]. Fig. 7 is the WTMM spectrum of Whistler (as given in Fig. 4) with large numbers of maxima lines. The results of analysis are given in Fig. 8 and Fig. 9.

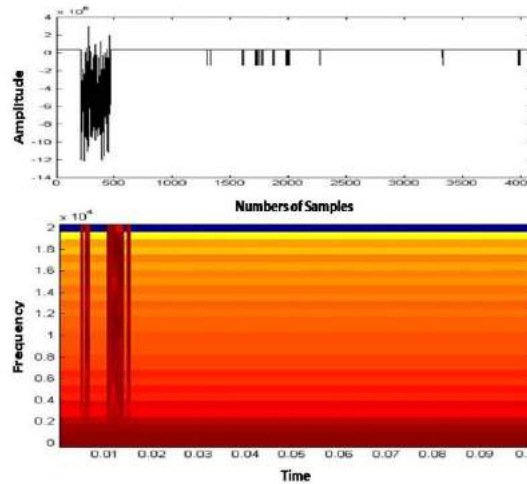


Fig. 8 Waveform of VLF whistler emission reconstructed by WTMM method and its WTMM curve (Lower panel)

It is found that VLF signal noises are suppressed after the occurrence of whistlers. The natural noise suppression by whistler is a relatively common magnetospheric phenomenon related to wave-particle interaction. Determination of onset and recovery times for the suppression effect were subject to uncertainty since most events showed suppression before the arrival of the 3-hop whistler and the onset was almost always obscured by the presence of multipath whistler traces or whistler triggered emissions[6]. Measurements of the recovery time were similarly complicated due to activity fluctuations, which made determination of the recovery point difficult. To overcome this problem DWT is used, which showed in Fig. 9. It gives exact time of onset and recovery time of Whistlers suppression events and also shows that signal has highly disturbed in frequency band 20-10 kHz.

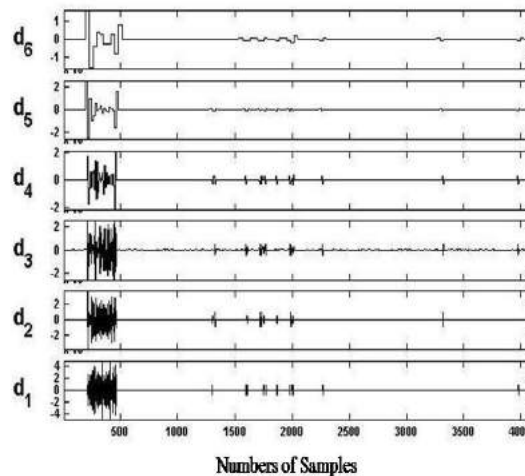


Fig. 9 Identification and localization of disturbance in VLF whistler emission using Haar wavelet at Level 6.

VI. CONCLUSION

In this paper, a method for VLF signal disturbance identification and localization using Wavelet transform modulus maxima and wavelet decomposition is proposed. WTMM detects the singularities of VLF signal by eliminating the unwanted noise. We found that the inner decomposition level of VLF signal is normally adequate to detect and localize any disturbance in signal. In order to increase the classification performance, features extraction is a pre-processing for removing the redundant information substantially without sacrificing significant information. In this work we transfer the VLF signal to the space-scale plane by using Wavelet Transform to extract important spectral features. The wavelet transform can focus on localized signal structure with scaling and dilation of a wavelet. The disturbances in VLF signal are thus detected automatically by WTMM.

ACKNOWLEDGEMENTS

D.K. Sondhiya is thankful to the University Grant Commission, New Delhi (India) for providing financial support through Special Assistance Program (SAP).

References:

- [1] C.F. Kennel and F. Engelmann, "Velocity space diffusion from weak plasma turbulence in a magnetic field," *Phys. Fluids*. 9, 12, 1966.
- [2] J.C. Foster and T.J. Rosenberg, "Electron precipitation and VLF emissions associated with cyclotron resonance interaction near the plasmapause," *Journal of Geophysical Research*, 81, pp. 2183-2192, 1976.
- [3] R.A. Helliwell, D.L. Carpenter and T.R. Miller, Power threshold for growth of coherent VLF signals in the magnetosphere. *J. Geophysic. Res.*, 85, 1980, pp. 3360.
- [4] H.C. Chang and U.S. Inan, "Quasi-relativistic electron precipitation due to interactions with Coherent VLF waves in the magnetosphere," *J. Geophys. Res.* 88 (A1), pp. 318-328, 1983.
- [5] C.F. Kennel and H.E. Petschek, "Limit on stably trapped particle fluxes," *J. Geophysic, Res.* 71, 1, 1966.
- [6] W.B. Gail and D.L. Carpenter, Whistler induced suppression of VLF noise, *Journal of Geophysical Research*. 89, pp. 1015-1022, 1984.
- [7] N. Cornilleau-Wehrin, R. Gendrin, F. Lefeuvre, M. Parrot, R. Grard and D. Jones, "VLF waves observed onboard GEOS-1," *Space Sci. Rev.* 22, pp. 371-382, 1978.
- [7] V.S. Sonwalkar and U.S. Inan, "Wave normal direction and spectral properties of Whistlers mode hiss observed on the DE 1 Satellite," *Journal of Geophysical Research: Space Physics*. 93(A7), pp.7493-7514,1988.
- [8] P. Kumar and E. Foufoula-Georgiou, "Wavelet analysis for Geophysical Application *Review of Geophysics*. 35, 4, pp. 385-412, 1997.

- [9] A.W.C. Liew and D.T. Nguyen, "Reconstruction from Wavelet Transform Modulus Maxima using Non-expansive Projections," *Electronics Lett.* 31 (13), pp. 1038-1039, 1995.
- [10] G. Cervone and M. Kafatos, D. Napoletani, R.P. Singh, "Wavelet maxima curves of surface latent heat flux associated with two recent Greek earthquake," *Natural Hazards and Earth System Sci.* 4, (3), pp. 359–374, 2004.
- [11] K. Wapenaar and R. Ghose, G. Toxopeus, J. Fokkema, The wavelet transform as a tool for geophysical data integration. *Integrated computer-Aided engineering.* 12 , 5-23.2005
- [12] X., Liu, "Time-Arrival Location of Seismic p-wave a based on Wavelet transform Modulus Maxima, *Journal of Multimedia,*" 8 (1), pp.32-39, 2013.
- [13] S. Mallat and H.Liang, Singularities detection and processing with Wavelets, *IEEE Transactions on Information theory.* 38 (2), pp.617-643, 1992.
- [14] D. Donoho and I. Johnstone, "Adapting to Unknown Smoothness via Wavelet Shrinkage," *Journal of the American Statistical Association,* 90, pp.1200-1244, 1995.
- [15] S. Mallat, "Multifrequency Channel Decompositions of Images and Wavelet Models, *IEEE Trans. on Acoustics, Speech, and Signal Processing.* 37 (12), pp.2091-2110, 1989.
- [16] W. Burtis and R.A. Helliwell, "Magnetospheric chorus; Occurrence patterns and normalized frequency," *Planet Space Sci.* 24, pp. 1007–1024, 1976.
- [18] H.C. Koons, "The role of hiss in magnetospheric chorus emissions," *J. Geophys.Res.* 86, pp. 6745–6754, 1981.
- [19] D.A. Gurnett, and B.J. Obrien, "High latitude Geophysical studies with Satellite Injun3, *Journal of Geophysical Research.* 69 (1), pp. 65-89, 1964.
- [20] S.S. Sazhin, 'Magnetospheric chorus Emissions: A Review,' *Planet Space Sci.* 40 (5), pp.681-697,1992.
- [21] K. Hattori, M. Hayakawa, D. Lagoutte, M. Parrot and F. Lefeuvre, "Further evidence of triggered chorus emissions from wavelets in the hiss band," *Planet Space Sci.* 39, pp.1465–1472, 1991.
- [22] R.A. Helliwell and M.G. Morgan, "Atmospheric whistlers," *Proc. IRE,* 47, pp. 200-208, 1959.

Detection of Seismo-ionospheric Anomalies using Wavelet based techniques

¹Anjana Sonakia, ²D.K. Sondhiya, ³S.K. Kasde, ⁴Harsha Jalori and ⁵A.K. Gwal
^{1,2,3,5}Department of Physics, Barkatullah University, Bhopal-462026, India
⁴Institute for Excellence in Higher Education, Bhopal-462021, India

Abstract: A number of papers have reported on anomalous variation in ionospheric foF2 parameter and/or ionospheric total electron content (ITEC) in the vicinity of earthquake's epicenter few days prior to the earthquake. In this work empirical dependency for the seismo-ionospheric disturbances relating the earthquake magnitude and the epicenter distance are obtained. They have been shown to be similar to those obtained earlier earthquakes. The dependences indicate the process of spreading the disturbance from the epicenter towards periphery during the earthquake preparation process. Large lead times for the precursor occurrence (up to 34 days for $M=5.8-5.9$) tells about a prolong preparation period. It is shown that different analyses of observed foF2 values lead to different conclusions regarding possible ionospheric precursors. Here we analyze the foF2 and ITEC observations over Greece prior to the three very large earthquakes of January 08, 2006, February 14, 2008 and June 08, 2008, using the wavelet based techniques.

Keywords: Wavelet Transform, ionospheric anomalies and foF2 parameter

I. Introduction

Earthquake is still an unpredictable natural disaster up to now, although there have been increasing interests in studying the ionospheric anomalies prior to earthquakes during the last three decades. Observation of ionospheric anomalies related to earthquake by ground-based equipment is a beneficial attempt to explore the impending earthquake prediction. The book of Ionospheric Precursors of Earthquakes, written by Pulnits and Boyarchuk [1], summarizes a large number obvious disturbance of the critical frequency observed by the ground-based ionospheric vertical sounding a few days before the quake.

Scientists observed anomalies appearing in electron densities of the ionospheric F-region few days before the strong earthquakes [2-3]. Liu et al. examined the ionospheric plasma frequency (or electron density) recorded by a local ionosonde and found that the critical frequency of the F2-peak (foF2), significantly decreased few days prior to $M \geq 6.0$ earthquakes in the Taiwan area between 1994 -1999 [3]. Ionosondes have been the most popular instrument probing the ionospheric electron density for more than seven decades [4]. Many results show anomalous behavior of ionospheric foF2 parameter few days before earthquake [5-12]. Xu et al. briefly present the observations of the giant perturbations in the ionosphere foF2 parameter prior to the Wenchuan earthquake and introduce the network of ground-based high-resolution ionospheric observation (GBHIO), using vertical and oblique ionosondes for monitoring seismo-ionospheric anomaly [13].

The goal of this work is not to explain the possible connection between ionospheric anomalies and earthquakes, since this is still under debate in the scientific community. Our first goal is to demonstrate the variation of ionospheric foF2 parameter and Ionospheric Total Electron Content (ITEC) during earthquake occurred at Greece. Secondly, we shows some new results from the unpublished data and increase the reliability of the results of the farfield sites in the previous studies using Wavelet based techniques. The result shows some unusual perturbations foF2 and ITEC some days before the main shock. This anomalous behavior of perturbations may be used as earthquake precursor.

II. Wavelet Analysis

General overview of Wavelet analysis may be found in [14-16]. Wavelet analysis uses a time localized oscillatory function as the Mother Wavelet. Using the Mother Wavelet function $\Psi(t)$ the continuous wavelet transform of ionospheric parameter $f(t)$ is defined as:-

$$(wf)(a,b) = \frac{1}{\sqrt{a}} \int_{-\infty}^{\infty} f(t) \bar{\psi}\left(\frac{t-b}{a}\right) dt \quad \dots\dots\dots (1)$$

Where,

a =dilation parameter

b = translation parameter

$\bar{\Psi}$ = complex conjugate of $\Psi(t)$

To ensure the existence of inverse wavelet transform mother wavelet satisfy the condition of admissibility given by-

$$C_{\Psi} = \int_{-\infty}^{\infty} \frac{|F_{\Psi}(\omega)|^2}{|\omega|} d\omega < \infty \quad \dots\dots\dots (2)$$

Where $F_{\Psi}(\omega)$ = Fourier transform of $\Psi(t)$

The signal $f(t)$ may be synthesized or reconstructed by an inverse wavelet transform of $(wf)(a, b)$ as defined by

$$f(t) = \frac{1}{C_{\Psi}} \int_{-\infty}^{\infty} \int_{-\infty}^{\infty} (wf)(a, b) \Psi\left(\frac{t-b}{a}\right) \frac{1}{a^2} da db \quad \dots\dots\dots (3)$$

In practice discrete wavelet transform is used in which the dilation parameter a and the translation parameter b are discrete. These procedures become much more efficient, if dyadic values of parameters a and b are used.

$$a = 2^j, b = 2^j k \quad j, k \in Z \quad \dots\dots\dots (4)$$

Where Z = set of positive integer

For a special cases of $\Psi(t)$, corresponding discretized wavelets $\psi_{jk}(t)$ is used, which is given by

$$\psi_{jk}(t) = 2^{\frac{j}{2}} \Psi(2^j t - k) \quad \dots\dots\dots (5)$$

Which constitute an orthogonal basis for $L^2(R)$ [15], [17-18]

In discrete wavelet transform a signal can be represented by its approximations and details. The details at level j are defined as:

$$D_j = \sum_{k \in Z} a_{jk} \psi_{jk}(t) \quad \dots\dots\dots (6)$$

and approximation at this level

$$A_j = \sum_{j=J} D_j \quad \dots\dots\dots (7)$$

Its become obvious that

$$A_{j-1} = A_j + D_j$$

$$\text{And } f(t) = A_j + \sum_{j \leq J} D_j \quad \dots\dots\dots (8)$$

These equations provide a tree structure of a signal and also a reconstruction process for the signal.

III. Data Selection

In this study data of ionospheric foF2 parameter and ionospheric total electron content (ITEC) were taken from NOAA's National Geophysical Data Center (NGDC) available online at www.ngdc.noaa.gov. For the proper selection of Ionosnde station famous Dobrovolsky equation was used in this work. Analytically written as [19]:

$$\rho = 10^{0.43M} \text{ km} \quad \dots\dots\dots (9)$$

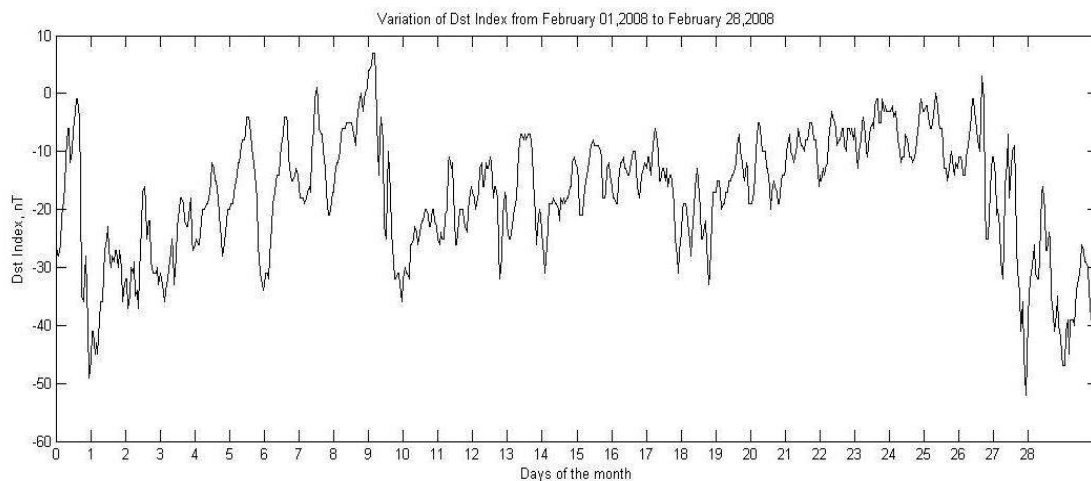
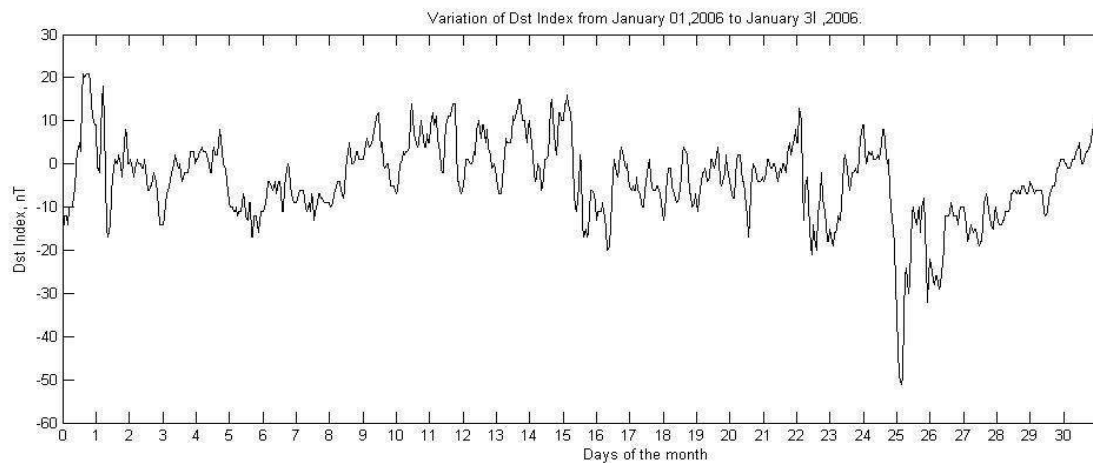
Where ρ is the radius of the earthquake preparation zone and M is the magnitude. The validity of the Dobrovolsky's formula for estimating the size of a modified area in the ionosphere before earthquakes used [20] and [21].

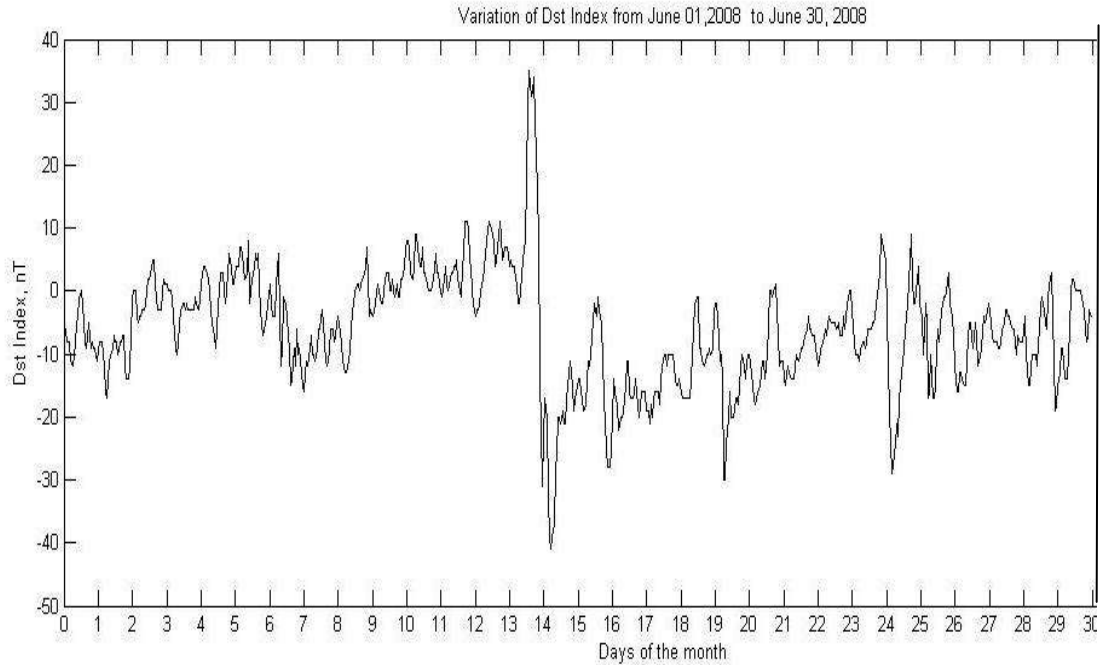
We have select three earthquakes near Athens ionosnde station for the study. The characteristics of these earthquakes were summarized in Table -1.

Table-1
Characteristics of Earthquakes

SN	Earthquake	Date	Epicenter	Time	M	Depth (km)	Name of nearest Ionosonde station	Distance between epicenter and Ionosonde station
1	Greece-southern	08/01/2006	36.30°N,23.36°E	11:34:55	6.8	66	Athens 38°N,24°E	197 km
2	Greece-southern	14/02/2008	36.64°N,21.83°E	10:09:23	6.9	29	Athens 38°N, 24°E	200 km
3	Greece-peloponnese	08/06/2008	38.02°N,21.46°E	13:25:00	6.4	16	Athens 38°N, 24°E	222 km

In order to classify the effect of geomagnetic activity on considered parameter during the earthquake geomagnetic Dst index should be checked. It is collected from WDC Kyoto, Japan and OMINI web data server. According to international classification the geomagnetic disturbance classified as a magnetic storm if the Dst index exceeds the value of -51 nT [22]. The variation of Dst index for the month of January 2006, February 2008 and May 2008 are shown in Fig. 1. It was noticed that for all earthquake Dst values were below the threshold level.





(c)

Fig. 1 Daily variation geomagnetic Dst Index for the moth (a) January, 2006 (b) February, 2008 and (c) June, 2008

IV. Case Study And Results

Analysis of ionospheric parameters revealed some anomalous common feature of ionospheric variability few days before main shock. These anomalies are expressed in terms of variation in ionospheric foF2 parameter and Ionospheric Total Electron Content (ITEC). We present three cases of earthquakes in which ionospheric perturbations were observed. Results related to these earthquakes are described below.

1.1 Greece – Southern Greece Earthquake occurred on January 08, 2006

The earthquake discussed took place on January 9, 2006, at 1:34 pm local time in Southern Greece (36.30°N, 23.36°E). Its depth was 66 km and the magnitude was $M = 6.8$. Variation in foF2 (upper panel) parameter and ITEC (lower panel) was illustrated in Fig. 2. Discrete Wavelet Transform (DWT) of foF2 parameter and ITEC were given in Fig. 3 (a) and Fig. 3 (b) respectively. In figure upper panel shows the variation in parameter middle and lower panel shows the variation in wavelet detail coefficient and values of selected wavelet coefficient on 2D graph. It gives abrupt change in ionospheric parameter six day (i.e. January 04, 2006) before the earthquake. The Continuous Wavelet Transform (CWT) displays the scale-dependent structure, so that the CWT provides a view of the frequency versus time behavior of the signal and therefore has great potential as a preliminary tool for investigating wideband, non-stationary or other types of signals having time-dependent spectral characteristics. Fig. 4 (a) and 4 (b) shows the step by step mode of continuous wavelet 1-D of foF2 and ITEC parameter. It is found that both parameters exhibit highly non-stationary nature before the earthquake.

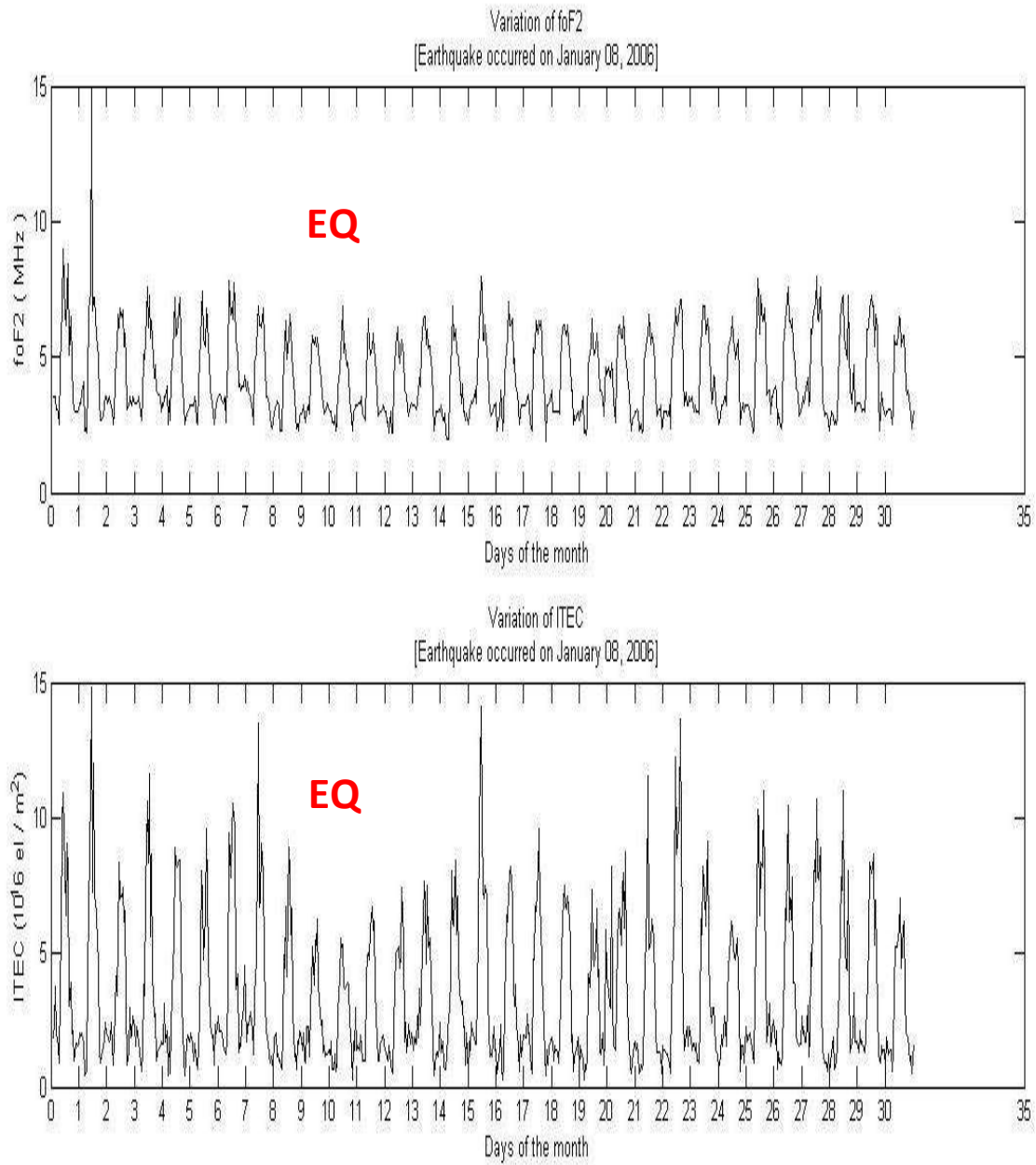


Fig. 2 Variation of ionospheric foF2 parameter and ionospheric Total Electron Content (ITEC) during Southern Greece Earthquake occurred on January 08, 2006

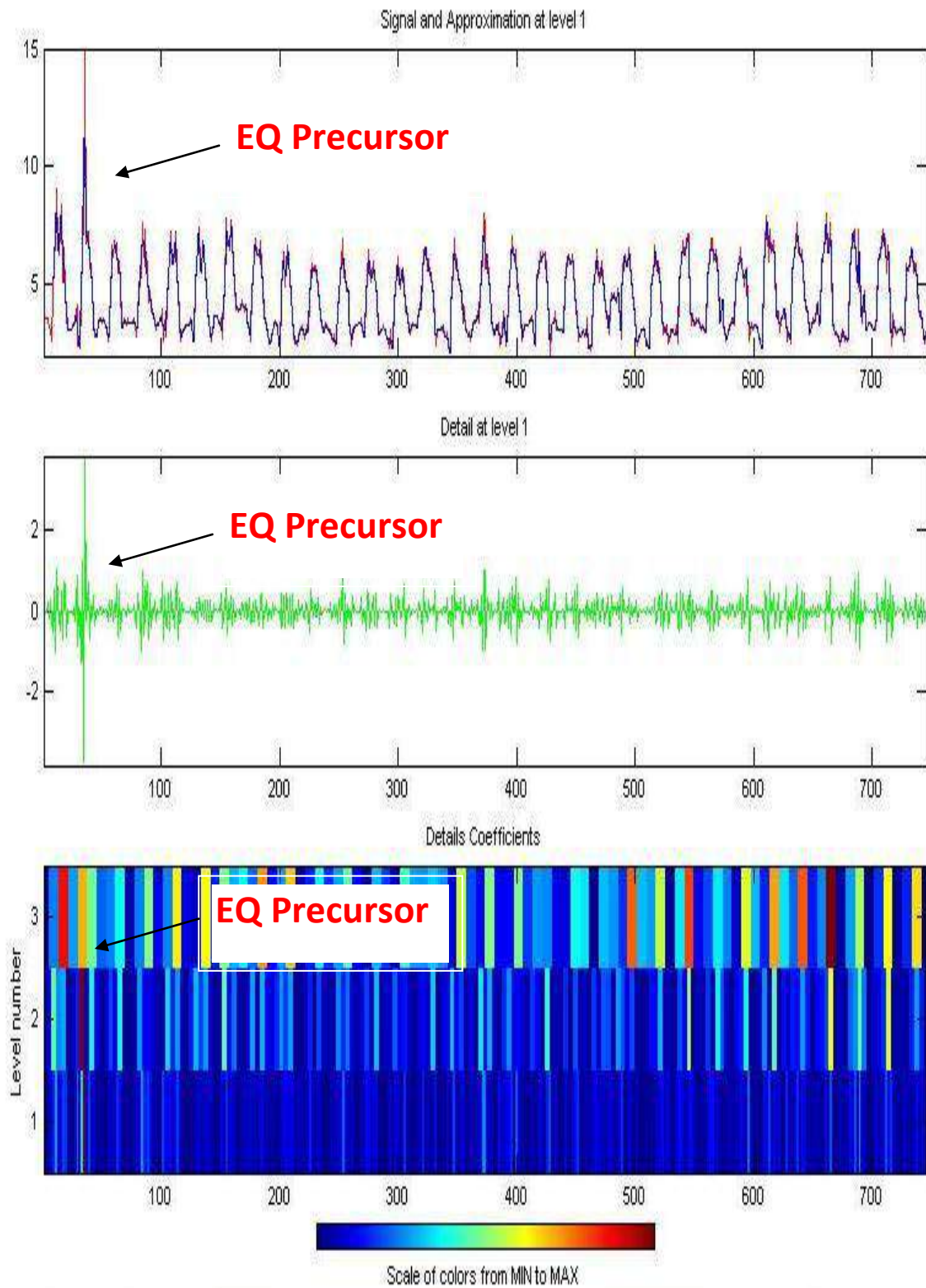


Fig. 3 (a) Discrete Wavelet Transform of Ionospheric foF2 parameter during Southern Greece Earthquake occurred on January 08, 2006

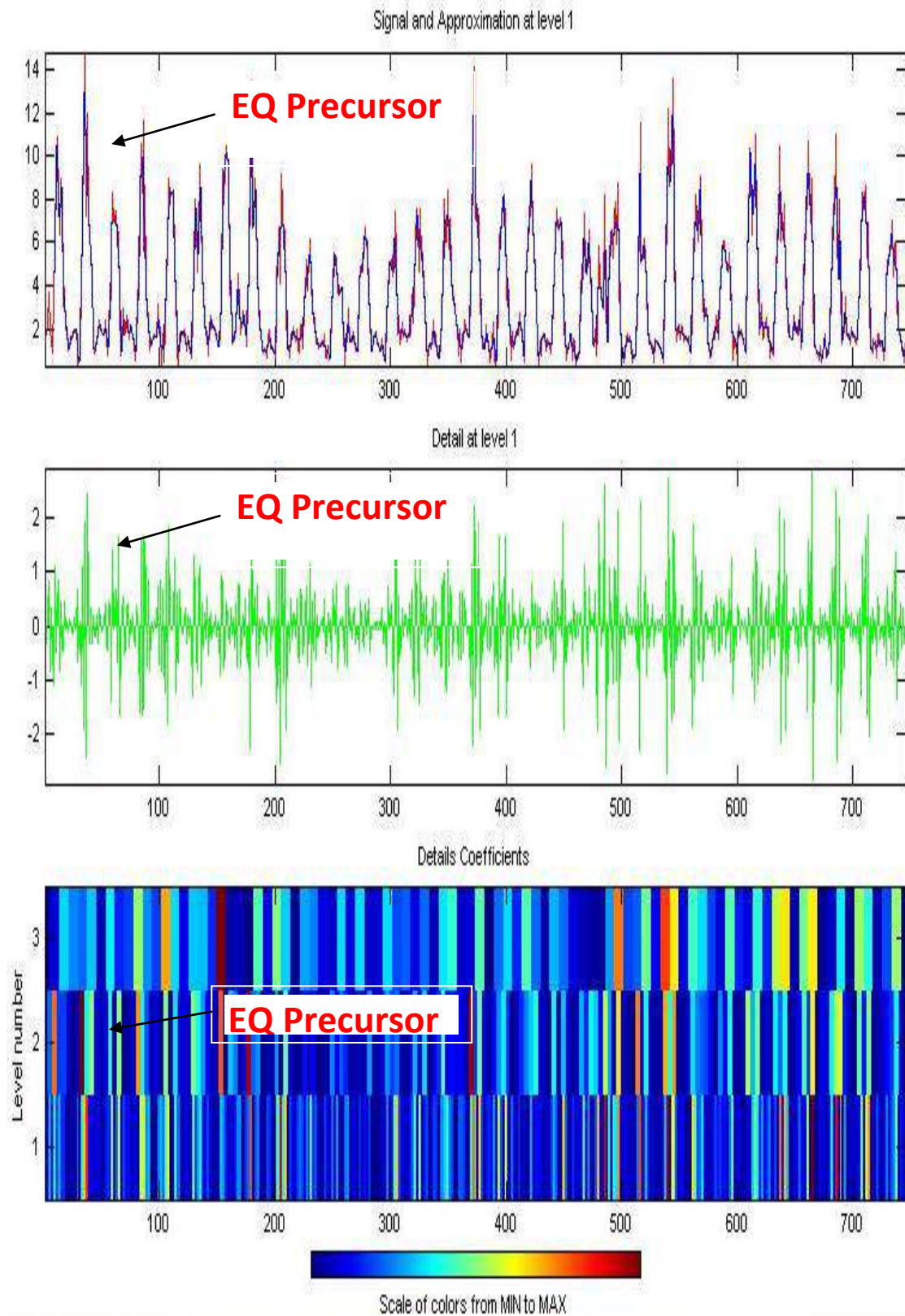


Fig. 3 (b) Discrete Wavelet Transform of Ionospheric Total Electron Content (ITEC) during Southern Greece Earthquake occurred on January 08, 2006

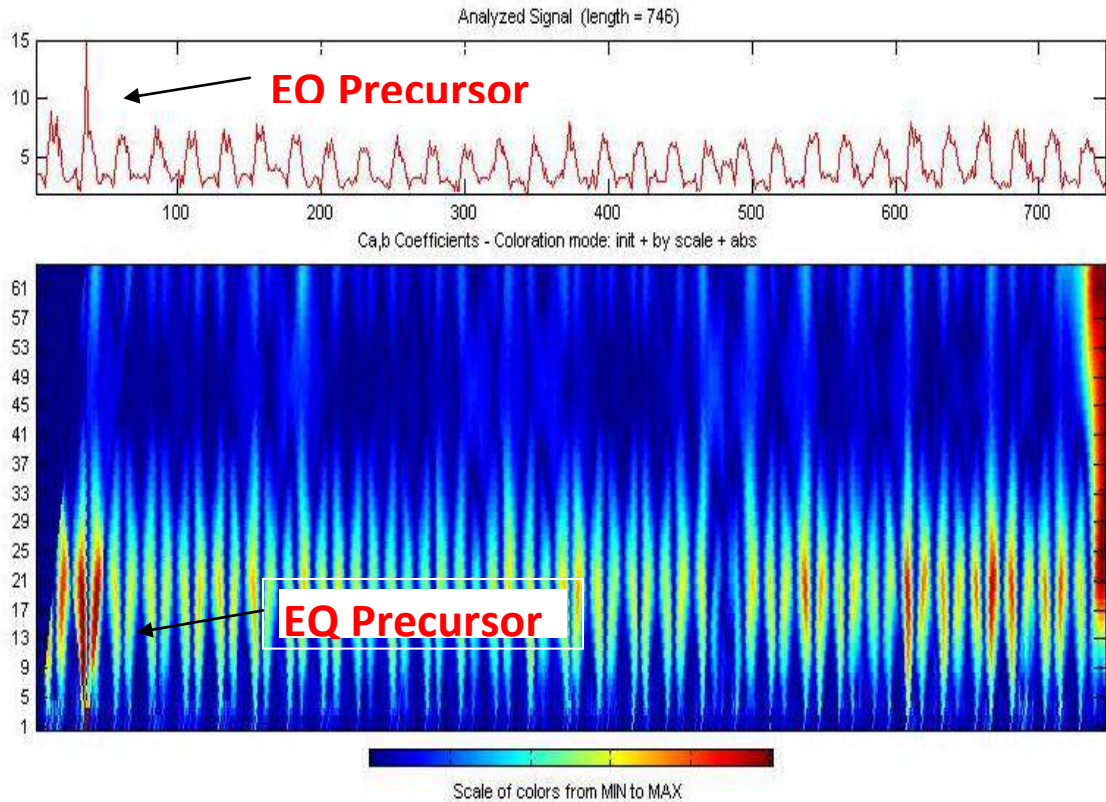


Fig. 4 (a) Continuous wavelet transform of Ionospheric foF2 parameter during Southern Greece Earthquake occurred on January 08, 2006

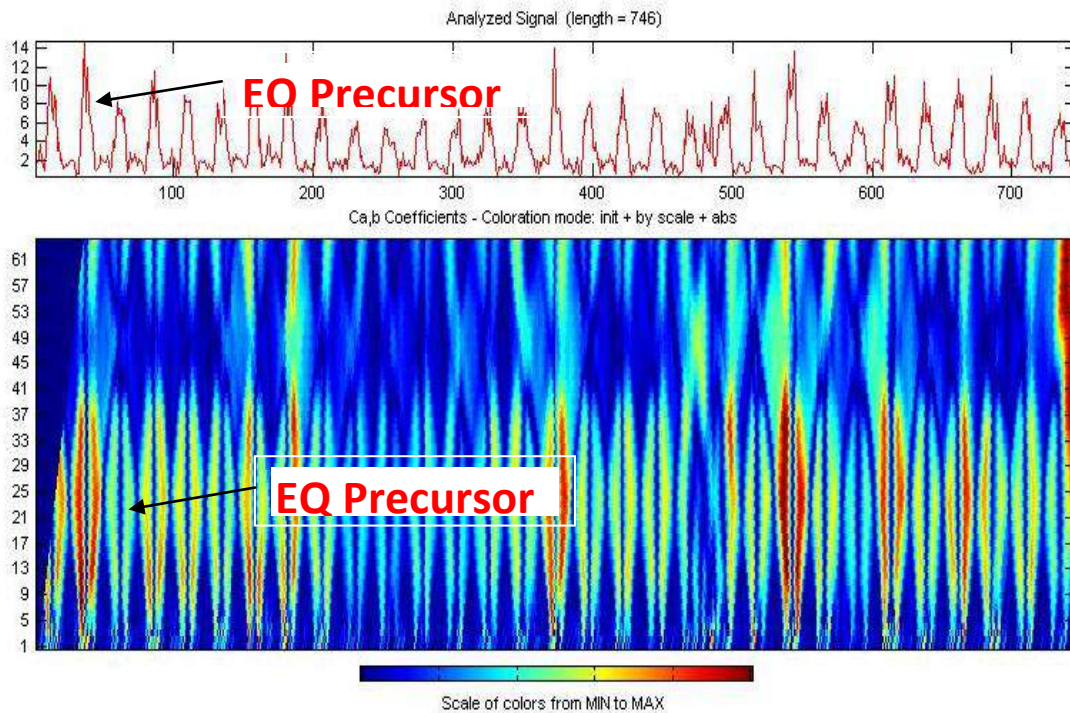


Fig. 4 (b) Continuous wavelet transform of ionospheric Total Electron Content (ITEC) during Southern Greece Earthquake occurred on January 08, 2006

1.2 Greece-Southern Earthquake occurred on February 14, 2008

Strong and dangerous earthquake with recorded magnitude of 6.9 struck Southern Greece (36.646°N, 21.833°E) on February 14, 2008 at 10:09:23 UTC. It was depth 29 km. Anomalous variation in foF2 and ITEC observed before six days from the main shock. Fig. 5 shows the variation of ionospheric foF2 parameter and

ITEC. Fig. 6 to 7 shows the wavelet analysis variation pattern for foF2 parameter and ITEC. It was noticed that these parameters shows highly abnormal behavior at February 07, 2008 seven day before the main shock and it was also noticed that the signal shows non-stationary behavior during this time.

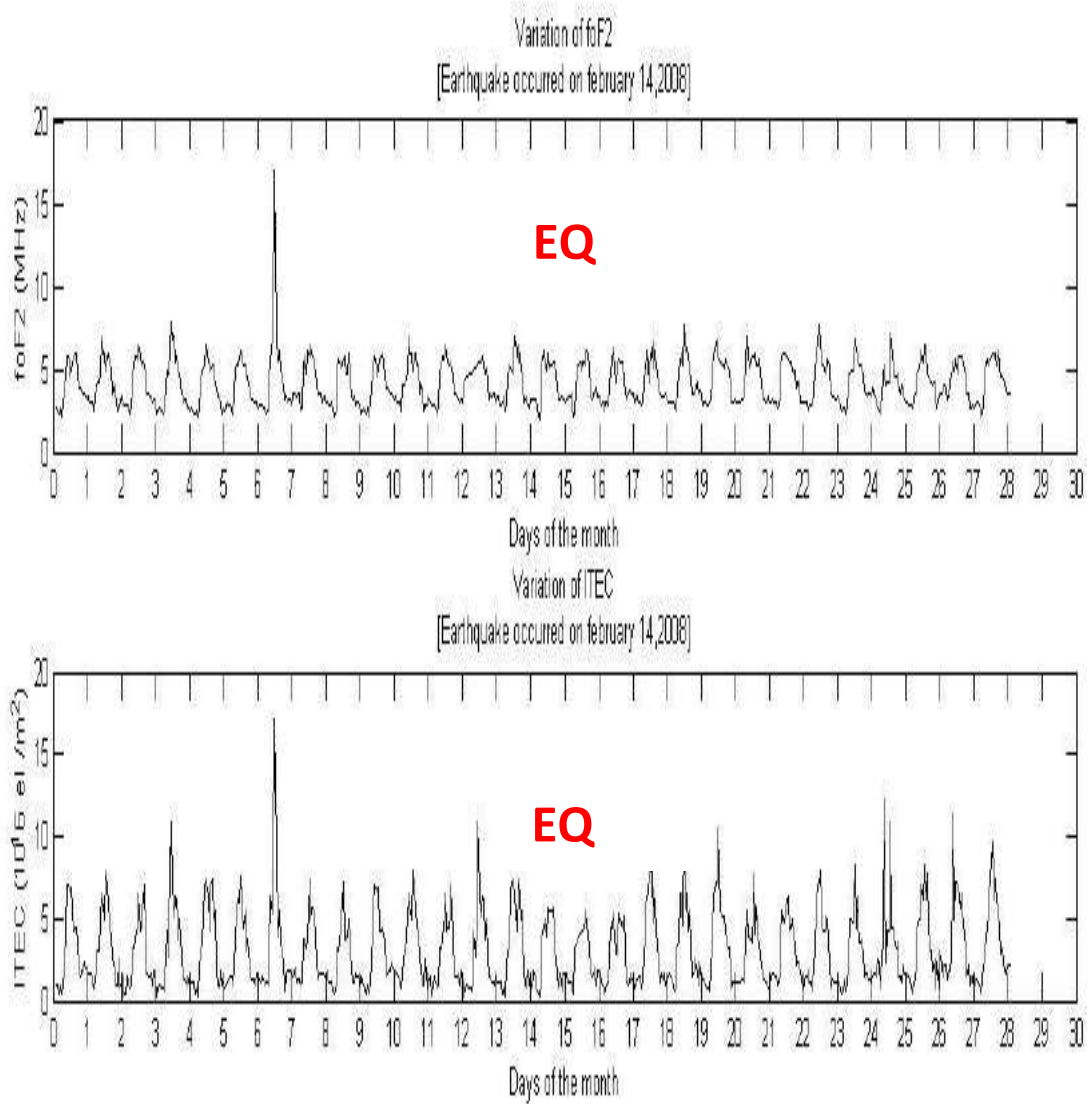


Fig. (5) Variation of ionospheric foF2 parameter and ionospheric Total Electron Content (ITEC) using Southern Greece Earthquake occurred on February 14, 2008

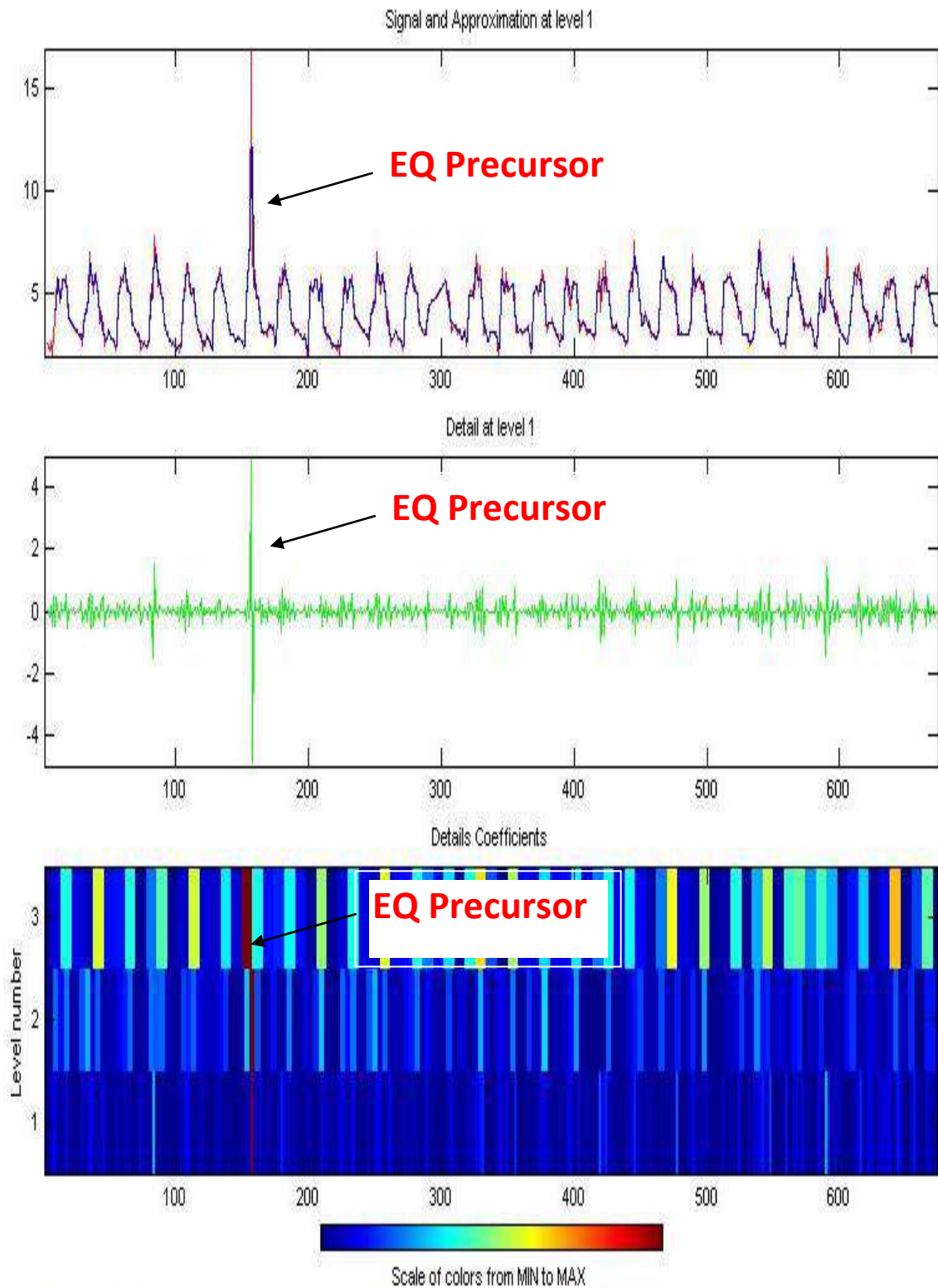


Fig. 6 (a) Discrete Wavelet Transform of Ionospheric foF2 parameter during Southern Greece Earthquake occurred on February 14, 2008

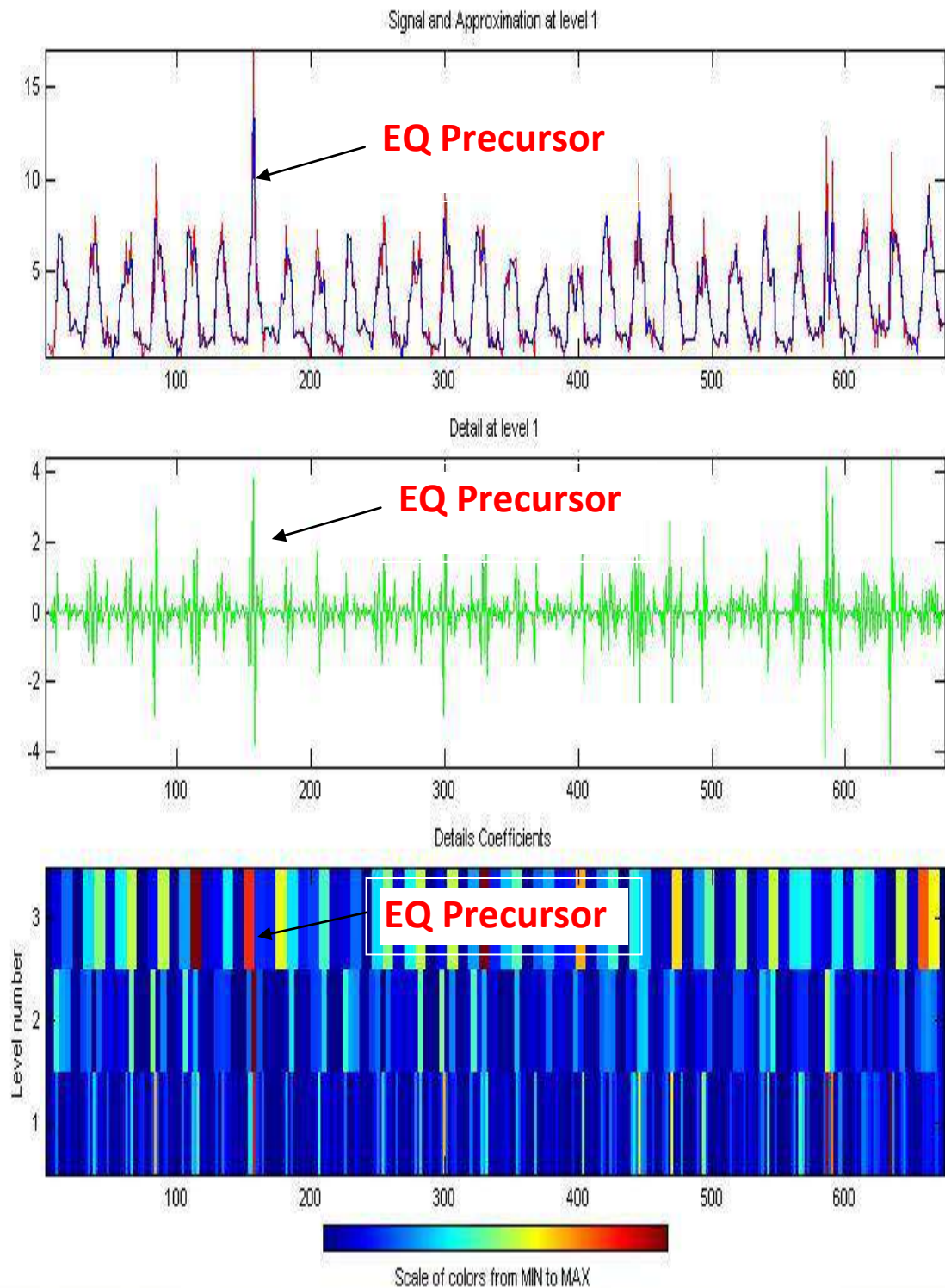


Fig. 6 (a) Discrete Wavelet Transform of Ionospheric total electron content (ITEC) parameter during Southern Greece Earthquake occurred on February 14, 2008

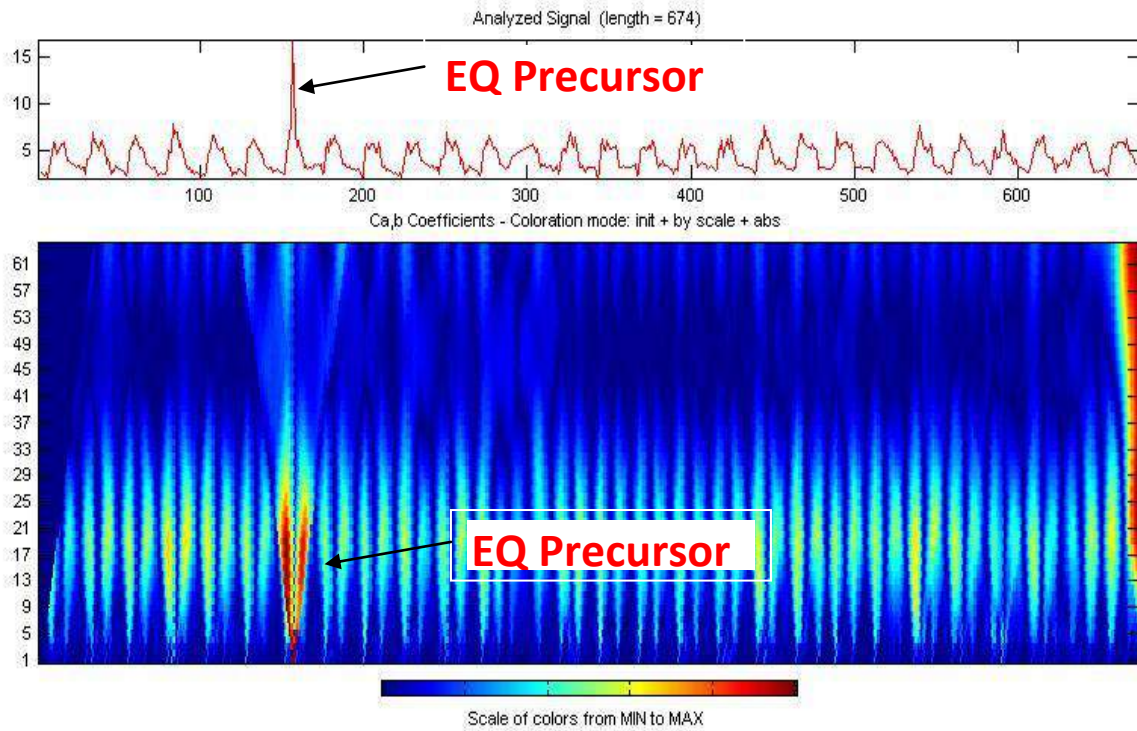


Fig. 7 (a) Continuous wavelet transform of Ionospheric foF2 parameter during Southern Greece Earthquake occurred on February 14, 2008

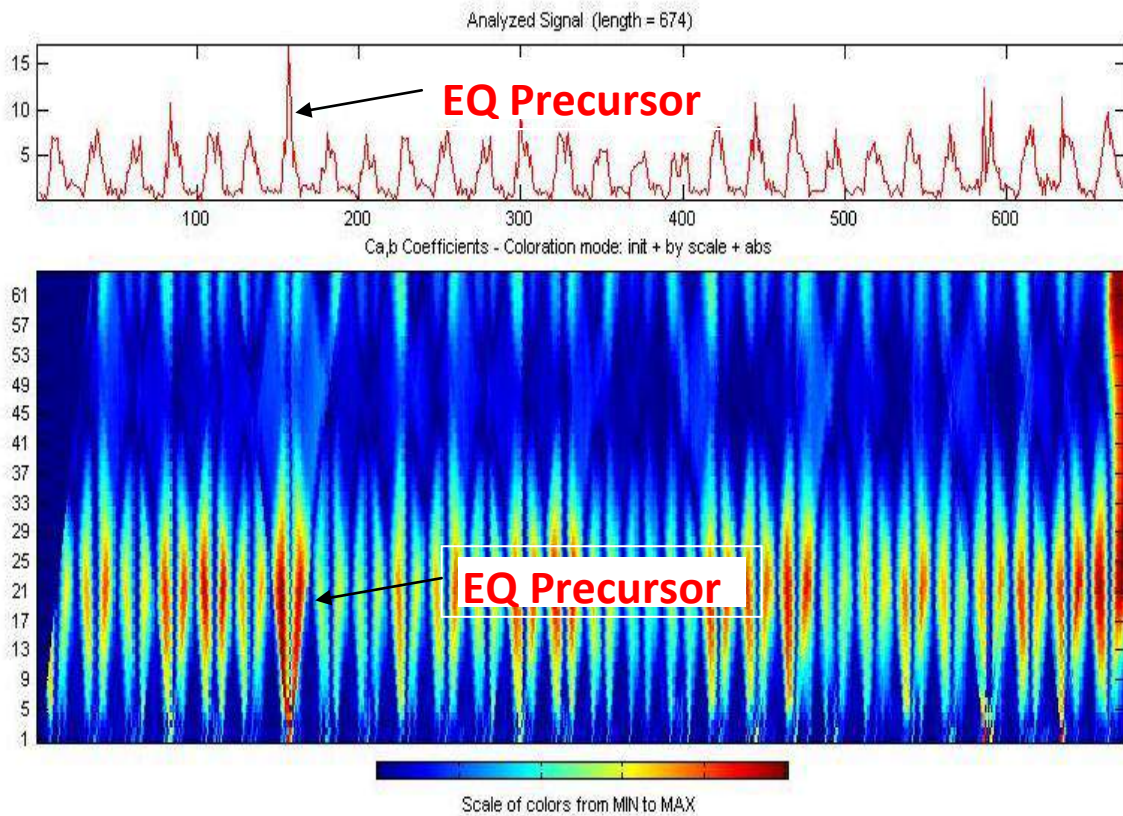


Fig. 7 (b) Continuous wavelet transform of Ionospheric total electron content (ITEC) parameter during Southern Greece Earthquake occurred on February 14, 2008

V. Greece-Peloponnese Earthquake Occurred On June 08, 2008:

A strong earthquake measuring 6.4 magnitudes on the Richter scale took place on June 08, 2008, at 13:25 UT in Peloponnese Greece (38.029°N, 21.464°E). Its depth was 10.5 km. Variation of ionospheric foF2 and ITEC parameters are shown in Fig. 8. The result of analysis was illustrated in Fig. 9 for discrete wavelet transform and Fig. 10 for continuous wavelet transform. It shows highly abnormal behavior at June 01, 2008 seven day before the earthquake and it is also noticed that the signal shows non-stationary behavior during this time.

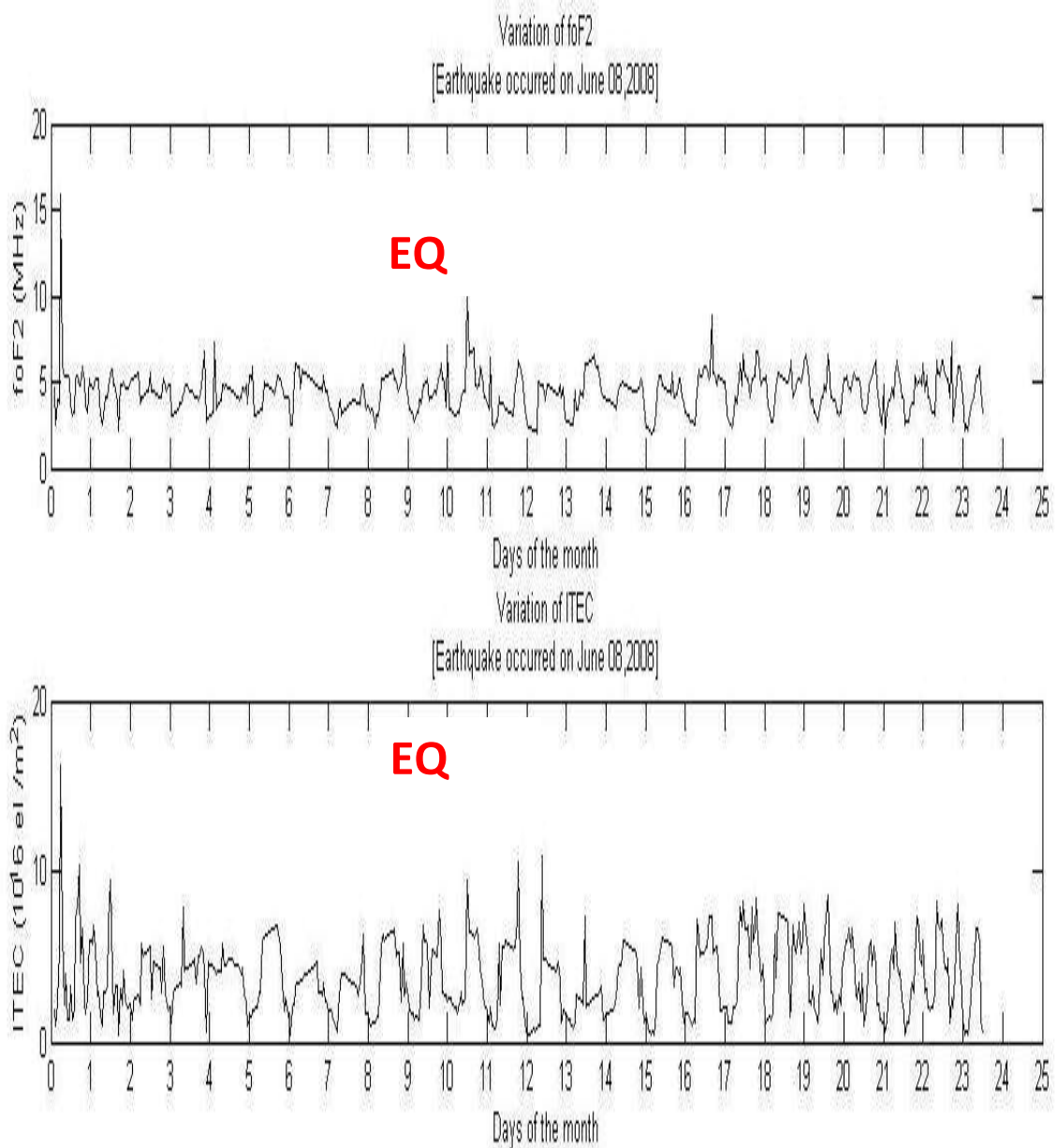


Fig. 8 Variation of ionospheric foF2 parameter and ionospheric Total Electron Content (ITEC) during Peloponnese Greece Earthquake occurred on June 08, 2008

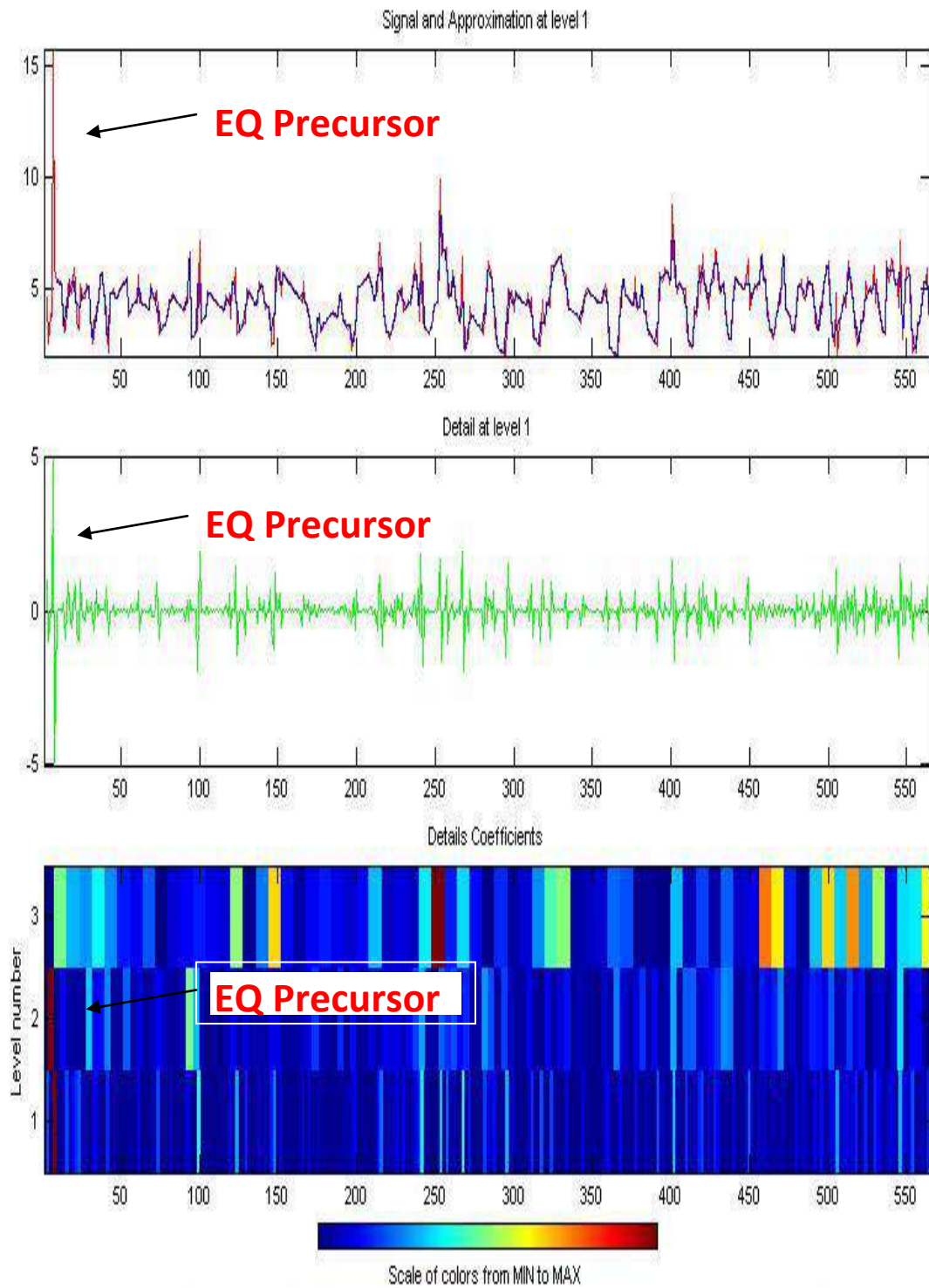


Fig. 9 (a) Discrete Wavelet Transform of Ionospheric foF2 parameter during Peloponnese Greece Earthquake occurred on June 08, 2008

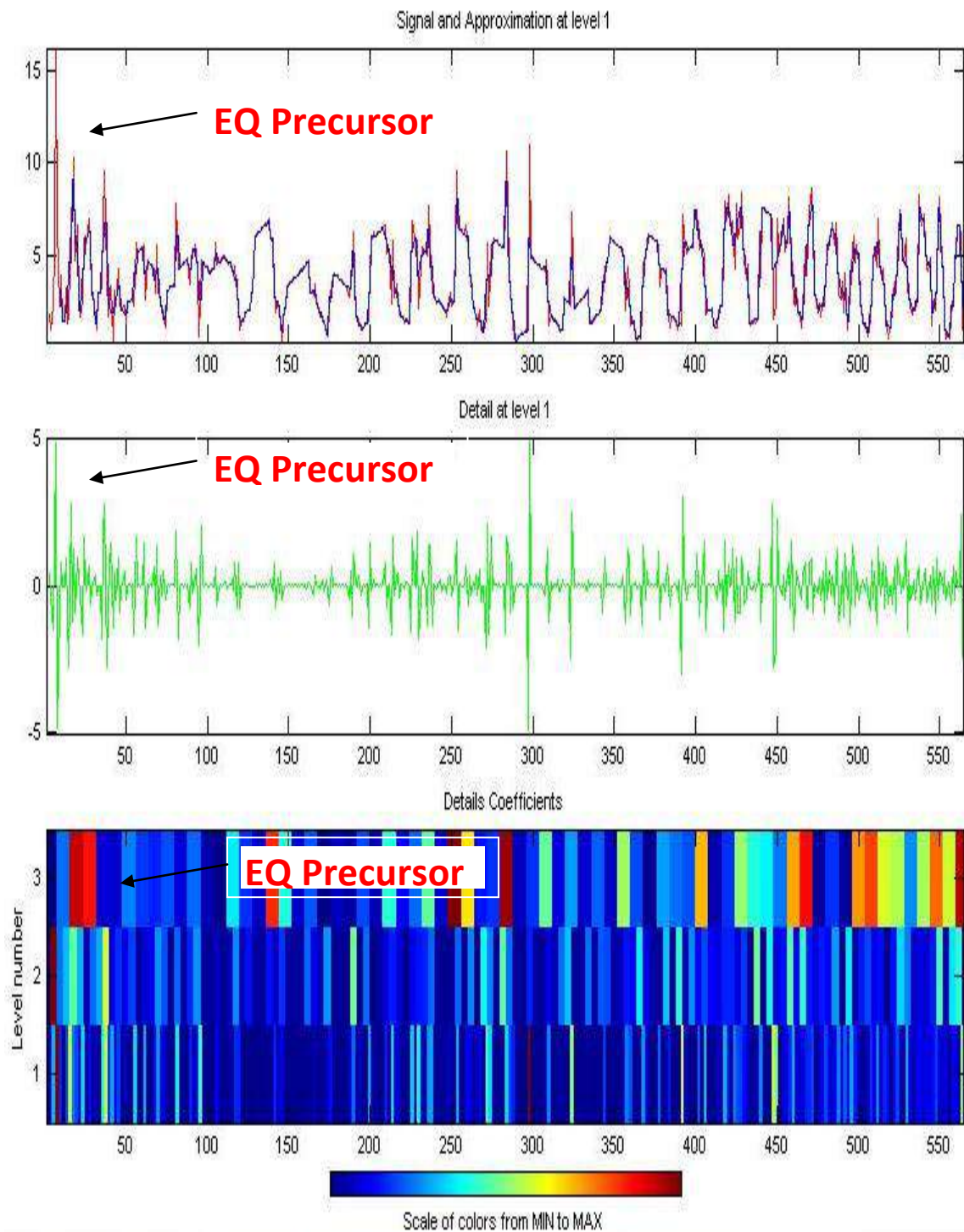


Fig. 9 (b) Discrete Wavelet Transform of ionospheric Total Electron Content (ITEC) during Peloponnese Greece Earthquake occurred on June 08, 2008

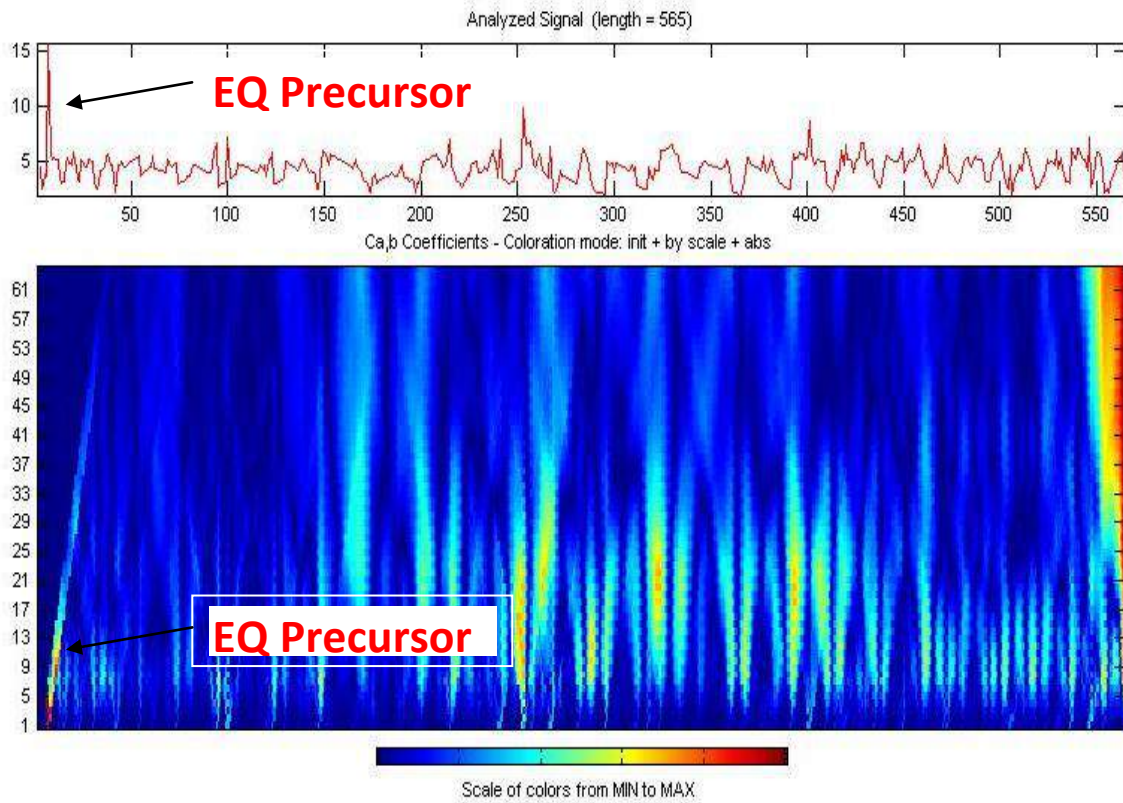


Fig. 10 (a) Continuous wavelet transform of Ionospheric foF2 parameter during Peloponnese Greece Earthquake occurred on June 08, 2008

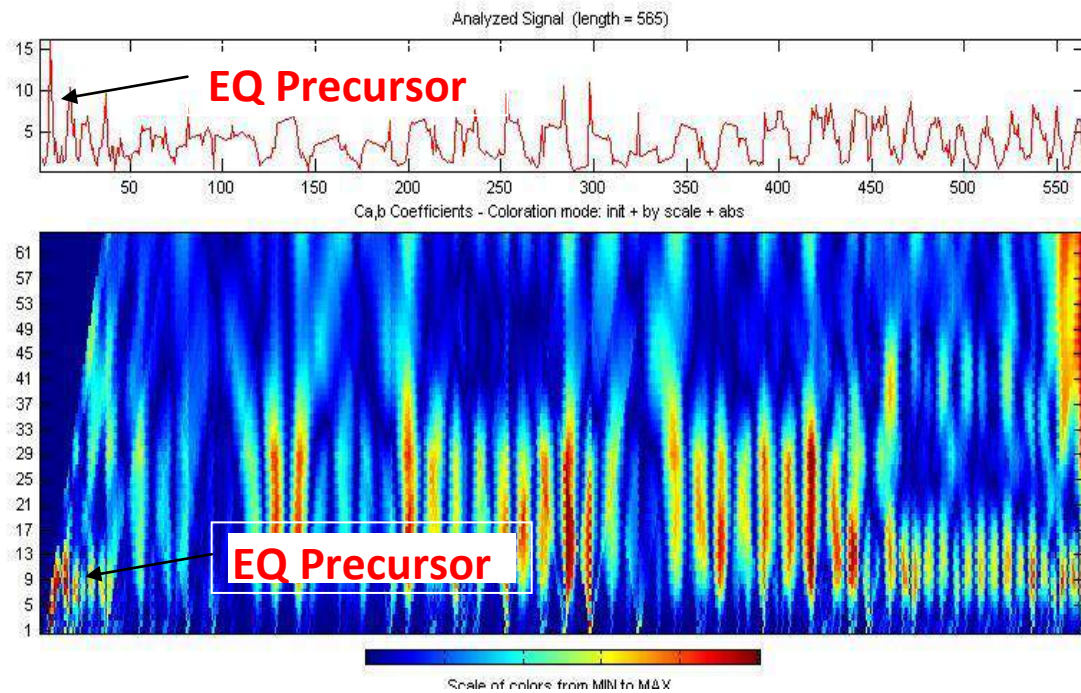


Fig. 10 (b) Continuous wavelet transform of Ionospheric foF2 parameter during Peloponnese Greece Earthquake occurred on June 08, 2008

VI. Discussion And Conclusions:

In this work the features of seismo-ionospheric variations registered by ground - based techniques that appear before the earthquakes have been demonstrated. These variations include the variation in ionospheric foF2 and ITEC parameters. The ionosonde measurements show ionospheric perturbations after the occurrence of the main shock. Also, these variations were independent of geomagnetic storm as the Dst values were quiet or moderate during these days with no geomagnetic storm during this period. The ITEC and foF2 measurements confirm that the ionosphere was disturbed some days before the earthquake at greater distance from the epicenter. The ionospheric variations have been observed during the earthquakes using different parameters ITEC and foF2 obtained from different techniques. The area of the variations of ionospheric parameters is of the same order of magnitude as size of the earthquake preparation zone on the ground surface [19]. Thus the present detection of anomalies during the earthquakes leads us to believe that coordinate measurements of ground based observations of ionospheric parameters can help in reliable detection of ionospheric precursors with more observations obtained from several stations.

The ionospheric perturbations observed in the F-layer are the most important ones as it is the most dense and most dynamical layer of the ionosphere. Pulinets used the data of Alouette-1 and Intercoms -19 satellites to study the variation in the critical frequency of F2 layer during earthquake [2]. They reported the formation of large - scale irregularities of electron concentrations in F2 region of the ionosphere during the preparatory phase of destructive earthquakes. The ground based ionospheric measurements using ionosonde shows strong anomalous disturbances in the ionosphere near the earthquake epicenter. The anomaly in the foF2 data was found before three to nine days from the main shock. Chen et al. analyzed the foF2 data associated with $M > 5$ earthquakes and found the chance of observing the precursor within five days prior to the earthquakes [23]. The ionospheric precursors of earthquake and reported observed precursors some days prior to the main shock [1], [3]. The main cause of above observed ionospheric anomalies might be due to the upward propagation of seismogenic electric fields, which are initially generated near the surface of the earth during the earthquake preparation period [24]. This dynamical process modified the height distribution of electric conductivity and induced the additional electromotive force in the lower ionosphere by the closed global electric circuit in the earth ionosphere system. This modification leads to perturbation in the F- region ionosphere; so as to change in ITEC and foF2 values. This anomalous behavior may be used as earthquake precursors.

References:

- [1] S.A. Pulinets, and K.A. Boyarchuk, *Ionospheric Precursors of Earthquakes* (Springer, Berlin, Germany, 2004).
- [2] S.A. Pulinets, A.D. Legenka, T.I. Zelenova, Local-time dependence of seismo-ionospheric variations at the F-layer maximum. *Geomagn.Aeronom*, 38, 1998, 400–402.
- [3] J.Y. Liu, Y.I. Chen, S.A. Pulinets, Y.B. Tsai, and Y.J. Chuo, Seismoionospheric signatures prior to MP 6.0 Taiwan earthquakes. *Geophys. Res. Lett.* 27, 2000, 3113–3117.
- [4] R.D. Hunsucker, *Radio Techniques for Probing the Terrestrial Ionosphere*, (Thomson Press India Ltd., 1991).
- [5] Y.I. Chen, J.Y. Liu, Y.B. Tsai, C.S. Chen, Statistical tests for preearthquake ionospheric anomaly, *Terr., Atm. Ocean Sci.* 15, 2004, 936–943.
- [6] V.H. Rios, V. P. Kim, V. V. and Hegai, Abnormal perturbations in the F2 region ionosphere observed prior to the great San Juan earthquake of 23 November 1977. *Adv. Space. Res.*, 33(3), 2004, 323–327, doi:10.1016/S0273-1177(03)00480-0.
- [7] R.S. Dabas, Rupesh, M. Das, K.M. Sharma, and K.G. Pillai, Ionospheric precursors observed over low latitudes during some of the recent major earthquakes, *J. Atmos. Sol.-Terr. Phy.*, 69(15), 2007, 1813–1824.
- [8] A.Kh. Depueva, A.V. Mikhailove, M. Devi, and A.K. Barbara, Spatial and time variations in critical frequencies of the ionospheric F region above the zone of equatorial earthquake preparation, *Geomagn.Aeron.*, 47(1), 2007, 129–133.
- [9] E.V. Liperovskaya, P.F. Biagi, C.V. Meister, and M.V. Rodkin, foF2 seismo-ionospheric effect analysis: actual data and numerical simulations, *Nat. Hazards Earth Syst. Sci.*, 8, 2008, 1387–1393, doi:10.5194/nhess-8-1387-2008.
- [10] E.V. Liperovskaya, V.V., Bogdanov, P.F. Biagi, C.V. Meister, V.A. Liperovsky, and M.V. Rodkin, Day-time variations of foF2 connected to strong earthquakes, *Nat. Hazards Earth Syst. Sci.*, 9, 53–59, 2009, doi:10.5194/nhess-9-53-2009.
- [11] K. Sharma, R.M. Das, R.S. Dabas, K.G.M. Pillai, S.C. Garg, and A.K. Mishra, Ionospheric precursors observed at low latitudes around the time of Koyna earthquake, *Adv. Space Res.*, 42(7), 1238–1245, 2008, doi:10.1016/j.asr.2007.06.026.
- [12] Tsolis, G. S. and Xenos, T. D.: A qualitative study of the seismoionospheric precursors prior to the 6 April 2009 earthquake in L'Aquila, Italy, *Nat. Hazards Earth Syst. Sci.*, 10, 133–137, 2010, doi:10.5194/nhess-10-133-2010.
- [13] T. Xu, Y.L. Hu, J. Wu, and Z.S. Wu, Anomalous enhancement of electric field derived from ionosonde data before the great Wenchuan earthquake, *Adv. Space Res.*, 47(6), 2011, 1001–1005, doi:10.1016/j.asr.2010.11.006.
- [14] C.K. Chui, *An introduction to wavelets* (Academic Press, San Diego, 1992).
- [15] I. Daubechies, *Ten lectures on wavelets* (SIAM, Philadelphia, 1992).
- [16] A. Sone and S. Yamamoto, *Wavelet analysis: Its origination, development, and applications* (in Japanese).
- [17] S. Mallat, Zero-crossings of a wavelet transform, *IEEE Transactions on Information Theory*, 37, 1991, 1019–1033.
- [18] B. Jawerth, W. Sweldens, An overview of wavelet based multiresolution analysis, *SIAM Review* 36 (3), 1994, 377–412.
- [19] I.R. Dobrovolsky, S.I. Zubko, and V.I. Mayachkin, Estimation of the size of earthquake preparation zones, *Pure Appl. Geophys.*, 117(5), 1979, 1025–1044.
- [20] S.A. Pulinets, K. A., Boyarchun, V.V. Hegai, V. P. Kim, and A.M. Lomonosov, Quasielectrostatic model of atmosphere-thermosphere-ionosphere coupling, *Adv. Space Res.*, 26(3), 2000, 1209–1281, doi:10.1016/S0273-1177(99) 01223-5.

- [21] S.A. Pulinets, K.A. Boyarchuk, A.M. Lomonosov, V.V. Khagai, J.Y. Liu, Ionospheric precursors to earthquakes: a preliminary analysis of the foF2 critical frequencies at Chung-Li ground-based station for vertical sounding of the ionosphere (Taiwan island), *Geomagn. Aeronom.* 42, 2002, 508–513.
- [22] W.D. Gonzalez, J.A. Joselyn, Y. Kamide, H.W. Kroehl, G. Rostoker, B.T. Tsurutani, and V.M. Vasyliunas, What is a geomagnetic storm? *J. Geophys. Res.*, 99, 1994, 5771-5792.
- [23] Y.I. Chen, J.Y. Chuo, J.Y. Liu, and S.A. Pulinets, Statistical study of ionospheric precursors of strong earthquakes at Taiwan area, XXVI URSI General Assembly, Toronto, 13-21 Aug. 1999, Abs., 745p.
- [24] M. Hayakawa, (Ed.), *Atmospheric and Ionospheric Electromagnetic Phenomena with Earthquakes* (TERRAPUB, Tokyo, 1999).